N72-13596
NASA-CR-72820
AI-71-31

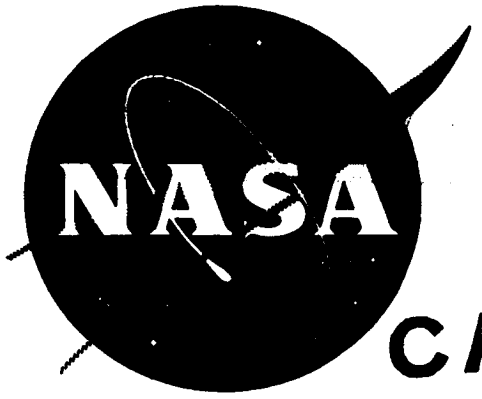

SUMMARY REPORT

EXPERIMENTAL PHYSICS CHARACTERISTICS OF A HEAVY-METAL-REFLECTED FAST-SPECTRUM CRITICAL ASSEMBLY

By

W. H. Heneveld, R. K. Paschall, T. H. Springer,
V. A. Swanson, A. W. Thiele, and R. J. Tuttle

ATOMICS INTERNATIONAL DIVISION
NORTH AMERICAN ROCKWELL CORPORATION

Prepared for
NATIONAL AERONAUTICS AND SPACE ADMINISTRATION
NASA LEWIS RESEARCH CENTER
CONTRACT NAS 3-12982

Paul G. Klann, Project Manager

NOTICE

This report was prepared as an account of Government-sponsored work. Neither the United States, nor the National Aeronautics and Space Administration (NASA), nor any person acting on behalf of NASA:

A.) Makes any warranty or representation, expressed or implied, with respect to the accuracy, completeness, or usefulness of the information contained in this report, or that the use of any information, apparatus, method, or process disclosed in this report may not infringe privately-owned rights; or

B.) Assumes any liabilities with respect to the use of, or for damages resulting from the use of, any information, apparatus, method or process disclosed in this report.

As used above, "person acting on behalf of NASA" includes any employee or contractor of NASA, or employee of such contractor, to the extent that such employee or contractor of NASA or employee of such contractor prepares, disseminates, or provides access to any information pursuant to his employment or contract with NASA, or his employment with such contractor.

NASA-CR-72820
AI-71-31

SUMMARY REPORT

EXPERIMENTAL PHYSICS CHARACTERISTICS OF A HEAVY-METAL-REFLECTED FAST-SPECTRUM CRITICAL ASSEMBLY

By
W. H. Heneveld, R. K. Paschall, T. H. Springer,
V. A. Swanson, A. W. Thiele, and R. J. Tuttle

ATOMICS INTERNATIONAL DIVISION
NORTH AMERICAN ROCKWELL CORPORATION
8900 DeSoto Avenue
Canoga Park, California 91304

Prepared for
NATIONAL AERONAUTICS AND SPACE ADMINISTRATION
JULY 30, 1971

CONTRACT NAS 3-12982
NASA LEWIS RESEARCH CENTER
CLEVELAND, OHIO
Paul G. Klann, Project Manager
Nuclear Systems Division

CONTENTS

Page

Abstract xv
Summary 1
I. Introduction 3
A. Background 3
B. Scope of Present Program 4
C. Purpose of Current Work 4
D. Brief Description of the Critical Assembly 5
E. Core Compositions 8
F. Organization of the Report 10
G. Units of Measurement 10
II. General Description of the Critical Assembly 13
A. The Reactor 13
1. General Layout 13
2. Control Drums 15
3. Fuel Element 17
B. Special Features 23
C. Instrumentation 29
III. Experimental Techniques 31
A. Reactivity 31
1. Inverse-Kinetics Technique 31
2. Pulsed-Neutron Technique 48
3. Inverse-Counting Technique 55
4. Drum-Worth Technique 57
B. Determination of the Ratio ℓ/β 57
C. Power Distribution Measurements 59
D. Neutron Spectrum Measurements 62
1. Proton-Recoil Method 62
2. Foil Measurements 69
IV. Results 73
A. Experimental Results and Discussion of Results 73
1. Core Material Masses 73
2. Critical Mass Values 75
3. Drum Calibrations 79

CONTENTS

Page

4. Neutron Energy Spectra 87
5. Core Material Worths by Substitution 89
6. Sample Reactivity Worths 95
7. Fuel Element Rotation Experiments 102
8. Neutron Lifetime 102
9. Reactivity Worth of a Void in the Outer Six Peripheral Locations 103
10. Power Distribution Measurements in Composition 5 103
11. Miscellaneous Experiments 113

B. Experimental Uncertainties 114

V. Concluding Remarks 117

APPENDIX A

Details of Experimental Program 119

I. Composition 1 119

A. Description 119

B. Experimental Results 119

1. Critical Mass 119
2. Drum Calibration 125
3. Neutron Spectrum 125
4. Fuel Element Interchange 127
5. Reactivity Worths of Various Materials 129
6. Fuel Element Rotation 132
7. Reactor Power Calibration 132

II. Composition 2 133

A. Description 133

B. Experimental Results 133

1. Critical Mass 133
2. Drum Calibration 135
3. Neutron Spectrum 135
4. Fuel Element Interchange 135
5. Reassembly Reproducibility 135

CONTENTS

Page

III. Composition 3 139
A. Description 139
B. Experimental Results 139
1. Critical Mass 139
2. Fuel Element Interchange 141
IV. Composition 4A 143
A. Description 143
B. Experimental Results 143
1. Critical Mass 143
2. Drum Calibration 145
3. Fuel Element Interchange 145
V. Composition 4 147
A. Description 147
B. Experimental Results 147
1. Critical Mass 147
2. Drum Calibration 148
3. Drum Interaction 148
4. Polyethylene Worth 149
VI. Composition 5 151
A. Description 151
B. Experimental Results 151
1. Critical Mass 151
2. Drum Calibrations 152
3. Power Distribution 153
4. Neutron Spectrum Measurements 159
5. Fuel Element Interchange 159
6. Fuel Element Rotation 159
VII. Composition 5A 165
A. Description 165
B. Experimental Results 165
1. Critical Mass 165
2. Drum Calibrations 166

CONTENTS

Page

3. Pulsed Neutron Measurements — Composition 5A(1) 166
4. Reactivity Worth of Some Large Samples in Composition 5A 168
5. Reactivity Worth of Small Samples in Composition 5A 169
6. Reactivity Worths of Fuel in Various Core Positions — Composition 5A 170
7. Reactivity Worth of a Void in the Outer Six Peripheral Locations 170
8. Control Characteristics — Composition 5A(2) 173

VIII. Composition 5B 175

A. Description 175

B. Experimental Results 175

1. Drum Calibration 175
2. Control Characteristics 175
3. A Measurement of the Ratio ℓ/β_e 176
4. Pulsed Neutron Measurements 177

IX. Power Flattened Core 179

A. Description 179

B. Experimental Results 179

1. Critical Mass 179
2. Drum Calibration 180
3. Control Characteristics 181
4. Spectral Power Distribution 181
5. Critical Mass with Four Drums In and Two Drums Out 191
6. Small-Sample Reactivity Worths 191

APPENDIX B

Chemical Impurities in Core and Sample Materials 193

I. Criteria 193

II. Conformance 201

CONTENTS

Page

APPENDIX C

Detailed Specification of the Critical Assembly 205
A. General Layout 205
B. Fuel Elements 205
C. Control Drums 211
D. Radial Reflectors 213
E. Core Filler Segment 216
F. Pressure Vessel Mockup 216
G. Reactivity Samples 216
H. Special Fuel Elements 217
I. Upper and Lower Grid Plates 217
J. Sample Holder Tubes 217
K. Oscillator Rods 217
L. Sample Changer and Oscillator Mechanism 222

APPENDIX D

Calculations in Support of the Safeguards Analysis Report 223
I. Introduction 223
II. Static Core Characteristics 225
A. Calculational Methods 225
B. Results 233
C. Conclusions 235
III. Dynamic Characteristics 241
IV. Summary 245
References 247

TABLES

1. Core Composition Description 9
2. Rossi-α Experimental Data 61
3. Detector Designation and Fillings 63

TABLES

Page

4. Radioactive Products Obtained in Foil Irradiation 70
5. Mass of Core Materials in Compositions 1, 2, 3, 4, 4A, 5, 5A, 5A(1), 5B, and the Power-Flattened Core 74
6. Summary of Critical Mass Data 76
7. Control Drum Worths in Power-Flattened Core 87
8. Foil Activation Data for Compositions 1, 2, and 5 92
9. Reactivity Worths of Various Materials in Composition 1 and 5A 93
10. Summary of Measured Reactivity Worths of Core-Length Samples in the Center of Composition 5A 94
11. Summary of Measured Reactivity Worths of Core-Length Samples in the Periphery of Composition 5A 96
12. Summary of Measured Void Reactivity Worths 100
13. Reactivity Worths of Small Samples in Composition 5A and the Power-Flattened Core 101
14. Estimate of Hydrogen Mass in Composition 1 124
15. Neutron Flux in Composition 1 126
16. Results of Foil Irradiations in Composition 1 128
17. Fuel Element Interchange Schedule 130
18. Neutron Flux in Composition 2 136
19. Results of Foil Irradiations in Composition 2 137
20. Reactivity Changes Accompanying Hf Addition — Composition 3 141
21. Reactivity Changes Accompanying Ta Addition — Compositions 4 and 4A 144
22. Drum Interaction Effects — Composition 4 149
23. Reactivity Changes Accompanying Tungsten Addition — Composition 5 152
24. Comparison of Total Worths of Each Drum in Composition 5 153
25. Radial Power Distribution — Composition 5 156
26. Axial Power Distribution — Composition 5 157
27. Axial Power Distribution — Composition 5 (Remeasurement) 158
28. Neutron Flux in Composition 5 160
29. Results of Foil Irradiation in Composition 5 162
30. Drum Worths as Determined by the Pulsed-Neutron Method 168
31. Drum Worths in Composition 5B 176

TABLES

Page

32. Power-Flattened-Cores Loading Scheme 179
33. Power-Flattened Core Loading Scheme (One Wire Added) 180
34. Control-Drum Positions for Power Distribution Measurements 183
35. Axial Power Distribution in Power-Flattened Core 186
36. Radial Power Distribution in Power-Flattened Core 187
37. Axial Power Distribution With Drums at -1.5% k 188
38. Radial Power Distribution With Drums at -1.5% k 189
39. Fuel Loading With Two Drums Out 192
40. Estimated Specific Reactivities 194
41. Impurity Concentrations Resulting in Reactivity Error of ±1¢ in Reactor Materials 196
42. Impurity Concentrations Resulting in Error of ±0.2% in Reactivity Samples 198
43. Impurity Listing for Reactor Materials 200
44. Impurity Listing for Reactivity Samples 202
45. Mass of Chemical Impurities in Reactor 203
46. Isotopic Compositions 203
47. List of Drawings 204
48. Physical Characteristics of Reactor Components 206
49. Theoretical and Measured Control-Drum Drive Speeds 211
50. 13-Group Cross Section Set 225
51. Atom Densities for Radial Cases With Drums Turned Fuel-In 228
52. Atom Densities for Axial Cases 229
53. Atom Densities for Radial Cases With Drums Turned Fuel-Out 229
54. 13-Group Source Spectra 232
55. Critical Loadings 233
56. Reactivity Calculational Results 234
57. Delay Neutron Fraction Calculations 235
58. WEP Input Data 244
59. Nuclear Parameters 245

FIGURES

Page

1. Sketch of Critical Assembly 6
2. Cross Sectional View of the Critical Assembly at the Core Midplane 12
3. Cross Sectional View of the Critical Assembly in the Vertical Direction
   a. Vertical Plane Passing Through the Axis of the Core and the Axis of a Drum 14
   b. Vertical Plane Passing Through the Axis of the Core and the Axis of the Fuel Element at a Point of the Star 14
4. Cross Sectional View of the Control Drum at the Core Midplane 16
5. Critical Assembly Fuel Element 18
6. Cutaway View of the Central Region of the Fuel Element 19
7. Top View of the Critical Assembly Without the Upper Grid Plate in Place 22
8. Photograph of Critical Assembly 24
9. Top View of the Critical Assembly With the Upper Grid Plate in Place 26
10. Proton-Recoil Detector Arrangement in Core Center 27
11. Neutron Detector Locations 28
12. Data Obtained for a Two-Step Reactivity Change
    a. Reactor Power vs Time 34
    b. Reactivity vs Time 34
13. Data Obtained During Scram of a Massive Mo Reflector
    a. Reactor Power vs Time 35
    b. Reactivity vs Time 35
14. Data Obtained for a Positive Reactivity Insertion
    a. Linear Power vs Time 36
    b. Reactivity vs Time 36
    c. Log Power vs Time 36
15. Data Obtained for a Stepwise Drum Calibration
    a. Power vs Time 40
    b. Reactivity vs Time 40
16. Comparison of the Worth of a Single Drum as Determined by Stepwise and Continuous-Drive Methods (Zero Degrees of Arc = Fuel Full-In) 41

FIGURES

Page

17. Power Trace Obtained During Small Sample Oscillations 44
18. Reactor Power Data Resulting from the Accumulation of Small-Sample Oscillator Cycles 45
19. Reactivity Data Derived from Accumulated Oscillator Cycles (Five Iterations) 46
20. Block Diagram of Instrumentation for Pulsed-Neutron Experiments 50
21. Results of Pulsed-Neutron Experiment Near $4 Subcritical 52
22. Block Diagram of Instrumentation for Rossi-α Experiment 58
23. Rossi-α Experimental Results 60
24. Block Diagram of Instrumentation for Proton-Recoil Spectrometer 64
25. Reactivity Worth of Drums 3 and 6 in Composition 1 (Zero Degrees of Arc = Fuel Full-In) 78
26. Reactivity Worth of Drum 6 in Composition 2 (Zero Degrees of Arc = Fuel Full-In) 80
27. Reactivity Worth of Drum 6 in Compositions 4 and 4A (Zero Degrees of Arc = Fuel Full-In) 81
28. Reactivity Worth of Drum 6 in Composition 5 (Zero Degrees of Arc = Fuel Full-In) 82
29. Reactivity Worth of Drums 3 and 6 in Composition 5A (Zero Degrees of Arc = Fuel Full-In) 83
30. Reactivity Worth of Drum 6 in Composition 5B (Zero Degrees of Arc = Fuel Full-In) 84
31. Reactivity Worth of Drum 6 in the Power-Flattened Core (Zero Degrees of Arc = Fuel Full-In) 85
32. Reactivity Worth of All Drums Ganged in Composition 5A (Zero Degrees of Arc = Fuel Full-In) 86
33. Neutron Spectrum in the Center of Composition 1 88
34. Neutron Spectrum in the Center of Composition 2 90
35. Neutron Spectrum in the Center of Composition 5 91
36. Radial Power Distribution — Composition 5 104
37. Axial Power Distribution — Top Half — Composition 5 106
38. Axial Power Distribution — Composition 5 107
39. Axial Power Distribution — Power-Flattened Core 108
40. Radial Power Distribution — Power-Flattened Core 110

FIGURES

Page

41. Axial Power Distribution – Drums at -1.5% $\Delta k/k$ 111
42. Radial Power Distribution – Drums at -1.5% $\Delta k/k$ 112
43. Changes in Inverse Multiplication From Addition of Mo Trapezoidal Pieces to Drums in Composition 1 120
44. Excess Reactivity and Inverse Multiplication – Composition 1 122
45. Excess Reactivity and Inverse Multiplication – Composition 2 134
46. Zones Corresponding to Hf Addition – Composition 3 140
47. Zones Corresponding to Ta Wire and Foil Additions – Composition 4A 142
48. Zones Corresponding to Large Diameter Ta Wire Additions – Composition 4 146
49. Zones Corresponding to W Addition – Composition 5 150
50. Power Distribution Wire Loading Scheme 154
51. Three-Zoned, Power-Flattened Core Loading Arrangement 178
52. Three-Zoned, Power-Flattened Core With Ta Absorbers Removed 182
53. Power Distribution Wire Loading Scheme – Power-Flattened Core (-1.5% $\Delta k/k$) 184
54. Power Distribution Wire Loading Scheme – Power-Flattened Core 185
55. Fuel Loading for Criticality With Two Drums Out 190
56. Li_3^7 Segment – Cross Sectional View 209
57. Eccentric Molybdenum Reflector – Cross Sectional View 210
58. Ta Absorber Segment – Cross Sectional View 212
59. Mo Reflector Segment – Cross Sectional View. 213
60. Trapezoidal Mo Filler Segment – Cross Sectional View 213
61. Scrammable Mo Reflector – Cross Sectional View 214
62. Stationary Mo Reflector – Cross Sectional View 215
63. Core Filler Segment – Cross Sectional View. 216
64. Fuel Element for Use With Proton-Recoil Detector 218
65. "Fuel Element" for Use With Sample Holder Tube 219
66. Sample Holder Tube 220
67. Oscillator Bar. 221
68. Core Layout 226

FIGURES

Page

69. Prompt Neutron Lifetime for Composition 1 236
70. Prompt Neutron Lifetime for Composition 5 237
71. Relative Axial Worth and Power Density – Composition 5 238
72. Relative Radial Worth and Power Density – Composition 5 239
73. Energy Release vs Ramp Rate 242
74. Core Map 249

ABSTRACT

A zero-power critical assembly has been designed, constructed, and operated for the purpose of conducting a series of benchmark experiments dealing with the physics characteristics of a UN-fueled, Li^7-cooled, Mo-reflected, drum-controlled compact fast reactor for use with a space-power electric conversion system. The experimental program consisted basically of measuring the differential neutron spectra and the changes in critical mass that accompanied the stepwise addition of $Li_3{}^7N$, Hf, Ta, and W to a basic core fueled with U metal in a pin-type Ta honeycomb structure. In addition, experimental results were obtained on power distributions, control characteristics, neutron lifetime, and reactivity worths of numerous absorber, structural, and scattering materials.

SUMMARY

A zero-power critical assembly has been designed, constructed, and operated for the purpose of conducting a series of benchmark experiments dealing with the physics characteristics of a UN fueled, Li^7-cooled, Mo-reflected, drum-controlled, compact fast reactor for use with a space-power electric conversion system. The critical assembly, which is a close geometrical simulation of the reference reactor, consists of a closely packed, six-pointed, star-shaped array of 181 Ta-clad, pin-type elements fueled with uranium metal and surrounded axially and radially by a Mo reflector. Nested between the points of the star-shaped core are 6 control drums each containing 11 fuel elements, a Mo reflector, and a Ta absorber segment.

The experimental program consisted basically of measuring the differential neutron spectra and the changes in critical mass that accompanied the stepwise addition of Li_3^7N (used to simulate the Li^7 coolant and the nitride in the fuel of the reference reactor), Hf, Ta, and W to the basic core which had a uniform distribution of uranium fuel. In addition, studies were carried out on power distributions, control characteristics, neutron lifetime and the reactivity worths of numerous absorber, structural, and scattering materials.

A three-zoned, power-flattened configuration was also assembled and used to determine: (1) the change in the power distribution relative to the uniformly loaded core, (2) the power distribution with drums banked, (3) the critical mass with (a) all drums full-in, and (b) with four drums full-in and two full-out, and (4) control characteristics involving various combinations of drum rotation.

The critical masses in the uniformly loaded systems varied from 179.64 kg of uranium (93% enriched in the U-235 isotope) for the "clean" core composition (only Ta and U) down to 171.75 kg for the fully-loaded core composition, the configuration containing Li_3^7N and all refractory metals. The critical mass of the power flattened core was 174.28 kg with all drums full-in and 181.54 kg with 4 drums full-in and 2 drums full-out. No major shift in the peak of the differential flux was observed between the clean core and subsequent cores; however, a prominent dip in the flux at 250 kev was observed when Li^7 was added to the system. Both radial and axial power distributions were determined in the

uniformly loaded composition. The ratio of the power at the center to that at the top edge of the core along the core axis was measured to be about 1.6, whereas the ratio of the power at the center to that at the edge along the core midplane was found to be about 1.8. Detailed mapping of the power in three dimensions in 1/12 sectors of the core was carried out. In the core midplane of the power-flattened core, the ratio of the power at the center to the power at the edge was reduced to 1.5. On the other hand, with the drums banked to about 0.2 of the way to the fuel-full-out position in the power-flattened core, the ratio of the power in the outermost drum fuel element to that at the core center was increased to 2.3, also within the core midplane.

All uniformly loaded core compositions appeared to exhibit roughly the same control characteristics, the worth of a single control drum varying from $2.22 for the clean core down to $1.90 for the fully loaded core. Intermediate compositions showed drum worths between these limits. However, as would be expected, the worth of a drum increased to $2.57 in the power-flattened core since additional fuel was moved into the outer periphery.

By the Rossi-α method, a determination for ℓ/β of 4.73 microseconds was made. Assuming that the value for β is 0.0067, one can derive a value for ℓ of approximately 32 manoseconds, which can be compared to the calculated value of 41 manoseconds.

Very extensive measurements of the reactivity worth of large as well as nearly infinitely dilute samples were made not only at the core center but also at the core edge in the uniformly fully loaded configuration. Most notable was the worth of U which varied from $+77 \times 10^{-3}$ ¢/gm for a large core length sample at the center to $+29 \times 10^{-3}$ ¢/gm for the same sample located at the core edge. The importance of neutron scattering at the edge of the core is exemplified by the fact that only B^{10} and Li^{6} exhibited significant absorption relative to a void, such materials as Ta, Hf, and U^{238} being positive in reactivity.

Numerous other physics characteristics of the critical assembly (such as reflector worths, the effects of a hydrogenous shield, and pulsed neutron decay constants) were investigated and provided information on basic core parameters that are useful for design purposes.

I. INTRODUCTION

A. BACKGROUND

The National Aeronautics and Space Administration has initiated a program for the purpose of designing a compact fast reactor for use in the generation of electric power in space. The reactor, which employs advanced concepts, is expected to operate at several megawatts, and is characterized by the exclusive use of high-temperature, high-strength refractory materials for structural, cladding, and reflecting purposes. The design goals for the reactor call for operation at high temperatures (1273°K) for periods of time of the order of 5 years.

An extensive series of neutronic calculations is being carried out by NASA on a reference design of one such reactor, a design that consists of a close-packed array of T-111 honeycomb tubes into which fuel pins are placed. These T-111 tubes are 2.159 cm(0.850 in.) in outside diameter (OD) and have a wall thickness of 0.0254 cm(0.010 in.). The fuel pin is also comprised of T-111 tubing which is 1.905 cm(0.750 in.) OD, has a wall thickness of 0.147 cm(0.058 in.), and is lined on the inside with a 0.013-cm(0.005 in.) thickness of W. Into this tubing is placed highly enriched hollow cylinders of uranium nitride (UN) fuel, the total height of which is about 37.59 cm(14.8 in.). A total of 181 fuel pins make up the stationary core and another 66 fuel pins are located in a series of six cylindrical control drums (11 fuel pins in each). With the fuel in the drums turned full-in, the core is roughly cylindrical in shape and has an effective diameter of about 35.5 cm(14 in.). Each control drum, which is about 14.6 cm(5.75 in.) in diameter and 60.2 cm(23.7 in.) high, also contains a massive TZM reflector which separates the fuel cluster from a T-111 absorber segment. The reference reactor is reflected axially by about 5.08 cm(2 in.) of TZM and radially by an effective 7.62-cm(3 in.) thickness of TZM.

Considering end-fittings on fuel pins and including the axial and radial reflectors, the overall height and diameter of the core are both about 55.88 cm(22 in.). The reactor is surrounded by a T-111 pressure vessel. Lithium-7 is proposed as the reactor coolant and flows principally in an annular space between the fuel pin and the honeycomb tube.

B. SCOPE OF PRESENT PROGRAM

Atomics International, under contract to NASA, designed, built, and operated a zero-power critical assembly that was a close geometrical mockup of this particular reference design. The experimental program, which is the subject of this report, consisted of measuring the differential neutron spectra and the changes in critical mass that accompanied the step-wise addition of the various refractory and coolant materials noted above to a basic core that was comprised solely of Ta and fully-enriched uranium metal uniformly distributed throughout the core. Cores containing all of the materials anticipated for use in the reference reactor were also used for determining: (1) the effects of fuel motion in the core, (2) the power distribution, (3) the reactivity worths of a wide variety of absorber, scattering, and structural materials, (4) certain core control characteristics, and (5) a variety of other information, such as neutron lifetime and decay constants, that pertains to dynamic and operating behavior of the reference reactor.

A redistribution of the uranium fuel was carried out for the purpose of achieving a three-zoned, power-flattened core, and the resulting configuration was used to measure the new power distribution not only for the case in which all drums were turned to the fuel-full-in position, but also for the case in which the drums were turned to achieve a decrease in k of 1.5%. The critical mass of this power-flattened core was measured for the condition corresponding to all-drums-in and for the condition corresponding to four drums in and two drums out. The reactivity changes accompanying the rotation of single drums, two diametrically opposing drums, five drums, and all drums from full-in to full-out were also determined, as was the reactivity control available in all drums with the Ta absorber segments removed.

C. PURPOSE OF CURRENT WORK

The purpose of the program was to conduct a well-defined and accurate series of experiments whose results can be used as a fundamental set of benchmarks against which current and future calculational techniques for this type of reactor can be checked.

Since the types, masses, purities, and locations of all materials making up the various compositions were carefully controlled and monitored, a very detailed and accurate geometrical and material representation of the core is available. This situation permits meaningful and detailed comparisons to be made between experimental and analytical data. At the same time, since the critical assembly is a reasonably close geometrical and material mockup of the reference reactor, many control and operating parameters are more or less directly applicable to an operating reactor. Finally, by systematically adding new materials in a step-wise fashion to a reasonably "clean" assembly (in terms of material composition), the adequacy of the various cross section sets applicable to the reference reactor and other fast reactor systems can also be ascertained.

D. BRIEF DESCRIPTION OF THE CRITICAL ASSEMBLY

The critical assembly was designed to be a reasonably good geometrical simulation of the reference reactor. An artist's sketch, showing the primary components of the system, is provided in Figure 1. The assembly is composed of a close-packed star-shaped array of 181 fuel elements surrounded radially by 6 massive Mo reflectors. Imbedded in the radial reflector region and also partly in the core region (between the points of the star) are 6 symmetrically located cylindrical control drums whose axes are parallel to the axis of the core. Each control drum contains 11 fuel elements and a molybdenum reflector and is backed by a massive Ta absorber segment. In order to provide a rapid-acting safety mechanism for the reactor, four of the 6 radial Mo reflector pieces are capable of falling away from the core (scramming) and thereby producing a substantial reduction in reactivity. This scram system consists of two independent and diametrically opposed safety elements to each of which are attached two of the Mo reflectors in a ganged fashion.

In the shutdown condition, four reflectors are located away from the core and all six control drums are rotated such that the Ta absorber segment in each drum is in the core region and the drum fuel elements are facing away from the core.

In order to achieve criticality, the four reflectors are raised into position (in juxtaposition with the core) by the safety element drive motors and then the

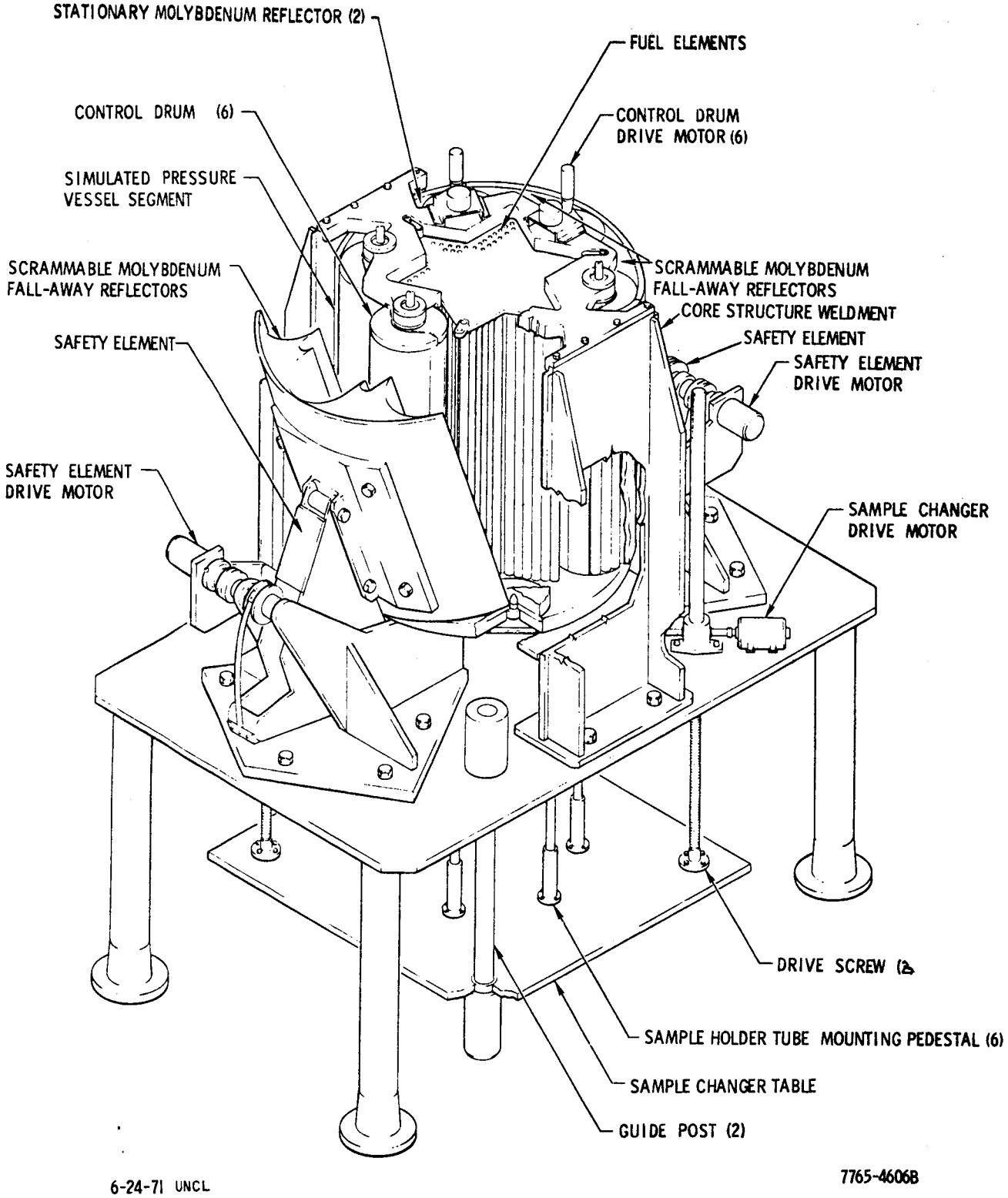

Figure 1. Sketch of Critical Assembly

control drums are sequentially "driven in"; i.e., rotated to bring fuel into the core. This drum control system simulates that proposed for the reference reactor.

Surrounding the massive Mo reflectors are four Ta segments which simulate in the radial direction the pressure vessel in the reference reactor. During reactor operation, when the reflectors are in the up-position, the four Ta segments form a cylindrical shell completely enclosing the reactor on the lateral surface.

Dimensionally, the critical assembly is 56.845 cm(22.38 in.) high, including upper and lower axial reflectors, and 57.15 cm(22.5 in.) in diameter, including the massive radial reflectors. The core proper is 37.508 cm(14.767 in.) high and has a "diameter" of 38.33 cm(15.09 in.) as measured from the center line of one fuel element at a point of the star to the center line of a diagonally opposite fuel element at the point of the star.

The critical assembly is mounted on a heavy steel plate below which is located a sample changer mechanism. This mechanism is used to insert or withdraw samples from the stationary core on either a rapid or slow drive-speed. Oscillator or single-sample replacement experiments can thus be performed.

Provisions have been made to allow for the removal of the central seven fuel elements from the critical assembly and for their replacement by a set of special elements which contain and enclose a spherical proton-recoil detector at the center of the core. This detector is used to measure the differential neutron spectrum in that location. In order to augment this spectrum data, sets of foils can also be inserted into the core center for irradiation.

Throughout an experimental program of this type it is necessary to have a means for identifying and locating individual fuel elements and the relative locations of control drums. The method used for this critical assembly is shown in a foldout diagram at the back of this document. The fuel element identification scheme consisted of assigning the designation 0-1 to the center fuel element location, 1-1 through 1-6 to the first ring of locations, 2-1 through 2-12 to the second ring of locations and so forth. Drum fuel elements are assigned designations in the 11 to 16 range so that the second digit designates the drum number. For example, 13-1 is a fuel element location in drum 3.

E. CORE COMPOSITIONS

The procedure in conducting the scope of work previously outlined for the experimental program consisted of first establishing a critical mass for a core comprised of 247 standard fuel elements containing no materials other than the uranium cluster, the Ta fuel and honeycomb tubes, a small amount of Ta spacer material, and the solid and eccentric Mo axial reflectors. This so-called "clean" core was designated Composition 1 and, insofar as the core proper was concerned, consisted only of U-235, U-238 (the balance of the uranium in the 93% enriched metal), Mo (a very small amount in the form of filler segments) and Ta. The radial and axial reflector regions remained in their normal positions throughout the experimental program. Several tests were conducted with Composition 1 and the experimental program then moved on to Composition 2 which involved only the addition of the $Li_3{}^7N$ segment to each of the 247 fuel elements. Thus, Composition 2 contained all of the materials in Composition 1 plus the $Li_3{}^7N$. Composition 3 consisted of all of the materials in Composition 2 in addition to Hf foil which was added to each fuel element. Similarly, Composition 4 consisted of all the materials in Composition 3 in addition to a coil of Ta foil in each fuel element and Ta rods in the fuel bundle and in the triflute spaces between honeycomb tubes. Finally, Composition 5 consisted of all the materials in Composition 4 in addition to a coil of W foil in each fuel element. For each of these compositions, the critical mass, control margin, and precision of the loading were measured. For some of the more important compositions, the neutron spectrum, control drum worths, and fuel displacement coefficients were also determined, and for Composition 5, measurements of neutron lifetime, decay constants, and sample worths in both the central and peripheral positions were conducted. In some instances, slight variations of particular compositions were studied, and, since the type of materials did not vary (only the quantities), a letter designation, as in Composition 4A, 5A, 5B, etc., was affixed to the composition number. Table 1 delineates these various cores according to their material types.

The power-flattened core was formed by decreasing, relative to Composition 5A, the mass of uranium in the fuel elements in the center of the core and increasing the mass in the fuel elements in the outer periphery. Whereas

TABLE 1

CORE COMPOSITION DESCRIPTION

Composition Number	Uranium Distribution	Major Materials in Core							
		U Fuel	Ta* Tubes	Li^7N	Hf	Ta Foil	0.28 Ta† Wire	0.36 Ta§ Wire	W Foil
1	Uniform	X	X						
2	Uniform	X	X	X					
3	Uniform	X	X	X	X				
4	Uniform	X	X	X	X	X	X	X	
4A	Uniform	X	X	X	X	X	X		
5	Uniform	X	X	X	X	X	X	X	X
5A	Uniform	X	X	X	X	X	X		X
5A(1)	Uniform	X**	X	X	X	X	X		X
5A(2)	Uniform	X††	X	X	X	X	X		X
5B	Nonuniform	X§§	X	X	X	X	X		X

*Honeycomb and fuel tubes
†0.279 cm(0.110 in.) diameter Ta wire located within the fuel bundle
§0.356 cm(0.140 in.) diameter Ta wire located between honeycomb tubes
**Re-constituted Composition 5 with minor change in total fuel loading
††Uniform removal of 3.2 kg of fuel from Composition 5A(1)
§§Re-distribution of fuel toward outer periphery of core.

Composition 5A consisted of 247 fuel elements each containing 6 rods and 7 large diameter wires of uranium, the inner zone (Zone 1) of the power-flattened core contained 6 rods and only 1 wire, the next zone (Zone 2) 7 rods and no wires, and the outer zone (Zone 3) 7 rods and 4 wires. Zone 1 was comprised of 73 fuel elements in positions 0-1 through 4-24, inclusive, plus positions 5-1, 5-5, 5-6, 5-10, 5-15, 5-16, 5-20, 5-21, 5-25, 5-26, and 5-30 (see foldout). Zone 2 was comprised of 90 fuel elements in the remaining core positions in the fifth ring, plus those in Positions 6-1 through 8-18, inclusive. Finally, Zone 3 consisted of 84 fuel elements in Positions 9-1 through 10-6, inclusive, and all of the drum fuel elements.

F. ORGANIZATION OF THE REPORT

In Section II of this report, a detailed description of the reactor is presented, and is followed, in Section III, by a discussion of the experimental techniques used for the various tests and experiments. Section IV contains a review and discussion of the major results of the program and Section V presents some concluding remarks.

A detailed discussion of the various experiments on a composition-by-composition basis is presented in Appendix A for use by those wishing to delve into the specifics of each experimental test and procedure.

Naturally occurring impurities in the various core materials have been carefully monitored. These are discussed and evaluated in Appendix B.

A detailed description of the reactor components, including extensive measurements of weights and dimensions and the statistical variations thereof is contained in Appendix C which should be referenced if detailed calculations are to be performed.

The operation of a new critical assembly required, according to normal procedures, the preparation of a Safeguards Analysis Report. Such a report was prepared for and submitted to the U.S. Atomic Energy Commission which, through its San Francisco Operations Office, gave approval to operate the reactor in an existing critical facility located at the Atomics International Field Laboratory near Canoga Park, California. This report encompassed, among other subjects, a series of calculations which scope, in broad generalities, the operating and physical characteristics of the reactor. These calculations are discussed in Appendix D and provide some rough analytical indications of the magnitudes of various physics parameters.

A very extensive pre-critical analytical effort in connection with the experimental program has been carried out by NASA and has been reported separately (see References 2, 3, and 4).

G. UNITS OF MEASUREMENT

All of the reactor components were designed, built, and checked to physical dimensions expressed in inches. Consequently, the International System of Units

used here for the unit of length is derived from the latter data. The masses quoted herein for fuel and other reactor materials were, however, measured directly in terms of grams. The proton-recoil spectrometer detectors were filled by an outside vendor to specified pressures expressed in atmospheres; therefore, for reporting purposes these units were converted to newtons/square meter. All other physical units of measurement, unless otherwise noted in the text, were based directly upon the units quoted.

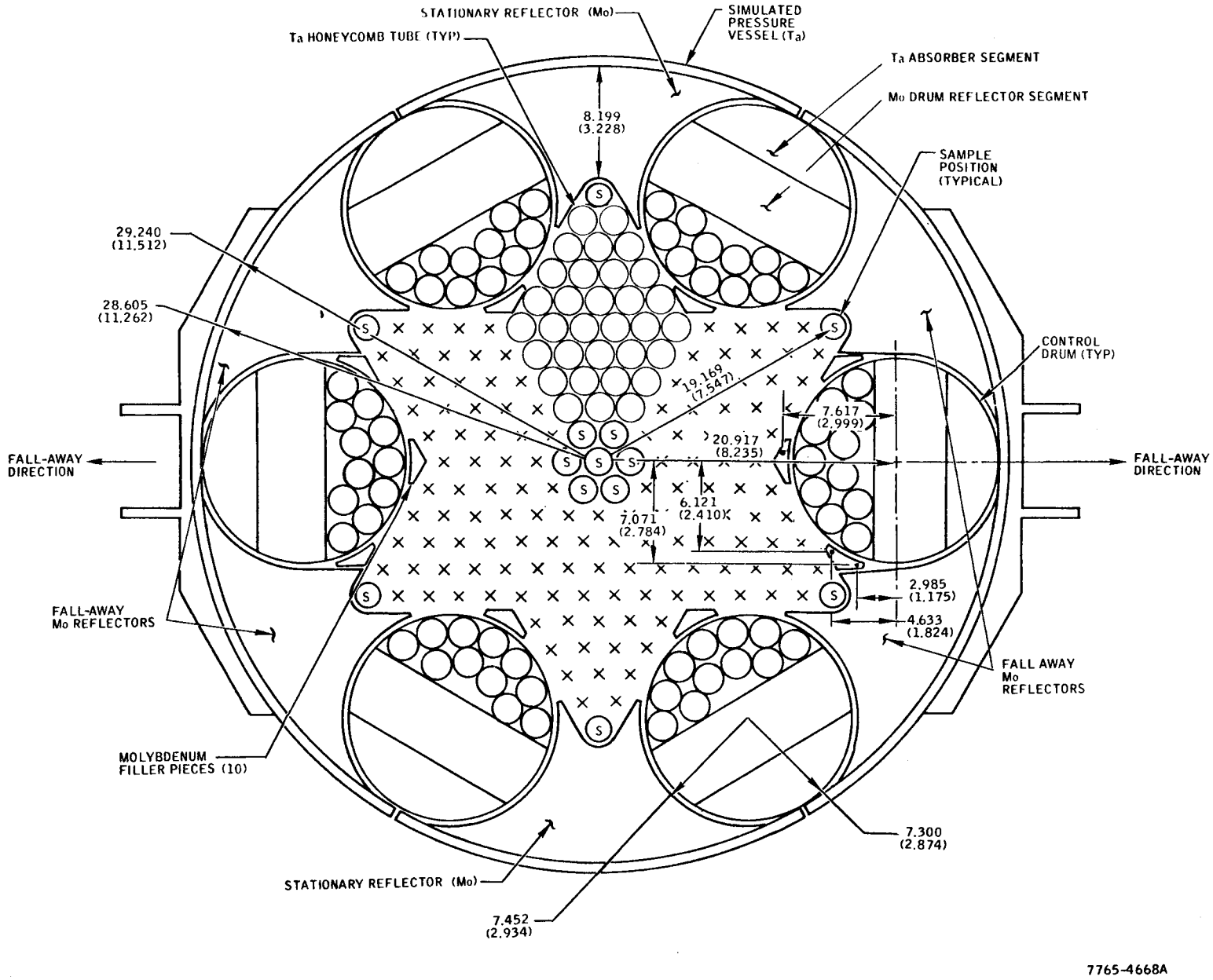

Figure 2. Cross Sectional View of the Critical Assembly at the Core Midplane

II. GENERAL DESCRIPTION OF THE CRITICAL ASSEMBLY

A. THE REACTOR

1. General Layout

The general features of the reactor can be seen by reference to Figure 2, which represents a cross-sectional view of the reactor at the core midplane. On the external surface, the reactor is surrounded by the Ta segments that simulate the pressure vessel in the reference reactor. One segment is located on each of the two fall-away safety-element systems and one on the outside of each of the two stationary reflectors. The segments have an outside radius of 29.23 cm(11.51 in.), a thickness of 0.691 cm(0.272 in.) and a height of 59.7 cm(23.5 in.). In the operating condition, the Ta segments form a tightly fitting cylindrical shell around the lateral surface of the reactor.

Inside the Ta pressure vessel mockup segments are the massive Mo reflectors. Each of the six reflectors is about 60.2 cm(23.7 in.) high and has an outside radius of 28.60 cm(11.26 in.). The thickness from the outer radius to the nearest fuel element is 8.20 cm(3.23 in.). The reflectors have circular cut-outs for accommodating the rotatable control drums and therefore wrap around the drums to some extent. However, in order to allow four of the reflectors to fall away from the core, a portion of these four reflectors has been cut away so that they "clear" the drums. Four small triangular Mo filler pieces are therefore installed in the stationary core in such a way that, when all reflectors are in the up-position, they are, for all practical purposes, identical. The two safety elements to which these four reflectors are attached are capable of removing about $12 reactivity in a time interval of the order of 450 milliseconds.

Located within the region occupied by these massive Mo reflectors and the six control drums is the star-shaped stationary core. The small circles shown in Figure 2 represent some of the 181 Ta honeycomb tubes that simulate the primary core structural member in the reference core. The location of the center line of the remainder of the core elements are shown by an "X" in the figure. The honeycomb tubes are 59.941 cm(23.599-in.) high, are 2.159 cm(0.850 in.) in outside diameter, have a 0.0254 cm(0.010 in.) wall, and are located on a 2.125 cm(0.872 in.) lattice pitch. In order to conduct certain experiments, the

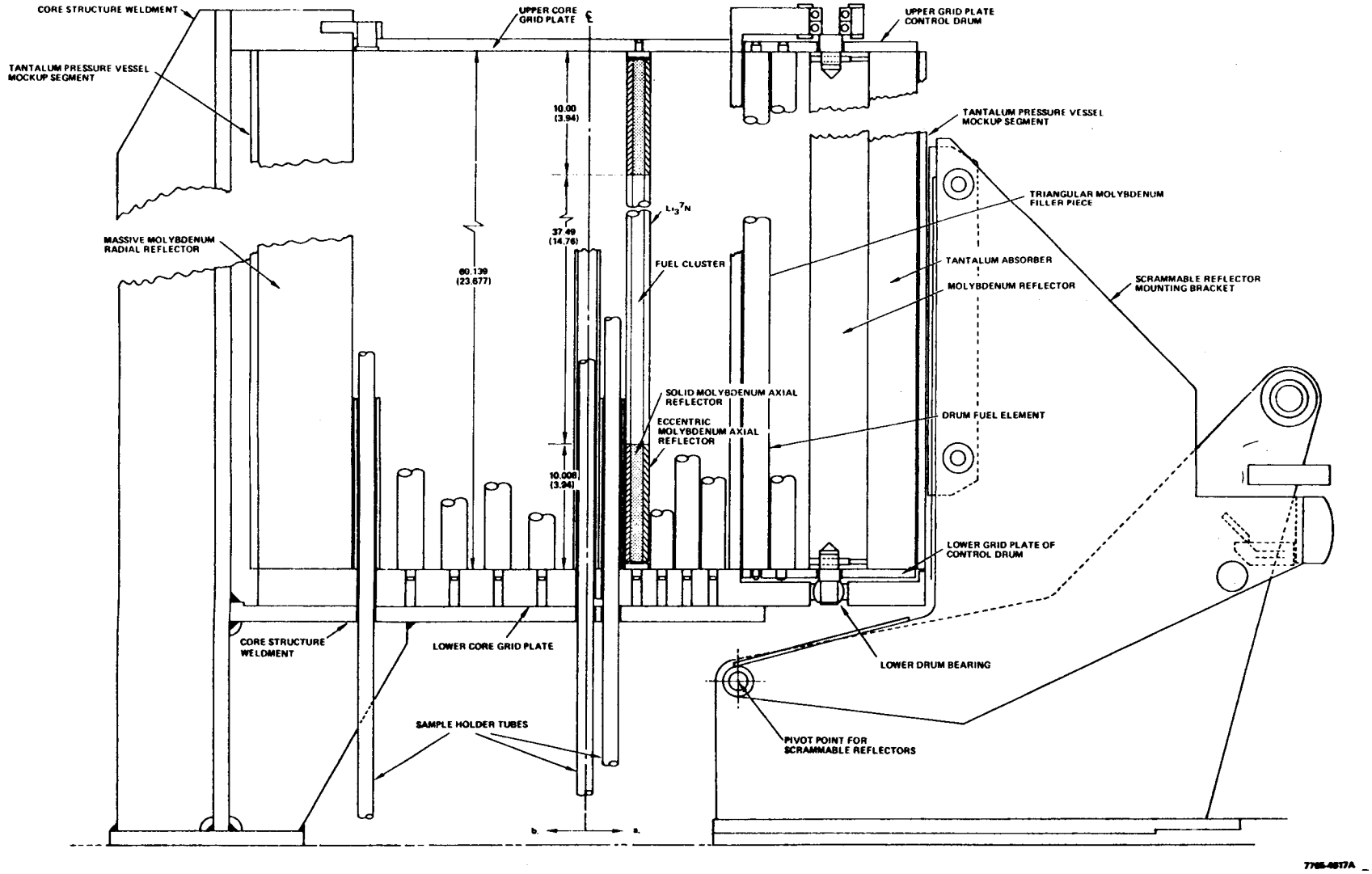

View b. Vertical Plane Passing Through the Axis of the Core and the Axis of the Fuel Element at a Point of the Star

View a. Vertical Plane Passing Through the Axis of the Core and the Axis of a Drum

Figure 3. Cross Sectional View of the Critical Assembly in the Vertical Direction

standard elements marked in the figure with the letter "S" can be removed and replaced by special fuel elements. In particular, the outer six peripheral positions are used for determining the worth of a group of large core-length samples. The central seven are used for a similar purpose as well as for inserting a spherical proton-recoil detector and selected foil materials for measuring the neutron spectrum. The central element position alone is used for small-sample reactivity measurements.

Six additional triangular-shaped Mo pieces, apart from the four noted above, are placed in the core to fill up the void space that exists between the hexagonal array of honeycomb tubes and the control drums.

In overall size, the critical assembly is 56.845 cm(22.38 in.) high, including upper and lower axial reflectors, and 57.15 cm(22.5 in.) in diameter including the massive radial reflectors. The core proper is 37.508 cm(14.767 in.) high and has a "diameter" of 38.33 cm(15.09 in.) as measured from the center line of one fuel element located at a point of the star to a diametrically opposite fuel element located at a point of the star. A cross sectional view of the core as produced by a vertical section formed by passing a plane through the axis of the core and the axis of a control drum is shown in the right-hand half of the center line of the drawing of Figure 3. The left half of the figure is the view that would be seen along a section formed by passing a plane through the axis of a fuel element at the point of the star. To provide an indication of the relative positions of the fuel element components to the other core components, an outline of one fuel element is depicted in the figure.

2. Control Drums

The axis of each of the six control drums is parallel to the axis of the core and located on a 20.917-cm(8.235 in.) radius. Each drum controls about $2 in reactivity but is not used for rapid shutdown since its speed of rotation, both for the case in which fuel is going into the core and the case in which fuel is going out, is low (about 0.12 revolutions per minute). The detailed layout of the control drum is shown in cross sectional view at the drum midplane in Figure 4. The main structural member of the drum is the massive Mo reflector piece to which an upper and lower drum grid plate are attached. This Mo piece is 60.2 cm(23.7 in.) high (the effective height of the control drum). Each drum has a Ta absorber segment which is also 60.2 cm(23.7 in.) high.

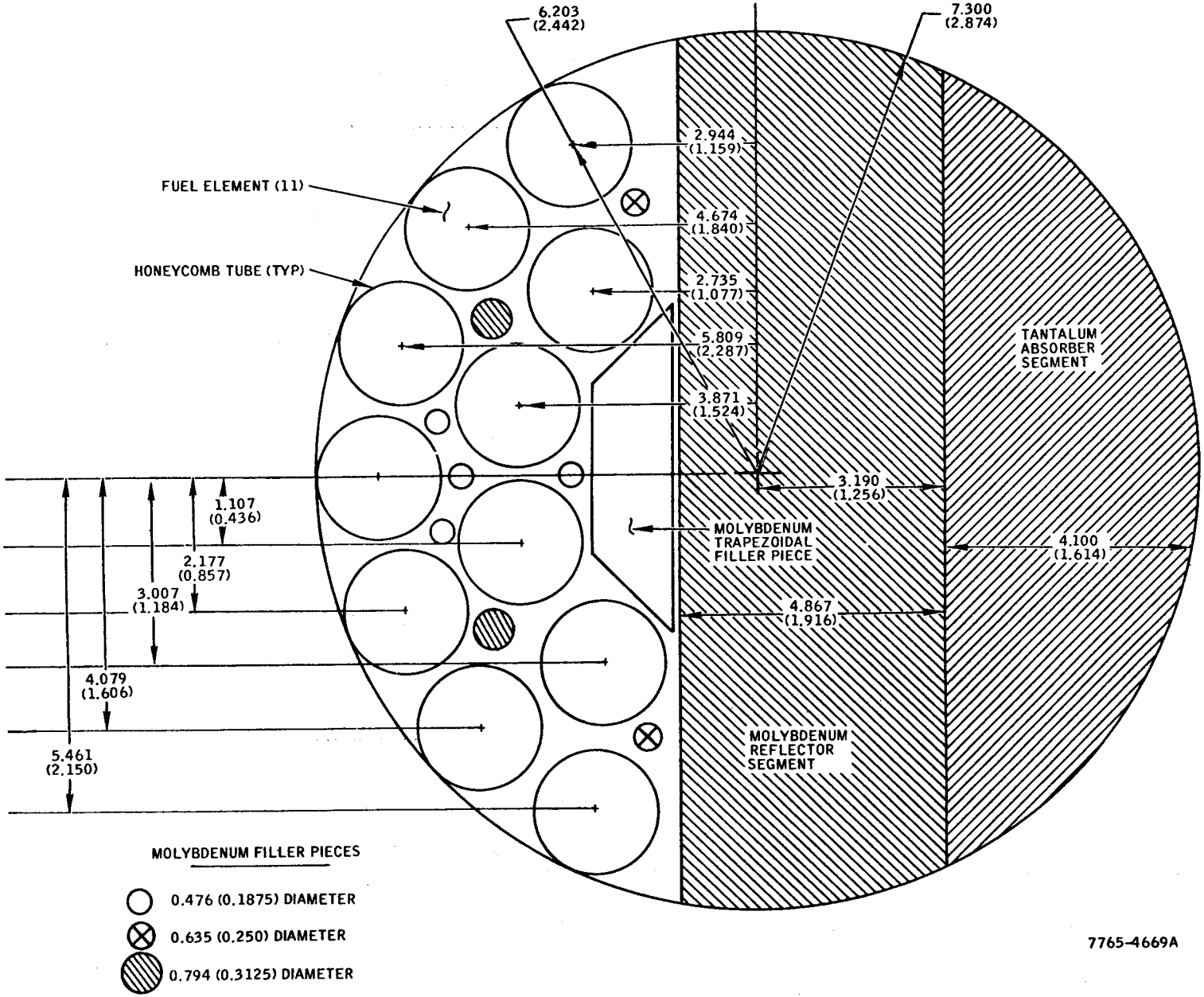

Figure 4. Cross Sectional View of the Control Drum at the Core Midplane

On the opposite side of the drum is a region which contains a group of honeycomb tubes identical to those in the stationary portion of the core. Since the void fraction in this region would be rather high with honeycomb tubes alone, several round Mo filler rods are inserted. All of these rods are 60.2 cm(23.7 in.) high, but vary in diameter, as indicated in the figure. In addition to the round rods, a large trapezoidal-shaped filler piece 60.2 cm(23.7 in.) high, is also utilized to fill the gap between the Mo reflector segment and the inner ring of honeycomb tubes.

3. Fuel Element

Within each Ta honeycomb tube is located eccentrically a Ta fuel tube which is used to contain the uranium fuel. This tube (see Figure 5) is 58.09 cm(22.87 in.) long, has an outside diameter of 1.575 cm(0.620 in.) and a wall thickness of 0.0254 cm(0.010 in.). Its center line is offset from the center line of the honeycomb tube by 0.0508 cm(0.020 in.). This eccentricity is established and maintained by an eccentric Mo reflector piece, 2.09 cm(0.823 in.) in outside diameter, 1.595 cm(0.628 in.) in inside diameter, and 10.00 cm(3.94 in.) long, one of which is located on each end of the element. In order to form a more or less continuous axial reflector, a solid Mo reflector is also placed at each end of the element and within the fuel tube. The latter reflectors are 1.493 cm(0.588 in.) in diameter and are also 10.00 cm(3.94 in.) long. Between the solid, axial, Mo reflector cylinders is located the uranium fuel, which consists of a cluster of uranium metal rods, each 0.432 cm(0.170 in.) in diameter, the number of rods in each cluster normally varying from six to seven depending upon the particular experiment. A typical 7-rod cluster is shown in Figure 6. Each rod of fuel in the fuel cluster is made up of two shorter rods, one 15.24 cm(6 in.) long and one 22.268 cm(8.767 in.) long, placed end to end to make a total length of 37. 37.508 cm(14.767 in.), the height of the active core. In order to make the fuel cluster more stable dimensionally the 15.24-cm and 22.268-cm lengths are stacked alternately so that there are actually two parting planes. In addition, a Ta centering ring, whose inside diameter corresponds to the circle circumscribing the fuel cluster, 1.295 cm(0.510 in.), is placed at the top and bottom of the cluster. To provide further rigidity to the fuel bundle, a two-turn or three-turn wire wrap of Mo is utilized, in some cases, at various positions along the height of the cluster.

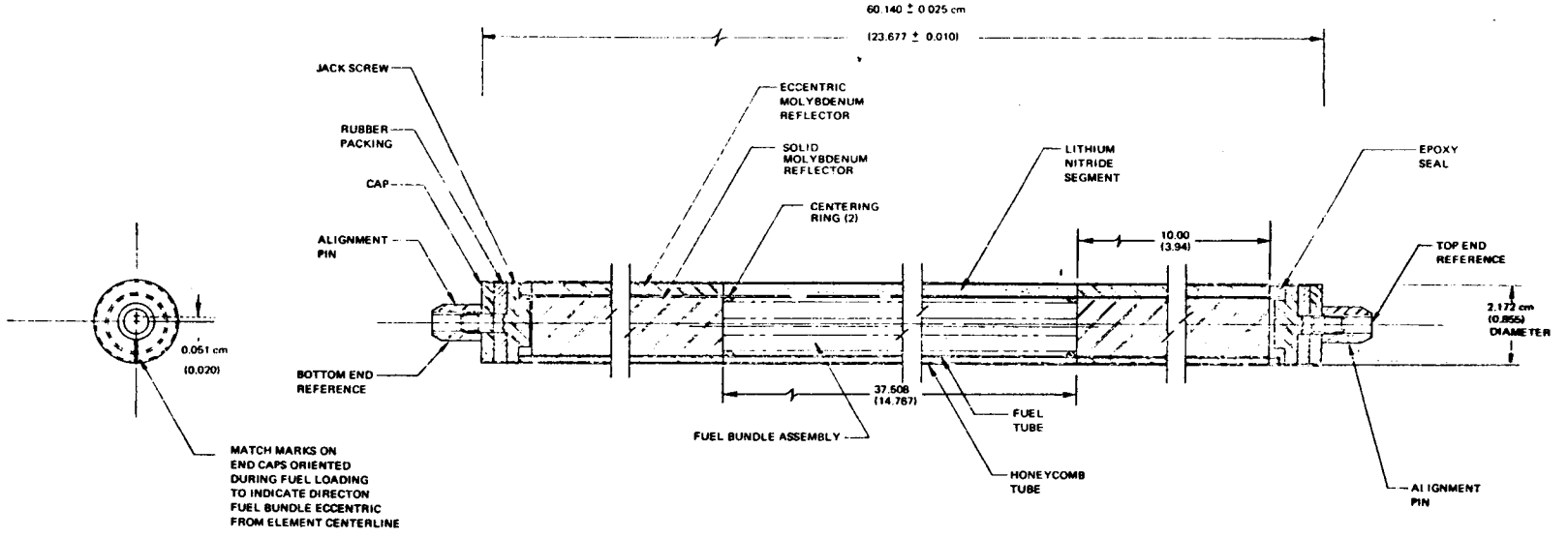

Figure 5. Critical Assembly Fuel Element

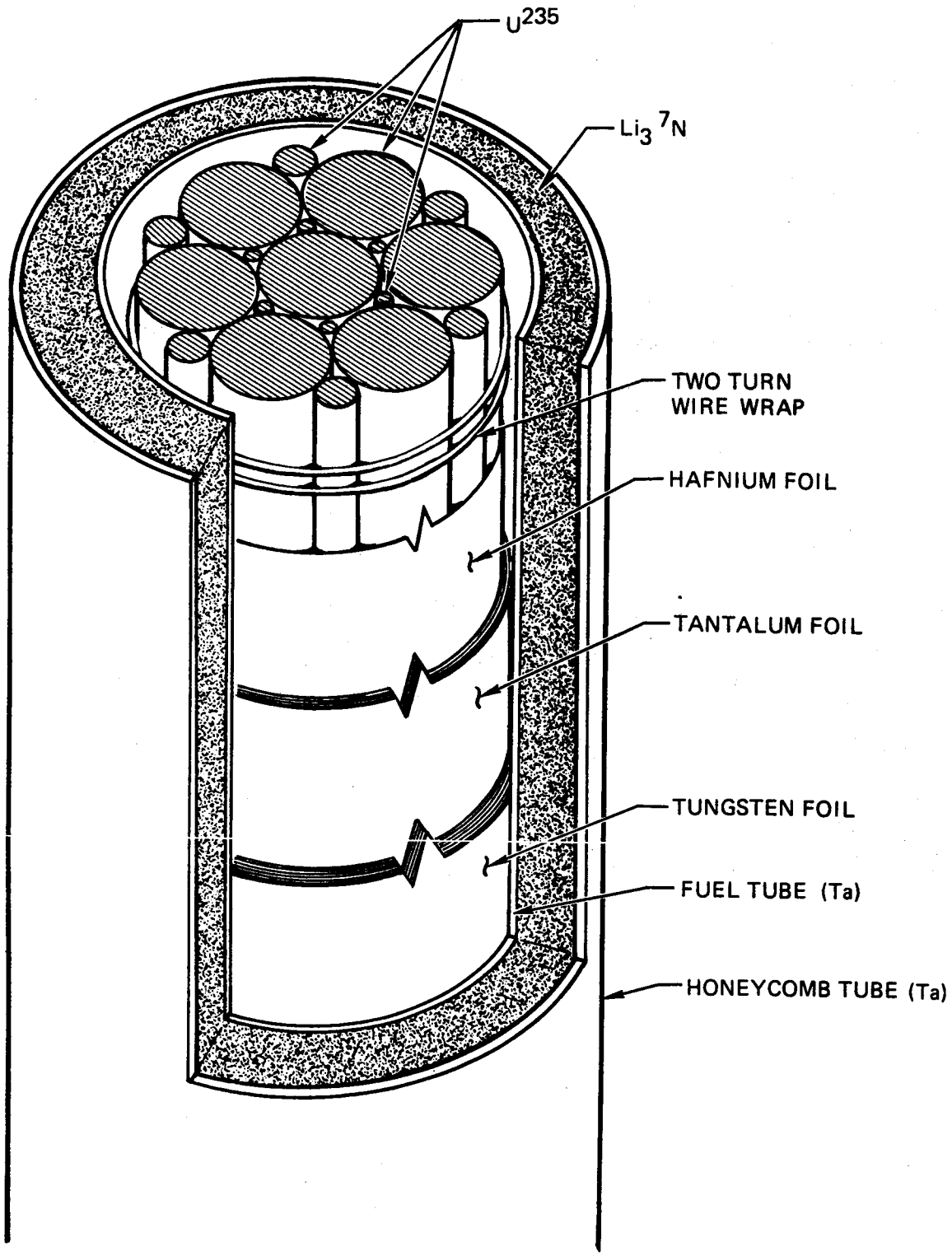

Figure 6. Cutaway View of the Central Region of the Fuel Element

Since, in some core configurations, more fuel than is contained in a 7-rod cluster of rods is required for criticality, some additional types of uranium were needed. Also, inasmuch as very fine and uniform fuel adjustments were needed for certain experiments, a smaller subdivision than that consisting of single rods was needed. These two requirements were met by swaging some of the uranium metal rods into wire, one of which was 0.152 cm(0.060 in.) in diameter by 37.465 cm(14.75 in.) long and the other 0.066 cm(0.026 in.) in diameter by 37.465 cm(14.75 in.) long. The 0.152-cm(0.060 in.)-diameter wire was designed for insertion into the cusp spaces around the outer periphery of the fuel cluster, whereas the 0.066-cm(0.026 in.)-diameter wire was inserted into the triflute spaces on the inside of the cluster as shown in Figure 6. Since 15.24-cm(6 in.) and 22.225-cm(8.767 in.) lengths of fuel rods are never used separately in a standard fuel cluster (i.e., they are always placed end-to-end), the term rod is used in this report to designate a column 0.432 cm(0.170 in.) in diameter by 37.508 cm(14.767 in.) long.

The uranium fuel rods and wire were enriched to 93.145% in the U-235 isotope and, as has already been noted, were of a metallic form.* Since the reference core is designed to use UN fuel, a suitable method for incorporating, the element nitrogen was required. This requirement was satisfied by the use of $Li_3{}^7N$, a ceramic-like material that would also satisfy the need for a simulation of the lithium-7 coolant proposed for the reference reactor. This $Li_3{}^7N$ material was fabricated into a free-standing body with a clam-shell form and was inserted in the annular space between the fuel tube and the honeycomb tube. Since this space does not have a uniform gap width because of the eccentricity in the location of the Ta tubes, the $Li_3{}^7N$ had a corresponding non-uniform wall thickness. It had, nominally, an inside diameter of 1.600 cm(0.630 in.) and outside diameter of 2.078 cm(0.818 in.) and a length of 37.34 cm(14.70 in.). It is thus confined only to the core proper.

Whereas the fuel and honeycomb tubes are pure Ta in the critical assembly, the reference reactor calls for T-111 tubing for these components. Also, the

*In order to reduce contamination that would result from frequent handling of bare uranium metal, all fuel was coated with a thin layer of nonhydrogenous plastic paint.

specifications for the reference reactor call for a very heavy-walled fuel tube with a W liner. T-111 is an alloy of Ta containing 8.5 wt % W and 2.3 wt % Hf. In order to provide these two additional materials (W and Hf), as well as additional Ta, metallic foils of these elements were coiled and inserted into the fuel tube around the fuel cluster in the manner depicted in Figure 6. The Hf segment was formed by coiling a 36.83-cm(14.5 in.)-high by 4.77-cm(1.88 in.)-wide by 0.0076-cm(0.003 in.)-thick foil into a single 36.83-cm(14.5 in.)-high tube. The W segment was formed by coiling a 36.68-cm(14.4-in.)-high by 15.24-cm(6.0 in.)-wide by 0.0051-cm(0.002 in.)-thick foil into a tube 36.83 cm(14.5 in.) high containing about 4 turns, and the Ta segment was formed by coiling a 36.83-cm(14.5 in.) high by 11.00-cm(4.33 in.)-wide by 0.0127-cm(0.005 in.)-thick foil into a tube 36.83 cm(14.5 in.) high containing about 3 turns. Thus, the refractory metal foils were also confined only to the core proper.

Even with the additional Ta foil in the critical assembly, the total mass of this material was still less than that contemplated for the reference reactor; consequently, another method for further increasing the total Ta loading was devised for specific experiments. This method consisted of inserting a 0.279-cm(0.110 in.)-diameter by 37.39-cm(14.7 in.)-long Ta wire into the center of the fuel cluster when it consisted of less than 7 rods. Also, a 0.356-cm(0.140 in.)-diameter by 59.69-cm(23.5 in.)-long Ta wire was inserted into the triflute spaces between honeycomb tubes in the stationary part of the core. A total of 300 such spaces, which are totally surrounded by honeycomb tubes, was available for this purpose.

Since $Li_3{}^7N$ reacts with moisture in the air to form ammonia, among other products, the annular region between the honeycomb tube and the fuel tubes had to be hermetically sealed. An epoxy cement was used for this purpose and was confined to the annular gap in the region outside of the reflectors, as can be seen in Figure 5. Thus the internal volume of the fuel tube remained accessible for purposes of fuel and material adjustments once the seal was made on the $Li_3{}^7N$.

To maintain the fuel cluster and other components in the proper position in the fuel tube, an aluminum end-plug was inserted into each end of the honeycomb tube. This plug also served to align the fuel elements (the term used here to

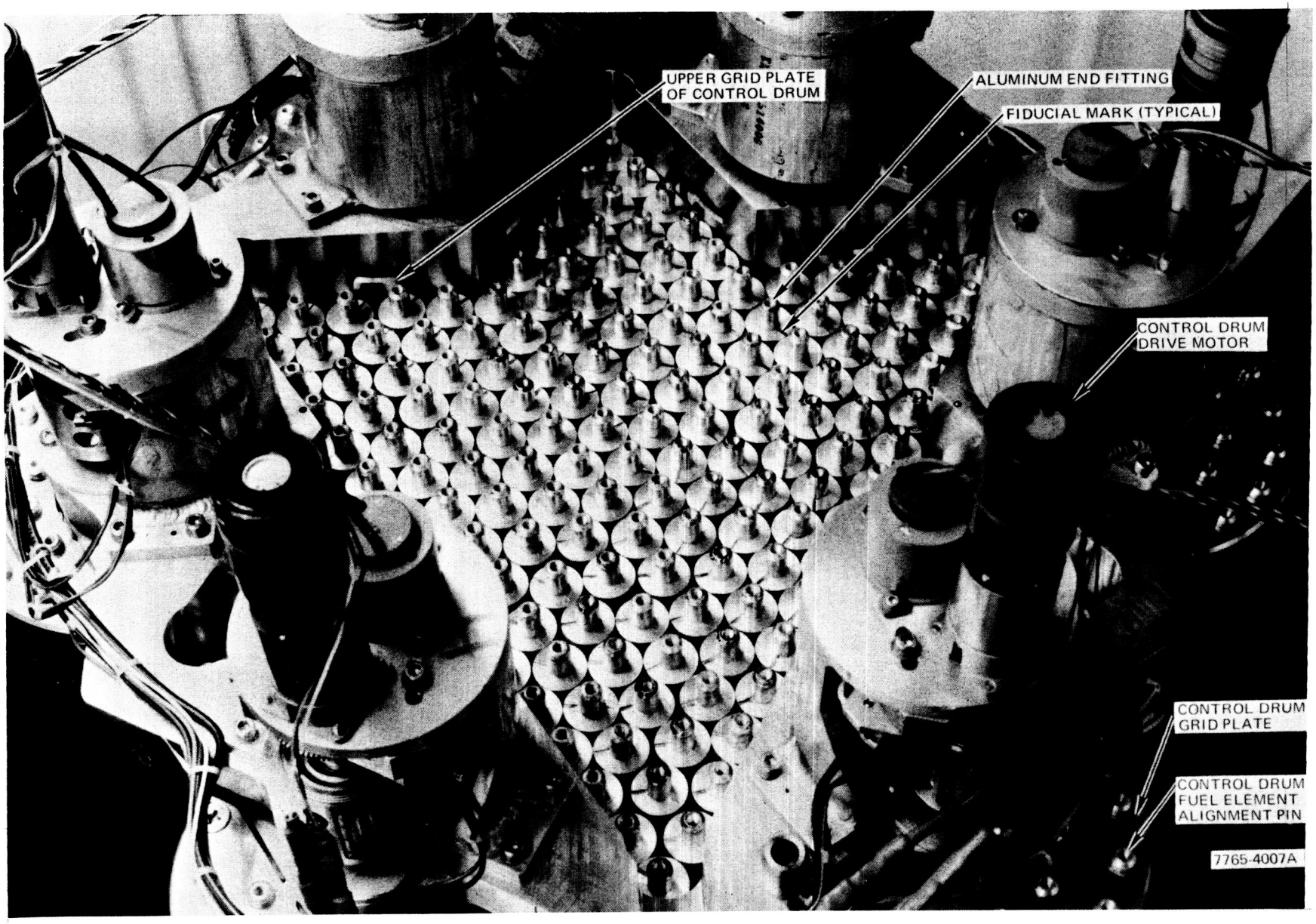

Figure 7. Top View of the Critical Assembly Without the Upper Grid Plate in Place

designate the combined fuel and honeycomb tubes) in an upper and lower grid plate. By tightening the alignment pin (see Figure 5), the rubber packing expanded out and made a reliable mechanical seal on the honeycomb tube.

A total of 181 of these fuel elements made up the stationary core and an additional 66 identical elements, 11 in each of 6 drums, were used in the movable drums to bring the total to 247 fuel elements.

The orientation of the fuel and honeycomb tubes in an eccentric fashion in the fuel element is intended to permit measurements of the reactivity effects of fuel displacement. In order to determine, relative to the axis of the core, the position of the fuel cluster in each element, a fiducial mark that was visible from the top of the core (see Figure 7) was made on the aluminum end-fittings. For all experiments, except those pertaining to fuel displacement, the fuel cluster in each element was located in a "null" position; that is, with the fiducial line perpendicular to the core radius. The fiducial mark indicated the position of the narrowest portion of the eccentric gap between the fuel and honeycomb tubes. In Figure 7, a complete fuel element loading is shown with the element orientation somewhat random. In order to line up all fuel elements, a clear plastic grid plate was placed over the elements and each was turned so that the fiducial mark coincided with a null-position mark in the plastic grid plate. To determine reactivity effects resulting from fuel motion, each fuel element was turned first to place the fuel cluster nearest the core axis and then farthest from the core axis.

B. SPECIAL FEATURES

In order to conduct some particular experiments associated with this program, some special mechanical features were built into the critical assembly. Primary among these features was a sample changer mechanism and its associated sample holder tubes which permit the insertion of samples into the core. A total of 13 such holder tubes were provided for, 6 in the outer periphery and 7 in the center. Special fuel elements that would accommodate these holder tubes were therefore required. Three of these, one at the point of the star, one at the center of the core, and one adjacent to the center, are depicted in Figure 3.

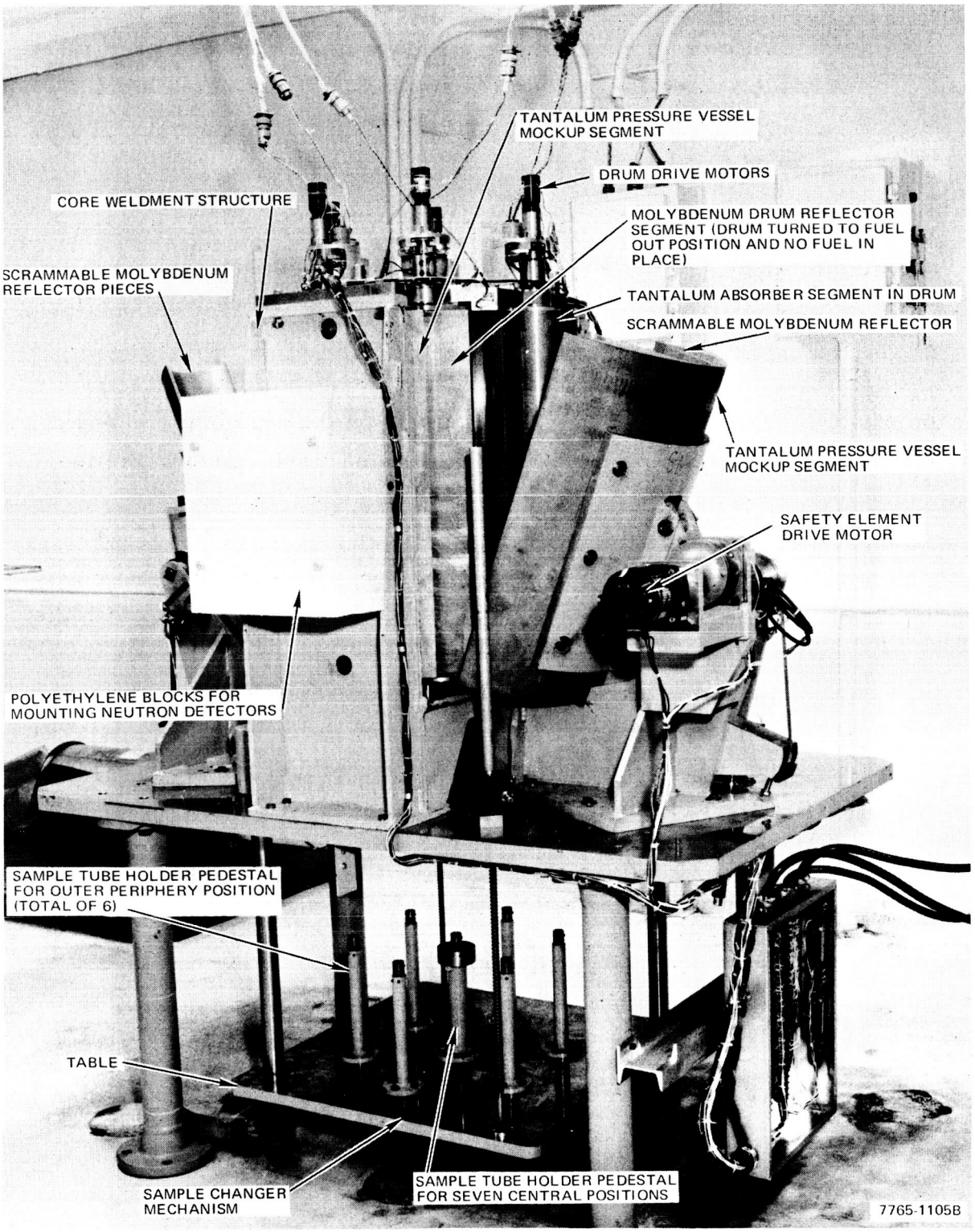

Figure 8. Photograph of Critical Assembly

As has already been indicated, during most experiments these special elements were not used and adaptor plugs that permit the use of standard fuel elements were placed in the upper and lower grid plates at the outer six peripheral positions and at the central seven positions. These special elements were identical to standard fuel elements except that no materials were placed inside the fuel tube, thus leaving a tubular passage for the sample holder tube. A $Li_3{}^7N$ segment and two eccentric Mo reflector pieces were retained in their usual positions and special aluminum end-fittings with a hole through the center were used to mount the elements (see Figure 65 in Appendix C). As can be seen in Figure 8, six sample-tube mounting pedestals are located on the changer mechanism to allow insertion of six peripheral samples simultaneously, and one pedestal is used to mount all seven central sample tubes. Samples are inserted or withdrawn from the core by a drive motor that raises and lowers the sample changer table.

Figure 9 is a photograph of the critical assembly and shows additional details about the core as well as the sample-holder tube arrangement. The upper grid plate is shown in place and the six peripheral sample-holder tubes are seen projecting through the core. A special bracket in the center of the grid plate held adaptor plugs (not in place in the photograph) in each of the seven central positions in order to locate each standard fuel element within its own grid position. When the adaptor plugs (see Figure 10) were not in place, the sample-holder tube passed through the large diameter hole. In Figure 9, the end-plugs on the standard fuel elements are seen in place below the bracket.

By removing the special bracket, the central seven fuel elements could be removed for the purpose of placing detectors and other materials in the center of the core. Figure 10 shows a spherical proton-recoil detector mounted at the center of the core. This type of detector was used to measure the differential neutron spectrum in the critical assembly. The diameter of the detector, over its spherical portion, was a maximum of 4.32 cm(1.70 in.); consequently, it could be located within the radial confines of the seven central elements.

Above and below the detector, and in place of the standard fuel elements, was placed a second type of special fuel element (a so-called "proton-recoil" element) which served to minimize the perturbation caused to the core by the

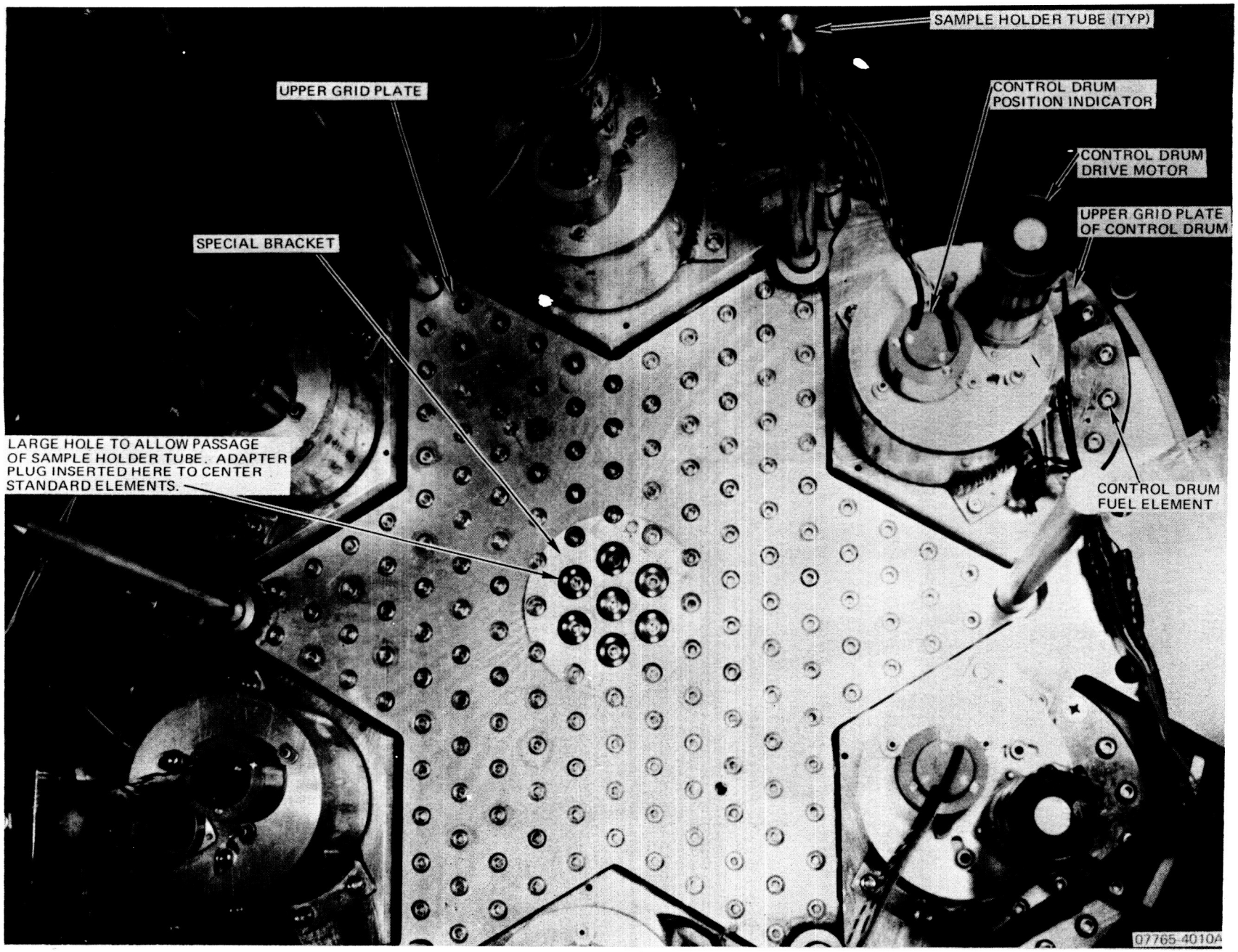

Figure 9. Top View of the Critical Assembly With the Upper Grid Plate in Place

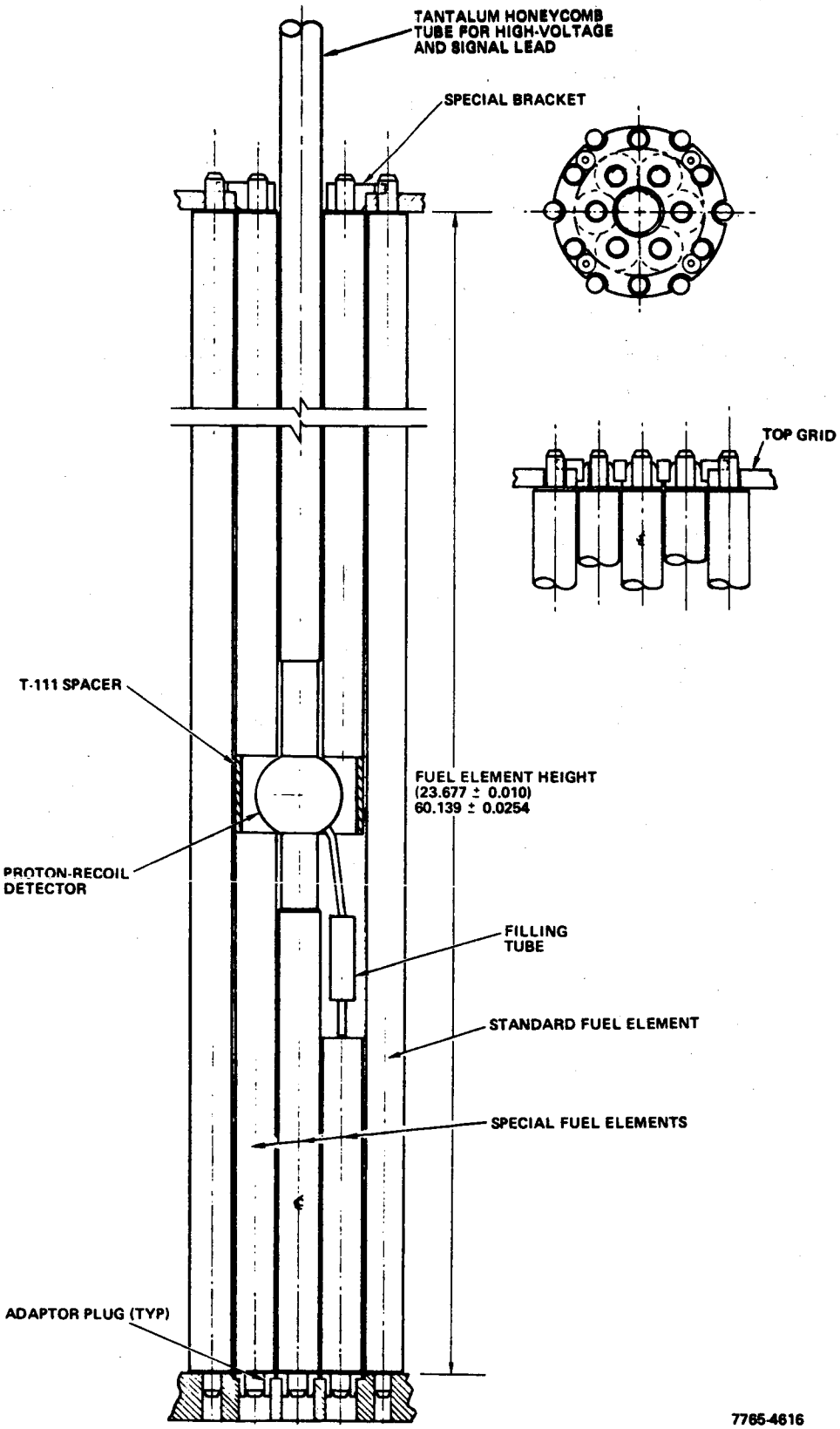

Figure 10. Proton-Recoil Detector Arrangement in Core-Center

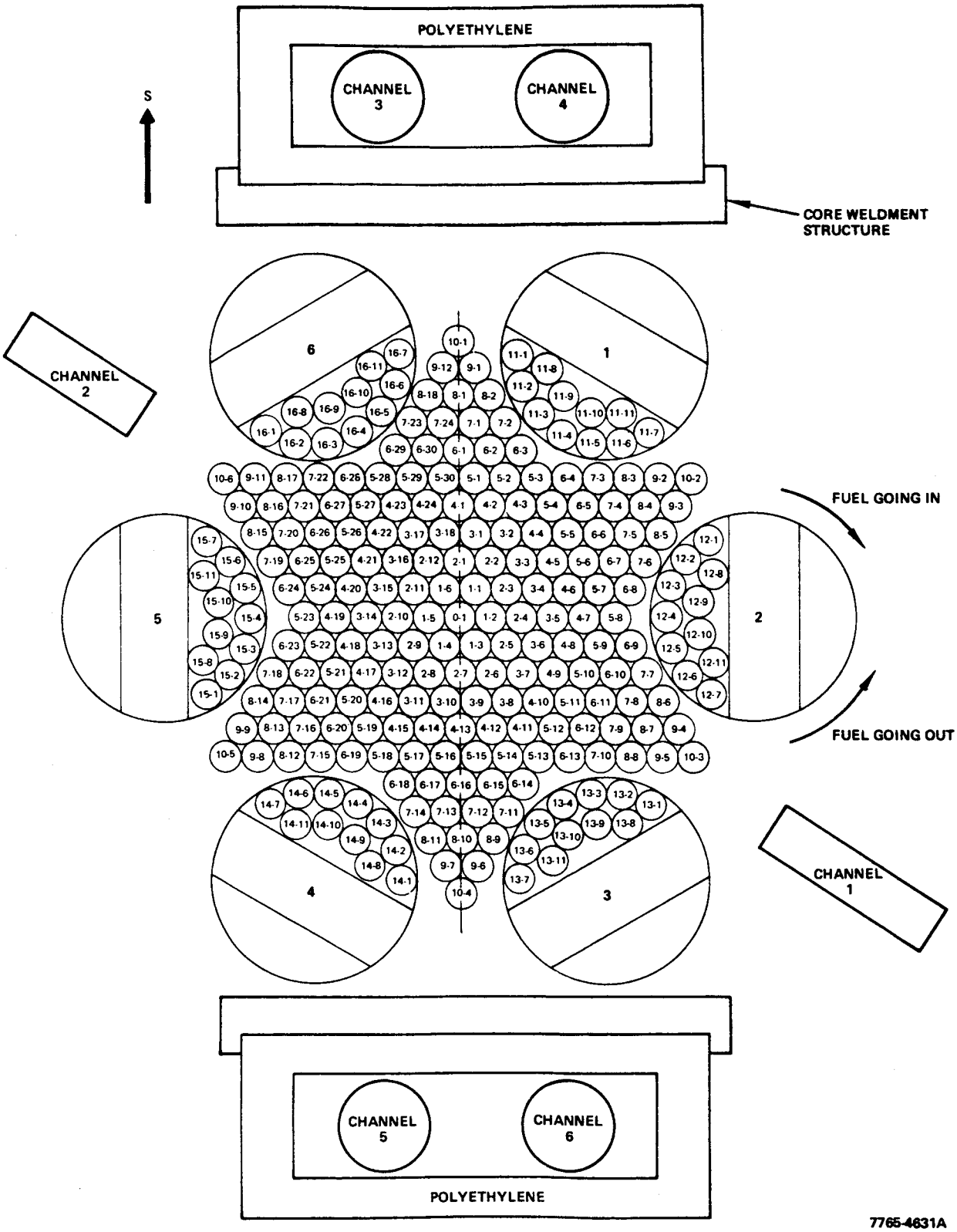

Figure 11. Neutron Detector Locations

insertion of the detector. These special fuel elements (see Figure 64 in Appendix C) were identical to standard elements except that they were of shorter lengths. One group had an overall length of 28.113 cm(11.068 in.) and was placed in the six peripheral positions immediately surrounding the detector in the top half of the core. These elements were prevented from falling into the core by the T-111 spacer sleeve. Since the filling tube on the detector projects significantly beyond the detector casing, only five of these elements could be located below the detector. A medium length, 23.985-cm(9.443 in.), special element was placed in the center fuel element position below the detector and a still shorter length, 18.588-cm(7.318 in.), element was placed below the filling tube. In the central fuel element position above the detector, a special section of Ta honeycomb tube, which carried the high voltage signal lead, was placed and was connected directly to the detector.

All of these special fuel elements contained all of the nonfuel materials (cut to shorter lengths) normally placed in standard elements. Fuel, however, was placed only in the long proton-recoil elements. To prevent these materials from falling out of the end opposite the aluminum end-plug, a Ta cap was welded into place by means of electron-beam techniques. This plug also maintained the previously defined eccentricity.

For purposes of foil irradiations all fuel element positions except the center one were filled by standard elements. In the center position were placed two of the 28.113-cm(11.068 in.)-long elements normally used with the proton-recoil detector. A 3.81-cm(1-1/2-in.)-high cavity was thus created at the core center.

C. INSTRUMENTATION

Insofar as nuclear instrumentation is concerned, a total of six detectors was normally employed for both operational and experimental information. These detectors are shown schematically in Figure 11. Two detectors (Channels 3 and 4) were located on one side of the reactor and two detectors (Channels 5 and 6) were located on the other. All four were B-10 lined, current-type chambers and, in order to increase their sensitivity, were placed in massive polyethylene "boxes," one of which can be seen in Figure 8. A single polyethylene box held two detectors side by side. An identical box mounted in an identical

way on the opposite side of the core weldment structure held the other two. The axes of the sensitive volumes of the detectors were parallel to and about 40.6 cm(16 in.) from the axis of the core. The midplane of the detector was located at approximately the midplane of the core. Two additional fission-type chambers (Channels 1 and 2) were located 45.72 cm(18 in.) below the core midplane and slightly to the side of the core. These chambers were also surrounded by polyethylene boxes. The axes of the chambers were perpendicular to the core axis and lay along a diametral line. In one, the center of the active volume was about 35.6 cm(14 in.) from the axis of the core and, in the other, it was diametrically opposite by an equal distance. Scaler readouts were used for Channels 1 and 2 and meter readouts for Channels 3, 4, and 5. Channel 6 was the primary channel for experimental information and its output was fed to a micro-microammeter whose output, in turn, was fed to a voltage-to-frequency (analog to digital) converter. This digitized output was then monitored by either a scaler with preset counting intervals or by a multichannel analyzer operated in the time mode. Channel 6 was initially an uncompensated chamber but was later replaced by a similar, but compensated chamber.

III. EXPERIMENTAL TECHNIQUES

A. REACTIVITY

1. Inverse-Kinetics Technique

The fundamental method for measuring reactivity in this experimental program is the inverse kinetics or reactivity vs time. The method has been employed for several years at Atomics International primarily in the work being conducted at the Epithermal Critical Experiments Laboratory (ECEL) split table critical assembly where the technique, which had been previously used irregularly by other laboratories, was coded and put to routine use. The basic principles are described in Reference 5. Since the initiation of its routine use at the ECEL in 1960, it has been further improved, particularly in the area of the inclusion of the effects of a constant neutron source.[6] It is now utilized in a routine manner at several other laboratories, including Argonne National Laboratory and at Karlsruhe, Germany.

The name "inverse kinetics" is based on the fact that, whereas normally one assumes that a known reactivity change is made and subsequently calculates the change in the neutron population with time, in this technique the change in the neutron population is measured directly by the neutron detector and from this information the reactivity is derived. The fundamental equation is

$$\frac{1}{\beta_e}\frac{\Delta k_e}{k_e} + \frac{\ell}{\beta_e k_e}\frac{S_e}{n} = 1 + \frac{1}{n\,k_e}\left[\frac{\ell}{\beta_e}\frac{dn}{dt} - \sum_i \frac{\beta_e^i}{\beta_e} e^{-\lambda_i t}\left(n_0 + \lambda_i \int_o^t k_e n e^{\lambda_i t}\, dt\right)\right]$$

where

k_e = the effective multiplication constant for all neutrons

$\Delta k_e = k_e - 1$

ℓ = neutron lifetime (sec)

β_e^i = effective delayed neutron fraction for the $i^{\underline{th}}$ group

β_e = effective delayed neutron fraction, $\sum \beta_e^i$

n = number of neutrons in the reactor

n_0 = number of neutrons in the reactor at equilibrium

t = time (sec)

λ_i = decay constant for i^{th} precursor group $(sec)^{-1}$

S_e = effective source strength (n/sec).

If the output of one of the neutron detectors in the assembly is fed to a multichannel analyzer operating in the time mode, the change in the neutron population as a function of time is directly measured. From this power trace, the derivative, dn/dt, can also readily be extracted. Since the constant source term is, in most cases, virtually negligible, and ℓ and β_e can be calculated with a reasonable degree of accuracy, the reactivity as a function of time can be derived. Indeed, it can be shown that the reactivity is very insensitive to values of ℓ and β_e; consequently, large errors in the calculated values of these quantities result in negligible errors in the results. Thus, only the term in the summation contributes substantially to the measured reactivity worth. Since β_e occurs within the summation sign as a ratio with $\beta_e{}^i$, the actual parameter of interest there is the fractional yield of delayed neutrons in group i, a_i, which is equal to $\beta_r{}^i/\beta_e$, assuming that all of the delayed neutrons have the same relative effectiveness.

The experimental arrangement was as follows: the output of Channel 6 was used as input to a micromicroammeter whose voltage output was, in turn, fed to a voltage-to-frequency converter. The voltage output of the micromicroammeter was directly proportional to the input current. The output of the converter, which produces 100 kHz/v input, is therefore directly proportional to the power, or neutron population, in the reactor. The converter's pulse train was then fed to a multichannel analyzer operated in the time mode; that is, the analyzer counted pulses for a preselected time interval, stores these in a channel, and then moves to the next channel. The time width of each channel could be varied over a wide range, but for most of the experiments conducted here it was 0.8 sec. Thus the analyzer stored in each channel successively the number of pulses that occur in that time interval.

The experimental procedure consisted of maintaining the reactor at level power for some period of time in order that the delayed neutron precursors can have achieved equilibrium. This period of time (typically 1 minute) established n_0, whereupon some process such as driving a control rod or inserting a sample

was initiated, and resulted in a change in reactivity. The ensuing power trace, as obtained from the analyzer, was then used in a code which calculated the reactivity at each point in time corresponding to the channel width. One therefore obtained the reactivity vs time.

A typical example of this technique, involving two separate and sequential reactivity changes, is shown in Figure 12. In Figure 12-a, the reactor power is plotted as a function of time as it would appear on the multichannel analyzer scope. In Figure 12-b, the power trace has been analyzed by the inverse kinetics code to produce reactivity vs time. As would be expected, the reactivity was zero over the first 60-sec time interval at the end of which a control drum was driven in. The drum reached its full-in position at about t = 90 sec, where it remained stationary as did the reactivity. At t = 155 sec, six Be samples that were located in the outer six peripheral positions were started out of the core and were full-out by t = 250 sec. Since no further changes were made, the reactivity should again have been a constant. This situation was found to be the case.

Numerous checks on the validity of the inverse kinetics method were carried out in its early stages of use at the ECEL. One of these methods involved scramming sequentially all eight safety rods in the ECEL critical assembly and determining the reactivity vs time. A well-behaved stair-step function was observed and the total worth ($\sim$\$7) of all eight rods as determined in one measurement agreed within 5% with the sum of the worths of each rod measured individually.[5,7] Moreover, the worth of a specific safety rod in the single sequential-type of measurement was the same whether it was scrammed first or last in the sequence. Analysis of the worth of a safety rod by the rod-drop method also produced a result in agreement with inverse kinetics, as did a series of positive period measurements.[6]

Two of these checks were also carried out in this critical assembly. In the first one, one of the safety elements was scrammed and the reactivity vs time was determined. The results of this experiment are shown in Figure 13. The reactor power was held constant at about 40 watts until t = 2.64 sec (see insert in Figure 13-a), whereupon the two Mo reflector pieces on one safety element were allowed to fall away. The measured worth by the inverse kinetics method is seen to be \$6.25 (see insert in Figure 13-b). By extrapolating to t = 2.64 sec, the power curve which is observed after the scram, and by using the equation

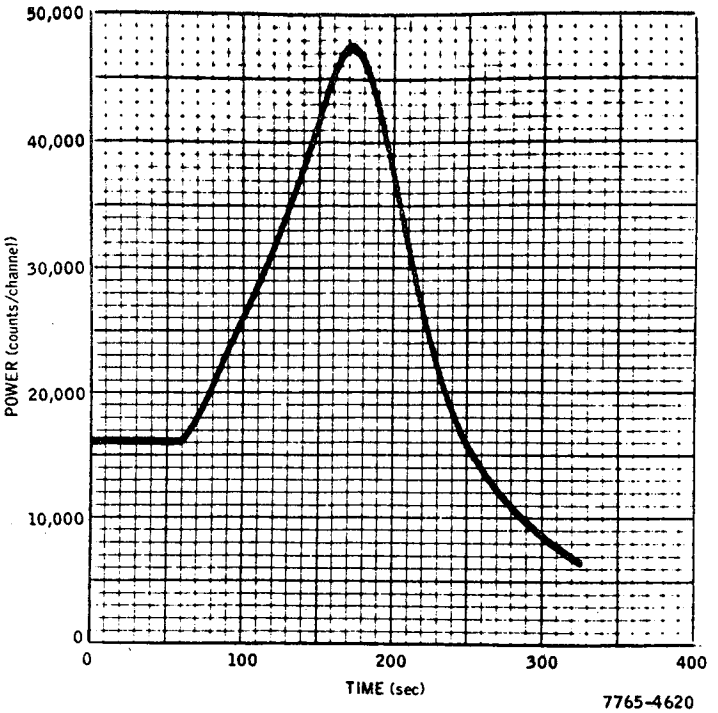

a. Reactor Power vs Time

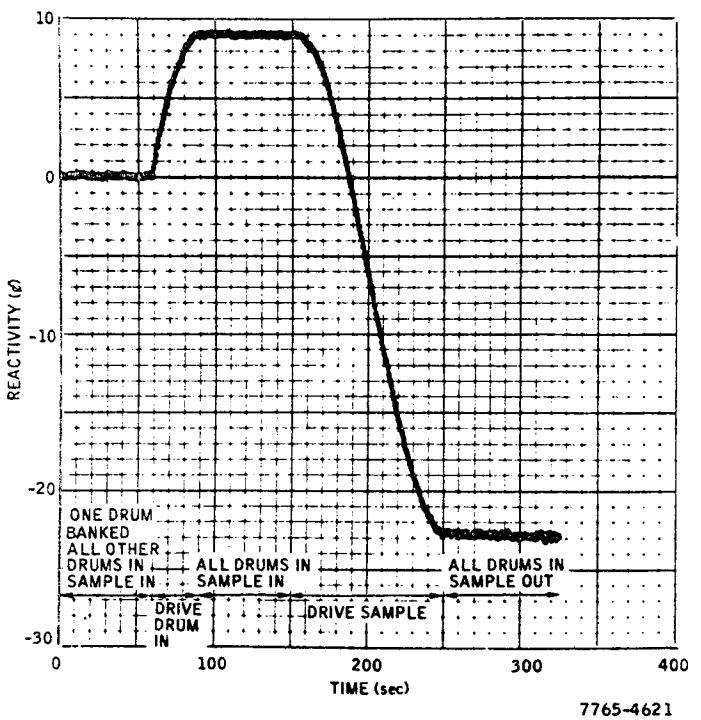

b. Reactivity vs Time

Figure 12. Data Obtained for a Two-Step Reactivity Change

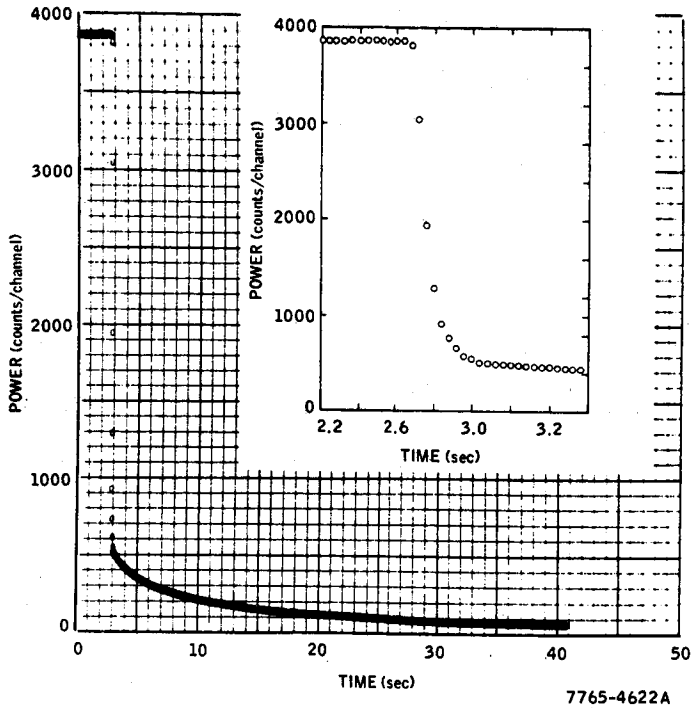

a. Reactor Power vs Time

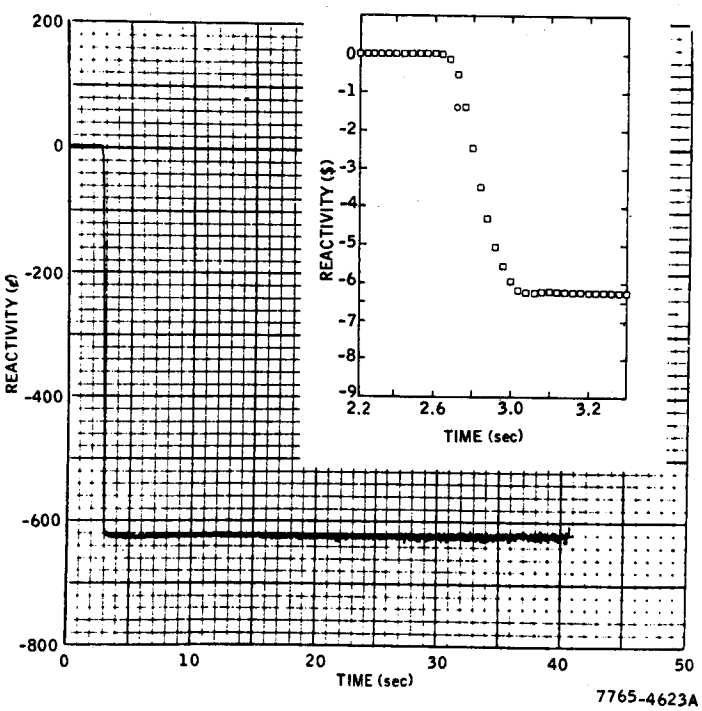

b. Reactivity vs Time

Figure 13. Data Obtained During Scram of a Massive Mo Reflector

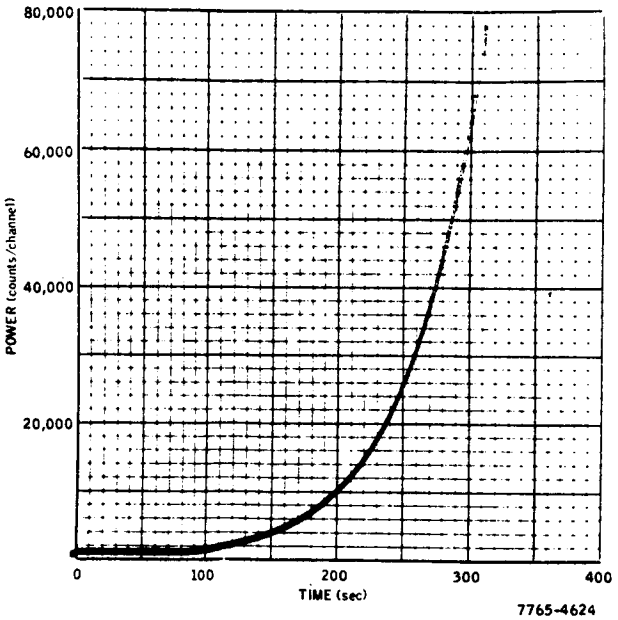

a. Linear Power vs Time

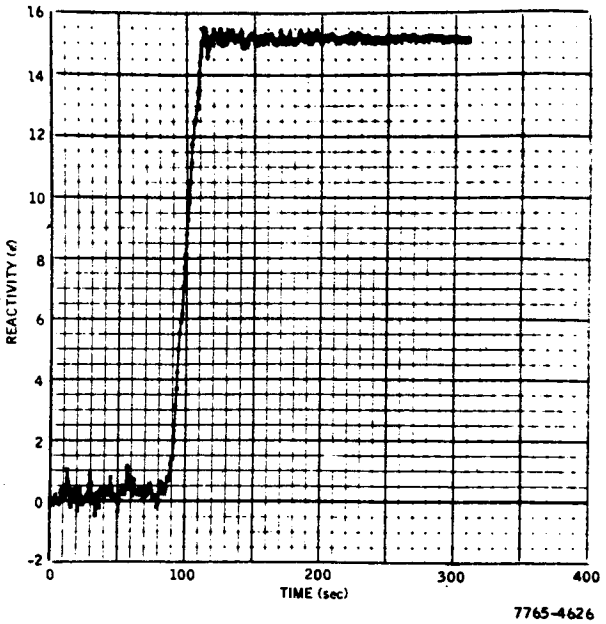

b. Reactivity vs Time

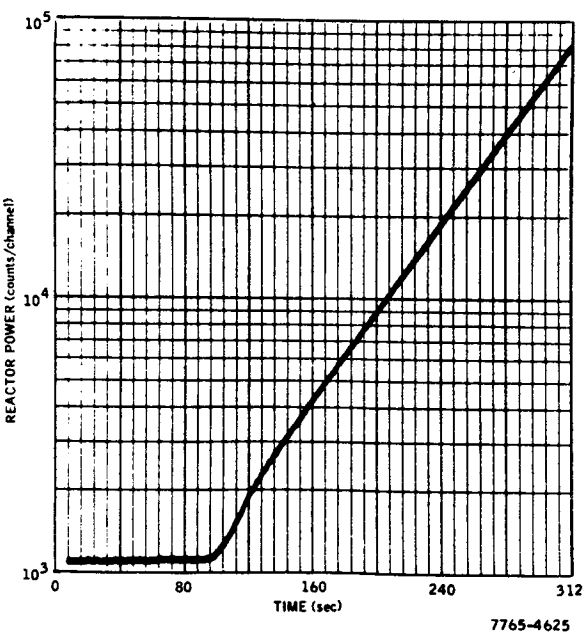

c. Log Power vs Time

Figure 14. Data Obtained for a Positive Reactivity Insertion

$$\frac{\Delta k}{k} = \beta_e\left(\frac{P_0}{P} - 1\right) \quad ,$$

one obtains

$$\frac{\Delta k}{k} = \$5.95 \quad ,$$

which is a minimum value for the worth of the safety element. In this case, P_0 is the power (in counts/channel, a quantity which is directly proportional to power in watts) before the negative step and P the power obtained at t = 2.64 sec by extrapolation of the power after the step (see Figure 13-a). The change in reactivity can be bounded on the higher side by taking P equal to the value soon after the step change, at t = 3.00 sec, for example. In this case, $\Delta k/k$ = \$6.52. Thus the inverse kinetics results are in excellent agreement with a simplified analysis by the rod-drop method.

A second check on the method by means of a small positive reactor period was also conducted and is shown in Figure 14. The experiment consisted of maintaining a constant power at some low level where data collection was initiated in the manner normally employed in the reactivity-vs-time technique. After about 80 sec, a control drum was driven in to a position such that a reactor period of about 54 sec was achieved. The driving time for the drum was about 35 sec whereupon the drum was held stationary and the power was allowed to increase exponentially for about an additional 190 sec. The linear power level, in terms of courts/channel, is shown for this experiment as a function of time in Figure 14-a. Analysis of this power trace by the standard reactivity-vs-time code gave an excess reactivity of 15.152 ± 0.005¢ as can be seen in Figure 14-b. A plot of the power-vs-time on semilog scale (Figure 14-c) yielded a reactor period of 54.3 sec using data over a time interval corresponding to 140 to 305 sec. A simple "hand calculation" of the reactivity using the inhour equation and this measured period gave an excess reactivity of 15.14¢, thus showing that the calculational procedures used in the reactivity-vs-time code are correct. In order to reduce the uncertainty in the results of this analysis period a mathematical fit to the power data was subsequently carried out using a least-squares technique. The mathematically determined period was 54.16 ± 0.04 sec and yielded a reactivity of 15.16 ± 0.04¢ using the inhour equation.

Some limitations on the inverse-kinetics method should be noted. Under most circumstances the method, which has been shown to be accurate down to as low as \$10 or \$12, is based upon a rapid removal of reactivity such that the power level at the end of the reactivity withdrawal is relatively high. One of the difficulties that has been encountered in this critical assembly concerns the fact that, where control drums are involved, reactivity changes cannot be made very rapidly (0.720° of rotation/sec). For example, the power level typically decreases by a factor of the order of 5×10^4 by the time a drum is driven from full-in to full-out. If the micromicroammeter being used to measure the power remains on a fixed current scale, the signal soon becomes smaller than, or of the same order of magnitude as, the zero setting on that current scale. The ensuing fluctuations in the output voltage are interpreted by the code as true power variations; consequently, the apparent reactivity undergoes wild oscillations and the data are useless. One must, under these circumstances, confine the use of the inverse-kinetics method, speaking roughly, to large reactivity changes ($\sim$\$10 or \$12) if they occur rapidly ($\sim$10 sec) or to small changes ($\sim$\$2) if they take place slowly ($\sim$200 sec).

One method for mollifying this limitation to some extent concerns the use of range-changing on the micromicroammeter. As the power level decreases into the low end of the scale, the range, or current scale, can be changed by a factor of 10 to bring it into the high end of the lower scale. By properly manipulating the data which are obtained during the range change (which can be performed over several decades), an analysis of the data can be carried out by a modified version of the inverse-kinetics code to yield results that are valid over a greater range of reactivity. For reasons that are not understood at this time, the inverse kinetic technique with range changing does not appear to yield valid results beyond \$4 or \$5 at the slow removal rate characteristic of these control drums. Thus range-changing only extends the range of validity a few dollars, at most.

It is apparent that a step-wise method of reactivity change is not a necessary requirement in the inverse-kinetics technique. The reactivity values derived while a drum or sample is in motion are just as valid as they are during a period of no reactivity changes (subject to the above noted limitations); consequently, a continuous reactivity change can be made and analyzed to derive a

"continuous" measure of the reactivity-vs-time within the limits imposed by the preselected channel width. In the measurement of the worth of a single control drum, the continuous-drive technique, with or without range changing, had the advantage of yielding results with a minimum of reactor operation. The reactor was brought to critical, allowed to stabilize, and then the drum was driven out. This technique was often employed to establish the worth of a single drum where detailed information on the shape of the worth-curve at or near the full-in position was useful.

A step-wise drum calibration was, however, most accurate at the full-out position. The step-wise technique involved only small reactivity changes; consequently, the validity of the results was less subject to question. In this technique, a drum, No. 6 for example, was placed with fuel in the full-in position and the diametrically opposite drum (No. 3 in this case) was banked out such that, with all other drums full-in, the reactor was delayed critical. After a period of time during which the reactor power was level, data collection was initiated. Drum No. 6 was then turned out a few degrees and maintained at that position for about one minute. Drum No. 3 was then turned in by an amount that not only offset the small negative reactivity produced by Drum No. 6, but also provided a small amount of excess. Again, all drums remained stationary for about one minute, whereupon Drum No. 6 was turned out a few degrees more. Drum No. 3 was then moved in and the process was repeated in this step-wise fashion, the worth of Drum No. 6 being measured as it was stepped out and the worth of Drum No. 3 as it was stepped in. The integral worths were established by algebraically summing the step-wise reactivity values. Figures 15-a and -b show the power and reactivity, respectively, as a function of time for a step-wise drum calibration. A comparison of a drum calibration by the continuous drive method, with and without range changing, and by the step-wise method is shown in Figure 16. Without range changing, the results become invalid when the drum reaches about 115 degrees of arc.

The inverse-kinetics method of measuring reactivity was applied during this experimental program to the measurement of large and small reactivity samples. This application was alluded to in the example discussed above. A set of seven identical samples of 16 different materials were procured for the purpose of determining their reactivity worths. Almost all sets consisted of

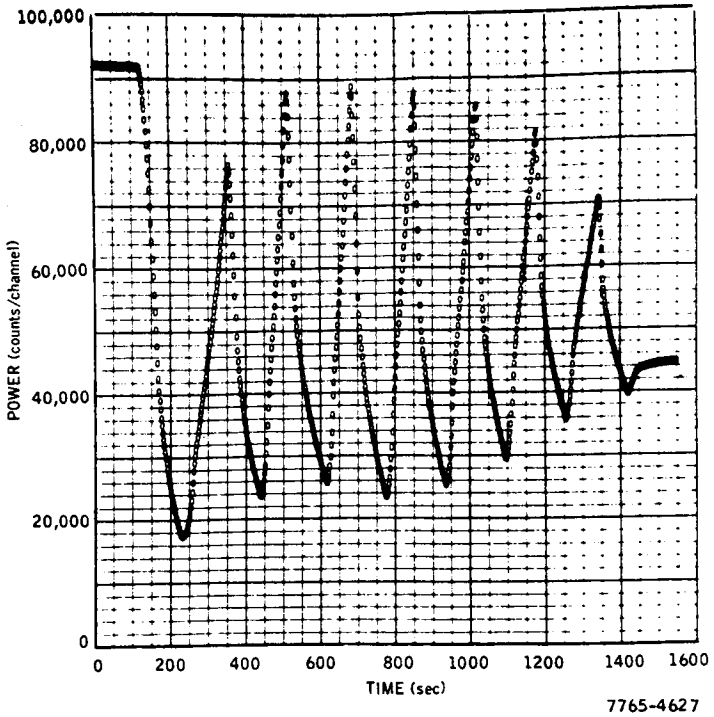

a. Power vs Time

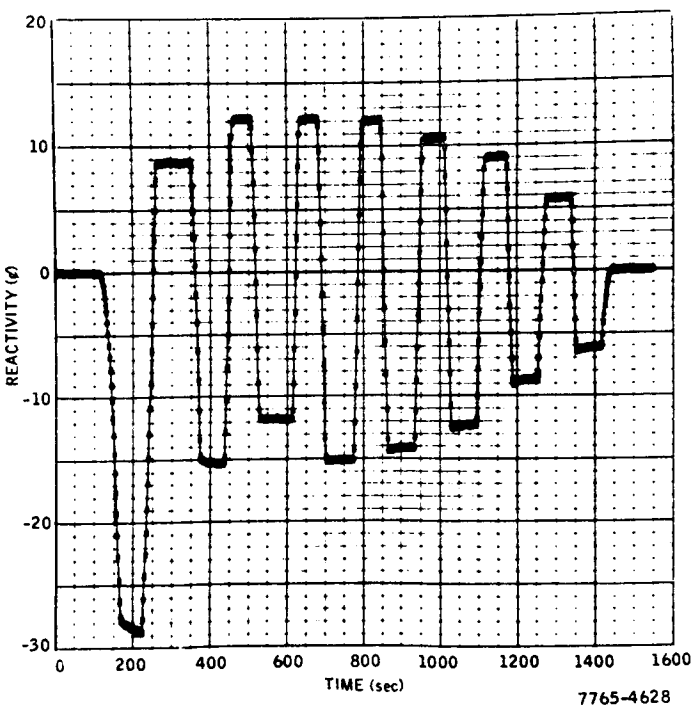

b. Reactivity vs Time

Figure 15. Data Obtained for a Stepwise Drum Calibration

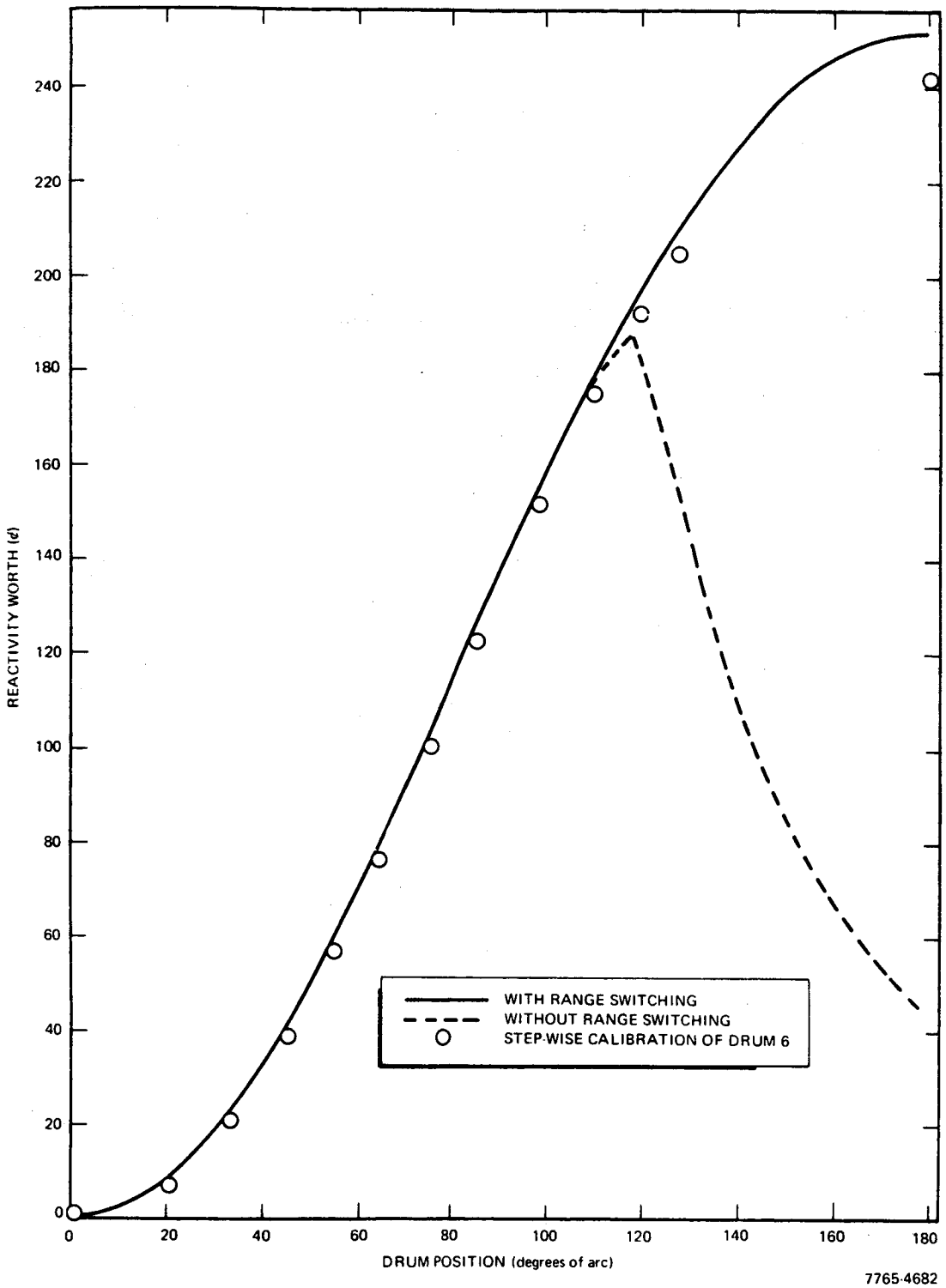

Figure 16. Comparison of the Worth of a Single Drum as Determined by Stepwise and Continuous-Drive Methods (Zero Degrees of Arc = Fuel Full-In)

samples which were 1.308 cm(0.515 in.) in diameter by 37.508 cm(14.767 in.) long. When measurements were conducted in the outer periphery, six of the seven samples in each set were used simultaneously. For central worths all seven were required. A set of samples was located either in the outer six or in the inner seven sample holder tubes which were connected to the sample changer mechanisms. The reactor was brought to critical and was held at level power (~40 watts) for several minutes before data acquisition was initiated. Data were then accumulated for about another minute whereupon the sample was inserted or withdrawn from the reactor and replaced by a void, the direction of sample motion being such that the reactor power always decreased. After the sample reached its new position, data were accumulated for an additional length of time corresponding to the new steady-state reactivity value. On the basis of the measured reactivity-vs-time, the gross worth of the sample corresponded to the algebraic difference between the two steady-state reactivity values, the first being approximately zero (depending upon how level the initial power actually was). In the above measurements the drums were normally all banked equally so that the core had six-fold symmetry.

A slight variation on this procedure, which is called the all-drum-in method, involved adjusting the core uranium loading in such a way that a controllable excess reactivity existed with all drums turned full-in. In this case, after level power had been achieved and the data accumulation had been started, the drums were all turned to the fuel-full-in position where they remained for about 1 min before the sample position was altered. This procedure was usually used for measuring the reactivity worths of samples located in the outer six peripheral positions where control-drum position could potentially affect the measured worth of the sample. An example of the reactivity history for the all-drums-in method was given in Figure 12-b. The gross reactivity change due to the sample was roughly -22.8¢ − (+9¢) = -31.8¢.

The application of the inverse-kinetics technique to the measurement of the reactivity worth of a group of small samples placed in the center of the core was somewhat different. These samples had the form of thin-walled tubes with an outside diameter of about 1.37 cm(0.54 in.), a wall thickness of generally 0.0254 cm(0.010 in.), and a length of about 5.08 cm(2.0 in.). A single sample is mounted in a single-sample-holder tube that passes through one of the special

elements placed in the center fuel element position only. The single-sample-holder tube is mounted in the usual way on the changer mechanism. Since none of these samples was expected to be worth more than 1.0¢ and some were expected to be worth less than 0.01¢, the use of a single drive in or out of the sample in the manner described above would yield very poor results statistically. An oscillator technique in which the sample was inserted and withdrawn from the core in a cyclic pattern was therefore employed. The reactivity was then calculated by an iterative inverse-kinetics program.

Measurements were made after a dynamically stable power had been established with the oscillator in operation. After sufficient time for stabilization, the multichannel analyzer was started, in synchronism with the oscillator, so that the sample changed position 42.4 sec after the start of data acquisition. Data were recorded during eight full cycles of the oscillator. A recorder chart showing a typical power trace is shown in Figure 17. In order to compress the data, the time analyzer was set to store only two pairs of cycles, with subsequent data added in phase with and cumulatively to the initial data. The result of this mode of data storage, shown in Figure 18, was to produce the equivalent of one pair of cycles at a power four times as high. In the standard inverse-kinetics analysis the delayed-neutron precursors were in static equilibrium at the start of the data; that is, no power change had occurred prior to the tenth data point. (The first 10 data points were used to define the equilibrium power or n_0.) This assumption was clearly not true for a steady oscillation; rather, the delayed-neutron precursors were in a dynamic equilibrium as determined by the cycle time and the amplitude of the oscillations. This problem was solved by calculating the reactivity in a series of iterations. At the end of each iteration, the current precursor values, adjusted for relative power, were used as the initial value for the start of the next pass through the data. This method was extremely effective; after one iteration, the discrepancy from the final result was less than 10^{-3}¢. Five iterations were used, after which the discrepancy was less than 5×10^{-6}¢. This value was far below the uncertainty due to reactor noise at the power used here. Analysis of the power data shown in Figure 18 resulted in the reactivity data shown in Figure 19.

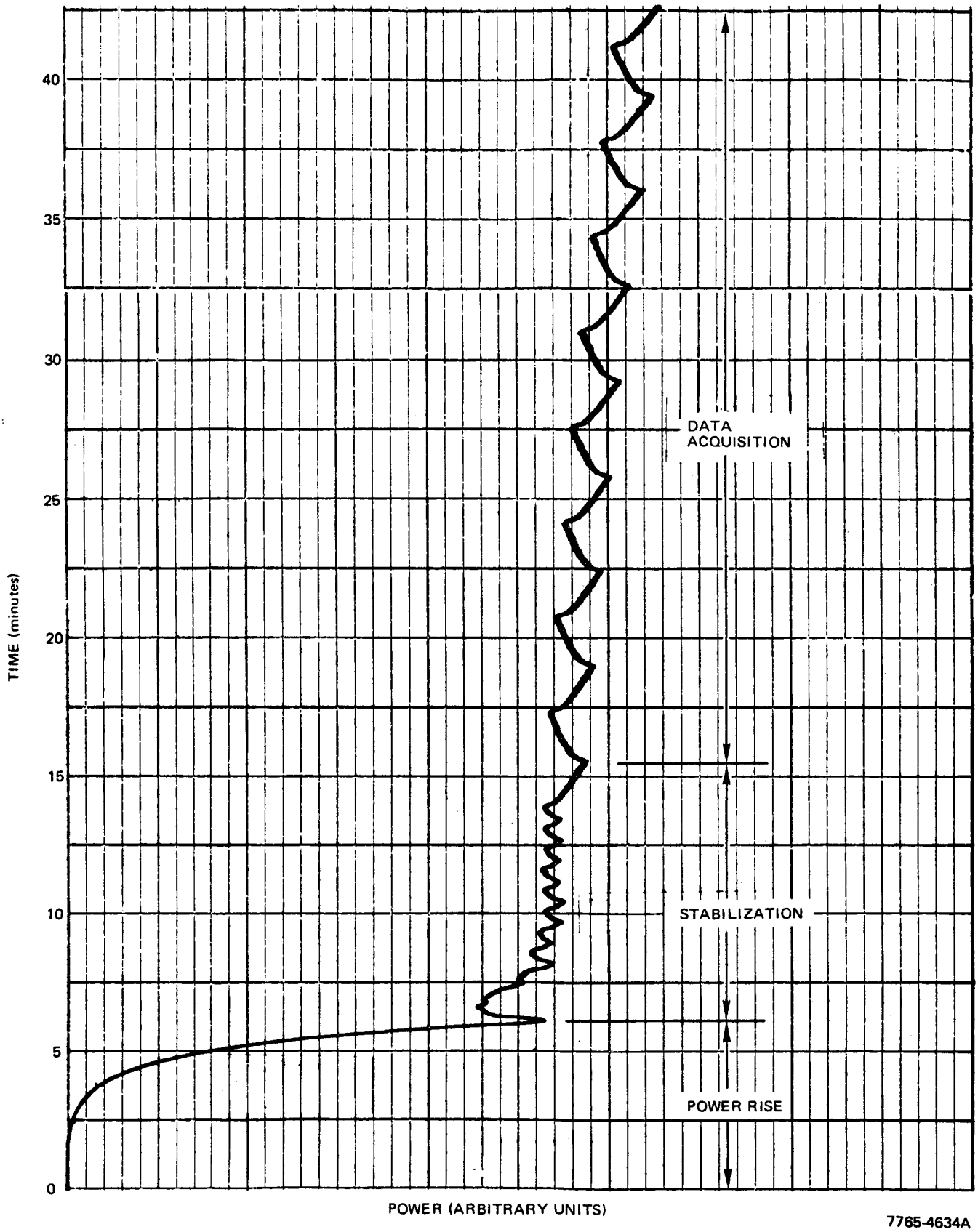

Figure 17. Power Trace Obtained During Small Sample Oscillations

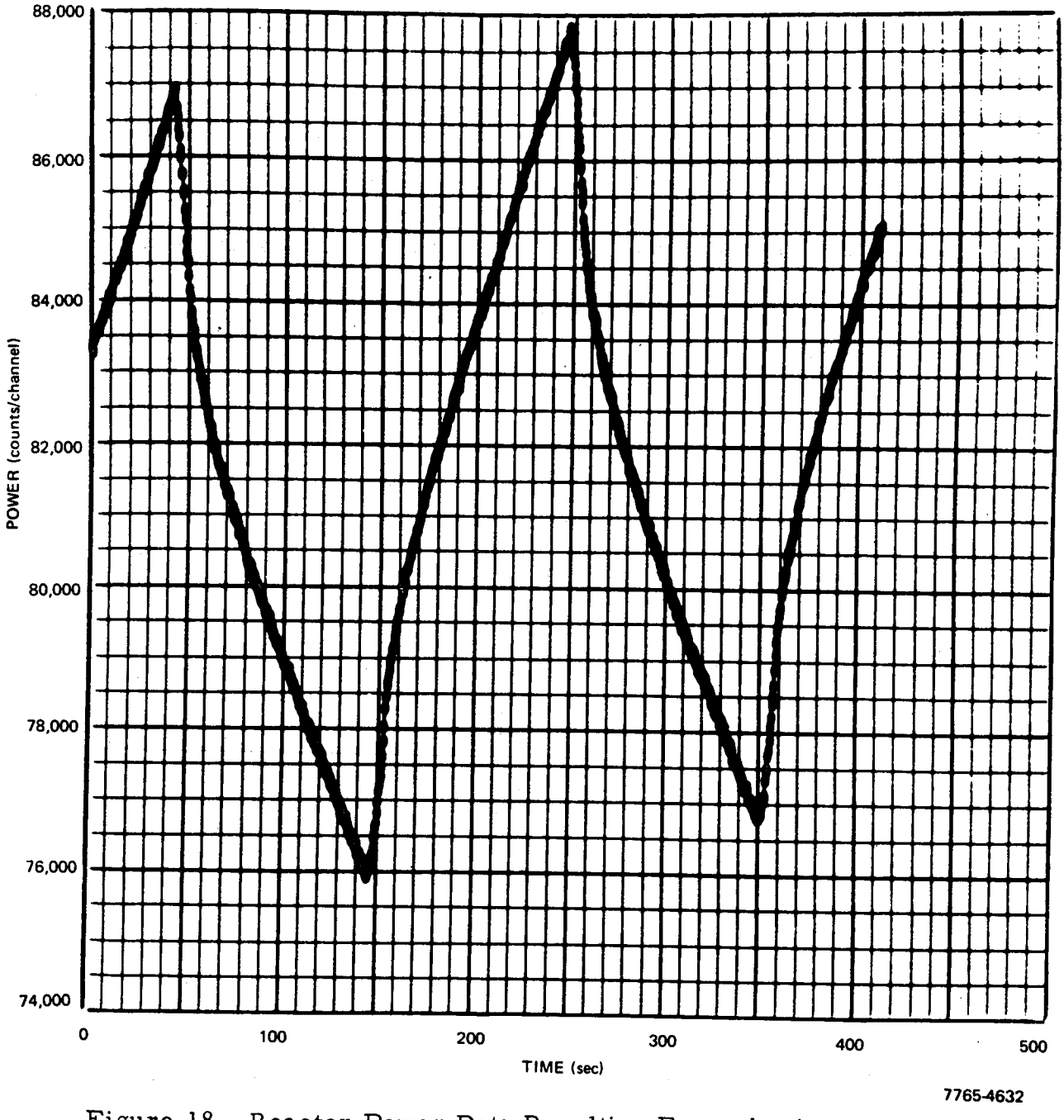

Figure 18. Reactor Power Data Resulting From the Accumulation of Small-Sample Oscillator Cycles

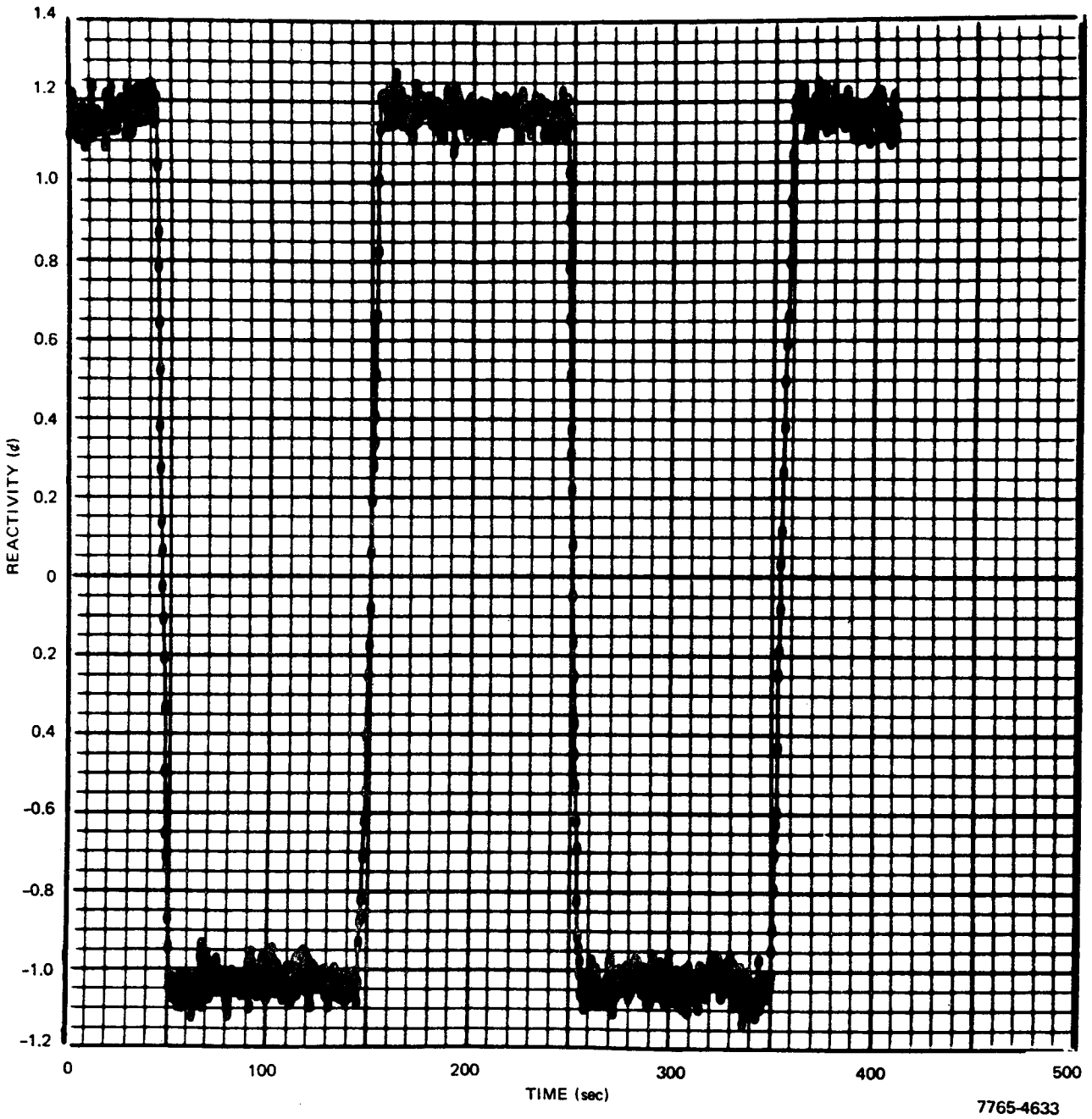

Figure 19. Reactivity Data Derived From Accumulated Oscillator Cycles (Five Iterations)

The reactivity values in each group of constant reactivity (oscillator full-up or full-down) was averaged and the standard deviation calculated. The reactivity difference was calculated from the expression

$$\Delta\rho = [-2(\rho_1 + \rho_5) + 9\,(\rho_2 + \rho_4) - 14\,\rho_3]/18^{*} \quad ,$$

where the ρ_i values were based on average values from groups 1, 2, 3, 4, and 5. This method eliminated both linear and quadratic drift.

For example, data were taken with the sample out of the core at the start and with the sample at the core center at the start. This technique was followed in order to verify that the method of determining the reactivity difference was independent of the reactivity sign or initial direction.

To check that there is no remaining dependence on reactivity sign or initial stroke direction, the reactivity differences for each pair were summed (without changing sign). If there were no systematic error, the average avlue of this sum would be zero. The average for 15 pairs was $(2.9 \pm 10.4) \times 10^{-3}$¢. The observed standard deviation, ±0.01¢ for a pair of values, implies a standard deviation of $\pm 7 \times 10^{-3}$¢ for a single measurement.

The inverse-kinetics technique was also applied, indirectly, to the determination of the critical mass of the various core compositions. Once a critical configuration was achieved, a drum calibration by the inverse-kinetics method was conducted. From the drum-worth curve and the known position of a drum at critical, the total excess reactivity could be determined. A uniform fuel adjustment was then made and a new excess reactivity determined. This process was continued for several more steps in order to generate a table of excess reactivity values as a function of uranium mass loading. The excess reactivity values were then plotted against uranium mass, and to these data points a straight line was fitted by the least-squares method. By extrapolating this line

*Subsequent to this work a more exact expression of the form

$$\Delta\rho \quad \frac{\rho_1 - 4\rho_2 + 6\rho_3 - 4\rho_4 + \rho_5}{8}$$

was derived. The error in the above equation is less than one part in one thousand, however.

to zero excess reactivity, the critical mass was obtained. An equivalent process involved the use of the slope of this line, the slope being a measure of the core-averaged worth-per-unit-mass of uranium. The latter number can be divided into the excess reactivity value in order to derive a value for the mass of uranium, which, if uniformly removed from the core, would render the reactor exactly critical. Once this core-averaged worth-per-unit-mass of uranium was established, it was used as a conversion factor to derive the critical mass of some other composition which had been formed by making small, uniform changes in the mass of some components. This process assumed that the conversion factor remained valid from one core to the next, an assumption that was justified if reactivity changes from one composition to the next were small, say, less than $1.

2. Pulsed-Neutron Technique

a. Experimental Apparatus and Arrangement

A second and independent method for measuring reactivity in the critical assembly was also used, but was only moderately successful. This method was based upon pulsed neutrons generated by the D-T reaction in an accelerator using a transformer-type power supply. Pulsing was accomplished by the use of deflection plates located in a bent drift tube. The pulse rise and decay times were of the order of 0.3 microseconds. A neutron production rate of about 5×10^{10} neutrons/sec was achieved during steady-state operation. Due to the small size of the core and other mechanical difficulties, such as cooling the target without using light scattering materials, it was not possible to place the target in the reactor. As a result, the assembly was pulsed from the side with the tritium target located about 56 cm from the axis of the core and in the core midplane, the midplane being defined as the plane perpendicular to the core axis and passing through the axis at a point halfway between the top and bottom of the fuel region. The neutrons interacting in the assembly as a result of the neutron pulse were detected by a liquid scintillator coupled to a fast photomultiplier tube. This detector also had to be located outside of the core, not only because of its size but also because it consisted of a large mass of hydrogeneous material that would have severely perturbed the core spectrum. The detector was located diametrically opposite the neutron source for some experiments and on top of the reactor along the axis for others. A small detector capable of

being placed in the core, not containing hydrogenous or light scattering materials, and having a sufficiently fast response was not available for these experiments.

In the usual pulsed neutron experiment, the initiation of the neutron pulse starts the sweep in a multichannel analyzer operating in the time mode. In most standard analyzers, the minimum channel width is 10 μsec. If the decay of the resulting neutron population is not too fast relative to the channel width, the decay can be recorded as a direct function of time. In this critical assembly, however, the decay time for the neutron population was of the order of a few microseconds near critical; consequently, the entire process occurred in less than one channel width. A method for circumventing this difficulty was therefore used. It consisted basically of using a time-to-pulse-height converter (TPHC) whose output was connected to an analyzer operating in a pulse-height mode. Thus the pulse from the neutron generator started the generation of a ramp function in the TPHC and the detection of a subsequent neutron event turned it off. The peak voltage reached by the ramp was used to generate a pulse whose peak voltage was proportional to the ramp voltage and therefore directly proportional to the time interval between the initiation and termination of the ramp. The higher this voltage pulse, the higher the channel number of the analyzer into which the pulse fell. The channel number in the analyzer was therefore directly proportional to the time interval between the initiation of the pulse from the neutron generator and the detection, either directly or after interaction with the core, of a neutron resulting from that pulse. The channel numbers in the analyzer were calibrated in terms of time units by noting the maximum time interval preselected on the TPHC and the channel number corresponding to its maximum voltage output. This channel number, divided by the time interval, yielded the effective channel width.

A block diagram of the instrumentation used in the pulsed neutron experiments is shown in Figure 20. In addition to the TPHC discussed above, a second one was used to discriminate between neutron and gamma events in the liquid scintillator. This TPHC functions in the following way. When an event occurs in the scintillator, a linear signal is taken off the ninth dynode and fed, through a pulse amplifier and crossover pick-off, to the start gate of the TPHC. The crossover pick-off serves to distinguish a neutron from a gamma event

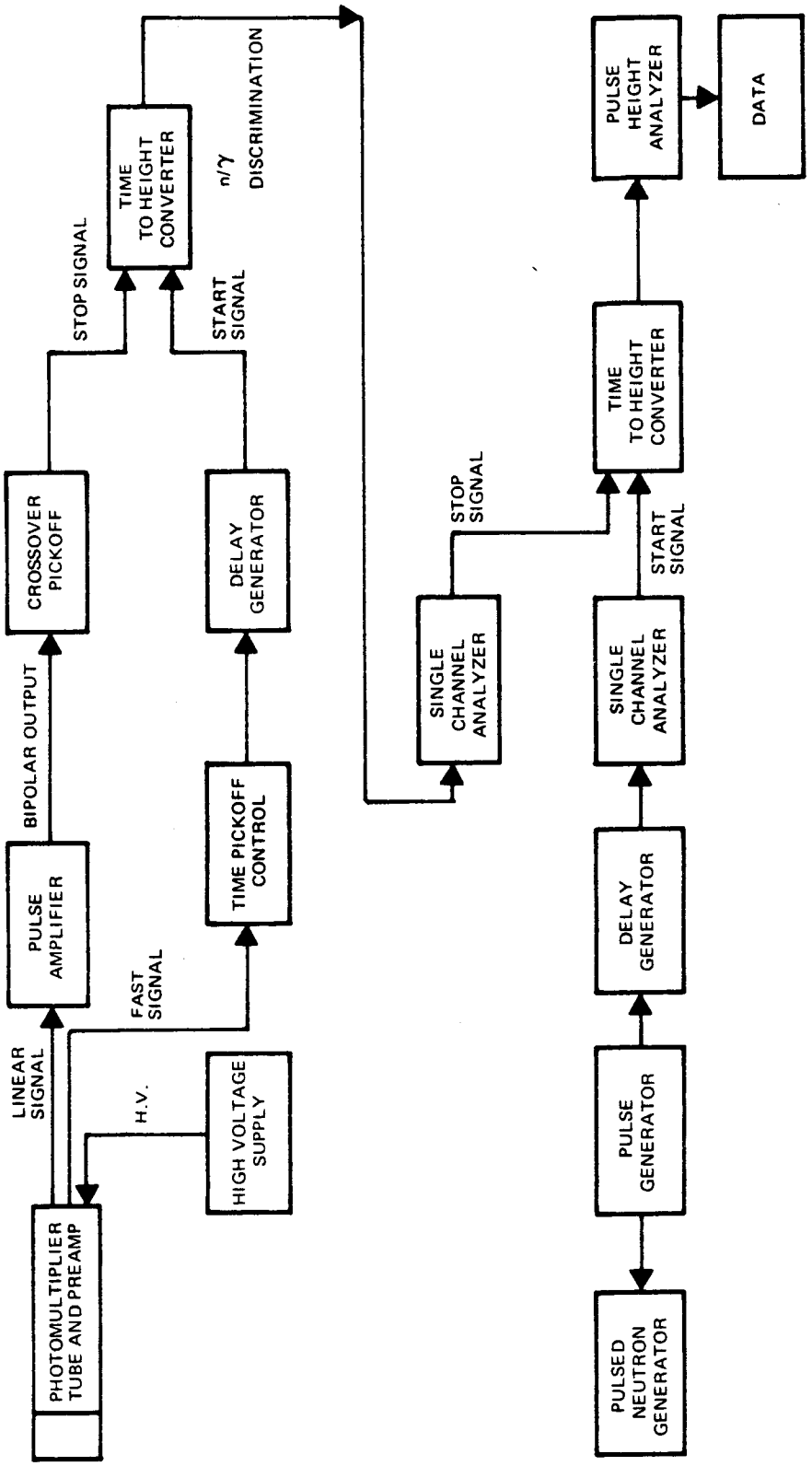

Figure 20. Block Diagram of Instrumentation for Pulsed Neutron Experiments

since the crossover times differ slightly. A second signal from the same event is also taken off the anode of the photomultiplier and fed to a time pick-off control and delay generator. This pulse serves to open the gate on the TPHC. Since the crossover time of the pulse caused by a gamma event in the scintillator occurs somewhat earlier in time than that for a neutron event, the time between the opening and closing of the start and stop gates in the TPHC is short and its output pulse is correspondingly low in voltage. On the other hand, the crossover time for the pulse caused by a neutron event in the scintillator is long. The pulse from the TPHC is therefore higher than in the case of the gamma event and, by feeding the pulse to a single channel analyzer (SCA) whose discriminator is set to reject pulses whose peak voltage does not exceed a preselected value, gamma events can be distinguished from neutron events. Thus the number of gamma events that ultimately give rise to a stop pulse in the TPHC leading to the analyzer is significantly reduced, the ratio of neutron to gamma events reaching the latter TPHC being of the order of 500.

b. Data Analysis

A typical curve of the "decay" of a neutron pulse in the reactor at about $4 subcritical is shown in Figure 21. Such curves are the result of pulsing the assembly repetitively for long periods of time, typically 5000 pulses/sec for 20 or 30 min. In general, one event is recorded by the analyzer as a result of each neutron pulse. Events are accumulated in each channel until curves of the type shown are obtained. It is a "decay" curve only in the sense that the channel number can be correlated with a probability of an event occurring as a function of time. Thus there is a high probability that a neutron will be detected soon after the pulse and this probability decreases with time. The channel width for the pulsed data of Figure 21 is 0.161 microseconds; therefore, between Channels 30 and 70, the total elapsed time is 6.4 microseconds.

One of the methods used for deriving the subcritical reactivity from the data in Figure 21 is based upon the Simmons-King analysis. In this analysis the decay constant, α (sec^{-1}), is related to the decay constant, α_c, at critical by the equation

$$\alpha = \alpha_c (1 - \$)$$

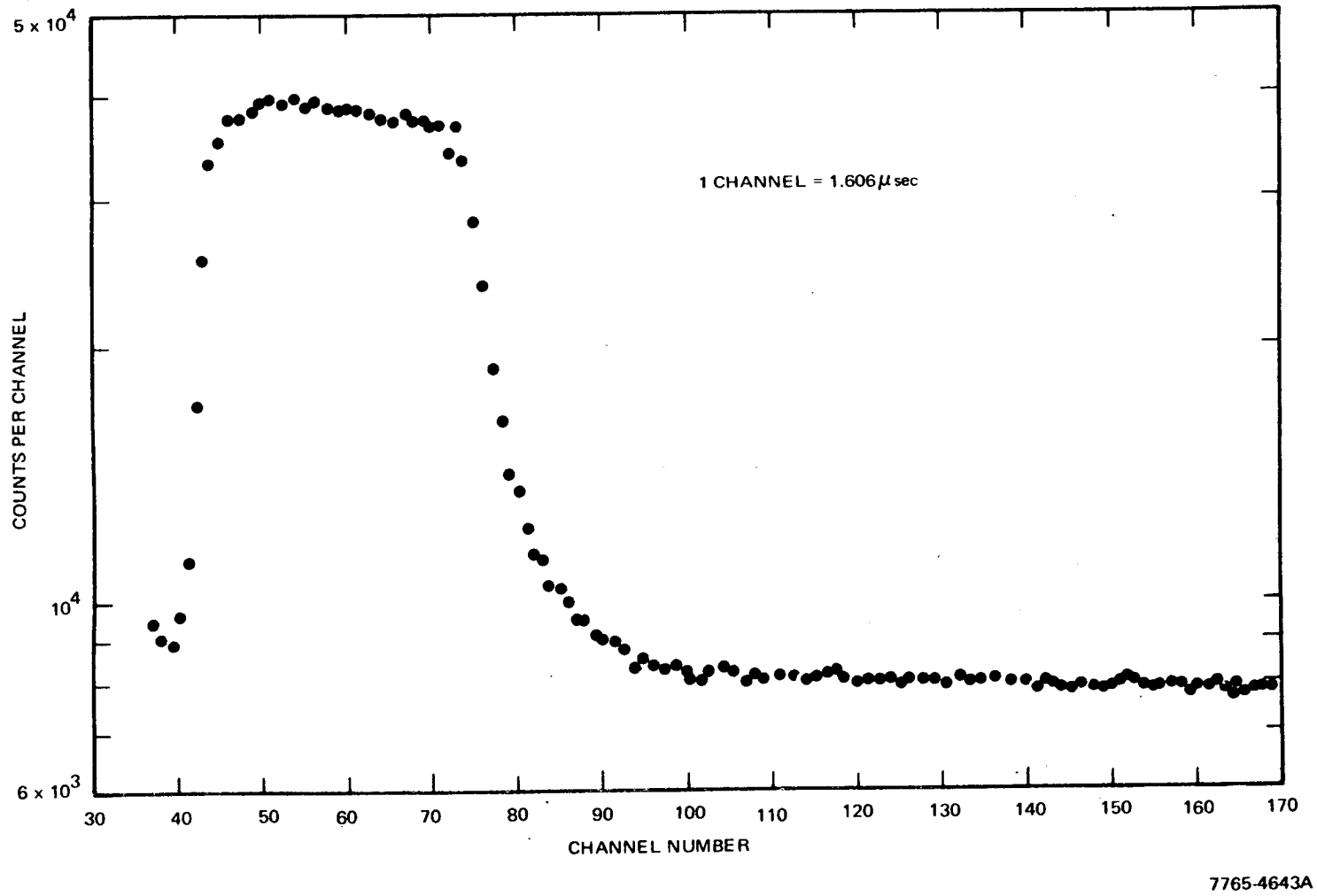

Figure 21. Results of Pulsed-Neutron Experiment Near $4 Subcritical

where \$ is the degree of subcriticality in \$. The value for α can be obtained by subtracting the constant background channel by channel from the decay curve. The differences can be plotted on semilog paper and generally show good exponential behavior over a sufficient number of points that the inverse of the time required for the pulse to change by a factor of e can be ascertained. This quantity is defined as α and has the value of 1.062×10^6 sec^{-1} for the data in Figure 21.

If the pulsed neutron experiment is carried out at delayed critical, the decay constant, α_c, is determined and can then be used in the above equation to yield the degree of subcriticality corresponding to some other decay constant. Alternatively, α_c can be determined by a Rossi-α experiment (an experiment that will be discussed subsequently) or by measuring α at some known degree of subcriticality, the latter being determined by inverse-kinetics techniques. Both of the latter methods were employed in this experimental program, but only the α_c obtained from the Rossi-α experiment seemed to yield reasonably good results.

An attempt to determine the degree of subcriticality by other types of analyses of the decay curves was also made. The GRIPE-II code[8] was used for this purpose. The code was successfully used to obtain decay constants (with statistical uncertainties) that had greatly improved accuracy relative to the hand plotting mentioned above. The code then attempts to calculate subcriticality by three methods: the area ratio,[9] the extrapolated area ratio[10] and the Garelis-Russell.[11] These analyses were not successful, primarily because most of the methods depend to one degree or another on having: (1) a neutron pulse width that is narrow relative to the inverse decay constants, and/or (2) a well-defined time-zero at which the pulse occurs. In addition, the necessity for locating the neutron source and detector external to the core may have created difficulties in data interpretation. The pulsed neutron experiments were generally conducted with a pulse width of 5.6 microseconds, a value very much larger than the inverse decay constant (0.46 microsecond) that was observed with the reactor in its least reactive control-drum condition; that is, with all drums turned fuel-full-out. Subsequent work on the neutron pulse generator has made it possible to achieve narrower pulse widths, but additional experiments have not been undertaken.

c. Check on the Method

A check on the pulsed neutron method for measuring large negative reactivity values was undertaken in one of the reactor compositions by using a set of seven B^{10} samples located in the center of the reactor. The worth of the seven B^{10} samples was determined by inverse-kinetics methods to be -\$2.74. A pulsed neutron measurement was conducted at a degree of subcriticality of 25¢ and yielded a decay constant of 3.03×10^5 sec^{-1}. From this value and the above equation, α_c is found to be 2.42×10^5 sec^{-1}. By the use of this value of α_c and a measured decay constant of 7.63×10^5 sec^{-1} with the B^{10} samples in place, the pulsed neutron method predicted a worth of -\$2.15 for the B^{10} samples.* This value is not in particularly good agreement with the inverse kinetics value shown above, the difference being of the order of 22%.

In the equation $\alpha = \alpha_c (1 - \$)$, it is assumed that the reactor is very close to critical such that $k \cong 1$. For large subcritical conditions, the more exact expression for calculating the reactivity is

$$\$ = \frac{1 - \alpha/\alpha_c}{1 - \alpha/\alpha_c \beta_e} \quad .$$

The use of this equation tends to improve the agreement slightly.

It is of interest to investigate the degree of agreement if the above data are analyzed in a way that utilizes a value of α_c as determined in a Rossi-α experiment. Suppose, for example, that the value of α_c as obtained above is, for some reason, in error. Then, if a value for α_c of 2.11×10^5 sec^{-1} (as determined by a Rossi-α experiment) is used, along with the measured decay constant of 7.63×10^5 sec^{-1} as determined in the pulsed neutron experiment, a worth of \$2.62 for the seven B^{10} samples is derived. The value is in considerably better agreement with the inverse kinetics value. There is, however, no independent experimental basis at this time for rejecting the α_c value as determined by the pulsed neutron method at -25¢; consequently, the preference for α_c of 2.11×10^5 is entirely arbitrary. However, it will be shown later in this report that the use of the latter value of α_c, along with the pulsed neutron data pertaining to the worths of the control drums, also yields much better agreement

with another experimental method – namely, the inverse counting technique, a method which will be described in the following section of this report.

3. Inverse-Counting Technique

A third method for measuring reactivity – in particular, large negative reactivities – is based upon inverse-counting techniques. In this technique, a Cf^{252} source ($\sim 2 \times 10^6$ n/sec) was placed in the center of the reactor and the neutron detectors described previously were used to measure the neutron population. The number of events occurring in the pulse detectors over some preselected time interval or the steady-state current achieved in the current detectors was recorded as a function of various subcritical reactor configurations. By making measurements at or very near a configuration where the reactivity is known directly by inverse-kinetics measurements, the method was normalized and then used to derive the reactivity for the unknown conditions. The conversion of the counting data to reactivity can be derived as follows:

By definition

$$\frac{1}{M} = 1 - k \quad .$$

Since C, the total counts for some fixed time interval, is directly proportional to M, one can write that

$$C = \epsilon M \quad .$$

Therefore

$$\frac{\epsilon}{C} = 1 - k \quad .$$

For some known normalization reactivity value k_n,

$$\frac{\epsilon}{C_n} = 1 - k_n \quad .$$

Therefore, by taking the ratio,

$$\frac{C_n}{C} = \frac{1 - k}{1 - k_n} \quad .$$

Since $k = 1/\beta\rho - 1$, where ρ = reactivity in dollars, one can eliminate k and solve for reactivity in dollars. Thus, the reactivity, in terms of the ratio of the counts, C, at some unknown reactivity to the counts, C_n, at some normalization value, is

$$\rho = \frac{\left(\frac{C_n}{C}\right)\rho_n}{\beta\rho_n\left[1 - \left(\frac{C_n}{C}\right)\right] - 1} ,$$

where ρ_n is the known normalization reactivity in dollars. The value for β is calculated, the value for ρ_n is determined by inverse-kinetics measurement at a place close to critical, and, since C_n/C is measured, the reactivity can be obtained.

The inverse-counting technique was applied with apparently good success to the measurement of large negative reactivity values where inverse-kinetics techniques yielded clearly erroneous results and where the pulsed neutron method appeared to be marginally valid. The degree of success of the inverse-counting technique is based, however, largely upon the fact that, once normalized at small negative reactivity values (up to \$1.40), it predicted the worths of single drums ($\sim$\$2.50) quite well and predicted a total worth for all drums turned full-out in good agreement with the worth of one drum multiplied by six. The latter manipulation assumes, of course, that there is little or no drum interaction, a conclusion that is supported by calculation.

The inverse-counting technique was also applied, in the classical manner and without the necessity for normalization, to approach-to-critical experiments. Under these circumstances, the total counts obtained over some preselected time interval are measured for the case in which no fuel is located in the reactor and only the neutron source is present. Uranium fuel in appropriate and safe increments is then added to the assembly and a new series of counts, usually for the same time interval, are made. This process is continued step-by-step and the total counts observed at each fuel addition are then divided by the counts obtained with no fuel. The resulting quotient is plotted as a function of fuel mass added to the core or as a function of some mass-dependent parameter.

4. Drum Worth Technique

A fourth and final type of reactivity determination that was routinely used during the experimental program involved the measurement of both positive and negative reactivity values on the basis of changes in the position of a calibrated control drum. This method is, of course, only a secondary technique since the drum itself is also calibrated initially by inverse kinetics techniques. It is, however, a very convenient and rapid method for ascertaining the magnitude of reactivity changes within a few cents.

Typically, the drum position is noted at which a base reactor configuration or composition is just critical. From the drum worth curve, the total excess reactivity is determined. A change, such as substitution of a fuel-loaded fuel element for an empty one or the addition of Ta wires to the core, is made and a new critical position for the calibrated drum is noted. This new position yields a new total excess reactivity value which, when algebraically subtracted from the former one, yields the reactivity change caused by the operation.

B. THE DETERMINATION OF THE RATIO ℓ/β

One of the objectives of the experimental program was the determination of the ratio of the prompt neutron lifetime, ℓ(sec), to the effective delayed neutron fraction, β_{eff}, the end result being an evaluation of ℓ on the basis of a calculated β_{eff}. Two methods for measuring the parameter were used.

One method involves the analysis of the decay curve following the pulsing of the reactor by a neutron source in the manner previously outlined in Section III-A-2 above. It was noted in that section that, if the reactor were pulsed at critical, a decay constant, designated α_c, could be derived. It can be shown that α_c is equal to β_e/ℓ;[12] consequently, the extraction of the decay constant from a decay curve obtained at critical provides a measure of β_e/ℓ. Also as noted in Section III-A-2, if the decay constant, α, at some known degree of subcriticality were measured, α_c would be derived from the equation $\alpha = \alpha_c$ (1 - \$), an equation that assumes that ℓ is independent of the degree of subcriticality. This is one method that was used to obtain a measurement of ℓ/β_e.

A second method for measuring α_c, or β_e/ℓ, is a Rossi-α experiment. One variation of this experiment consists, in brief, of determining the time

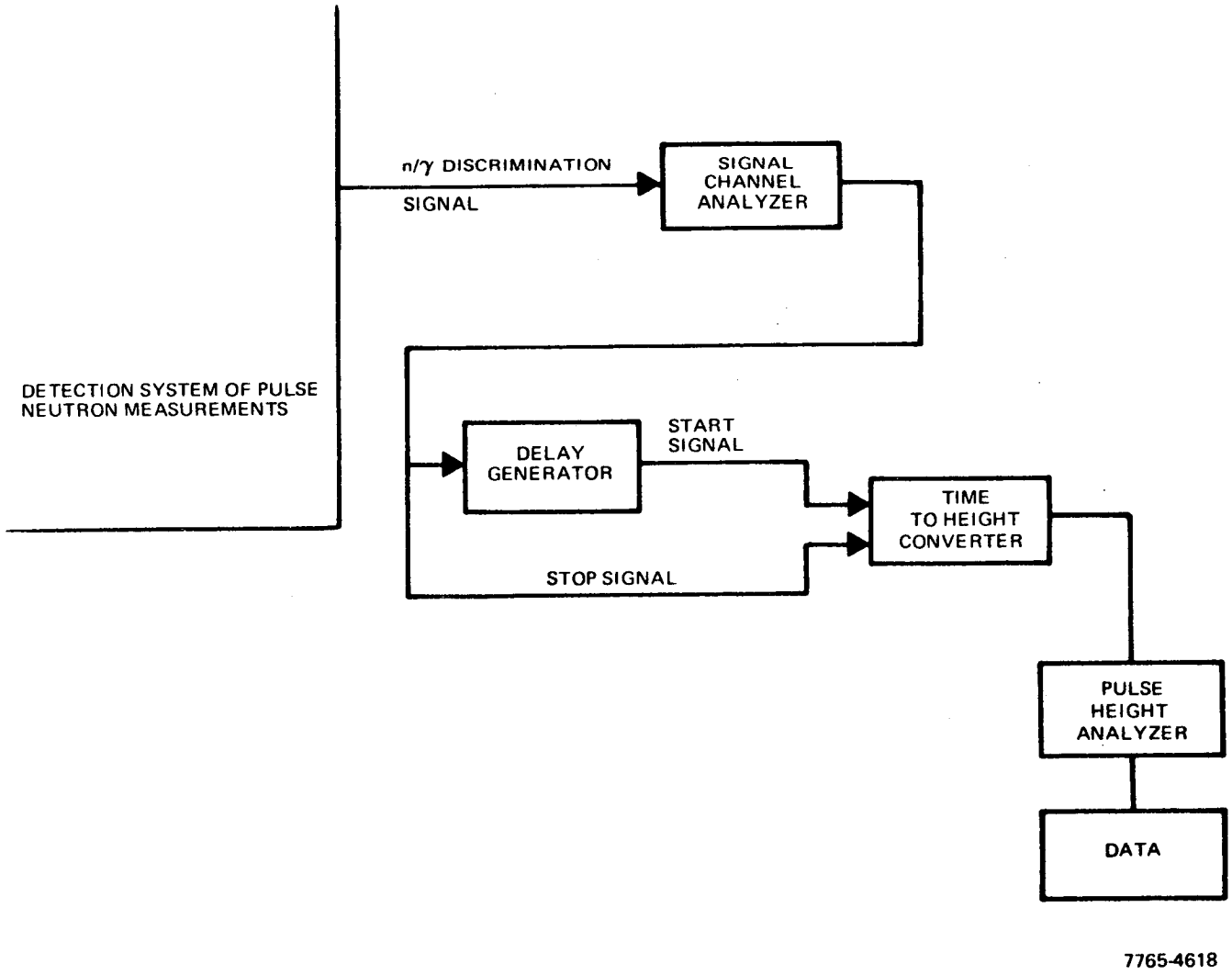

Figure 22. Block Diagram of Instrumentation for Rossi-α Experiment

interval between the detection of a neutron in a detector and the detection of another neutron in the same chain at a later time in the same detector.

A block diagram of the experimental apparatus for performing this measurement is shown in Figure 22. The same liquid scintillator used in the pulsed neutron measurements was placed in identical positions outside the core. With the reactor at critical and at a very low power, a chance neutron interaction occurs in the scintillator and creates a pulse which is handled, insofar as discriminating between gamma and neutron events is concerned, in the same way that was used in the pulsed neutron experiment. Thus the output of the first time to pulse height (TPHC) as shown in Figure 20 is again fed to the single channel analyzer (SCA) shown in Figure 22. The output of the SCA is then fed into the stop gate in a TPHC where it terminates a previously initiated ramp and causes the TPHC to produce, in the usual way, a voltage pulse whose height is proportional to the time between the opening and closing of the gate. A delay generator provides a pulse that opens the gate, however, a short time later. The pulse arriving at the startgate than initiates a new ramp function which will be terminated by the detection of a second neutron. The output pulse from the TPHC is fed to a multichannel analyzer operating in the pulse height mode. The longer the delay between the two neutron events, the greater will be the output pulse of the TPHC and the higher the channel number in which the pulse is counted. Thus, as in the case of the pulsed neutron experiments, the analyzer channels are calibrated in terms of time. If this counting is continued for long periods of time ($\sim$20 min), data of the type shown in Table 2 and plotted in Figure 23 is obtained. The curve appears to be made up of at least two exponentially decaying functions, one with a long and one with a short time constant. If the exponential with the long time constant is subtracted, a decay time that is very roughly characteristic of the core is obtained.

C. POWER DISTRIBUTION MEASUREMENTS

The power distribution in Composition 5 of the critical assembly was measured by inserting a previously unirradiated 0.066-cm(0.026 in.)-diameter uranium wire into the fuel cluster in each of a group of fuel elements making up a one-twelfth sector of the core. The wires were irradiated at about 25 watts for a period of 1 hr at the end of which time the reactor was scrammed and the

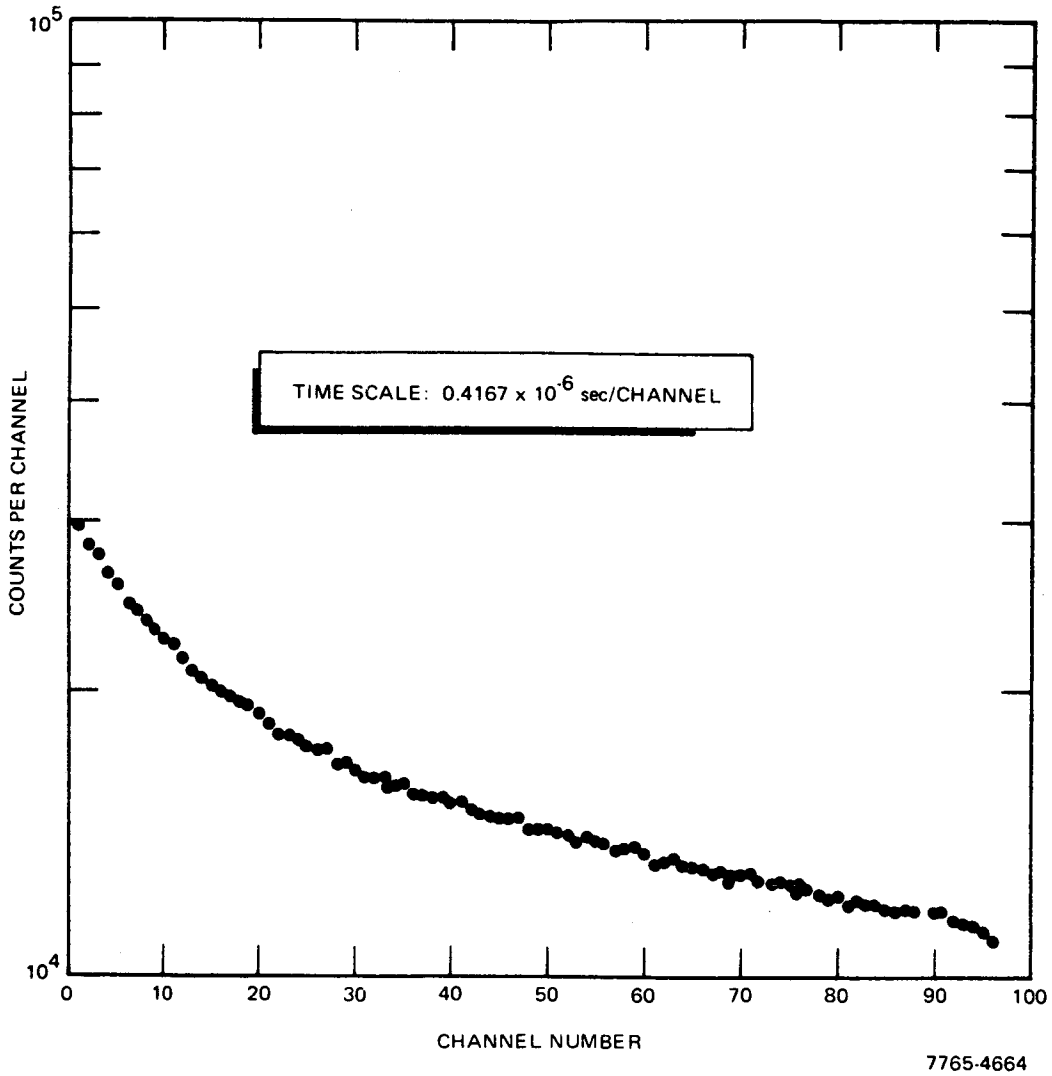

Figure 23. Rossi-α Experimental Results

TABLE 2

ROSSI-α EXPERIMENTAL DATA
(Time Scale: 0.4167×10^{-6} sec/channel)

Channel Number	Total Counts	Channel Number	Total Counts	Channel Number	Total Counts
1	29753	33	16208	65	13123
2	28241	34	15983	66	13125
3	27687	35	15976	67	12958
4	26482	36	15560	68	12983
5	25954	37	15531	69	12746
6	24862	38	15444	70	12869
7	24271	39	15410	71	12790
8	23833	40	15274	72	12655
9	23230	41	15288	73	12581
10	22723	42	15027	74	-
11	22282	43	14819	75	12736
12	21560	44	14684	76	12559
13	20958	45	-	77	12356
14	20586	46	14680	78	12332
15	20206	47	14703	79	12184
16	20010	48	14300	80	12189
17	19593	49	14336	81	11962
18	19484	50	14366	82	12160
19	19233	51	14366	83	12057
20	18835	52	14018	84	11984
21	18420	53	13981	85	11883
22	17952	54	14011	86	11785
23	17977	55	13978	87	11885
24	17781	56	13823	88	11809
25	17469	57	13600	89	-
26	17289	58	13686	90	11774
27	17460	59	13776	91	11702
28	16757	60	-	92	11512
29	16739	61	13564	93	11432
30	16437	62	13089	94	11390
31	16233	63	13201	95	11349
32	16208	64	13301	96	10995

foils removed. Wire segments, nominally 1.27 cm(0.50 in.) long, were cut from the full core-length wires at various positions along their length in order to measure axial power profiles and to map the power at various axial planes. These wire segments were weighed to an accuracy of ±0.1 mgm and had an average weight of about 69 mgm, of which about 1 mgm was contributed by the Kel-F coating.

The wire segments were counted on three gamma channels beginning a few hours after reactor shutdown. Standard NaI scintillation detectors were used with the amplifiers set for integral counting of gamma rays above 0.5 Mev. A fourth channel was employed to count a wire segment that was taken from near the center of the core and that was used as a monitor. A least-squares fit of the data from this monitor wire was used for decay correction. All four channels were controlled by the same time base and dual preset counter. Fifteen-minute counting intervals were generally used, but some wire segments were counted more than once. The three channels were normalized to one another by counting the same group of six wires in all three channels and comparing the resulting decay-corrected counts.

A second- or third-order polynomial was found to give the best (least-squares) fit to the data from the monitor wire, depending upon the time at which counting is initiated.

A computer code was used to correct the data for decay, background, mass normalization (after subtracting the weight of the Kel-F), and counter normalization. The resulting relative activities, which are directly proportional to power, were then plotted as a function radial and axial distance. The errors, due to counting statistics only, vary from 1/2 to 1-1/2%. The mass determination introduces an error of approximately ±0.2% and there is an uncertainty of about ±0.01 in. in the axial position of a wire within the fuel element.

D. NEUTRON SPECTRUM MEASUREMENTS

1. Proton-Recoil Method

The differential neutron spectrum from approximately 50 kev to 2.31 Mev was measured in various core compositions of the critical assembly by means of the proton-recoil spectrometer, an instrument which has been under development and test for several years.[13-15] The spectrum measurements utilized a

group of gas-filled spherical-type detectors as developed by P. W. Benjamin et al.[13] The spheres are 3.94 cm(1.55 in.) in inside diameter and have a 0.058-cm(0.022 in.) wall thickness. The central anodes consist of 0.00254-cm (0.001 in.)-diameter tungsten wire. Each of the detectors in the group had a different filling of hydrogen and/or methane gas. These fillings are listed in Table 3. Most of the detectors also had a small amount of nitrogen or He^3 gas for energy calibration [in a thermal neutron flux, the $N^{14}(n,p)C^{14}$ reaction produces a 615-kev pulse from the proton plus C^{14} ion, while the $He^3(n,p)H^3$ reaction produces a 770-kev pulse].

TABLE 3

DETECTOR DESIGNATION AND FILLINGS

Detector Designation*	Detector Description*	Detector Filling Pressure (newtons/m^2 x 10^5)
0.9 H_2	0.908 H_2 + 0.042 CH_4	0.920 H_2 + 0.043 CH_4
2.63 H_2	2.63 H_2 + 0.263 CH_4 + 0.132 N_2	2.66 H_2 + 0.263 CH_4 + 0.134 N_2
2.63 CH_4	2.63 CH_4 + 0.132 N_2	2.66 CH_4 + 0.134 N_2
2.63 CH_4 (He^3)	2.63 CH_4 + 0.0001 He^3	2.66 CH_4 + 0.0001 He^3
8.1 CH_4	8.09 CH_4 + 0.42 N_2	8.20 CH_4 + 0.43 N_2
8.1 CH_4 (He^3)	8.09 CH_4 + 0.004 He^3	8.20 CH_4 + 0.004 He^3

*The numerical values in these two columns refer to pressure in atmospheres. Thus 0.908 H_2 + 0.042 CH_4 describes a detector filled with H_2 to 0.908 atm and with CH_4 to 0.042 atm.

The detectors were operated with a positive high voltage on the anode wire and the outer sphere was grounded. Neutrons entering a detector create recoil protons in the hydrogenous gas. Each proton ionizes the gas, and the electrons are collected on the central anode wire. The collected charge is proportional to the energy of the proton. Neutrons of a given energy produce a continuous energy distribution of recoil protons from zero up to the energy of the neutrons. Figure 24 is a block diagram of the electronics network used to amplify, measure, and analyze the signals from the anode. The energy channel

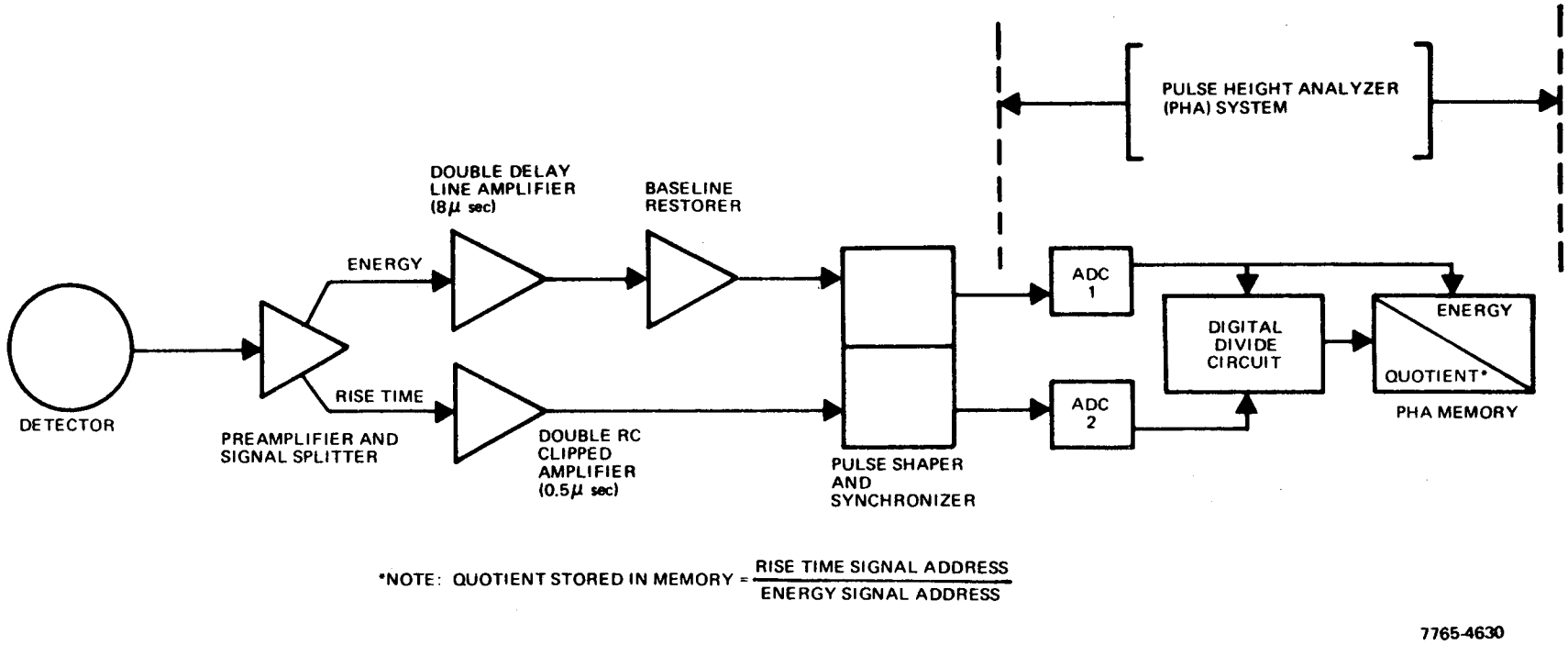

Figure 24. Block Diagram of Instrumentation for Proton-Recoil Spectrometer

is used for all of the measurements. The rise-time channel is used simultaneously with the energy channel at low energies to help remove gamma-induced background from the data before it is finally analyzed.

In each experiment, many gammas are present with the neutrons. The gammas strike the detector walls and knock off electrons which ionize the gas along with the protons; however, the electrons produce considerably less ionization per unit path length than do the protons. Thus, an electron travels much farther than a proton while losing an equivalent amount of energy in the gas. The electron deposits the largest amount of energy in the gas while traveling approximately along a diameter of the detector. All deposits above this energy are strictly neutron-induced events while those below can be neutron-induced or gamma-induced. The "cut-off" energy varies with detector gas pressure only, since all the detectors are the same size. Thus, each detector has a lower energy limit for data taking.

The influence of gammas below this energy limit depended upon the ratio of neutrons to gammas in each reactor composition or for each arrangement of lead shielding. The lower the gas pressure, the lower this limit was. With the lowest pressure detector (designated 0.9 H_2), this limit was approximately 50 kev. The lower limit with the detector designated 2.63 H_2 (which was used in some experiments for two-parameter data analysis) was approximately 100 kev.

Below this energy, gamma-induced events were removed by two-parameter (energy and rise-time) gamma discrimination.[14] Since a proton and an electron of the same energy have considerably different path lengths while ionizing the gas, the time to collect the charge on the anode wire usually is quite different. By analyzing the rise times of the signals in coincidence with their pulse heights, many of the gamma-induced events can be removed from the total number of events at each energy before further data processing is performed. A simple discrimination (yes, no) cannot be used on each event, since there is some overlapping of rise times. For instance, an electron traveling somewhat parallel to, and close to the anode wire will have a relatively fast rise time; while a proton perpendicular to the anode wire and near the detector wall will have a relatively slow rise time. Also, an energetic proton which leaves the gas after depositing a small amount of its energy in the gas causes a longer rise

time than one of low energy which stops in the gas, since the specific ionization increases rapidly just before the particle stops. These factors require that the shapes of the rise-time curves at each energy be examined and compared with data from a pure gamma source to accurately subtract the gamma-induced events from the total. Two-parameter data, taken with a gamma source as produced by the reactor in a shutdown condition, were normalized and subtracted from the reactor data below 100 kev before proceeding with the final analysis.

As was indicated in Section II of this report, in order to place a detector at the core center, seven standard central fuel elements were removed from Positions 0-1 through 1-6 inclusive. Then, seven special short elements were inserted at the bottom of the core, the detector was placed on top of them (centered in the core), and six special elements were inserted above the detector. A T-111 cylinder [3.81 cm(1.5 in.) high, see Figure 10] located around the detector maintained a fixed separation between top and bottom elements. Located in fuel element Position 0-1 was a 36-cm(14.2 in.)-long Ta honeycomb tube. This tube connected the detector to the line driver (gain-of-one amplifier) which, in turn, connected to the preamplifier by cable. The Ta tube had an axial wire which provided high voltage to the detector anode and carried the signal from the detector to the electronic system.

A 4096 two-parameter multichannel analyzer is used to store, either in the one- or two-parameter mode, data obtained from the proton-recoil detector. This information is then printed out for computer processing either as punched paper tape or as parallel printing on adding machine paper. The analysis of the data of the one-parameter type is based upon a computer code developed by P. W. Benjamin et al[16] and requires the following input:

1) Detector radius,

2) Filling gas and pressure,

3) Energy calibration factor (Mev per channel),

4) Lowest energy to be analyzed,

5) Highest energy to be analyzed,

6) A number proportional to reactor power so that all runs are normalized to a constant power, and

7) A neutron spectrum (calculated or measured) above the highest energy to be analyzed.

Output from the code is the calculated flux on an absolute scale related to reactor power. Internal and external errors are also calculated and an option for numerical smoothing of the original data is available.

Benjamin describes the four main steps in the analysis of a proton recoil spectrum which has a significant amount of wall effect. These are:

1) Generate a matrix of recoil proton distributions due to discrete neutron energies below E_{max}, the highest energy to be analyzed;
2) Generate a recoil spectrum due to neutrons above E_{max};
3) Subtract 2 from the experimental spectrum; and
4) Unfold 1 from 3.

For each detector gas filling, there is an upper neutron energy detection limit which depends on the type of gas and its pressure. Protons have shorter ranges in methane than in hydrogen at the same pressure. In every detector, some protons strike the wall before depositing their energy in the gas. The code calculates a correction for this wall effect. Errors in this calculated correction limit the upper energy for data analysis in each detector.

Steps 1 and 2 must allow for wall effect and can be calculated either by a Monte Carlo process or by an analytical method. In this code, the analytical method reported by Snidow[7] is used.

The expression relating the neutron flux, $\varphi(E)$, to the observed recoil proton distribution, M(E), is:

$$\varphi(E) = \frac{dM(E)}{dE} \cdot \frac{E}{\sigma(E)VN_p} \quad ,$$

where $\sigma(E)$ is the (n,p) scattering cross section at energy E, V the volume of the detector, and N_p the number of protons (i. e., the number of hydrogen atoms) per cm^3 of the detector. This equation is exact only if the full energy of each recoil proton is deposited in the detector gas. The wall effect calculations

give for the number of protons C(E) dE which will deposit an energy between E and E + dE in a spherical counter

$$\frac{C(E)}{C_T} = \frac{F(E)}{E_n} + \frac{1}{E_n}\int_E^{E_n} \frac{dR}{dE}(E' - E)N[R(E') - R(E' - E)]dE' \quad ,$$

where C_T is the total number of recoil protons, E_n is the neutron energy, and R(E) is the range of a proton having energy E. N(L) dL is the probability that protons will see a path length to the counter wall between L and L + dL and is given by

$$N(L)\,dL = \frac{3}{4a}\left(1 - \frac{L^2}{4a^2}\right)dL \quad ,$$

where a is the counter radius. Integration of this equation between R(E) and L_{max} gives F(E), the fraction of protons with energy E which will stop inside the counter; thus,

$$F(E) = 1 - \frac{3R(E)}{4a} + \frac{R^3(E)}{16a^3} \quad .$$

The computer code calculates $C(E)/C_T$ for any E and E_n. A table of range-vs-energy for each detector gas is input to the code as the first set of data.

As previously mentioned, input to the code includes a spectrum above the energy to be analyzed (E_{max}). The spectra calculated by NASA personnel for the various core compositions were used for this purpose.

The effects on the derived neutron spectrum below E_{max} of using, above E_{max}, an input spectrum that may not be known very accurately has been investigated by P. W. Benjamin, et al., and is discussed on Pages 10 and 11 of Reference 16. In brief, the effects were investigated by analyzing a single set of experimental proton-recoil data by using two different neutron spectra as input. The flux per unit lethargy of one input spectrum varied from 11.5 at an energy of 1.2 Mev down to zero at 6.4 Mev. The flux per unit lethargy of a second input

neutron spectrum varied from 8.8 at 1.2 Mev down to zero at 6.0 Mev. Between these energy intervals (i.e., between 1.2 Mev and about 6.0 Mev), the two spectra varied from zero up to 50% (at 4.0 Mev) from one another. However, a comparison of the two neutron spectra that were derived from the single set of proton-recoil data shows no variations greater than 4% over the energy interval from 140 kev to 1.2 Mev.

Another factor of importance in the proton-recoil spectrometer technique concerns the reactor power level at which measurements are made. If the power level is too high, several pulses can be taking place in the detector while a previous one is being processed in the electronic system. Since the counts/channel in the pulse height analyzer increase exponentially with decreasing channel number, more counts may be lost in low channels than in high ones. This situation could give a flatter proton-recoil distribution than would normally be the case, and, thus, a lower neutron flux, since the flux is proportional to the shape of the counts/channel curve.

In order to investigate this phenomenon, proton-recoil data were taken in one of the reactor compositions over a large range of power levels. A definite increase in flux, particularly where it should indeed normally be increasing rapidly, occurred as the power level was reduced to a point at which pulses no longer overlapped significantly in time. Special care was therefore taken to maintain very low power levels during the proton-recoil spectrometer measurements conducted during this program.

2. Foil Measurements

As a means of obtaining some integral data pertaining to the neutron energy distribution in the various core compositions, a series of "foil" irradiations were performed. For these experiments, only the fuel element in Position 0-1 is removed, all others remaining standard. In its place, are inserted two of the largest special proton-recoil elements normally used for the proton-recoil measurements. One of these is placed at the bottom of the core; then a thin-walled stainless-steel spacer tube 3.81 cm(1.5 in.) high is inserted. On top of this spacer tube is placed the second special element which occupies the remaining space below the upper grid plate. Thus a 3.81-cm(1.5-in.)-high cavity is formed at the center of the core into which 2 groups of foils were placed.

Both groups were usually identical, both containing four or five different foils and one serving as a check on the other. One foil of each of the following materials was normally included in a group: S, Cu, In-Sn, Al, and Na_2CO_3. Attempts to utilize a Co foil were not successful because of interfering activities; consequently, it was not further considered. The In-Sn foil is a mixture of 40% by weight In and 60% by weight Sn. The reactions measured are shown in Table 4.

TABLE 4

RADIOACTIVE PRODUCTS OBTAINED IN FOIL IRRADIATIONS

Reaction	Approximate Activation Energy or Range	Half Life of Product
$_{16}S^{32}(n,p)_{15}P^{32}$	1.8 Mev Threshold	14.3 days
$_{16}S^{34}(n,\alpha)_{14}Si^{31}$	5.0 Mev Threshold	2.6 hours
$_{29}Cu^{63}(n,\gamma)_{29}Cu^{64}$	Entire Spectrum	12.8 hours
$_{29}Cu^{65}(n,p)_{28}Ni^{65}$	3.0 Mev Threshold	2.564 hours
$_{49}In^{113}(n,\gamma)_{49}In^{114m}$	Entire Spectrum	50 days
$_{49}In^{115}(n,\gamma)_{49}In^{115m}$	1.46 ev Resonance	54 minutes
$_{49}In^{115}(n,n')_{49}In^{115m}$	0.4 Mev Threshold	4.5 hours
$_{13}Al^{27}(n,p)_{12}Mg^{27}$	2.5 Mev Threshold	9.5 minutes
$_{13}Al^{27}(n,\alpha)_{11}Na^{24}$	6.0 Mev Threshold	15 hours
$_{11}Na^{23}(n,\gamma)_{11}Na^{24}$	2.85 kev Resonance	15 hours

The foils were irradiated at about 38 watts for about 1 hour. After irradiation, the foil activities, except for $_{49}In^{114m}$, were measured in beta counters. Each beta counter consisted of a 0.5-mm(0.02 in.)-thick anthracene crystal, 5.08 cm(2.0 in.) in diameter, mounted on a 5.08-cm(2.0 in.) photomultiplier tube. In general each foil was counted for 5 or 10 min, starting from a few minutes to several hours after shutdown; counting continued for several days

or until the activity was negligible. Shorter counting times (~1 min) had to be employed for such products as Mg^{27}, which has only a 9.5-min half-life. The reaction product $_{49}In^{114m}$ was gamma-counted using a 5.08-cm x 5.08-cm(2.0 in. x 2.0 in.) NaI crystal.

The foil activities were analyzed by a computer code which fits a sum of exponentials to the raw counting data by a least-squares method. Only one exponential occurs in those foils that, when irradiated, produce only one radioactive product; in most cases, several products, each with a different half line, are generated. The code solves the equation

$$C(t) = \sum_i C_i \, e^{-\lambda_i t}$$

where

$C(t)$ = the measured number of counts per second occurring in the foil at time t after shutdown (sec)

C_i = the number of counts per second at reactor shutdown for the i^{th} decay mode

λ_i = the decay constant for the i^{th} decay mode (sec^{-1}).

The values for C_i derived from this code are then used to obtain absolute saturated activities, S_i, according to the equation

$$S_i = \frac{C_i}{\epsilon (1 - e^{-\lambda_i t})}$$

where

T = the reactor irradiation time (sec) and

ϵ = the detector counting efficiency.

Detector efficiency factors for most of the reaction products were established on the basis of experiments conducted prior to the existence of this program. For some radioactive products, such as $_{14}Si^{31}$, $_{29}Cu^{64}$, and $_{28}N^{65}$, the

efficiency was estimated since no direct calibration had been performed. The absolute saturated activity, S_x, of a single radioactive species is therefore related to the flux in the reactor by the following equation:

$$S_x = \frac{C_x}{\epsilon(1 - e^{-\lambda_x T})e^{-\lambda t}} = V \int \sum_a (E)\varphi(E)\, dE$$

where

C_x = the measured count rate at time t after removal from the reactor

V = the volume occupied by the target material leading to the particular (cm^3) radioactive product

$\sum_a$ = the macroscopic cross section for the specific reaction leading to the radioactive product (cm^{-1})

$\varphi(E)$ = the neutron flux (n/cm^2 sec) and

all other terms have the definition noted above.

IV. RESULTS

A. EXPERIMENTAL RESULTS AND DISCUSSION OF RESULTS

1. Core Material Masses

By using the experimental techniques that were discussed in detail in the preceding section, an extensive series of experiments was undertaken in the heavy-metal reflected, fast-spectrum critical assembly. The experiments were conducted in six basic core compositions, five of which were constructed by adding successively to a base composition, designated Composition 1, Li_3^7N and various refractory metals in the form of foils and wires. The sixth basic core was a power-flattened version of Composition 5.

Thus Composition 1 contained, in the core proper, only Ta, U, and a small amount of Mo. Composition 2 contained all of the above materials plus Li_3^7N. Compositions 3, 4, and 5 consisted of the materials in Composition 2 to which were added cumulatively Hf, more Ta, and W, respectively. In addition to these five primary uniformly-loaded cores, investigations were carried out in several cores which consisted of adjustments, but not total withdrawal, of some of the nonfuel materials making up the primary core. Composition 4, for example, was constructed by adding Ta foil, 0.279-cm(0.110 in.)-diameter Ta wires, and 0.356-cm(0.140 in.) diameter Ta wire to the materials already in Composition 3. The 0.356-cm(0.140 in.)-diameter wire, which was added to the triflute spaces between the honeycomb tubes, could be readily removed; consequently, certain core characteristics that might be expected to depend upon the Ta loading could be conveniently measured in a composition devoid of these wires. This configuration was designated Composition 4A. Similar distinctions were made with the primary Composition 5 core. Initially it contained all available materials, including the 0.356-cm(0.140 in.)-diameter Ta wire; however, when these Ta wires were again removed from this basic core, the configuration was designated Composition 5A. Another, more or less major, alternation in the quantity of materials in Composition 5 concerned the addition of a seventh U rod to the normal six-rod cluster making up the fuel elements in the drums and in the tenth ring. In the primary core, a uniform six-rod cluster was used throughout the reactor. The seventh rod was added to the outer periphery in order to offset reactivity

TABLE 5

MASS OF CORE MATERIALS IN COMPOSITIONS 1, 2, 3, 4, 4A, 5, 5A, 5A(1), 5A(2), 5B AND THE POWER-FLATTENED CORE

Type of Material	Description	Mass (kg)										
		Compositions										Power-Flattened Core
		1	2	3	4	4A	5	5A	5A(1)	5A(2)	5B	
Ta	Fuel Tubes (247)	32.41§										
Ta	Honeycomb Tubes (247)	44.84**										
Ta	Centering Rings	0.86	0.45	0	0	0	0	0	0	0	0	0
Ta	Foil [0.0128-cm(0.005-in.) thick]	0	0	0	21.70							
Ta	0.110-in.-diam wire	0	0	0	9.54						6.57	0
Ta	0.140-in.-diam wire	0	0	0	30.08§§	0	30.08†	0	0	0	0	0
Hf	Foil	0	0	4.12	4.12							
Ta	Foil [0.0051-cm(0.002-in.) thick]	4.64††	0	0	0	0	0	0	0	0	0	0
Steel (1020)*	Wire Wrap	0	0	0.05	0	0	0	0	0	0	0	0
W	Foil	0	0	0	0	0	15.15					
Li_3^7N	Segments	0	10.13									
Mo	Axial Reflector Solid Cylinder (247)	88.40										
Mo	Axial Reflector Eccentric Cylinder (247)	71.94										
Mo	Wire Wraps	0.30	0.30	0	0	0	0	0	0	0	0	0
Mo	Radial Reflectors (6)	399.28										
Mo	Drum Reflectors (6)	246.88										
Mo	Core Filler Segments (10)	11.28										
Mo	Drum Filler Segments (6)	16.55										
Mo	Drum Filler Rods (48)	8.59										
Ta	Pressure Vessel	120.31										
Ta	Drum Absorber Segments (6)	230.63										
U	Uniform Core Loading†	184.16	174.96	174.96	174.96	174.96	174.96	174.96	174.84	171.62	180.54***	174.99***

*The Mo wire wraps lacked sufficient strength to hold the Hf foil in place; consequently, they were replaced by two rings of 0.016-in.-diam mild steel spring wire.
†The uranium masses shown include the nonhydrogenous plastic coating which represents a very small fraction of the total. See Table 14 and Table 45 for exact values.
§64.6% by weight (i.e., 20.94 kg) in core proper
**62.6% by weight (i.e., 28.7 kg) in core proper
††Used in Composition 1 to prevent upper eccentric reflector from falling into core since no Li_3^7N was in place
§§Since these wires extend into the upper and lower reflectors, only 62.8% of this mass (18.90 kg) is in the core
***Nonuniform loading

losses caused by the removal of the seven central fuel elements for purposes of sample worth measurements. This core was designated Composition 5B.

In general, a uniform adjustment in the fuel loading of a core composition did not require a new designation nor did minor fuel adjustment in a few isolated fuel elements. An exception to this policy was made in the case in which, after a several-months time delay, and considerable fuel manipulation, Composition 5A was reconstituted as nearly as possible to its former condition. Since some differences in total uranium loading were inevitable, this core was designated Composition 5A(1). Also, since several types of physics experiments were conducted in a core comprised of the Composition 5A but with a uniform removal of one 0.152-cm(0.498 in.)-diameter U wire, a Composition 5A(2) designation was employed. With the notable exception of Composition 5B and the power-flattened cores, all compositions had a uniform uranium loading through the core, the variation in the mass of any given element not varying from the average by more than ±2 gm out of a total 600 or 700 gm/element. Table 5 summarizes the masses of the various core components making up all of the core compositions.

2. Critical Mass Values

One of the primary characteristics of the various core compositions studied on this program was the critical mass value. A major effort was expended to establish the critical mass in each case to within an uncertainty of ±0.15%. These values are listed in Table 6 for each composition, along with various other parameters, including the total excess reactivity that would exist in the system if all drums were turned fuel-full-in. As indicated in Section III, critical mass values are established either by direct means, that is, by making several uniform fuel adjustments in the core and plotting the resulting excess reactivity values against U mass, or by making a single measurement of the total excess reactivity and using a conversion factor based on some other core. The former method was used for Compositions 1, 2, and 5A(1) and the latter for Composition 3, 4, 4A, 5, and 5A. The conversion factor for the latter cores was 0.51¢/kg as determined in Composition 2. A column entitled, "Change in Reactivity Relative to Composition 2" has been included in the table to provide an indication of the magnitude of the changes in going from Composition 2 to the other compositions where this conversion factor was applied.

TABLE 6

SUMMARY OF CRITICAL MASS DATA

Composition Number	Excess§ Reactivity as Measured (¢)	Excess Reactivity Corrected for Polyethylene (¢)	Core From Which Drum Calculation is Taken	Total Mass of Uranium Loaded Into Core (kg)	Change in Reactivity Relative to Composition 2	Critical Mass (kg)	
						Measured (corrected for poly-ethylene)	Calculated (see References 2 and 4)
1	236.0	222.0	1	184.16	-	179.64	179.8
2	186.0	172.0	2	174.96	0.0	171.39	172.0
3	189.2	175.2	2	174.96	3.2	171.32	171.9
4A*	139.3	125.3	4A	174.96	-46.7	172.32	-
4	94.2	80.2	4	174.96	-91.8	173.23	173.0
5	139.5	125.5	5	174.96	-46.5	172.32	172.6
5A†	193.6	179.6	5A	174.96	+7.6	171.24	-
5B	45.0	31.0	5B	180.54	-	-	-
5A(1)	182.5	168.5	5A(1)	174.84	-	171.75	-
5A(2)	6.86	-7.1	5A(2)	171.62	-		-
	52.0	38.0	Power-flattened core**	174.99	-	174.28	174.5
	134.0	120.0	Power-flattened core††	183.79	-	181.54	-

*All Ta foil and 0.110-in.-diameter Ta wire added; no 0.140-in.-diameter Ta wire
†Composition 5A is identical to Composition 5 except that all 0.140-in.-diameter Ta wire has been removed
§All-drums-in (not corrected for polyethylene)
**For the case in which all drums are full-in
††For the case in which two drums are turned fuel-full-out and four drums are turned fuel-full-in

The reactivity changes that resulted from the addition of 4.12 kg of Hf to Composition 2 was sufficiently small that the drum calibration for Composition 2 was also used to ascertain the total excess reactivity.

Compositions 5A and 5A(1) are identical except for minor uranium loading differences; consequently, their critical mass values should be the same. There is a substantial difference, although the two values fall within ±0.15% of the average.

The critical mass value tabulated for the power-flattened core (with all drums turned to the fuel-full-in position) was based upon two measurements. In once, the total excess reactivity was determined with the normal three-zoned fuel arrangement. In the other, the total excess was measured after one 0.152-cm(0.060in.)-uranium wire was added to each of the 247 fuel elements throughout the core and drums, thus approximately preserving the original power distribution. The total uranium added was 3.237 kg and the reactivity change resulting from this addition was $1.73. These two values yielded a core-averaged worth for fuel of 0.534 $/kg. The excess reactivity value of 38.0¢ would therefore correspond to an excess uranium mass of 0.71 kg. If this quantity of uranium were removed uniformly from the core, a critical mass of 174.28 kg would be obtained. Since the average weight of fuel in each fuel element in Zones 1, 2, and 3 was 628.13, 717.24, and 768.86 gm, respectively, the tabulated critical mass refers to a power-flattened core in which the average mass of uranium in each fuel element in Zones 1, 2, and 3 would be 625.26, 714.37, and 765.99 gm, respectively.

In the case of the power-flattened core in which two drums were turned to the fuel-full-out position, the critical mass was derived by converting the excess reactivity of $1.20 to an excess mass of 2.25 kg through the use of the conversion factor 0.534 $/kg as derived above.

As was described in the Section II, two massive polyethylene boxes were used around Detectors 3, 4, 5, and 6 in order to increase their sensitivity. The box contributed, of course, to the overall system reactivity by scattering neutrons back into the system in an energy range of higher importance. This phenomenon causes the measured excess reactivity to be greater than the value that would exist if no polyethylene were present. The magnitude of this effect was measured in Compositions 1 and 2 and found to be 14¢. A corrected excess reactivity is therefore included in Table 6 in order to indicate the true excess

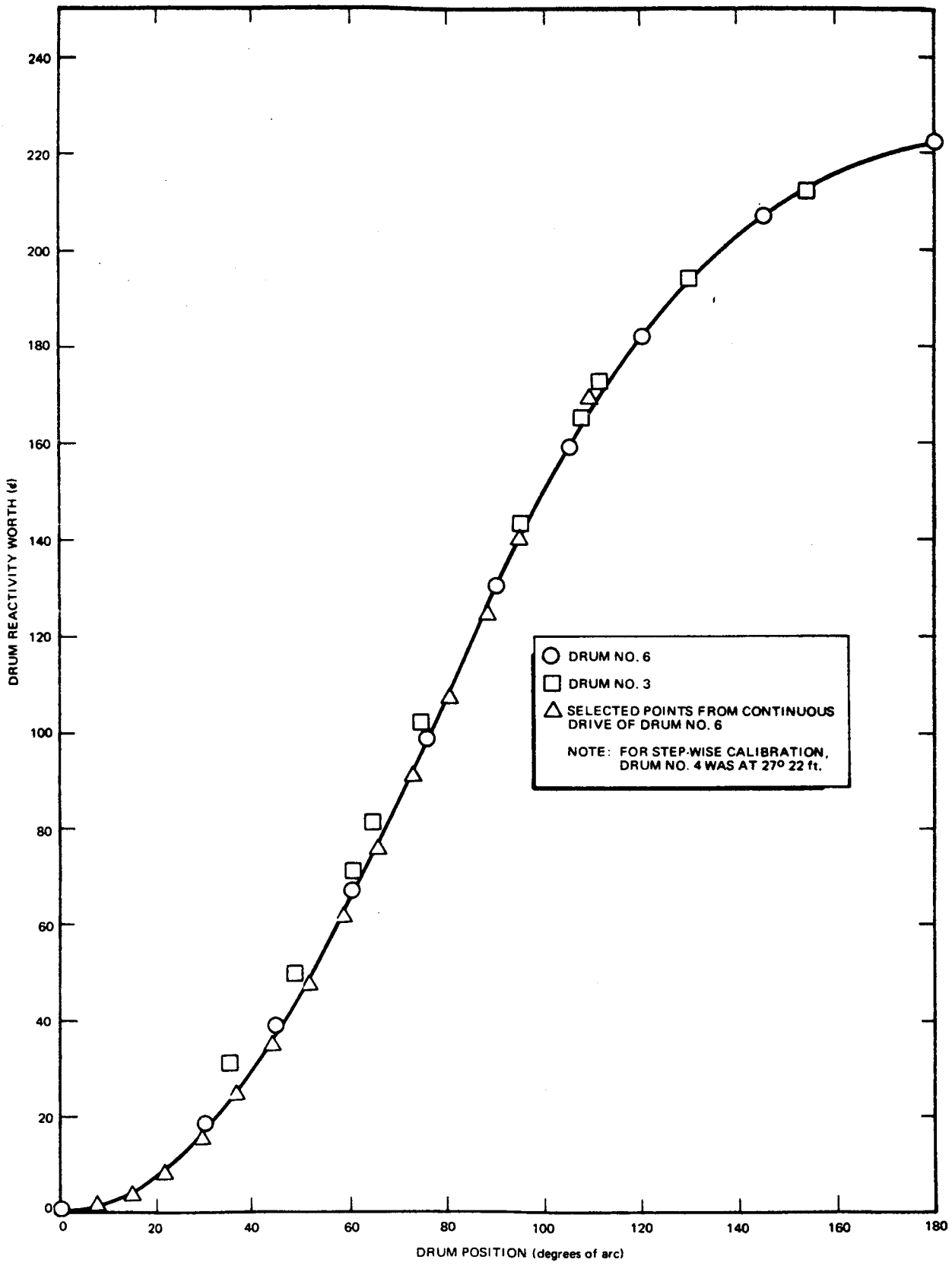

Figure 25. Reactivity Worth of Drums 3 and 6 in Composition 1 (Zero Degrees of Arc = Fuel Full-In)

reactivity of the isolated system. The worth of the polyethylene is assumed to be the same for all compositions. Other materials in the vicinity of the critical assembly, including the walls of the cell in which the reactor is located and the table on which the critical assembly is built, also contribute to the measured excess, but these are expected to be of much smaller magnitude and were not evaluated. Critical mass values, shown in Table 6, have been corrected for the effect of the polyethylene boxes. Also shown are the calculated values for the critical masses of some of the compositions. These calculations were performed by NASA and are reported in References 2 and 4. The agreement is quite good, although the calculations include a "bias factor" that was derived from prior analyses of some other, quite different, compact fast assemblies. This bias factor is of the order of 3.6% in k for Composition 1 and 3% for the others. Since the calculations were conducted and reported prior to the performance of the specific experiment to which they applied, they contain no adjustments or normalizations relative to the present experimental results in regard to the critical masses.

Although one correction to the experimentally derived critical mass data was required and made (i.e., the polyethylene boxes), other ones, which pertain to the hydrogen contained in the Kel-F coatings on the fuel, to the hydrogen and oxygen impurities in the Li_3^7N, and to a few other minor chemical impurities, have not. These corrections could be derived experimentally, but were not part of this phase of the program. In Composition 1, for example, where the total mass of hydrogen contained in the Kel-F coating on the fuel is of the order of 1.3 grams (see Table 14 in Appendix A), a very crude estimate of the increase in the critical mass that would occur if the hydrogen were not present is 0.1 kg. This estimate is based on the assumption that the specific worth (i.e., worth per unit mass) of hydrogen is about 80 times that of U^{235} (see Table 15 in Appendix B).

3. Drum Calibrations

A calibration over all or most all of the drum travel was conducted in most of the critical assembly compositions, the only exceptions being Compositions 3 and 5A(2). The results of these studies are shown in Figures 25 through 31, inclusive. All of these calibrations were performed by the stepwise method as discussed in the section on experimental techniques.

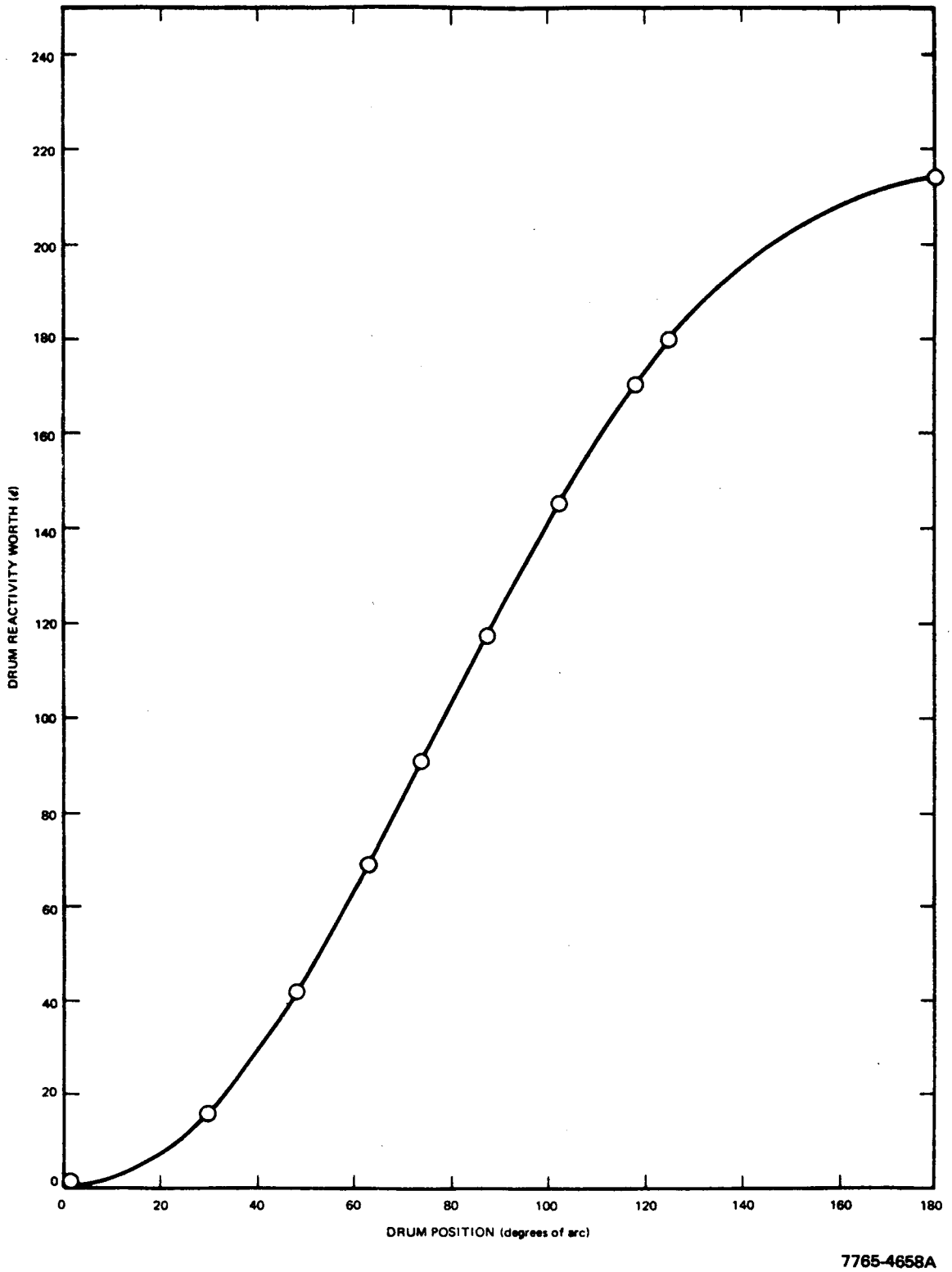

Figure 26. Reactivity Worth of Drum 6 in Composition 2
(Zero Degrees of Arc = Fuel Full-In)

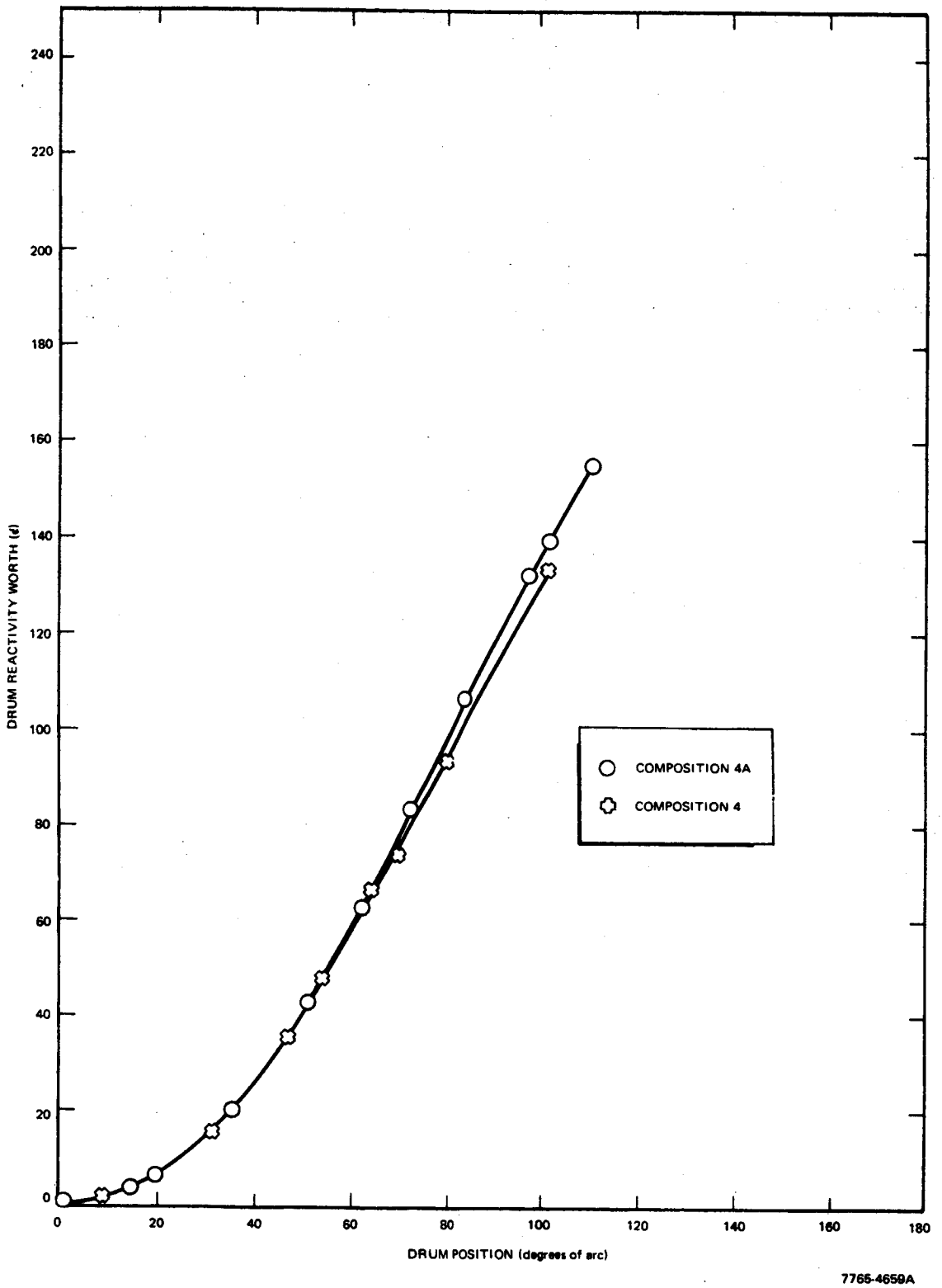

Figure 27. Reactivity Worth of Drum 6 in Compositions 4 and 4A (Zero Degrees of Arc = Fuel Full-In)

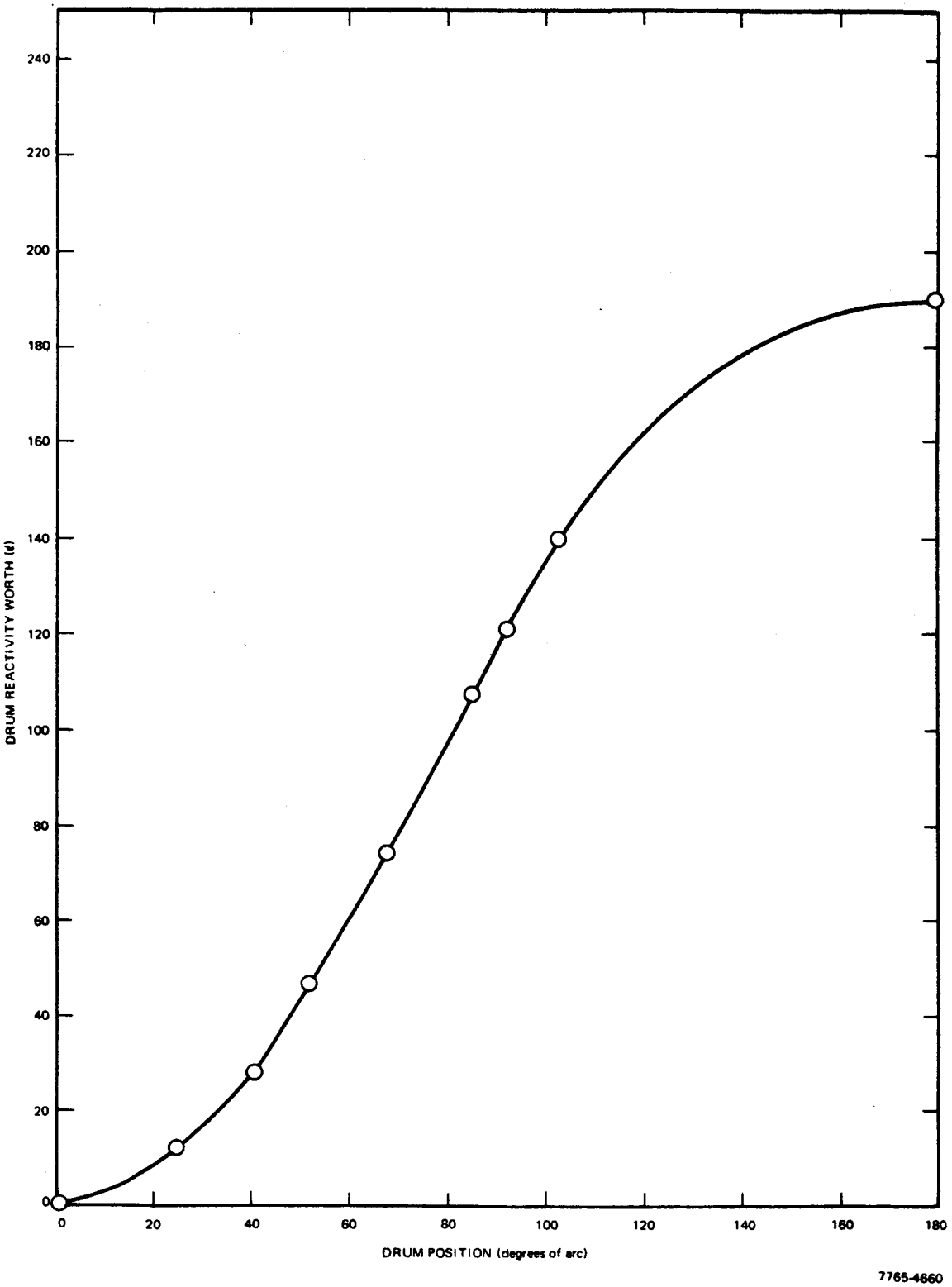

Figure 28. Reactivity Worth of Drum 6 in Composition 5
(Zero Degrees of Arc = Fuel Full-In)

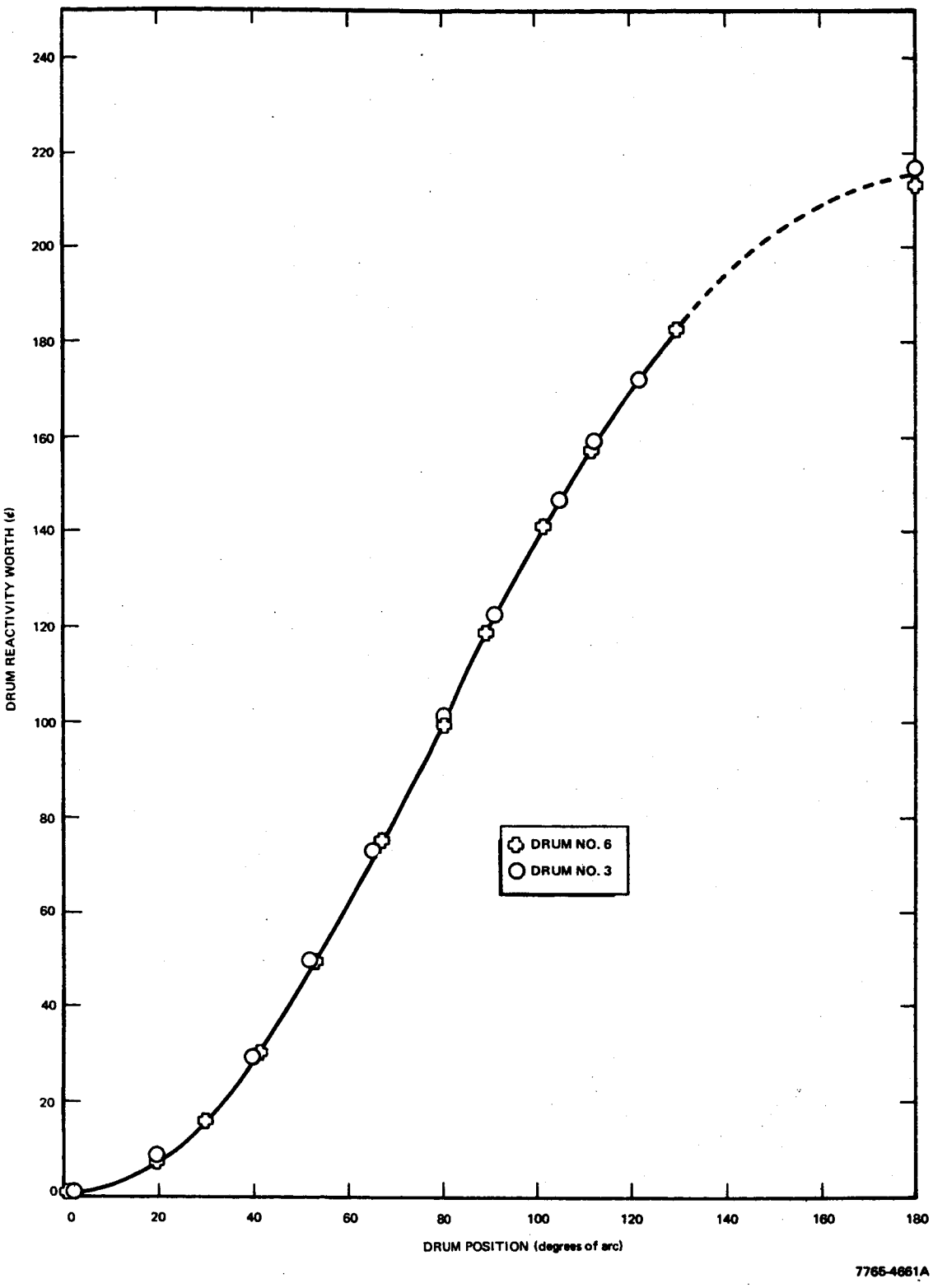

Figure 29. Reactivity Worth of Drums 3 and 6 in Composition 5A (Zero Degrees of Arc = Fuel Full-In)

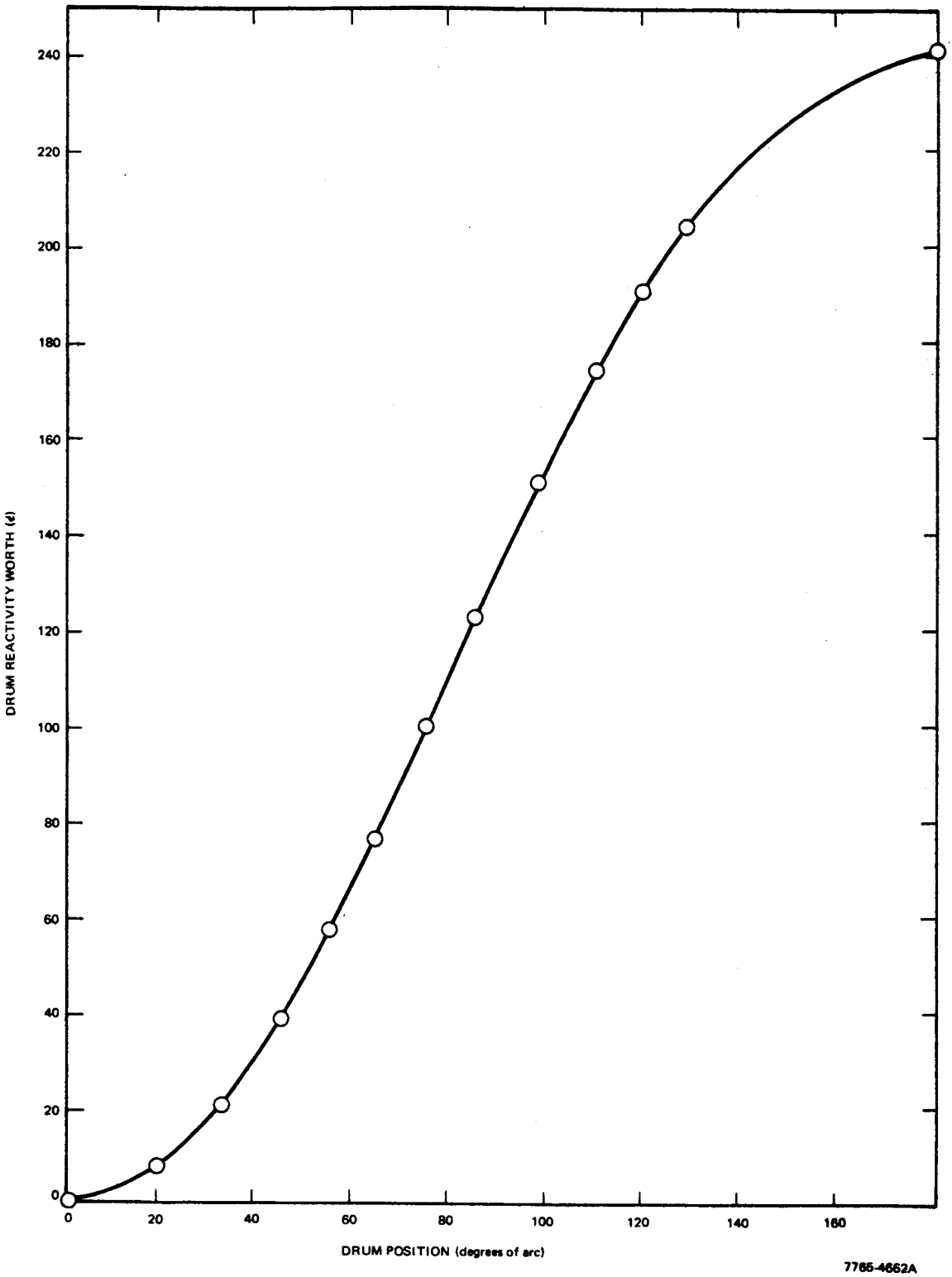

Figure 30. Reactivity Worth of Drum 6 in Composition 5B (Zero Degrees of Arc = Fuel Full-In)

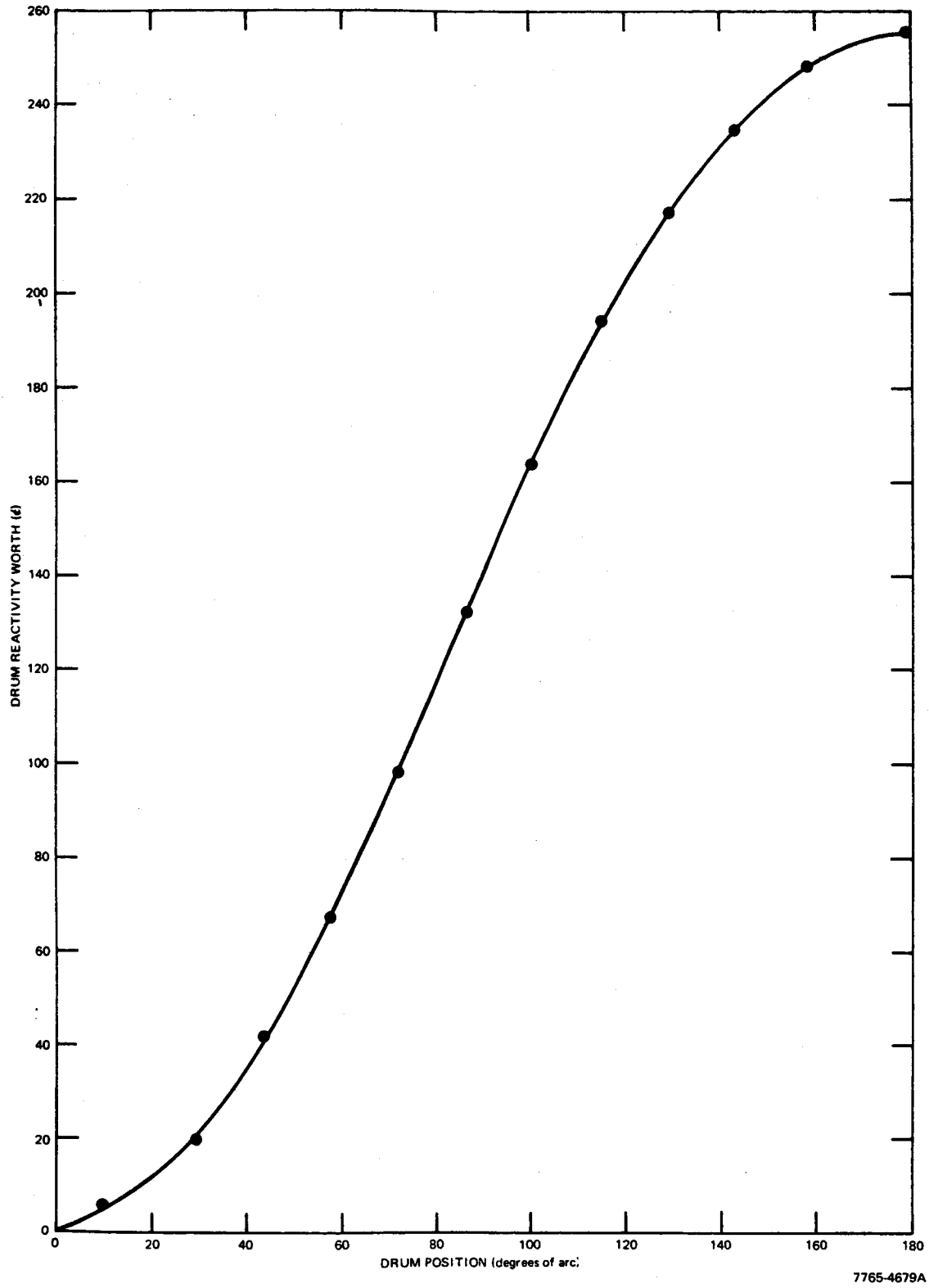

Figure 31. Reactivity Worth of Drum 6 in the Power-Flattened Core (Zero Degrees of Arc = Fuel Full-In)

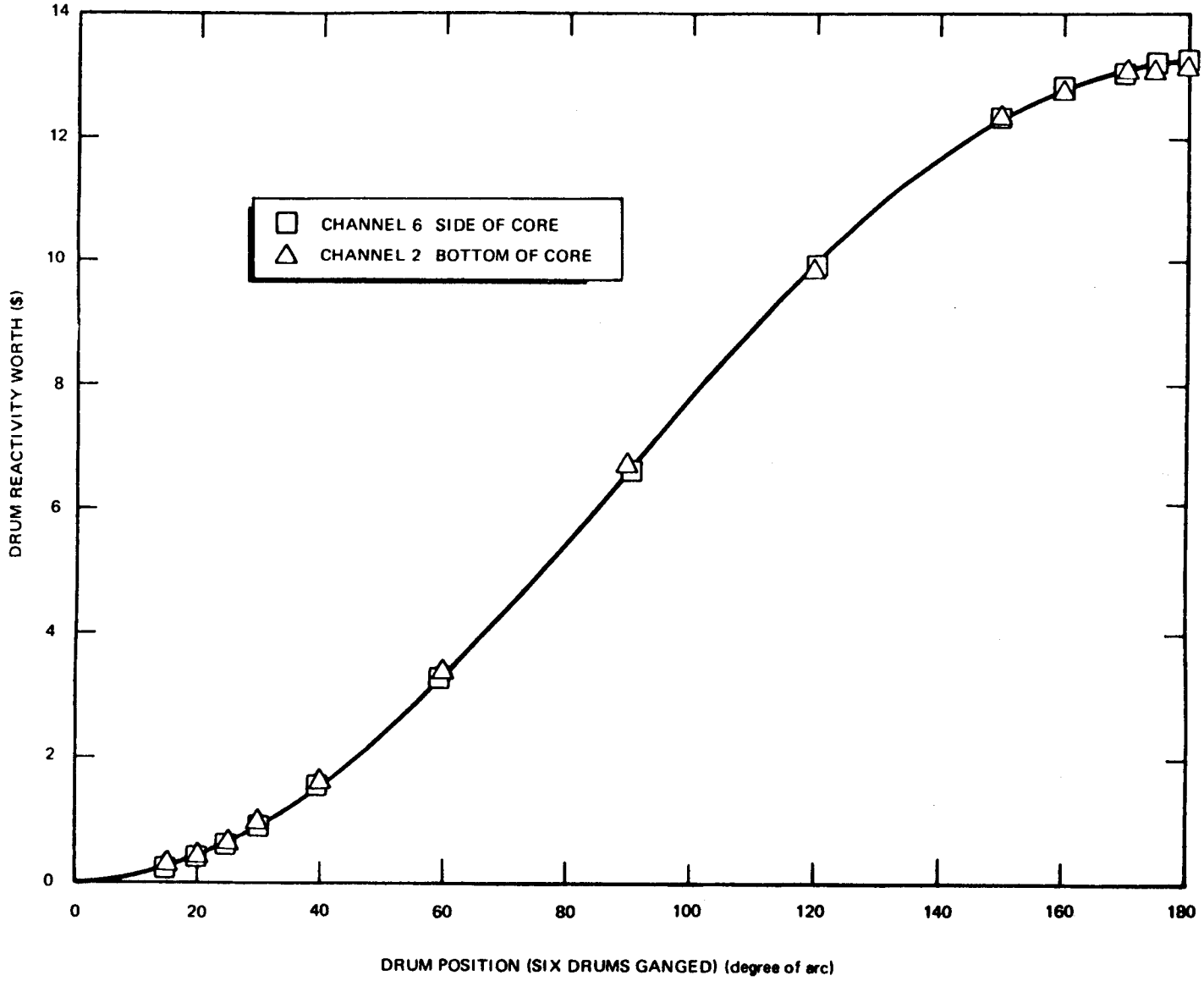

Figure 32. Reactivity Worth of All Drums Ganged in Composition 5A (Zero Degrees of Arc = Fuel Full-In)

A measurement of the worth of all six drums ganged was conducted in Composition 5A(1) and is shown in Figure 32. The inverse counting method was employed in this case and was normalized on the basis of a worth of -$1.44 for all drums banked to 40 degrees of arc. The worth of all drums as determined in terms of Channel 6, the current detector, and in terms of Channel 2, a pulse detector, gave virtually identical results as can be seen. The total worth is about -$13.45 and is roughly in agreement with the worth of a single drum (-$2.15) in Composition 5A(1) multiplied by six (i.e., -$12.90).

Drum reactivity worths for the power-flattened core, as obtained by the inverse counting and inverse-kinetics techniques, are presented in Table 7 and in Figure 31. Since the relative fuel loading in the outer periphery of the core was increased, the drum worths also became somewhat larger, the worth of all drums increasing, for example, from $13.45 to $17.66. In view of previously noted difficulties concerning systematic uncertainties, those results except for single drums, derived by the inverse-kinetics method should only be considered as rough indications (±20%) of the magnitude of the actual reactivity. As can also be seen in the table, the worth of all drums with the Ta absorber segments removed is 83% of that with the absorbers in place.

TABLE 7

CONTROL DRUM WORTHS IN POWER-FLATTENED CORE

Drum Number	Worth ($)	
	Inverse Multiplication	Inverse Kinetics
6	2.21	2.57
6 (Ta Absorber Removed)	-	2.43
3 and 6	4.83	5.62
2, 3, 4, 5, and 6	13.40	16.00
All Drums	17.66	20.60
All Drums With Ta Removed	14.73	17.14

4. Neutron Energy Spectra

The energy distributions of neutrons in the center of Compositions 1, 2, and 5 were measured by means of the proton-recoil spectrometer discussed in the

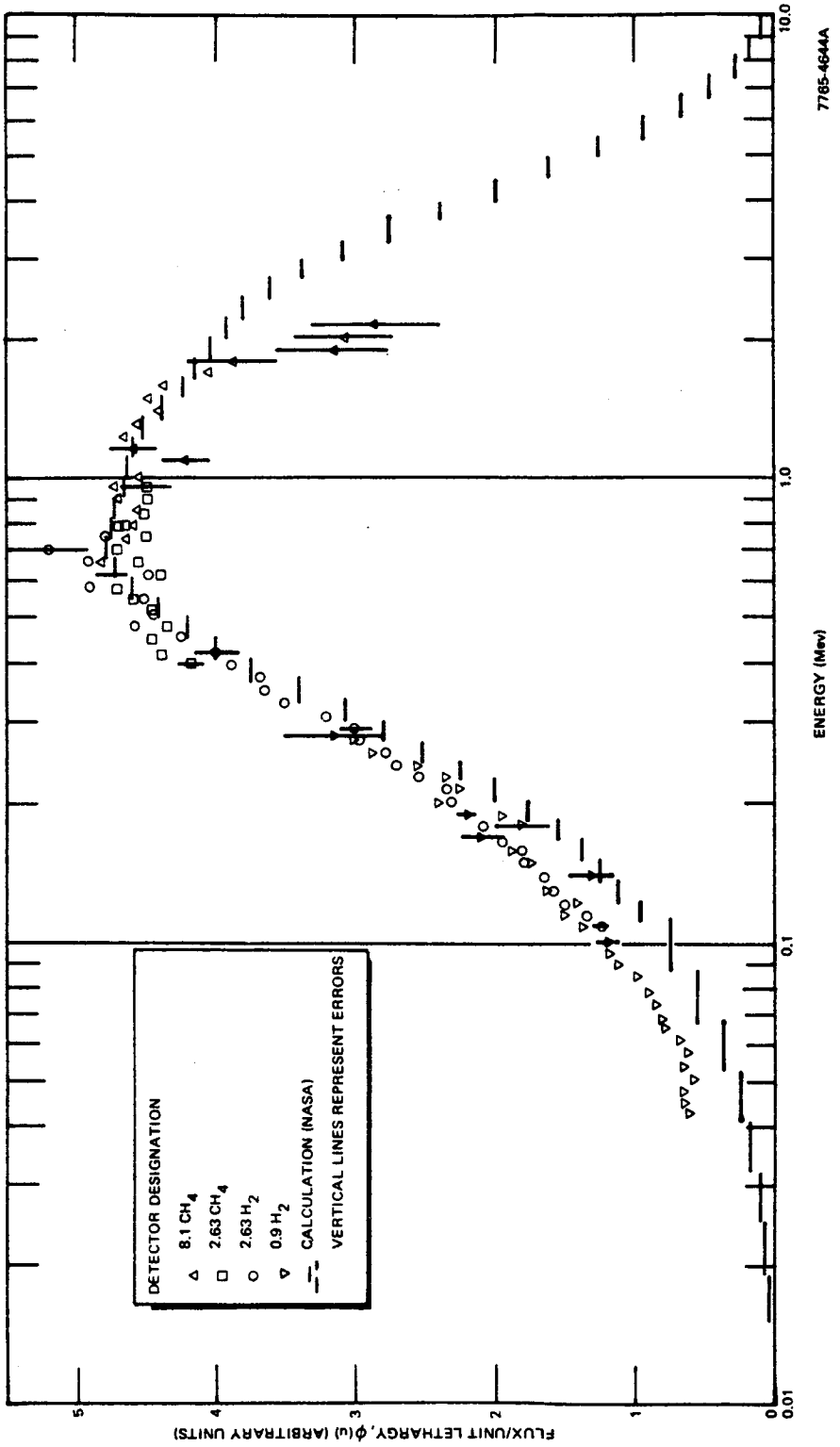

Figure 33. Neutron Spectrum in the Center of Composition 1

section on experimental techniques and are presented graphically in Figures 33, 34, and 35. In Compositions 1 and 2, the measurements extended from about 40 kev to about 2.2 Mev and involved one-parameter analysis only. In Composition 5, a two-parameter analysis was performed and yielded data down to about 20 kev. The existence of Li_3^7N in the reactor is clearly indicated by the spectrum dip at 250 kev in Compositions 2 and 5. This dip is the result of the scattering resonance in Li^7 at that energy.

The solid horizontal bars in Figures 33, 34, and 35 represent the group fluxes as calculated by NASA.[2,3] The calculated spectrum for Composition 1 appears to be slightly harder than measured. In Compositions 2 and 5, the agreement is better.

The results of a selected series of foil activation measurements from which integral flux values can be obtained are presented in Table 8. Some of the results, those indicated by a double asterisk, are based upon estimated values for the counting system efficiency.

5. Core Material Worths by Substitution

Although the measurement of the reactivity worths of various core materials as a function of position was only an incidental experiment in Compositions 1 and 5A, some information about the reactivity change that occurs upon removing the fuel cluster from a standard fuel element and replacing it with a void and other materials can be of use in core operation as well as in the reference core design. These experiments are performed by first noting the drum position for criticality with the core composed of standard fuel elements. One fuel element, the one in Position 4-1 for example, is then removed and replaced by an element identical except that no uranium is present. The new position of the control drum for achieving criticality is found, and the reactivity change is established by noting these two drum positions on the control drum worth curve. This difference is the worth of the fuel cluster in that position relative to a void. If a sample is then inserted into that fuel element in the position normally occupied by the fuel, its worth relative to a void can be ascertained. By using several core positions, preferably along a radial line, the worth of the various materials can be determined as a function of this radial position. The result of a series of experiments of this type are shown in Table 9. It should be noted that these experiments are

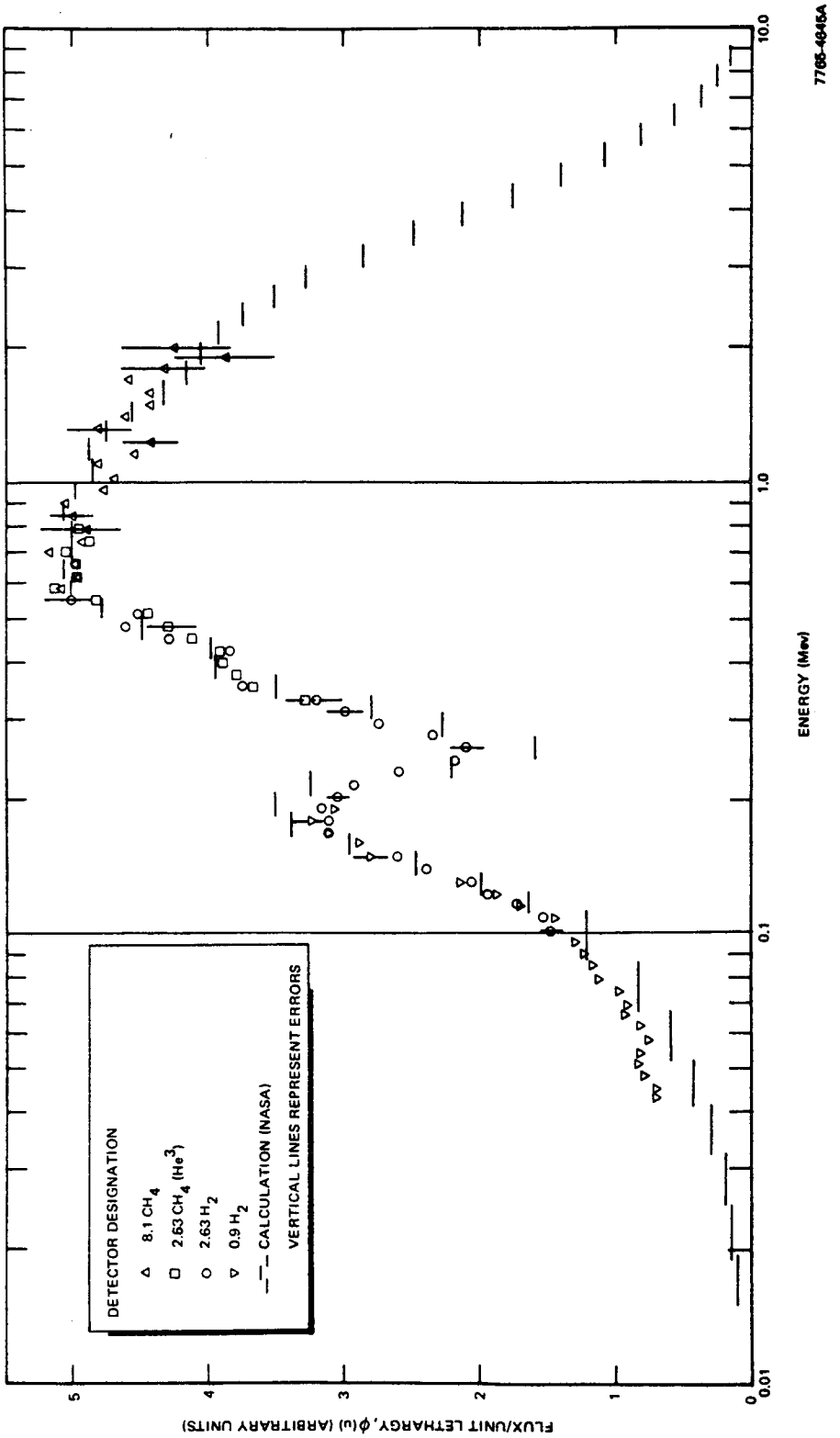

Figure 34. Neutron Spectrum in the Center of Composition 2

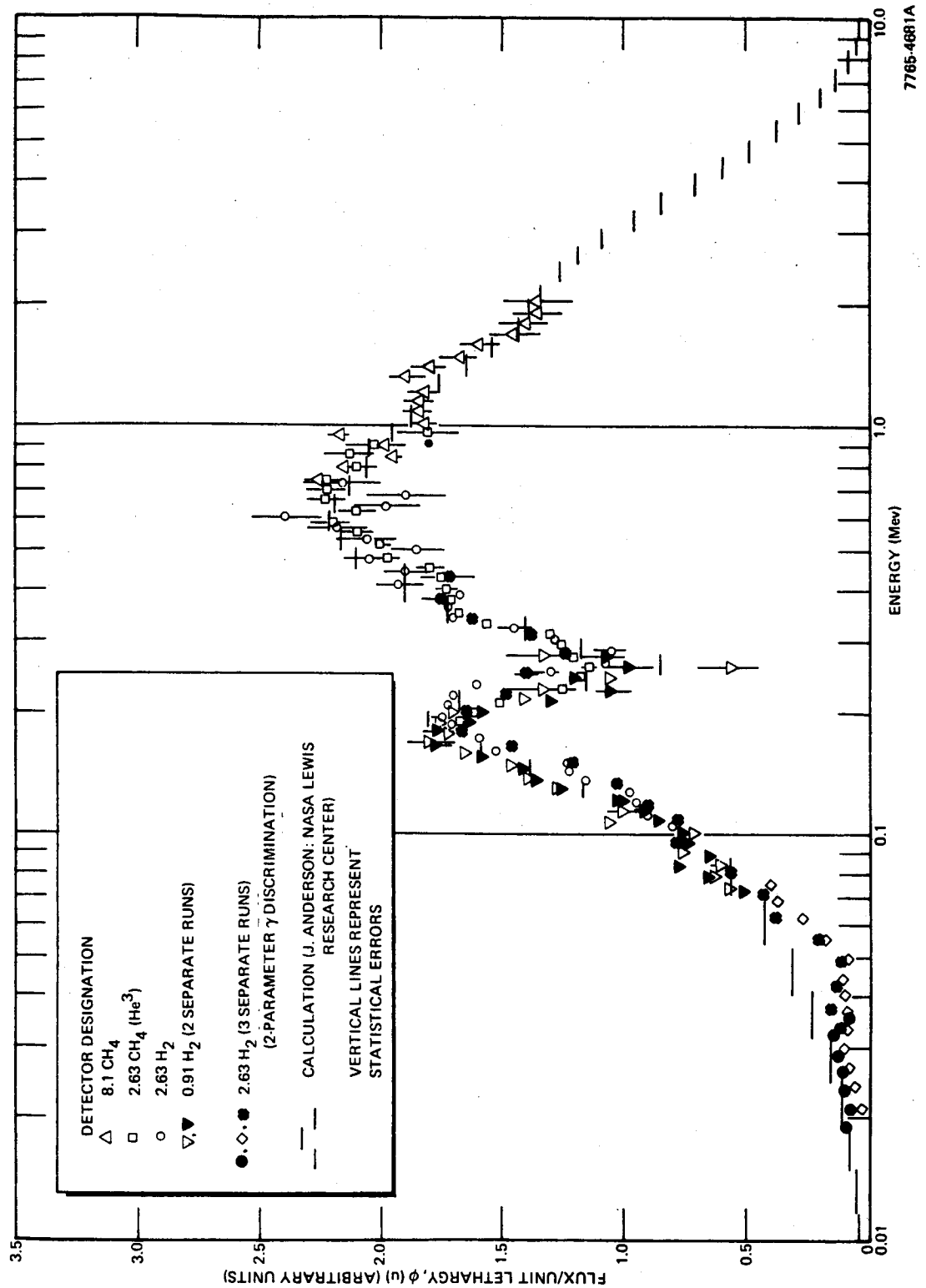

Figure 35. Neutron Spectrum in the Center of Composition 5

TABLE 8

FOIL ACTIVATION DATA FOR COMPOSITIONS 1, 2, and 5

Foil	Foil Volume (cm^3)	Foil Mass (gm)	Reaction	$T_{1/2}$	Composition 1 Saturated Activity		Composition 2 Saturated Activity		Composition 5 Saturated Activity	
					(dis/sec)	σ(%)	(dis/sec)	σ(%)	(dis/sec)	σ(%)
Na_2CO_3	0.391	0.586†	$_{11}Na^{23}(n,\gamma)_{11}Na^{24}$	15 hr	-	-	8.08×10^3	0.38	1.00×10^4	0.29
Al	0.224	0.561	$_{13}Al^{27}(n,\alpha)_{11}Na^{24}$	15 hr	1.10×10^4	0.37	8.86×10^3	0.25	8.98×10^3	0.19
S	1.80	3.05	$_{16}S^{32}(n,p)_{15}P^{32}$	14.3 days	2.78×10^6	0.10	2.36×10^6	0.07	2.36×10^6	0.066
Cu	0.0485	0.383	$_{29}Cu^{63}(n,\gamma)_{29}Cu^{64}$	12.8 hr	$4.47 \times 10^{4**}$	0.30	$4.87 \times 10^{4**}$	0.19	$5.87 \times 10^{4**}$	0.14
In-Sn*	0.0376	0.266	$_{49}In^{115}(n,n')_{49}In^{115m}$	4.5 hr	$1.52 \times 10^{6**}$	0.16	$1.36 \times 10^{6**}$	0.13	$1.37 \times 10^{6**}$	0.15
In-Sn*	0.0376	0.266	$_{49}In^{115}(n,\gamma)_{49}In^{116m}$	54 min	2.62×10^5	0.12	2.69×10^5	0.04	3.08×10^5	0.036

*Foil consists of an alloy of Sn and In (40 wt % In, 60 wt % Sn). Mass is that of foil; therefore, mass of In is 0.106 gm.
†Total mass of Na_2CO_3 pellet. Mass of Na is 0.254 gm.
§σ = Standard Deviation
**Efficiency factor, ϵ, estimated for this reaction product.

TABLE 9

REACTIVITY WORTHS OF VARIOUS MATERIALS
IN COMPOSITIONS 1 AND 5A

Material	Form	Mass (gm)	Worth (¢)	Position
Composition 1				
U	7 fuel rods plus fuel wire	745.23	+52.0	0-1
U	7 fuel rods plus fuel wire	745.97	+50.2	2-1
U	7 fuel rods plus fuel wire	744.33	+45.0	4-1
U	7 fuel rods plus fuel wire	746.60	+38.7	6-1
U	7 fuel rods plus fuel wire	745.09	+29.7	8-1
U	7 fuel rods plus fuel wire	745.17	+17.7	10-1*
Ta	0.515 in. diameter by 14.767 in. long	845.68	-1.0	0-1
Ta	0.515 in. diameter by 14.767 in. long	845.68	-0.5	4-1
Ta	0.515 in. diameter by 14.767 in. long	845.68	+5.0	8-1
Ta	0.515 in. diameter by 14.767 in. long	845.68	+5.0	10-1*
Mo	0.515 in. diameter by 14.767 in. long	517.49	+4.0	0-1
Mo	0.515 in. diameter by 14.767 in. long	517.49	+6.5	10-1*
Be	0.515 in. diameter by 14.767 in. long	93.96	+10.7	0-1
Be	0.515 in. diameter by 14.767 in. long	94.96	+7.3	10-1*
Composition 5A				
U	6 fuel rods plus wire	708.63	+46.3	4-1
U	6 fuel rods plus wire	708.36	+36.6	6-1
U	6 fuel rods plus wire	707.74	+26.1	8-1
U	6 fuel rods plus wire	708.09	+18.8	10-1*

*The reactivity values quoted for Position 10-1 have a systematic error in the sense that the values would be expected to change if all drums were in the fuel full-in position. In these determinations, Drum No. 6, which is adjacent to Position 0-1, was banked to achieve criticality. See page 111 of text.

TABLE 10
SUMMARY OF MEASURED REACTIVITY WORTHS OF CORE-LENGTH SAMPLES IN THE CENTER OF COMPOSITION 5-A

Principal Element/ Isotope in Sample	Sample* Mass (gm)	Reactivity† Worth (¢)	Specific Reactivity Worth (¢/gm x 10^{-3})	Principal§ Impurity	Mass of Principal Isotope/ Element (gm)	Reactivity Worth Correction for Impurities (¢)	Specific Reactivity Worth Based on Mass of Principal Isotope/gm (¢/gm x 10^{-3})
Li	188.341	-6.228	-33.068	G	188.32	-6.23 ±0.12	-33.07 ±0.61
Li^6	147.133	-128.280	-871.864	Li^7	139.36	-128.56 ±1.32	-922.50 ±9.51
Li^7	168.952	+6.175	+36.549	G	168.72	±6.18 ±0.07	36.65 ±0.41
$Li_3{}^7N$	278.810	+5.491	+19.694	$Li_2{}^7O, Li^7OH$	266.60	+5.18 ±0.07	19.44 ±0.26
Be	656.243	+44.797	+68.263	G	651.97	+44.80 ±0.41	68.71 ±0.63
BeO	1022.287	+37.896	+37.070	G	1021.11	+37.90 ±0.34	37.11 ±0.33
B^{10}	379.351	-272.041	-717.122	B^{11}, C, O_2	325.51	-273.54 ±2.76	-840.33 ±8.49
C	605.087	+18.690	+30.888	G	604.13	+18.69 ±0.15	30.94 ±0.25
Nb	2840.510	-1.605	-0.565	Zr	2800.88	-1.74 ±0.08	-0.62 ±0.03
Mo	3624.810	+4.695	+1.295	G	3610.31	+4.73 ±0.07	1.31 ±0.02
Hf	4615.408	-25.723	-5.573	Zr	4467.72	-25.92 ±0.30	-5.80 ±0.07
Ta	5920.999	-44.941	-7.590	G	5876.59	-44.94 ±0.49	-7.65 ±0.08
W	6764.653	-8.988	-1.329	G	6762.82	-8.99 ±0.14	-1.33 ±0.02
Re	2619.330	-34.368	-13.121	G	2609.40	-34.37 ±0.39	-13.17 ±0.15
U^{235}	5013.84	+388.234	+77.432	U^{238}	4670.14	+386.68 ±3.85	82.80 ±0.82
U^{238}	6559.203	+30.378	+4.631	U^{235}	6544.77	+29.61 ±0.27	4.52 ±0.04
Small Void Capsule	358.610	-4.103	-	-	-	-	-
Large Void Capsule	303.065	-4.143	-	-	-	-	-

*The values in this column represent the total mass of the sample exclusive of cladding, but include all "impurities."

†Measured worths of sample without corrections for impurities, isotope difference, etc.

§The symbol "G" represents general impurities in the sample, no one of which usually exceeds a few hundred parts per million, but taken collectively may add up to a few tenths of a percent. (See Tables 44 and 46 in Appendix B.)

not as accurate as those involving the sample changer. For one thing, the reactor must be shut down, an element substitution performed, and then the reactor restarted in order to make the measurement, a manipulation that involves an uncertainty of the order of ±1¢. Moreover, the worths are determined by reference to a drum worth curve that cannot be "read" to much better than 0.5¢. The values quoted in the table have, therefore, an uncertainty of the order of ±1¢; consequently, the worth of a Ta rod in Positions 0-1 and 4-1 is statistically zero. It is, moreover, important to note that the drum used for these experiments was Number 6. This drum is therefore adjacent to Sample Position 10-1 and can influence its worth. This effect has been measured for U^{235} and has been shown to cause the measured worth of the sample to be low by about 7%.

6. Sample Reactivity Worths

The reactivity worths of a total of sixteen sets of large samples were measured in Composition 5A and 5B by means of the sample changer mechanism and are tabulated in Tables 10 and 11. As previously indicated there are seven identical full core-length samples in each set available for measurements. The sets are composed of the materials listed in the lefthand column of each table.

In the normal procedure for conducting reactivity worth measurements, the sample, clad in a 0.0254-cm(0.010 in.)-wall Mo tube with Mo end-caps, is placed in the upper part of the sample holder tube (see Figure 66 of Appendix C). The lower part of the holder tube contains only an empty Mo tube (with Mo end caps) which is identical to the cladding around the sample. Thus, when the sample changer mechanism is driven up or down, the net effect is to replace in the core the full-core length sample material by a full core-length void. Under ideal circumstances, the reactivity change concomitant with the exchange of the sample with a void could yield the worth of the sample, exclusive of cladding. However, on the one hand, the upper and lower halves of the sample holder tubes are not exactly identical in mass and, on the other, the motion of the table and pedestals on which the sample holder tubes are mounted affects the reactivity. Thus, a so-called "void" run is made in which an empty Mo tube (with end-caps) is placed in the upper portion of the sample holder tube. Replacing the upper void by the lower void results in a reactivity change of the order of 3 or 4¢, the major portion of which is caused by an increase in neutron reflection from the table on which the

TABLE 11
SUMMARY OF MEASURED REACTIVITY WORTHS OF CORE-LENGTH SAMPLES IN THE PERIPHERY OF COMPOSITION 5-A

Principal Element/ Isotope in Sample	Sample* Mass (gm)	Reactivity† Worth (¢)	Specific Reactivity Worth (¢/gm x 10^{-3})	Principal§ Impurity	Mass of Principal Isotope/ Element (gm)	Reactivity Worth Correction for Impurities (¢)	Specific Reactivity Worth Based on Mass of Principal Isotope/gm (¢/gm x 10^{-3})
Li	161.412	+4.390	+27.197	G	161.39	+4.36 ±0.07	+27.00 ±0.43
Li^6	126.114	-38.827	-307.872	Li^7	119.45	-38.96 ±0.30	-326.19 ±2.49
Li^7	145.864	+7.966	58.267	G	145.66	+7.97 ±0.07	+54.71 ±0.49
$Li_3{}^7N$	238.980	+10.360	43.351	$Li_2{}^7O, Li^7OH$	228.51	+9.90 ±0.09	+43.32 ±0.38
Be	562.494	+35.039	+62.292	G	558.83	+35.01 ±0.32	+62.64 ±0.57
BeO	876.246	+38.848	+44.335	G	875.24	+38.82 ±0.36	+44.35 ±0.41
B^{10}	325.158	-83.151	-255.724	B^{11}, C, O_2	279.01	-85.24 ±0.88	-305.52 ±3.10
C	518.646	+23.471	+45.254	G	517.83	+23.44 ±0.21	+45.26 ±0.40
Nb	2434.722	+22.611	+9.286	Zr	2400.76	+22.18 ±0.20	+9.24 ±0.08
Mo	3106.980	+27.855	+8.965	G	3094.55	+27.82 ±0.25	+8.99 ±0.08
Hf	3956.064	+12.524	+3.166	Zr	3829.47	+11.35 ±0.10	+2.96 ±0.03
Ta	5075.142	+10.136	+1.997	G	5037.08	+10.10 ±0.08	+2.01 ±0.02
W	5798.274	+25.476	+4.394	G	5796.70	+25.44 ±0.23	+4.39 ±0.04
Re	2245.140	-0.912	-0.406	G	2236.63	-0.94 ±0.07	-0.42 ±0.03
U^{235}	4306.26	+126.022	+29.265	U^{238}	4011.07	+124.41 ±1.25	+31.02 ±0.31
U^{238}	5622.174	+30.733	+5.466	U^{235}	5609.80	+30.10 ±0.28	+5.37 ±0.05
Small Void Capsule	307.38	-2.744	-	-	-	-	-
Large Void Capsule	259.77	-3.277	-	-	-	-	-

*The values in this column represent the total mass of the sample exclusive of cladding, but include all "impurities."

†Measured worths of sample without corrections for impurities, isotope difference, etc.

§The symbol "G" represents general impurities in the sample, no one of which usually exceeds a few hundred parts per million, but taken collectively may add up to a few tenths of a percent. (See Tables 44 and 46 in Appendix B.)

sample holder tubes are mounted. The net worth of the sample is therefore obtained by subtracting the reactivity effect of the sample-void interchange from the reactivity effect of the void-void interchange, due regard being given to the direction of motion and the sign of the effect. The reactivity values obtained after the subtraction is made are tabulated in Column 3 of Tables 10 and 11. The magnitude of the void correction that has been used is shown in the row labeled "large void capsule."

It is frequently of interest to ascertain the reactivity worth of pure materials or isotopes. Since some samples frequently contain significant impurities and often cannot be made isotopically pure without very special efforts, corrections must be made to the measured quantitites. As an example, the so-called U^{235} sample actually consists of uranium enriched to about 93% in the U^{235} isotope. The U^{238} sample, on the other hand, contains only 0.22% U^{235}. Thus, the measured worth of the U^{238} sample can be used to carry out a first order correction for the U^{238} in the U^{235} sample. Similarly, the Li^{6} sample can be corrected for the Li^{7} content on the basis of the worth of the isotopically pure Li^{7} sample. The $Li_3{}^{7}N$ sample is actually 95.62% $Li_3{}^{7}N$, the balance being largely $Li_2{}^{7}O$ and $Li^{7}OH$. Corrections can be made for the Li^{7} that is not in the form of $Li_3{}^{7}N$ and for oxygen (using Be and BeO samples to determine the worth of oxygen. Finally, adjustments can be made for general impurities which collectively can add up to perhaps several thousand parts per million in a given sample. The latter adjustments are generally made on the assumption that the impurities have a reactivity worth about equal to that of an equivalent mass of molybdenum.

Corrections of the above type have been made on the samples measured in these cores and are shown in Column 7 of each table. The specific worth given in Column 8 is therefore the corrected worth divided by the "pure" sample mass.

The chemical and isotopic purity values which have been used in these corrections are discussed in Appendix B. The overall uncertainty for the sample reactivity worths corrected for the "void" effect and the isotopic and chemical impurities is seen to be typically of the order of ±0.08¢ for measurements of less than 5¢ and of the order of 1 or 2% for measurements greater than 5¢.

For peripheral worth measurements, six of the identical samples in a given set are used simultaneously, one in each of six sample holder tubes. One sample holder tube is mounted on each of the six peripheral pedestals located on the sample changer table. The six pedestals are located in such a way that one holder tube passes through the core at each of the Positions 10-1, 10-2, 10-3, 10-4, 10-5, and 10-6. In order to measure the worth, all six samples are driven into or out of the reactor (whichever leads to a decrease in system reactivity) simultaneously and replaced by the void.

For central worth measurements, all seven identical samples are used simultaneously, being driven by the sample changer into or out of the core in Positions 0-1, 1-1, 1-2, 1-3, 1-4, 1-5, and 1-6.

All peripheral worth measurements apply to Composition 5A, although adjustments in the fuel loading in one or more of the central seven fuel elements were made as required to permit all drums to be driven fuel-full-in before the samples were moved. This procedure prevented the control drums from influencing the worth values relative to a geometrically well-defined core. For central worth measurements, where the influence of control-drum position is negligible, all control drums were generally banked equally in order to achieve a level power before the samples were moved. Reactivity losses due to the removal of the seven central standard fuel elements, along with the contained fuel cluster, were partically offset by adding fuel rods to the fuel bundles in elements in Rings 9 or 10 or in the control drums. Most, but not all, of the large samples were measured with one extra fuel rod in each of the 11 fuel elements in each of the six drums (a total of 66) and one in each of the elements in the 10th ring. This configuration, as already noted, was designated Composition 5B. It was shown, by means of drum motion, that this nonuniform loading did not affect the measured worth of the sample; consequently, the results are applicable to Composition 5A where the peripheral measurements were made. A separate designation was given to Composition 5B since several ancillary experiments pertaining to properties of the reactor as a whole were conducted.

Two types of reactivity samples (U^{235} and Li^{7}) were segmented into several sections along their lengths so that, by the removal of one segment, a void would be created within a particular zone of the sample column. The Li^{7} sample was

made up of five segments which, when stacked end-to-end, made up a full core-length sample. The worths in Tables 10 and 11 refer to a full core-length configuration. Since the Li^7 material had to be sealed, each segment was encapsulated in a short Mo tube which had Mo end-caps. Thus, the amount of Mo cladding contained in end-caps was increased relative to the standard sample. A so-called "small void capsule" measurement was therefore conducted in which a set of five empty Mo capsules were placed in the upper half of the sample holder tube. The reactivity change associated with this void arrangement was somewhat less than that of the standard void, as would be expected as a result of the increased amount of Mo present.

In Table 12, the reactivity changes associated with creating a void zone at the center, at the top, and at a point half-way in between (designated "mid-void") in these samples are tabulated. The column labeled "void mass" is the difference in mass between the full-length sample column (see Tables 10 and 11) and the sample column with the void in the places noted. The column labeled "void worth" is the total worth of the full length sample stack minus the worth of the sample with the void. Finally, the column labeled "specific worth" represents the reactivity changes that would result from the removal of a unit mass of material if it were removed uniformly from the zone occupied by the void. Thus, a decrease in reactivity that is greatest at the core center, as expected, would be encountered upon removal of material.

A series of measurements of the reactivity worths of a group of small, nearly infinitely dilute samples placed in the center of Composition 5A are given in Table 13. For these experiments, all fuel element positions except 0-1 were filled with standard fuel elements. In Position 0-1, a special element of the same type used in large sample worths was placed. The oscillator tube, holding one small sample at a time, passes through this element and serves to introduce and remove the sample on a periodic basis.

A short series of small-sample oscillator measurements was also conducted in the three-zones, power-flattened core. These measurements utilized a U^{235} sample, a polyethylene foil [5.10 cm(2.008 in.) by 4.11 cm(1.620 in.) by 0.024 cm (0.0096 in.)] coiled into a tubular form [5.10 cm(2.008 in.) high by 0.024-cm (0.0096 in.)-wall] and placed in a V-1 type of capsule, and a cylindrical polyethylene sample 1.283 cm(0.505 in.) in diameter by 5.38 cm(2.118 in.) high also placed

TABLE 12

SUMMARY OF MEASURED VOID REACTIVITY WORTHS

	Central Measurements			Peripheral Measurements		
	Void* Mass (gm)	Void† Worth (¢)	Specific Reactivity (m¢/gm)	Void* Mass (g)	Void† Worth (¢)	Specific Reactivity (m¢/gm)
Void Displacing Fuel						
Void location relative to core midplane (cm)						
Top +11.73 to +18.75	877.98	-55.0 ±5.0	-62.6 ±5.7	760.14	-16.9 ±1.6	-22.2 ±2.0
Mid +3.51 to +11.01	1052.85	-99.0 ±4.8	-94.0 ±4.6	896.67	-31.1 ±1.5	-34.7 ±1.7
Center -3.51 to ++3.51	877.98	92.7 ±4.8	-105.6 ±5.5	760.14	-30.5 ±1.5	-40.1 ±2.0
Void Displacing Li^7						
Void location relative to core midplane (cm)						
Top +11.38 to +18.76	34.32	-2.14 ±0.07	-62.5 ±2.0	29.55	-1.32 ±0.07	-44.5 ±2.4
Mid +3.84 to +11.22	32.16	-1.00 ±0.07	-31.1 ±2.2	27.86	-1.65 ±0.07	-59.1 ±2.6
Center -3.69 to +3.69	34.61	-0.53 ±0.07	-15.2 ±2.0	29.54	-1.90 ±0.07	-64.4 ±2.4

*Mass of material displaced by void
†Worth relative to displaced material

TABLE 13

REACTIVITY WORTH OF SMALL SAMPLES IN COMPOSITION 5A AND THE POWER-FLATTENED CORE

Sample	Core Number	Mass§ (gm)	Worth (¢ + 0.007)	Specific Worth (10^{-3} ¢/gm)
Li^6	5A	0.258	-0.165**	-639 ± 27
Li^7	5A	0.290	-0.012	-41 ± 24
B^{10}	5A	0.816	-0.946	-1159 ± 8.6
Hf	5A	6.564	-0.093	-14.2 ± 1.1
Ta	5A	9.918	-0.148	-14.9 ± 0.7
W	5A	9.208	-0.066	-7.2 ± 0.8
U^{235}	5A	6.002	+0.517	+86.1 ± 1.2
U^{238}	5A	11.217	+0.065	+5.8 ± 0.6
Re	5A	7.962	-0.156	-19.6 ± 0.9
Thin Polyethylene	pf††	0.4723	+0.191	+404 ± 15
Cylindrical Polyethylene	pf	6.3180	+1.852	+293 ± 1.1
U^{235}	pf	6.002	+0.470	+78.3 ± 1.2
V-1*	5A	2.677	-0.010	-3.7 ± 2.6
V-2†	5A	4.680	-0.009	-1.9 ± 1.5

*V-1 designates the stainless-steel capsule used to contain all samples except Li^6, Li^7, B^{10}, and Re.

†V-2 designates the stainless-steel capsule used to contain the Li^6, Li^7, B^{10}, and Re samples. This capsule has an inner stainless-steel sleeve on which the samples are deposited.

§Measured mass of sample. No correction has been made for impurities.

**This value may be in error, since, upon inspection of the sample after the measurement, some chemical activity with the atmosphere was evident due to a leak in the capsule. The total weight gain in the sample was 0.0409 gm.

†† pf — power flattened core

in a V-1 type capsule. These results are given in Table 13. As would be expected, the worth of the U^{235} has been reduced at the center by the power flattening procedure.

The column labeled "worth" is the net worth of the sample material after correction for the stainless-steel capsule.

7. Fuel Element Rotation Experiments

In the normal fuel element orientation, the plane passing through the honeycomb tube axis and the fuel tube axis is perpendicular to the plane passing through the axis of the core and the axis of the honeycomb tube. In Composition 5, the drum position for criticality was measured first after all 247 fuel elements were turned so that the fuel cluster in the fuel tube was displaced by 0.0508 cm(0.020 in.) toward the center of the core, then measured again after the elements were turned so that the fuel cluster in the fuel tube was displaced by 0.0508 cm(0.020 in.) away from the core center. A change of reactivity, relative to the null position, of +22.5¢ occurred in the first operation and -25.3¢ in the second. In Composition 1, a reactivity change of -14¢ was observed upon turning the cluster outward.

8. Neutron Lifetime

A measurement of the neutron lifetime in Composition 5A was made by performing a Rossi-α measurement to obtain ℓ/β_e and using a calculated value for β_e. In this measurement, the detector was located outside the core and reflector at the midplane. The Rossi $-\alpha$ measurement yielded a value for ℓ/β_e of 4.73×10^{-6} sec. For β_e 0.0067, a value for ℓ of 31.7×10^{-9} sec is obtained, somewhat low compared with the expected value of 41×10^{-9} sec (see Appendix D). The result for ℓ/β_e of 4.13×10^{-6} sec as determined by the pulsed neutron method yields a value for ℓ of 27.6×10^{-9} sec. This result is not considered reliable, however, since the associated value of α_c did not yield good results when applied to reactivity measurements.

A more sophisticated analysis of the data can be performed based on the work of Kistner.[18] The above quoted value of 31.7×10^{-9} sec is obtained by peeling off the exponentially decaying response function that exists after about Channel 35 of the data of Figure 23. The resulting decay curve, which is also exponential in character, provides a rough indication of the core decay constant. Kistner has

developed a two-region (core and reflector) decay theory which may be more appropriate in this instance and in which the two decay constants are considered, the time behavior of the pulse being related to $A_1 e^{\alpha_1 t} + A_2 e^{\alpha_2 t}$. The quantities, A_1, A_2 α_1 and α_2 can be obtained from the decay curve of Figure 23. A value for the core lifetime can then be derived. Kistner's method results in a derived lifetime of about 42×10^{-9} sec, assuming $\beta_e = 0.0067$.

9. Reactivity Worth of a Void in the Outer Six Peripheral Locations

It is of interest from a calculational standpoint to know the reactivity effect of removing the fuel cluster from the fuel elements in locations 10-1, 10-2, 10-3, 10-4, 10-5, and 10-6. This effect was measured in several ways in Compositions 5A and 5A(1). One result, which is somewhat approximate, was based upon substituting for the six outer fuel elements a set of elements in which the fuel cluster was not present. By this technique, a reactivity change of -121.1¢ was obtained. It is approximate in that (1) reactivities were determined by "reading" drum worth curves, (2) a reactor startup, shutdown, fuel manipulation, and new startup had to be conducted, (3) three of the empty elements did not contain $Li_3{}^7N$ segments, and (4) only one drum was banked to make the reactor critical in both cases. Another method involves the use of the sample changer and a sample holder tube which is located so that a void exists in the outer six positions. If the reactor excess reactivity is reduced in one or more of the center seven positions so that all drums can be driven to fuel-full-in, the excess reactivity can be measured and used, in conjunction with known worths for fuel in the center of the reactor, to obtain a worth value for the void created in the outer periphery of the core. This method yielded a worth for the six voids of -128.1¢. A repeat of the same experiment at a later date produced a statistically identical value of -127.8¢. The latter two values are considered to be the most reliable since all shortcomings inherent in the former procedure were avoided.

10. Power Distribution Measurements in Composition 5

A series of power distribution measurements applicable to the case in which all drums were in the fuel-full-in position in Composition 5 were conducted by placing an 0.066-cm(0.026 in.)-diameter by 37.47-cm(14.75 in.)-long uranium wire in each of the 27 fuel elements making up a one-twelfth sector of the core. In all cases, three wire segments, each nominally 1.27-cm(0.50 in.) long, were

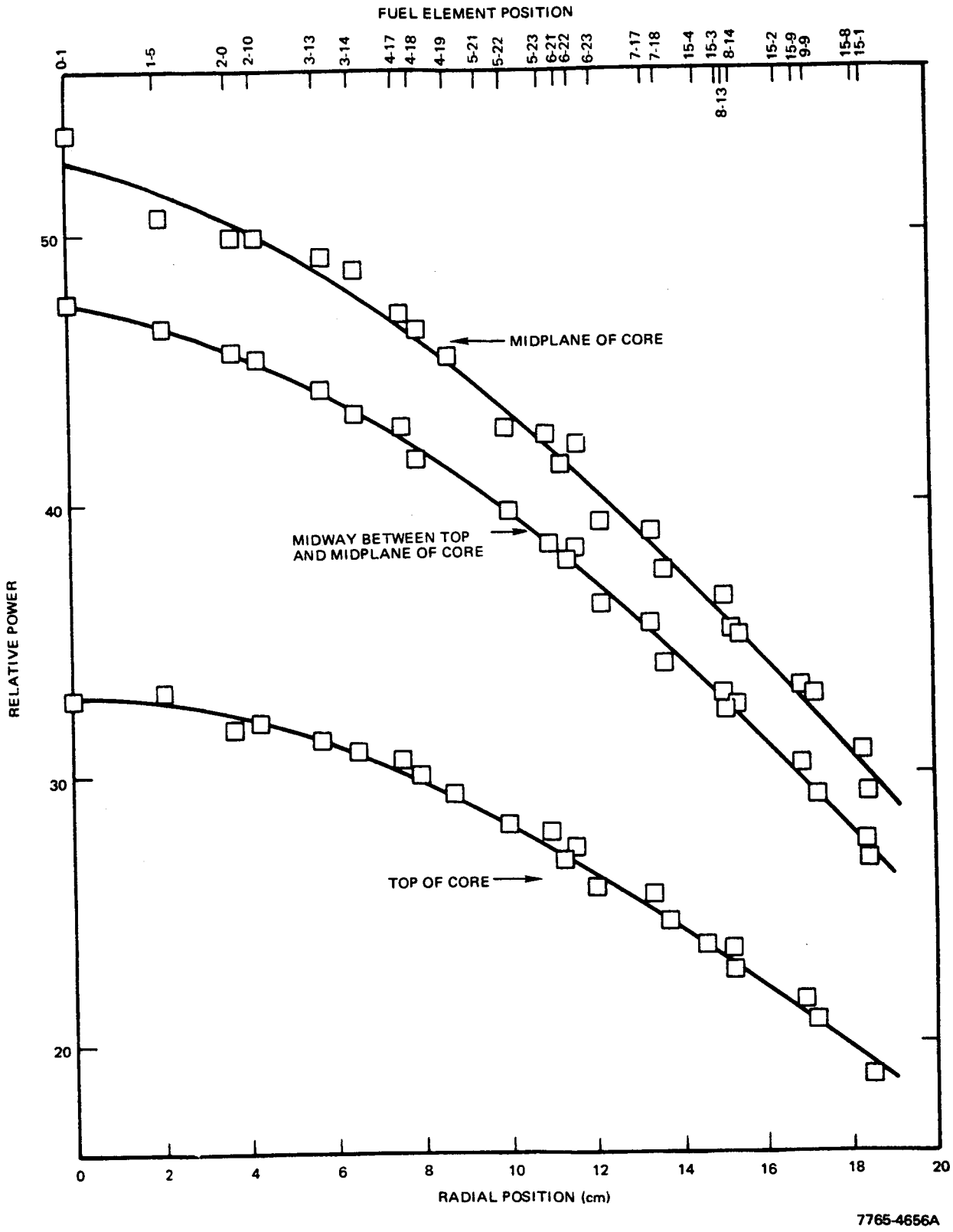

Figure 36. Radial Power Distribution – Composition 5

removed from each full-length wire, one from the top, one from the center, and one from a zone halfway in between these two points. These segments were counted and then analyzed in the manner described in the section on Experimental Techniques. A plot of the results in the radial direction at each axial plane is given in Figure 36. The scatter in the data appears to be the result of the fact that all radial planes emanating from the core axis are considered equivalent. Considerably smoother curves are obtained if only the segments lying in a given radial plane are plotted – the plane, for example, containing the axis of the core and the axis of the drum. This trend implies that there is some asymmetry in the power distribution, the asymmetry depending upon which radial plane is being followed. The fuel element location of each of the three segments is indicated at the top of the graph.

The results obtained for the power distribution in the axial direction primarily over the upper half of the core in each of the four elements (0-1, 5-23, 15-8, and 9-9) are shown in Figure 37. In this case, the upper half of each wire was completely segmented into nominally 1.27-cm(0.50 in.)-long segments. A few selected segments of identical size were also removed from the lower half of the wire. The relative power as a function of axial position appears, on the basis of these data, to show some unexpected peaking at the core midplane at all four radial positions. Above about 3.81 cm(1.5 in.), the data appear, however, to be quite consistent, and the selected segments (indicated by an "X") that were taken from the lower half of the core yield produced results in very good agreement with the upper half. This power peaking was assumed, on the basis of its position, to be related to the two parting planes in the fuel, planes that are associated with the junction of a 15.24-cm(6.0 in.)-long fuel rod and a 22.27-cm(8.767 in.)-long rod. Since the fuel bundle is composed of these rods placed end-to-end, first with a long rod on top and then on the bottom, the cluster has two parting planes. These planes would occur 3.51-cm(1.38 in.) above and below the midplane.

In a similar manner, an axial plot of the power distribution was made on the basis of segmenting the wires in Positions 0-1 and 8-10 over their entire lengths. Over the central 12.07-cm(4.75 in.) region of each wire, 0.635-cm(0.250 in.) segments were removed, and above and below this region 1.27-cm(0.50 in.) segments were removed. These segments were counted and the data were analyzed to yield the results plotted in Figure 38. A small asymmetry in the overall flux shape

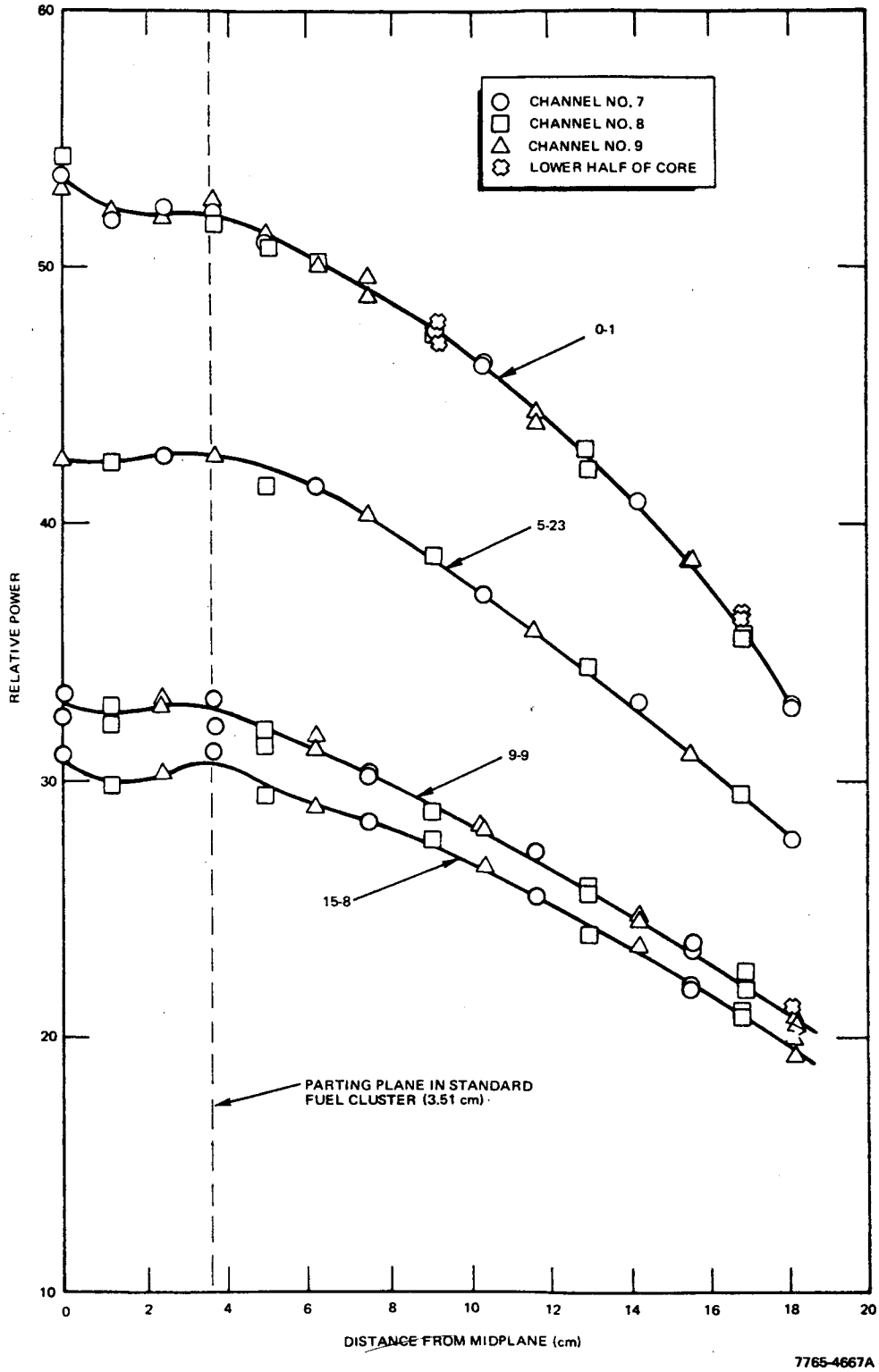

Figure 37. Axial Power Distribution – Top Half – Composition 5

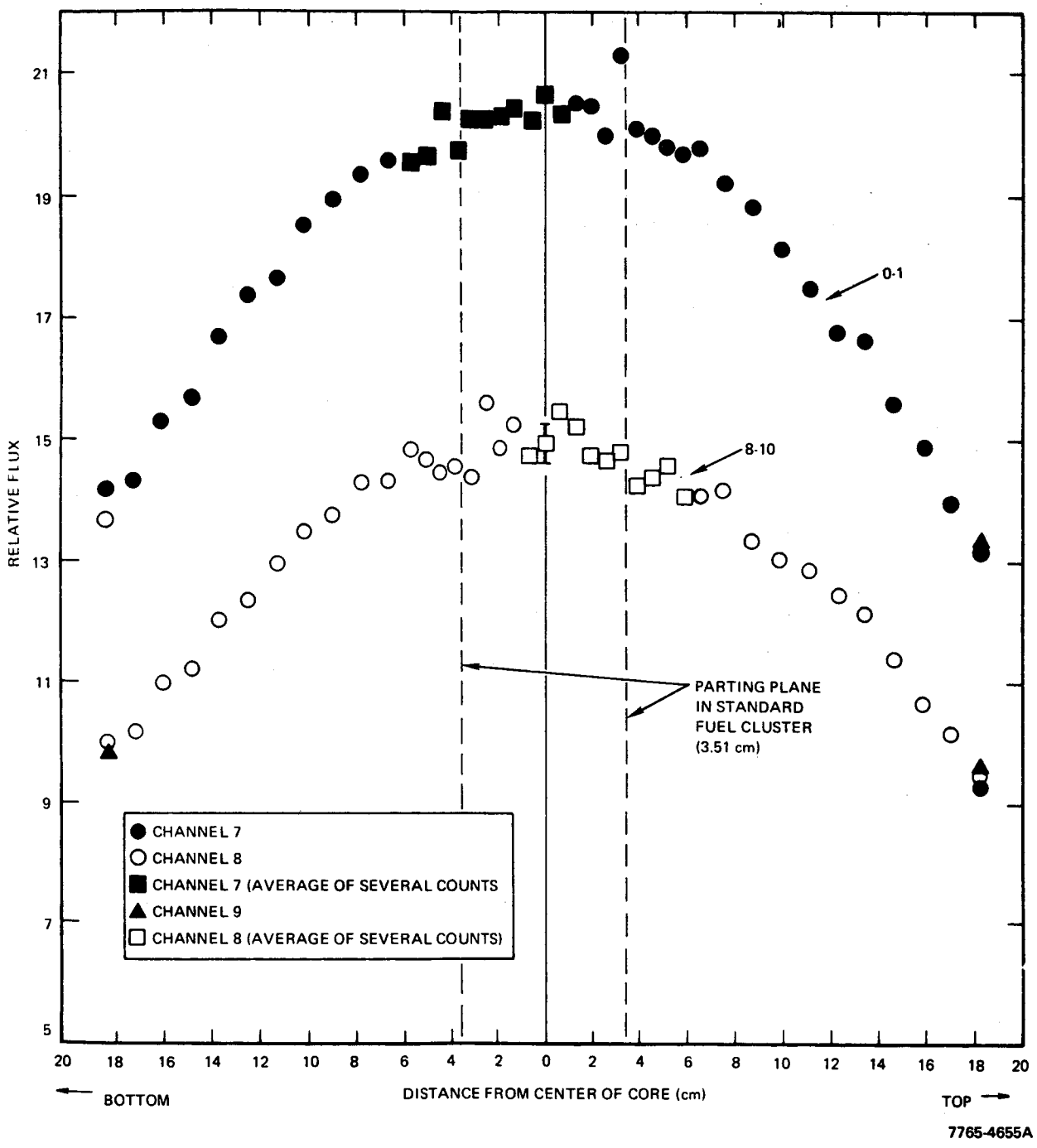

Figure 38. Axial Power Distribution – Composition 5

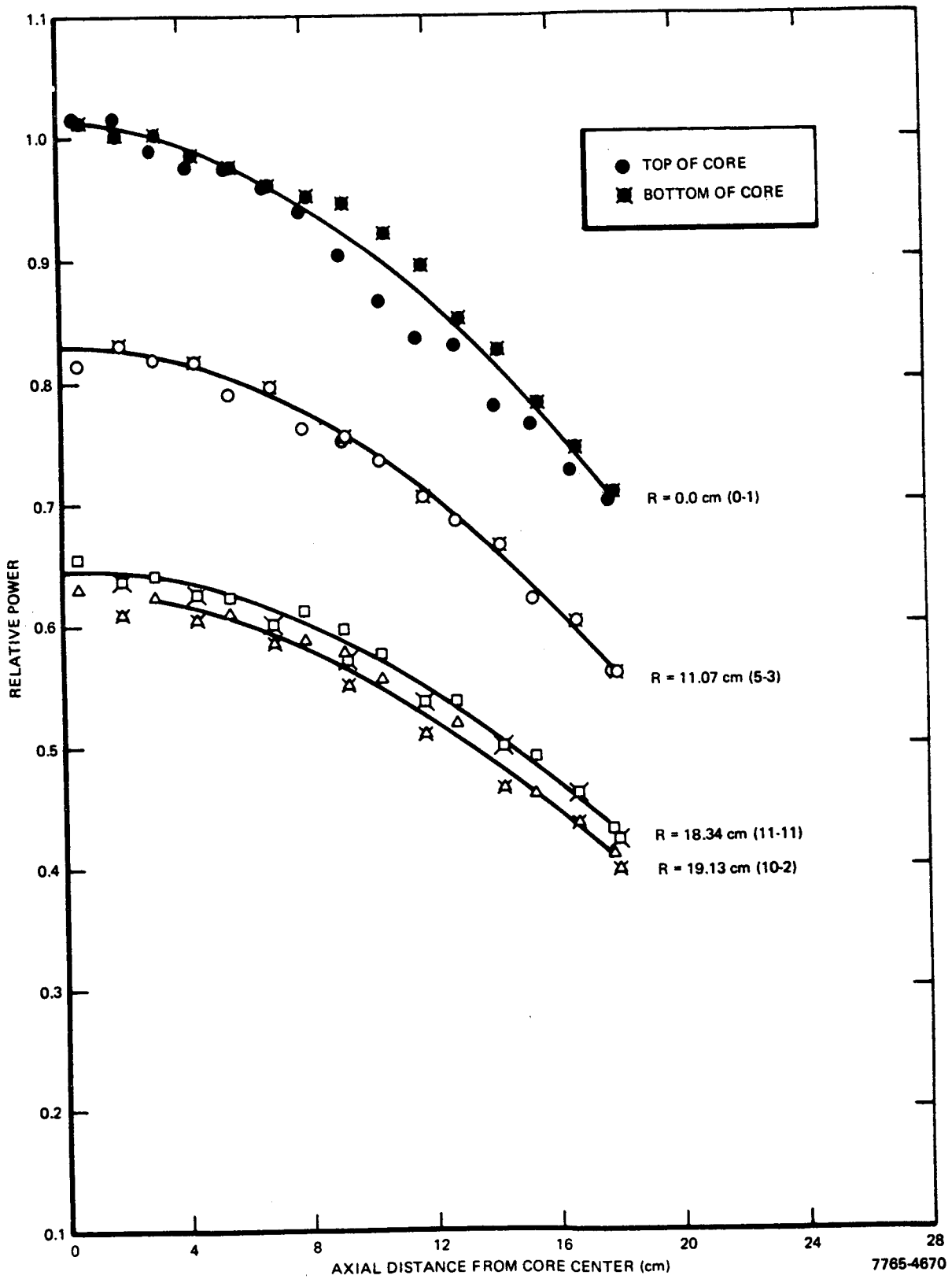

Figure 39. Axial Power Distribution – Power-Flattened Core

that is not obvious in Figure 37 can be seen; it is attributed to backscatter from the massive steel plate on which the critical assembly is built. The rather wide scatter in the points is caused by large statistical counting uncertainties due to the small size of the wire segments in the central zone of each wire.

In order to test the hypothesis that the peaking near the core midplane (see Figure 37) is associated with the parting plane in the fuel cluster, the fuel cluster in the fuel element in Position 8-10 was altered in such a way as to place all of the 22.27-cm(8.767 in.)-long fuel rods on the top end of the element and all of the 15.24-cm(6.0 in.)-long rods on the bottom. Although a somewhat smoother power distribution may be discernible over the top half of the wire in Position 8-10, the counting statistics preclude a positive identification of a parting plane effect.

Similar graphical representations of the power distribution in the power-flattened core are shown in Figures 39 and 40 for the case in which the three drums adjacent to the one-twelfth sector are in the fuel-full-in position. In the case of the axial power distribution, the entire uranium wires in Fuel Elements 0-1, 5-3, 11-11, and 10-2 were segmented into nominally 1.27-cm(0.50 in.) lengths and counted, thereby providing a check on the axial asymmetry noted above. In this case, no such phenomenon was observed.

A second series of power distribution measurements in the power-flattened core are shown in Figures 41 and 42. In these experiments, one uranium wire was irradiated in each of 40 fuel elements located in a one-sixth sector of the core. The three control drums adjacent to the sector were rotated out such that, if all six drums were rotated to this position, the reactor would be 1.5% subcritical. In order to establish the axial distribution, each of the uranium wires in 0-1, 5-8, 12-10, 10-2, and 10-3 were cut over their entire lengths into nominally 1.27-cm(0.50 in.) segments and counted. Again, the power distribution appears to be symmetrical.

In all of these figures, the lines drawn through the points are only approximations to the power distribution; no mathematical fit was performed.

The power distribution results presented here are intended to provide an indication of the general shape of the function. Additional results that provide more detail are presented in Appendix A long with tabulated values for the relative counting rates in the various wire segments.

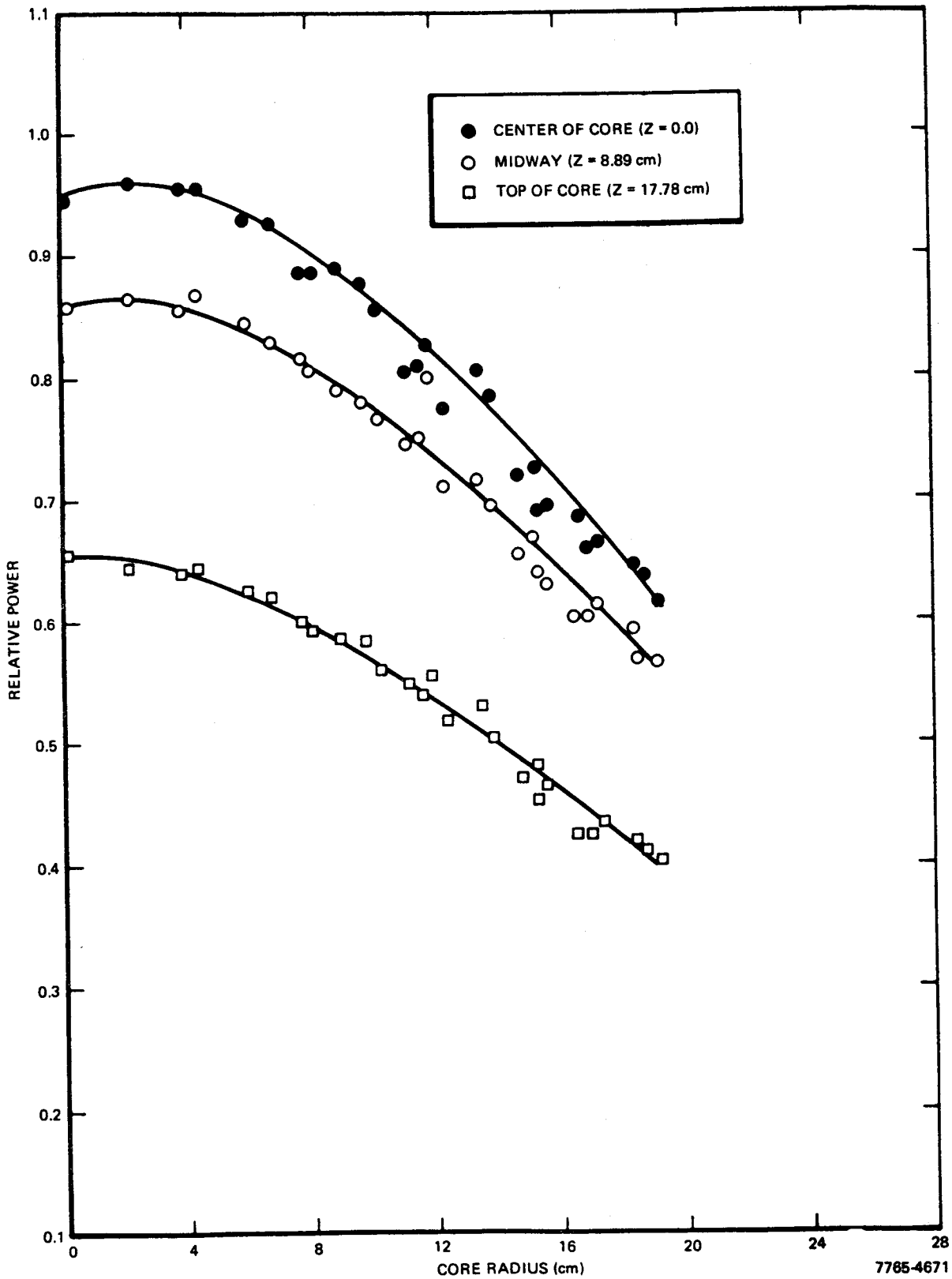

Figure 40. Radial Power Distribution — Power-Flattened Core

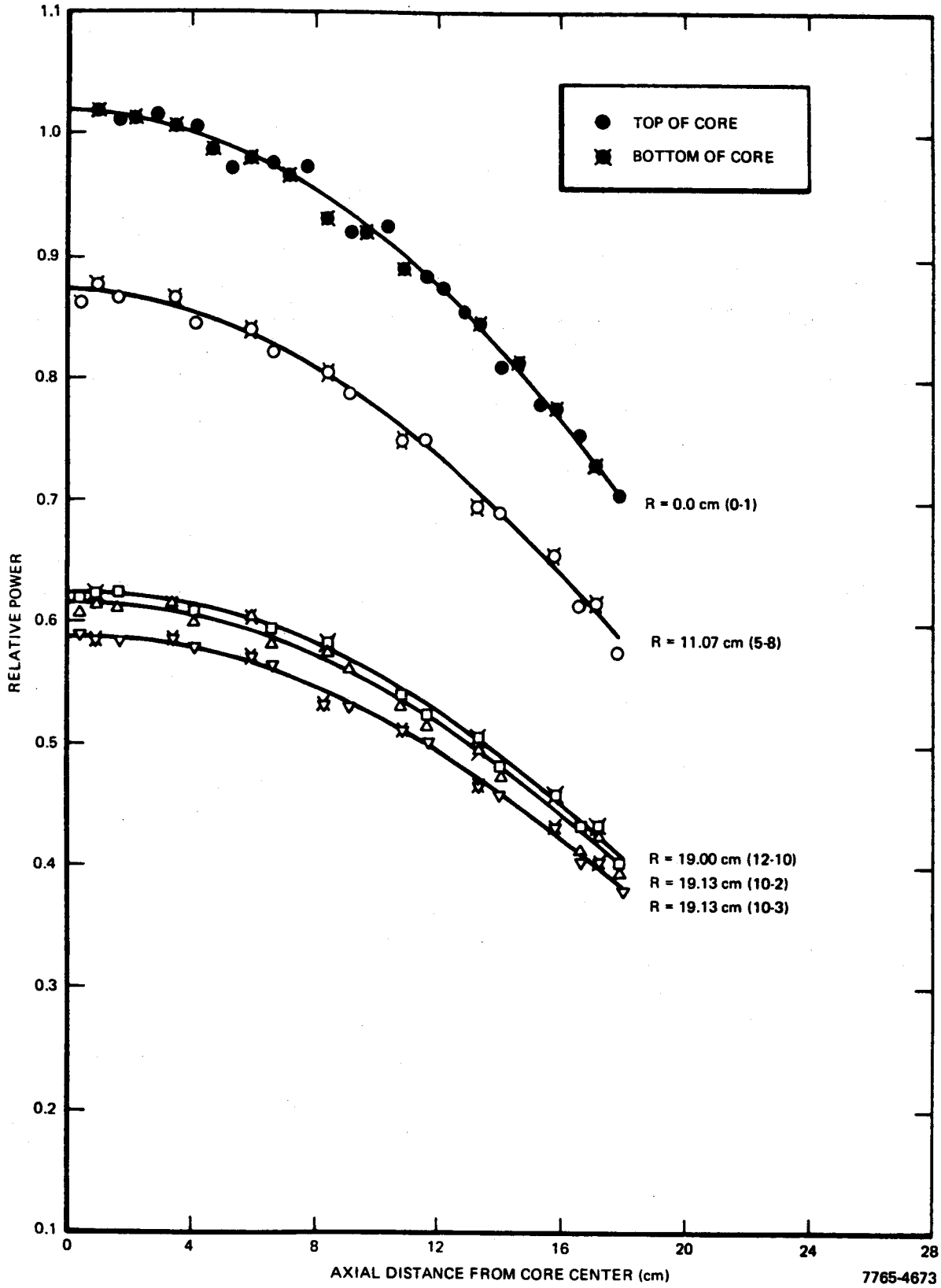

Figure 41. Axial Power Distribution – Drums at -1.5% $\Delta k/k$

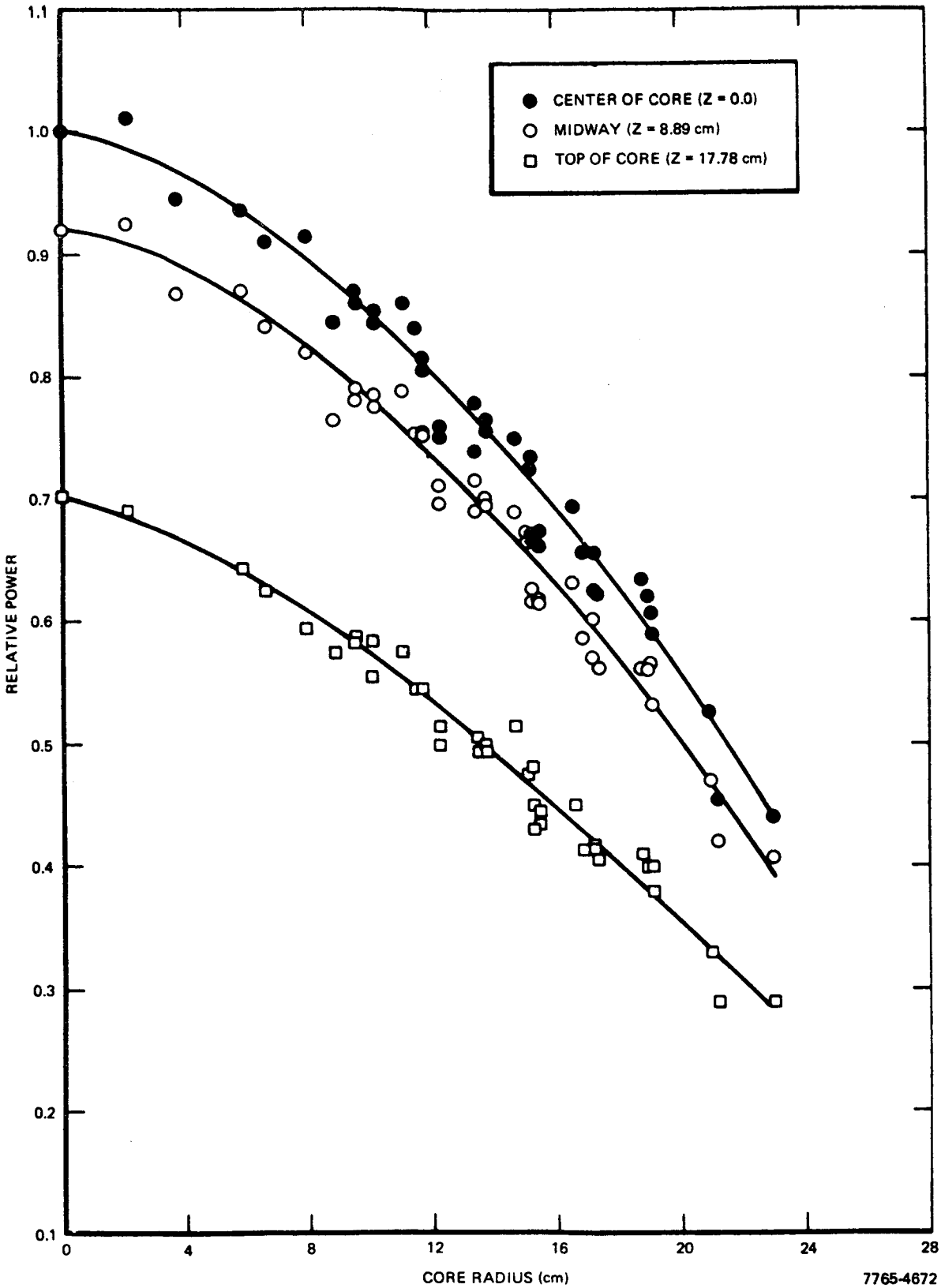

Figure 42. Radial Power Distribution – Drums at -1.5% $\Delta k/k$

11. Miscellaneous Experiments

Several other experiments pertaining to the physics characteristics of the reference reactor were conducted during this program. These experiments are described in detail in Appendix A. The results are summarized as follows:

1) The approximate worth of the six trapezoidal Mo filler pieces (see Figure 4) was found to be $1.17.

2) During the initial approach-to-critical in Compositions 1 and 2, two large blocks of paraffin were brought up to the core, one [22.8 cm(9 in.) in diameter by 3.8-cm(1.5-in.)-thick] placed on top of the core, another [30.5 cm(12 in.) by 30.5 cm(12 in.) by 45.7 cm(18 in.)] placed on the side. These blocks provided some approximate data on the effect of a hydrogenous shield and indicated that the total shutdown margin was roughly of the order of $25.

3) In order to estimate the error involved in measurements which required shutting down the reactor, making some adjustments, and then restarting again, the reproducibility of the excess reactivity was determined for the same drum position after several shutdowns and restarts. This reassembly reproducibility was found to be ±1¢.

4) During the course of adding the various refractory metals to one core in order to construct another, the excess reactivity was measured as the refractory metals were added in zones. This procedure was utilized primarily for ease in reactor operation, but provided useful data on the reactivity effects of adding material uniformly to the core zone by zone.

5) The reactivity worth of all control drums ganged was measured by the pulsed neutron method. Although the results are not considered as accurate as the values obtained by inverse counting, they are valuable in providing a rough substantiation of the inverse counting data. These pulsed neutron experiments are also described in Appendix A.

6) Routinely with each composition, the degree of uniformity in the make-up of each fuel element in the reactor was tested by interchanging 30 fuel elements in the central region of the core with 30 fuel elements in

the outer periphery. The reactivity change resulting from these interchanges never exceeded 2.5¢ for any composition.

B. EXPERIMENTAL UNCERTAINTIES

It was an experimental requirement to determine critical mass values of ±0.15%. In all cases the masses of the materials going into the core were measured to an uncertainty considerably less than this value, typically to 0.1% or better. The derivation of that mass of uranium which would make the reactor just critical with all drums in the fuel-full-in position is considerably more complicated. In Compositions 1 and 2, the uncertainty in the straight line fit to the data points relating the excess reactivity to the mass of uranium loaded is such that the intercept for zero excess is known to be ±0.1% or better. The inverse multiplication data that were taken at various loadings just below critical tend, in all cases, to confirm these values, but in themselves, probably have considerably higher uncertainties. In those compositions in which a conversion factor was employed to derive the critical mass, the excess reactivity was generally small enough that a considerable error (±10% or less) in the conversion factor can be made without incurring an error greater than ±0.15% in the critical mass. On the basis of the straight line fits to the data obtained for Compositions 1 and 2, the errors in the conversion factors do not exceed a few percent. There is, of course, a systematic error in applying to Composition 5A, for example, the conversion factor derived for Composition 2. However, the 10% change that occurred in the conversion factor in going from Composition 1 to Composition 2 is intuitively expected to be much greater than the change that might occur between Compositions 2 and 5A. Thus, the latter change is felt to be less than the statistical uncertainty.

Insofar as spectrum measurements are concerned, statistical errors are routinely less than 10% between 100 kev and 2 Mev. Below 100 kev, however, errors increase to perhaps ±20%, particularly where two-parameter techniques are used.

The assigned uncertainties on the large-sample-worth measurements are based upon the observed dispersion of repeated measurements uncorrected for the "void." These uncertainties are ±0.05¢ for gross worth less than 5¢ and ±1%

for gross worths greater than 5¢. The uncertainties are then combined quadratically with a similar uncertainty (±0.05¢) for the void correction. The uncertainties derived in this manner are slightly larger than the uncertainties resulting from reactor noise alone, but are considerably less than the anticipated uncertainties of ±0.3¢ or 2%, whichever was larger.

The counting statistics in the power distribution measurements are of the order of ±2%, although some systematic uncertainties of the order of 6% were found.

V. CONCLUDING REMARKS

A program has been conducted for the purpose of providing experimental data on some reactor parameters that are of crucial importance in the design and development of a compact fast reactor for space application. Through the use of a critical assembly that is a close geometrical mockup of the reference reactor, very carefully measured values for critical masses were obtained as a function of the types of materials that may be required in a reactor operating at high temperatures. These critical mass values provide not only basic benchmark information for substantiating cross section sets and calculational techniques but also provide direct estimates of the fuel loadings for this type of reactor. The addition of materials uniformly and sequentially to a basic "clean" core has been a very strong tool for understanding the nuclear characteristics of the various materials involved. This information is not only of interest to the specific reactor under design here but is also very valuable in the field of fast reactor physics in general.

The close geometrical simulation provided by this critical experiment also furnished some direct indications of the control characteristics of the reference reactor and the total amount of shutdown available. Drum interaction effects were investigated during the course of the program and provided data on an operating characteristic that would involve rather complex and expensive calculational schemes. The existence of control drums that operate in a fashion very similar to those in the reference design has proven to be very useful in providing rapid information on this facet of reactor design. It was found that the reactivity control afforded by a drum that did not contain the tantalum absorber segment was not greatly decreased, thus indicating that a drum of much reduced weight would be nearly as effective.

Detailed investigations of neutron spectra and power distributions furnished data that can be used to better understand the thermal and lifetime properties of the materials under consideration in the reference design. On the basis of experiments in the three-zoned core that simulated an operational configuration of the reference reactor, the approximate power distributions at the beginning and end of core life were determined.

Finally, the measurements dealing with reactivity effects of fuel motion or displacement are useful in understanding the safety characteristics of the reference design. Closely related to this type of investigation are the extensive sample-worth-measurements which not only furnish a check on calculational techniques and cross sections but also give an indication of the reactivity effects that will occur if one type of material must be substituted for another in the final design. Since the calculation of the large samples can become strongly dependent on the correct spectral representation of the neutron flux, the small samples, being essentially infinitely dilute and confined to a small zone in the core center, can be used to evaluate the adequacy of the central flux alone.

In general, all of the experimental techniques proved to be adequate in yielding the desired technical information. Two notable exceptions concerned the inverse-kinetics and the pulsed-neutron methods for measuring large negative reactivity values. As noted above, the inverse-kinetics method does not give reliable results if the reactivity changes were large and made too slowly. This behavior was attributed to the large changes (a factor of 10^4 or more) in neutron population that occurred; consequently, the method was used sparingly and with caution in this reactivity regime. It was originally expected that the pulsed neutron technique would provide adequate results in this area, but, in view of single drum worths and calculations, the values obtained by this method appear to underestimate reactivity control by as much as 17% for the all-drums-out case. Part of this difficulty is probably attributable to the fact that the minimum pulse-width is long compared to the decay constants involved in this assembly. Another difficulty pertains to the present impracticality of placing the source and/or detector inside the core. Since the pulsed neutron method is such a powerful tool for understanding the physics characteristics of the core, some technique for overcoming these problems would be advisable. The inverse-counting technique appeared to be adequate in providing the necessary information. On the basis of multiple measurements, this latter technique seems to be accurate to ±10%.

APPENDIX A

DETAILS OF EXPERIMENTAL PROGRAM

I. COMPOSITION 1

A. DESCRIPTION

Composition 1 was a relatively clean configuration and contained, in the core proper, only the Ta honeycomb and fuel tubes, some Ta foil and centering rings, and small amounts of Mo, in addition to the uranium fuel. Table 5 delineates, in the column headed "Composition 1," the exact mass of each material comprising the core and reflector. The 0.0051-cm(0.002 in.)-thick Ta foil, called out in the table, was used in the space that was to be occupied in later cores by the $Li_3{}^7N$ segment and was used to prevent the upper eccentric Mo reflector from accidentally falling into the core. The foil was coiled to form a tube approximately 37.51 cm(14.767 in.) high by 2.0 cm(0.8 in.) in diameter and was placed around the fuel tube. Serrations that extended axially from the top to the bottom were pressed into the foil in order to provide rigidity. The fuel in the fuel element consisted initially of a cluster of seven rods held together by 5 wire wraps, each made up of 1-1/4 turns of 0.076-cm(0.030 in.)-diameter Mo wire (0.250 gm each). The two Ta centering rings and the Mo wire wraps kept the fuel cluster centered in the fuel tube. As a result of some difficulties in installation, the six trapezoidal-shaped Mo filter pieces were not placed in the drums initially (see Figure 4).

B. EXPERIMENTAL RESULTS

1. Critical Mass

With each fuel element containing a seven-rod cluster of U rods, the approach-to-critical was initiated. A 5-curie ($\sim 10^7$ n/sec) Pu-Be neutron source was placed at the center of the top grid plate and a background count was made in each of the six channels without any of the fuel elements in the core. Next, all of the control drum locations (66) were filled with fuel elements. A new neutron count was then made and the inverse multiplication was computed by taking the ratio of the count in each channel when no fuel was present in the reactor to the count with the 66 fuel elements installed. Other fuel elements,

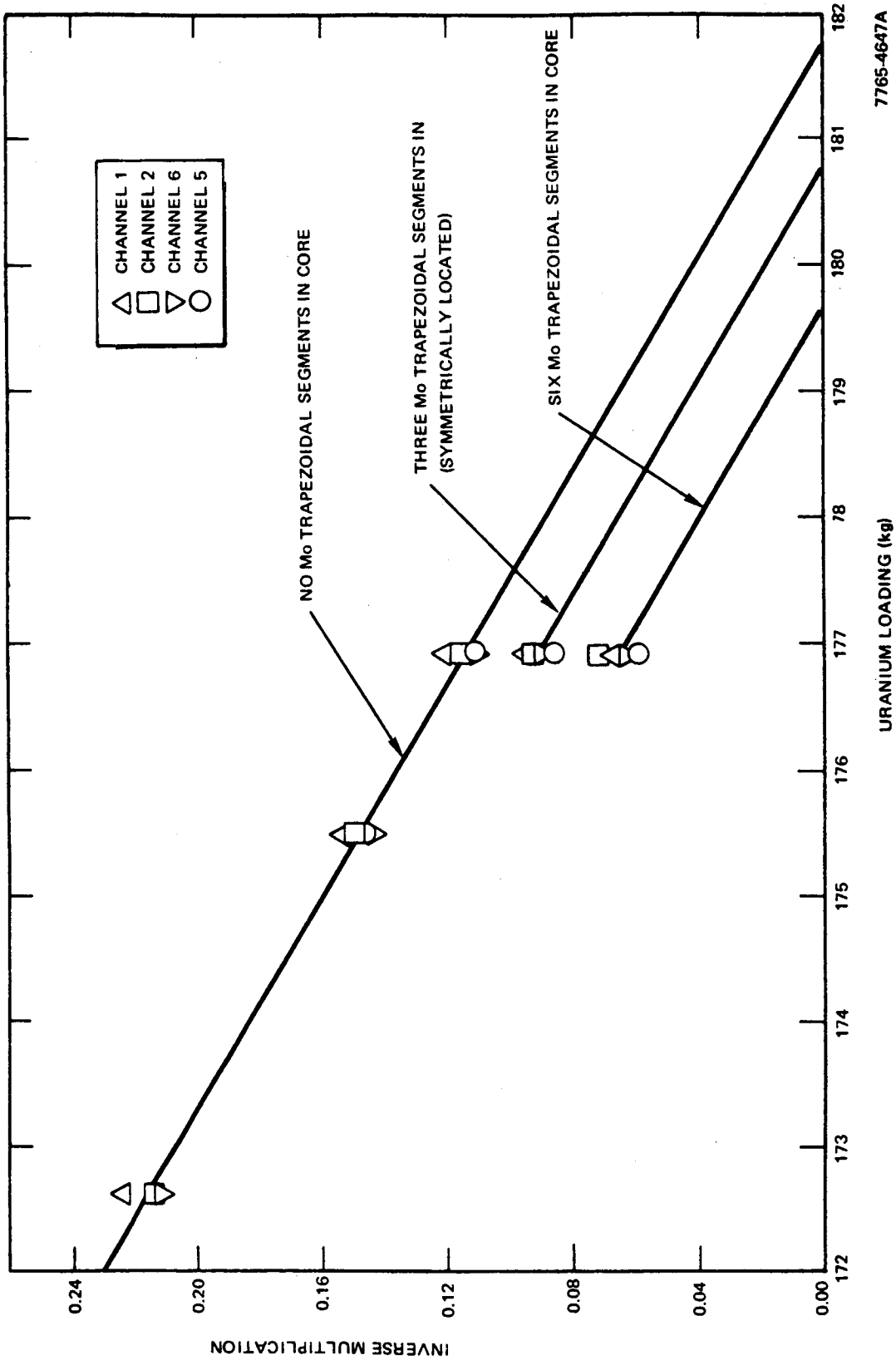

Figure 43. Changes in Inverse Multiplication From Addition of Mo Trapezoidal Pieces to Drums in Composition 1

initially in groups of 45, were added "uniformly" to the core proper in such a way that a more or less constant fuel density was maintained across the core. This process was carried out until all 247 fuel elements were inserted (176.92 kg of uranium). The inverse multiplication was, however, only of the order of 0.12; consequently some upward adjustment of fuel loading by means of uranium wire was necessitated. Before this procedure was initiated, one trapezoidal-shaped drum filler-segment was added to each of three control drums in a symmetrical fashion and an inverse multiplication determination was made. One of these Mo segments was then added to each of the remaining three drums and the inverse multiplication was again determined. These additions of Mo resulted in decreased values for 1/M and therefore a decrease in the extrapolated critical loading as indicated in Figure 43. Using an average value for the slope of the line determined by the three 1/M values preceding the addition of Mo (0.0234/kg of U) and an average value for 1/M from three chambers (1, 2, and 6) for each of the two cases of Mo additions, one obtains an average decrease in critical mass of 1.03 kg for each set of 3 Mo segments added. All six Mo segments therefore reduced the critical mass by about 2.06 kg.

From this point on, uranium wire was added to each fuel element in such a way that an excess reactivity of about $2 would be achieved and the maximum spread in the weight of uranium in all 247 elements would be less than or equal to ±1.2 gm. In order to establish the critical mass to within the required ±0.15%, the inverse multiplication parameter was measured as a function of uranium loading at several points just below critical. Similarly, the excess reactivity for several points above critical was also measured. The points so determined were then used to extrapolate to a delayed critical value as indicated in Figure 44. Based upon the four excess reactivity points corresponding to uranium mass loadings of 179.98, 180.78, 181.58, and 182.25 kg, an uncorrected critical mass of 179.36 ± 0.016 kg is predicted on the basis of a least-squares fit of a straight line, and this value is confirmed to within the required ±0.15% by the inverse multiplication data. Three additional excess reactivity values corresponding to fuel being loaded into Control Drums 1 and 4 (182.89 kg), Drums 2 and 5 (183.52 kg), and Drums 3 and 6 (184.16 kg) were also determined. Whereas the uranium mass additions corresponding to the first four excess reactivity values were carried out in a more or less uniform manner over the core

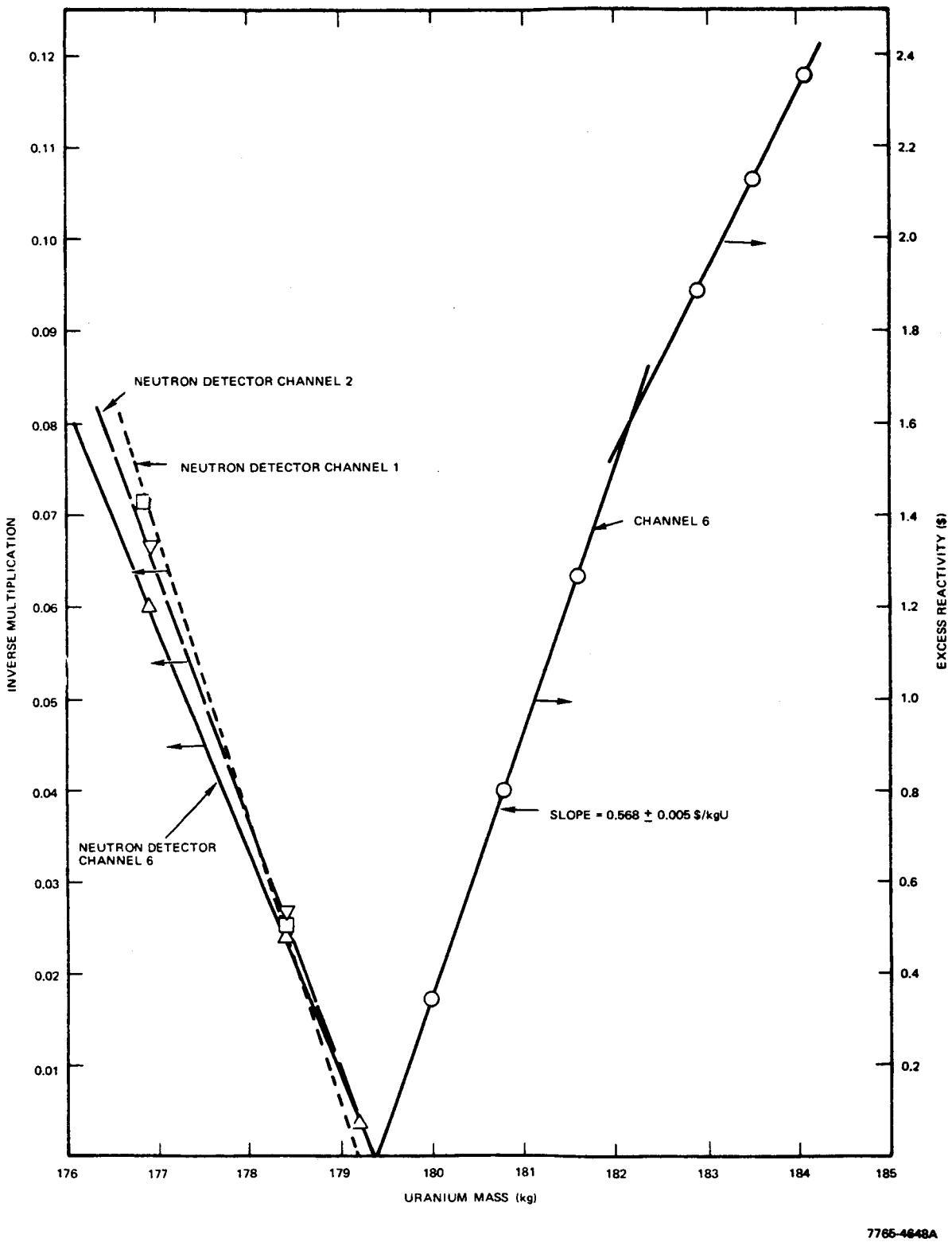

Figure 44. Excess Reactivity and Inverse Multiplication — Composition 1

proper, those associated with the last three applied only to drums, where the average fuel worth is less than for the core average. This fact is reflected in the change in the slope of the curve shown in Figure 44. A slope of 56.8 ± 0.5¢/kg was derived from the uniform core-loading data by the least-squares fit. By means of this slope, or conversion factor, the reactivity worth of the six Mo filler segments can be derived to be about $1.17.

Inverse multiplication data from a fourth detector, Channel 5, has arbitrarily not been included in Figure 44 inasmuch as it cannot be "read" to much better than ±10%.

At the final core loading (184.163 kg), a uniform uranium mass distribution was achieved in such a way that the mass of uranium in any given element did not deviate from the average by more than ±1.2 gm. Based upon exact weights for each element, the average mass of uranium in each fuel element was calculated to be 745.6 gm, with a standard deviation of 0.7 gm.

In order to increase sensitivity, blocks of polyethylene are placed around the various detectors used to monitor the neutron population. Two such detectors are mounted within a polyethylene "box" on each of the two vertical sides of the core structure weldment with their centers located at about the core midplane. The polyethylene surrounding the cylindrical detectors on all sides except the top forms a rectangular parallelepiped approximately 33 cm(13 in.) high by 20 cm(in.) deep by 28 cm(11 in.) wide, and has a volume of polyethylene of 14.45×10^3 cm^3(882 $in.^3$). This polyethylene is known to affect the reactor to some extent, and, in order to ascertain the magnitude of the effect, it was removed from one side of the core structure weldment. The change in the system reactivity was measured and found to be -7¢. It is assumed, therefore, that the removal of the polyethylene on both sides of the reflector would decrease the reactivity by 14¢. Using the experimentally determined value of 57¢/kg, one would predict that the removal of the polyethylene would increase the critical mass of the reactor by 0.25 kg. Thus the measured critical mass of the clean, unperturbed core (Composition 1) is 179.64 kg.

Another possible correction that should be noted pertains to the Kel-F coatings on the fuel rods and on the U wire. During the process of fabricating wire it was found necessary to remove the existing Kel-F coating. Groups of fuel

rods were weighed before and after cleaning in acetone. An analysis of the weight difference yielded an average weight of Kel-F of 0.0180 gm on each of 588 of the 6-in.-long rods and 0.0267 gm on each of 75 of the 8-3/4 in. rods.

After the cleaning, the rods were swaged down to the desired wire size [either 0.152 cm(0.060 in.) or 0.066 cm(0.026 in.) in diameter]. They were then cut to length 37.508 cm(14.767 in.) and coated with Kel-F. The wire segments, usually in groups of 36, were weighed before and after coating. From an analysis of the coating weight on 1260 of the 0.152-cm(0.060 in.)-diameter wires, the average weight of Kel-F on each was found to be 0.0697 gm. From a similar analysis of the coating weight on 560 of the 0.066 cm(0.026 in.)-diameter wires, the average weight of Kel-F on each was found to be 0.0251 gm. These results, along with an estimate of the total mass of hydrogen in Composition 1, are summarized in Table 14. An analysis performed at this laboratory in 1968 on some Kel-F coatings on some 5.08-cm(2 in.) by 5.08-cm(2 in.) by 0.32-cm(0.125 in.)-uranium plates indicated that Kel-F is 1.11% by weight hydrogen. Similar analyses carried out at Argonne National Laboratory showed a hydrogen content of 0.35 to 0.37 wt % hydrogen for the red-tinted Kel-F and 0.25 to 0.26 wt % for the clear Kel-F. We have used the 1.11 wt % value since the process of applying the Kel-F on the wire is the same as that used in 1968.

TABLE 14

ESTIMATE OF HYDROGEN MASS IN COMPOSITION 1

Type of Component	Average Weight of Kel-F per Component (gm)	Number of Components in Composition 1	Total Weight of Kel-F (gm)	Total Weight of Hydrogen (gm)
15.24-cm long rods	0.0180	1729	31.12	0.35
22.27-cm long rods	0.0267	1729	46.16	0.51
0.060-in. wire	0.0697	489	34.08	0.38
0.026-in. wire	0.0251	266	6.68	0.07
		Totals	118.04	1.31

Although the epoxy seals at the ends of each element are not considered to represent a significant reactivity effect, the average mass of epoxy has been approximately determined. By measuring weight differences, the weight of epoxy is estimated to be 0.4 gm per seal or 0.8 gm per standard fuel element.

In conjunction with the approach-to-critical, a set of measurements was made at each step on the worth of a hydrogenous phantom ("fat man"). The phantom consisted of a 30.48-cm(12.0 in.) by 30.48-cm(12.0 in.) by 45.72-cm (18 in.) paraffin block which was placed beside the reactor near the gap between the core and the fall-away safety element, and a 3.81-cm(1.5 in.)-thick by 32.86-cm(9 in.)-diameter paraffin disc which was placed on top of the reactor. The extrapolated critical mass with the phantom in position on a shutdown reactor was slightly in excess of 300 elements (i.e., $\sim$224 kg). This value represents an increase over the critical mass by 44 kg; consequently the reactor appears to have a shutdown margin of the order of (0.57 \$/kg) (44 kg) = \$25. This measurement is, of course, very crude and serves only to provide a "ball park" estimate of this effect.

2. Drum Calibration

In order to determine the total excess reactivity in the final core loading, a drum calibration was conducted. Both the step-wise and continuous methods using the inverse-kinetics techniques were employed, the latter without range changing. The results were previously presented in Figure 25. The continuous drum calibration values were not valid beyond about 110°; consequently they were not plotted in the figure. Also, only selected points were used for illustration even though values were actually determined every 0.8 sec. From Figure 25, the worth of a control drum from full-in to full-out is therefore seen to be of the order of \$2.22.

3. Neutron Spectrum

The seven central fuel elements in Composition 1 were removed from the core and 15 special fuel elements, in addition to a spherical proton-recoil detector, were inserted in their place. Under these conditions (which resulted in a decrease in reactivity of \$1.35), several measurements of the differential neutron energy distribution were made and covered the energy range from 50 kev to 2.2 Mev. A total of four different detectors were employed, each with a

TABLE 15

NEUTRON FLUX IN COMPOSITION 1

Detector Designation	0.9 H_2		2.63 H_2		Detector Designation	2.63 H_2		2.63 CH_4		8.1 CH_4	
E (Mev)	$\varphi(\mu)$	% Error	$\varphi(\mu)$	% Error	E (Mev)	$\varphi(\mu)$	% Error	$\varphi(\mu)$	% Error	$\varphi(\mu)$	% Error
0.043	0.62	4.2			0.330	3.50	3.3				
0.045	0.64	4.5			0.353	3.74	3.1				
0.048	0.65	4.9			0.376	3.68	4.0				
0.051	0.57	6.1			0.399	3.89	3.9	4.18	1.8		
0.054	0.64	7.0			0.425	3.99	3.8	4.39	2.0		
0.058	0.62	6.5			0.45	4.26	3.8	4.46	1.8		
0.062	0.69	6.9			0.48	4.58	4.2	4.35	2.2		
0.066	0.79	6.4			0.51	4.45	4.8	4.44	2.4		
0.069	0.81	7.3			0.55	4.51	4.4	4.57	2.5		
0.074	0.84	6.1			0.58	4.90	4.4	4.70	2.4		
0.079	0.90	6.7			0.62	4.47	5.4	4.38	2.9	4.76	2.1
0.085	0.98	7.4			0.66	4.91	5.0	4.56	3.1	4.83	1.9
0.090	1.12	7.5			0.70	5.20	5.3	4.75	2.8	4.75	2.2
0.095	1.18	7.7			0.74	4.79	6.0	4.50	3.6	4.64	2.5
0.101	1.18	6.6			0.79	4.67	7.5	4.69	3.4	2.58	2.4
0.107	1.37	7.3	1.25	2.3	0.84			4.50	3.8	4.57	2.7
0.115	1.50	6.0	1.36	2.3	0.90			4.47	3.7	4.70	3.2
0.123	1.41	8.5	1.50	2.2	0.96			4.49	3.9	4.83	3.0
0.130	1.62	o.9	1.57	2.3	1.02					4.55	3.4
0.138	1.70	13.4	1.64	2.0	1.09					4.21	4.0
0.147	1.76	7.3	1.78	2.2	1.15					4.59	3.9
0.157	1.87	6.9	1.80	3.2	1.23					4.67	4.3
0.167	2.09	7.0	1.95	2.6	1.31					4.57	4.6
0.179	1.81	10.5	2.08	2.7	1.39					4.39	5.7
0.189	1.95	9.3	2.19	2.4	1.47					4.48	5.3
0.201	2.41	8.1	2.32	3.2	1.57					4.37	6.4
0.214	2.25	9.1	2.35	2.9	1.68					4.05	7.4
0.229	2.34	8.4	2.56	3.0	1.78					3.87	8.2
0.242	2.55	10.3	2.71	3.2	1.90					3.16	12.9
0.258	2.87	8.4	2.78	2.9	2.02					3.07	11.8
0.275	3.02	9.0	2.98	3.2	2.16					2.86	15.3
0.293	3.16	11.0	3.00	3.8							
0.311			3.22	3.8							

different gas and/or pressure. Detectors designated 0.9 H_2, 2.63 H_2, 2.63 CH_4, and 8.1 CH_4 were used. The results of these measurements were shown graphically in Figure 33 and are tabulated in Table 15. Detectors with different fillings were normalized to each other in the overlapping energy regions. The normalization factors were, respectively, 1.0, 1.24, 1.55, and 2.220 for each of the above detectors.

It is not clearly understood why this inter-normalization was necessary. One assumption is that if the reactor power is too high, several pulses can occur while only one is being processed by the electronic system. Since the counts per channel in the pulse height analyzer increase exponentially with decreasing channel number, more counts will be lost in low channels than in high ones. This could give a flatter distribution of counts per channel and, thus, a lower flux (since the flux is proportional to the slope of the counts-per-channel curve). To test this theory, data were taken with one detector at two power levels (different by a factor of 2) in Composition 1, but no measurable difference was found. In a latter core, this effect was studied over large changes in power level (factors of 28, for example) and some changes were detected.

In support of the proton-recoil spectrometer measurements, two sets of five foils each (sulphur, cobalt, aluminum, copper, and indium) were irradiated within a cavity at the core center. The cavity was formed by removing the central (0-1) fuel element (all other positions containing standard fuel elements) and replacing it with two of the longest fuel elements made especially for accommodating the proton-recoil detector. These two special elements, when placed in the upper and lower grid plates, leave a cavity 3.81-cm(1.5 in.) high in the center of the reactor. To prevent the upper element from falling into this cavity, a 3.81-cm(1.5 in.)-long piece of honeycomb tube was placed at the core center and into this tube were placed the two sets of foils. A single irradiation was conducted and the foils were removed and counted in a β detector. The results of this counting procedure are shown in Table 16.

4. Fuel Element Interchange

In order to provide some indication of the degree of uniformity in the masses of the materials making up each fuel element, the 30 fuel elements in Rings 3 and 4 were interchanged with 30 fuel elements located in various peripheral

TABLE 16

RESULTS OF FOIL IRRADIATIONS IN COMPOSITION 1

Foil	Foil Diameter (cm)	Foil Thickness (cm)	Foil Volume (cm^3)	Foil Mass (gm)	Isotope	Isotope Abundance (%)	Isotope Mass (gm)	Isotope Density (gm/cm^3)	Isotope Number Density (atoms/cc x 10^{24})	Efficiency*	Reaction	Mother	Decay Mode	Daughter	Halflife	Decay Constant, λ (min^{-1})	Activity of Shutdown (counts/sec)	Saturated Activity (counts/sec)	Saturated Activity/Efficiency (counts/sec)	Standard Deviation (%)
Al(b)	1.905	0.0787	0.224	0.561	$_{13}Al^{27}$	100	0.561	2.50	0.0559	0.102	n,α	$_{11}Na^{24}$	β^-	$_{12}Mg^{24}$	15 hr	7.7×10^{-4}	5.00×10^{1}	1.11×10^{3}	1.10×10^{4}	0.37
(t)																	5.60×10^{1}	1.24×10^{3}		0.17
S(b)	1.905	0.632	1.80	3.05	$_{16}S^{32}$	95.0	2.90	1.61	0.0303	0.0402	n,p	$_{15}P^{32}$	β^-	$_{16}S^{32}$	14.3 day	3.37×10^{-5}	2.26×10^{2}	1.12×10^{5}	2.78×10^{6}	0.10
(t)																	2.57×10^{2}	1.27×10^{5}		0.06
(b)					$_{16}S^{34}$	4.25	0.13	0.07	0.00124	0.0402*	n,α	$_{14}Si^{31}$	β^-	$_{15}P^{31}$	2.6 hr	4.44×10^{-3}	3.96×10^{1}	1.69×10^{2}	4.2×10^{3}	4.2
(t)																	4.56×10^{1}	1.95×10^{2}		2.6
Cu(b)	1.905	0.0170	0.0485	0.383	$_{29}Cu^{63}$	69.1	0.265	5.46	0.0522	0.06*	n,γ	$_{24}Cu^{64}$	β^-	$_{30}Zn^{64}$	12.8 hr	9.02×10^{-4}	1.33×10^{2}	2.52×10^{3}	4.47×10^{4}	0.30
(t)										0.06*							1.51×10^{2}	2.85×10^{3}		0.25
(b)					$_{29}Cu^{65}$	30.9	0.118	2.43	0.0225	0.10*	n,p	$_{28}Ni^{65}$	β^-	$_{29}Cu^{65}$	2.564 hr	4.5×10^{-3}	2.0×10^{1}	8.42×10^{1}	9.12×10^{2}	7.0
(t)										0.10*							2.33×10^{1}	9.83×10^{1}		5.5
InSn(b)	1.905	0.0132	0.0376	0.266	$_{49}In^{113}$	4.3	0.0046	0.12	0.00062		n,γ	$_{49}In^{114m}$	γ	$_{49}In^{114}$	50 day	9.62×10^{-6}	4.37	7.57×10^{3}		4.7
(t)																	4.93	8.55×10^{3}		3.5
(b)					$_{49}In^{115}$	95.7	0.1014	2.70	0.0142	0.0860	n,γ	$_{49}In^{116m}$	β^-	$_{50}Sn^{116}$	54 min	1.28×10^{-2}	1.21×10^{4}	2.25×10^{4}	2.62×10^{5}	0.12
(t)										0.0968							1.33×10^{4}	2.48×10^{4}	2.56×10^{5}	0.09
(b)					$_{49}In^{115}$	95.7	0.1014	2.70	0.0142	0.0043*	n,n'	$_{49}In^{115m}$	β^-	$_{50}Sn^{115}$	4.5 hr	2.57×10^{-3}	9.35×10^{2}	6.54×10^{3}	1.52×10^{6}	0.16
(t)										0.0048*							1.05×10^{3}	7.35×10^{3}	1.53×10^{6}	0.12

*Estimates

positions as shown in Table 17. In order to make this measurement, the critical position on Drum No. 6 was noted with the standard elements in their standard locations (see foldout). The interchange of the elements in accordance with the table was then performed and a new critical position was found. In Composition 1, the differences between the critical positions were equivalent to -0.74¢, a value which is statistically zero within the uncertainty of ±1¢ for this technique of measurement.

5. Reactivity Worths of Various Materials

In order to obtain some idea of the reactivity changes caused by the removal of complete fuel elements from the core, the reactivity worths of the standard fuel elements in Positions 4-1 and 4-13 were determined. The experiment consisted of removing the two elements in these positions and noting the change in the drum position required for criticality. A reactivity change of -$1.07 was observed for the combined effect of both elements.

Each element contains approximately 335.01 gm of tantalum in the form of honeycomb and fuel tubes, spacer foil, and centering rings; 325.85 gm of Mo in the form of upper and lower axial reflectors, and wire wrapping; and two aluminum end caps that fit into the grid plates. Fuel Element Numbers 4-1 and 4-13 contained 744.23 and 745.02 gm of uranium, respectively.

In order to obtain some idea of the worths of some of the core materials and reactivity samples, a series of worth determinations was carried out in Composition 1 relative to a void. In this series of experiments, a standard, voided fuel element, made up of all the usual components except the uranium, was substituted for the standard fuel elements in Positions 0-1, 2-1, 4-1, 6-1, 8-1, and 10-1. In order to prevent the upper solid Mo reflector from falling to the bottom of the element, a tantalum foil, 0.002 in. thick, was inserted into the place normally occupied by the uranium fuel. The weight of such a foil is approximately 18.78 gm. The change in the critical drum position was noted in each case and this position was converted to reactivity from the drum calibration curve. The results of these experiments were previously outlined in Table 9 and are uncorrected for any mass variations between fuel elements other than for the sample under consideration. The worth of the uranium fuel cluster in Position 0-1 is seen to be +69.8¢/kg, a value that is somewhat larger than the core averaged worth of 56.8¢/kg, as would be expected.

TABLE 17

FUEL ELEMENT INTERCHANGE SCHEDULE

Original Position	Interchange Position
2-1	10-1
2-2	8-18
2-3	7-2
2-4	6-1
2-5	9-11
2-6	5-3
2-7	8-3
2-8	7-21
2-9	5-27
2-10	4-23
2-11	6-5
2-12	8-15
3-1	4-4
3-2	6-25
3-3	6-7
3-4	4-19
3-5	5-8
3-6	5-9
3-7	4-9
3-8	5-21
3-9	7-16
3-10	4-14
3-11	8-7
3-12	6-13
3-13	5-15
3-14	6-19
3-15	9-8
3-16	7-11
3-17	8-11
3-18	9-6

In a similar fashion, the worths of a large reactivity sample of Ta, Mo, and Be were determined in Composition 1. In this case, the voided element was loaded with a reactivity sample by removing the tantalum foil in the position normally occupied by the uranium fuel. By comparing the control-drum position for the case in which the voided element is in place with the drum position for the case in which a reactivity sample is inserted, one obtains a measure of the worth of the sample relative to a void, assuming that the tantalum foil has a negligible reactivity effect and that the other materials making up the fuel elements are virtually identical in mass and location. The results of the measurements with the reactivity samples were also summarized in Table 9. It was noted above that, upon insertion of the special proton-recoil elements in Composition 1, a reactivity loss of $1.35 occurred. This reactivity change was attributed primarily to a decrease in the uranium loading at the core center and was therefore of some significance in predicting the worth of fuel at this location. The decrease in uranium mass between the core that was comprised exclusively of standard fuel elements in all positions, and the core with the seven centrally located standard fuel elements removed and replaced by 13 proton-recoil elements, was 1762.55 gm. The net increase in the mass of tantalum introduced by the proton-recoil elements and the spacer sleeve was about 293 gm. From Table 9, one would conclude that the reactivity change due to the increase in tantalum mass was negligible; consequently the worth-per-unit mass of fuel would be about 76.6 ¢/kg. In view of the fact that this uranium was removed largely at the core center, this value compares reasonably well with the worth of 69.8 ¢/kg of uranium for the central fuel element (0-1) alone.

As was indicated above, in order to insert foils into the core, the central fuel element (0-1) is removed and replaced by two of the longest proton-recoil elements. This procedure results in a void cavity 3.81-cm(1.5 in.) high at the core center within the central fuel element location. The mass of uranium removed in this process was approximately 154.37 gm. A reactivity decrease of 10.7¢ was observed and resulted in a worth per unit mass of 69.3 ¢/kg. This value would be expected to be greater than the 76.6 ¢/kg noted above. No explanation for this discrepancy was uncovered, however.

In order to anticipate in Composition 1 the change in critical mass that would take place in proceeding from Composition 1 to Composition 2 (in which

approximately 10.13 kg of $Li_3{}^7N$ was added), the reactivity change accompanying the insertion into the core of a fuel element containing a 41.2 gm natural Li_3N segment was measured. The experiment consisted of replacing the standard element in Position 0-1 (745.23 gm of U) with another standard fuel element (746.60 gm of U) that contained, in addition to the other standard components, the Li_3N segment in the space between the honeycomb and fuel tubes. The reactivity change, without any corrections for U mass differences, was found to be zero within statistical and systematic uncertainties. Upon substitution of the natural Li_3N-loaded element for the standard fuel element (745.09 gm of U) in Position 8-1, a similar result, uncorrected for uranium mass differences, was found.

6. Fuel Element Rotation

In order to measure the reactivity change that results from a uniform radial displacement of the fuel, all fuel elements are rotated 90° from the normal null position with respect to the axis of the core. In the initial critical loading, the fuel elements were located in the null position; i. e., in the position in which the plane passing through the axes of the honeycomb and fuel tubes in each fuel element is at right angles to the plane passing through the axis of the core and the axis of the honeycomb tube. A reactivity change of -14¢ was observed when all fuel elements in Composition 1 were rotated to the full-out position, a rotation that displaced each fuel cluster by 0.0508 cm(0.020 in.) along the core radius. In this position, the fuel tube was farthest from the core axis.

7. Reactor Power Calibration

In order to calibrate the neutron detector readout against reactor power, several uranium foils were irradiated at the core center and core edge of Composition 1. This calibration consisted essentially of comparing the activities (gross gamma counting above 0.6 Mev) of the foils placed in the critical assembly with identical foils placed in a known thermal flux. Although this information is of importance only in terms of reactor operation, it is of interest, in terms of power distributions, that the foils at the radial edge of the core had an activity of the order of 0.5 to 0.6 of those at the center. By the use of the calculated peak-to-average activity ratio of the two foils and the mass of uranium in the reactor, it was possible to obtain a rough calibration of the readout of the detectors in terms of reactor power. The result was that 1.5×10^{-6} amp in Channel 6 corresponds roughly to 38 watts.

II. COMPOSITION 2

A. DESCRIPTION

The fuel elements comprising Composition 1 were removed from the core, the fuel cluster was extracted, and the element disassembled. The $Li_3{}^7N$ segments were then installed in the annular gap between the fuel and honeycomb tubes, and an epoxy seal was made as shown in Figure 5 to prevent air and moisture from contacting the $Li_3{}^7N$. The total mass of $Li_3{}^7N$ contained in the 247 fuel elements was 10.13 kg with an average mass per segment of 41.00 gm. All fuel elements were then reassembled and a fuel cluster consisting initially of 6 rods, 6 of the 0.152-cm(0.060 in.) wires, and 1 or 2 of the 0.066-cm(0.026 in.)-diameter wires was inserted into place. The masses of the various other core components are shown in the column labeled "Composition 2" in Table 5.

B. EXPERIMENTAL RESULTS

1. Critical Mass

The standard 1/M approach to critical was carried out, first by adding 66 elements to the drum locations, and then adding elements to the core in a uniform manner. As was done in Composition 1, values for the inverse multiplication were derived and plotted as a function of the uranium mass loading for the region just below critical, and excess reactivity determinations were made at several points above critical. These results are presented graphically in Figure 45. In order to obtain a sufficient excess reactivity for the spectrum measurements by the proton-recoil technique, a seventh 0.152-cm(0.060 in.)-diameter uranium wire was ultimately added to the fuel cluster in each element. The final loading (174.96 kg) was uniform to within ±1.6 gm maximum spread and an excess reactivity of $1.86 was achieved. The average mass of uranium per fuel element was 708.35 ± 0.55 gm. A least-squares fit of a straight line was made to the 5 excess reactivity values and yielded a zero intercept of 171.10 ± 0.15 kg. Two ($1.80 and $1.87) of these 5 values involved fuel addition in a nonuniform manner and consequently do not fit the straight line as well as would be expected for the other measurements. If these two points are omitted from the fit, a zero intercept of 171.11 ± 0.07 kg is obtained. The mass reactivity coefficient, or slope, obtained from these fits is 50.6 ± 0.3 and 51.0 ± 0.2 ¢/kg for the 5-point and 3-point analyses, respectively. Using a value for the

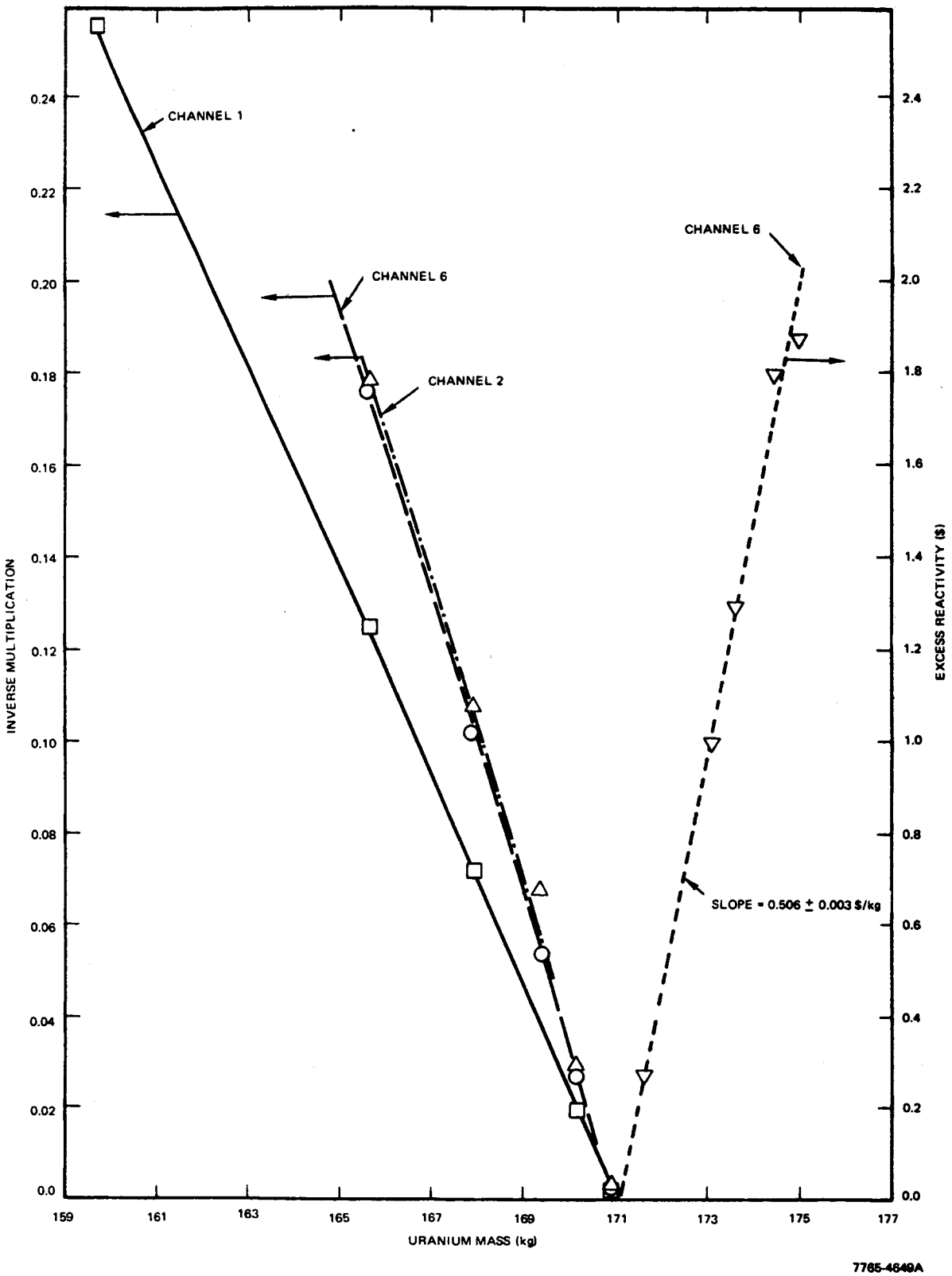

Figure 45. Excess Reactivity and Inverse Multiplication — Composition 2

zero intercept of 171.10 kg and a conversion factor of 51 ¢/kg to correct for the 14¢ contributed by the polyethylene box, one obtains a critical mass of 171.37 kg for Composition 2. The results of the inverse multiplication data appear to confirm the zero intercept value quite well.

2. Drum Calibration

After the final uranium loading was performed, a drum calibration by the step-wise technique was conducted and has already been shown in Figure 26. As can be seen, the total worth of the drum from full-in to full-out was $2.14, a value somewhat less than that observed in Composition 1.

3. Neutron Spectrum

The seven central fuel elements were removed from Composition 2 and the thirteen special elements plus the proton-recoil detector were installed in the usual manner. Differential spectrum determinations were then made using four detectors for the energy range from about 40 kev to 2.0 Mev. These results were previously shown in Figure 34 and are tabulated in Table 18. Most noticeable is the dip in the spectrum that is attributable to the Li^7 scattering resonance at 250 kev. Since the spectrum shows a dip at this same energy, the energy calibrations used in the detectors appear to be quite good. As in the Composition 1 task, an internormalization factor between detectors was required. These factors were 1.0, 1.20, 1.54, and 2.38 for the detectors designated 0.9 H_2, 2.63 H_2, 2.63 CH_4 (He^3), and 8.1 CH_4.

A series of foil irradiations were performed using, in this Composition, Na_2CO_3, Al, S, Cu, and In-Sn. These results are presented in Table 19.

4. Fuel Element Interchange

In accordance with standard procedures, the central 30 fuel elements in Composition 2 were interchanged with 30 fuel elements located in the outer zone of the core. The reactivity change observed on the basis of the position of Drum No. 6 indicated that a change of less than 0.1¢ occurred. This value is less than the error involved in the reassembly reproducibility (±1¢).

5. Reassembly Reproducibility

During the normal shutdown of the critical assembly, the scrammable reflectors are moved away from the core and all drums are turned out.

TABLE 18

NEUTRON FLUX IN COMPOSITION 2

Detector Designation	0.9 H_2		2.63 H_2		Detector Designation	2.63 H_2		2.63 $CH_4(He^3)$		8.1 CH_4	
E (Mev)	$\varphi(\mu)$	% Error	$\varphi(\mu)$	% Error	E (Mev)	$\varphi(\mu)$	% Error	$\varphi(\mu)$	% Error	$\varphi(\mu)$	% Error
0.043	0.72	3.8			0.330	3.20	3.7	3.28	2.8		
0.045	0.73	4.2			0.353	3.74	3.2	3.69	3.4		
0.048	0.81	3.7			0.376	3.79	4.1	3.79	2.5		
0.051	0.86	3.3			0.399	3.90	3.7	3.89	3.4		
0.054	0.84	4.8			0.425	3.85	4.0	3.92	3.2		
0.059	0.78	5.0			0.45	4.29	4.3	4.12	3.4		
0.062	0.84	5.2			0.48	4.61	4.2	4.29	3.8		
0.066	0.95	4.6			0.51	4.51	4.2	4.46	3.6		
0.069	0.93	5.5			0.55	5.01	4.1	4.81	3.4		
0.074	1.00	5.2			0.58	5.08	4.6	5.12	3.5	5.08	1.4
0.079	1.14	5.3			0.62	5.99	4.7	4.95	4.2	4.96	2.0
0.085	1.20	5.3			0.66	4.98	4.9	4.94	4.2	4.98	1.8
0.091	1.24	6.3			0.70			5.04	4.6	5.17	2.0
0.098	1.31	6.7			0.74			4.88	5.0	4.91	2.4
0.101	1.48	5.3			0.79			4.95	5.4	4.90	2.3
0.107	1.46	6.2	1.56	1.7	0.84					4.99	3.0
0.115	1.72	5.4	1.74	1.7	0.90					5.05	2.4
0.123	1.89	5.4	1.96	1.7	0.96					4.78	3.3
0.130	2.15	5.0	2.08	1.8	1.02					4.69	3.3
0.138	2.40	5.4	2.40	1.4	1.09					4.80	3.6
0.147	2.81	4.3	2.61	1.5	1.15					4.55	3.8
0.157	2.89	4.4	2.98	1.8	1.23					4.42	4.6
0.167	3.12	4.5	3.13	1.6	1.31					4.80	4.5
0.178	3.24	5.0	3.13	1.8	1.39					4.62	4.9
0.189	3.08	5.3	3.17	1.6	1.47					4.41	5.5
0.201			3.07	2.3	1.57					4.43	6.2
0.214			2.93	2.2	1.69					4.58	6.8
0.228			2.60	2.7	1.78					4.33	6.7
0.242			2.19	3.7	1.90					3.88	9.4
0.259			2.12	3.7	2.02					4.25	9.3
0.275			2.34	4.2							
0.295			2.74	3.9							
0.311			2.98	3.9							

TABLE 19

RESULTS OF FOIL IRRADIATIONS IN COMPOSITION 2

Foil	Foil Diameter (cm)	Foil Thickness (cm)	Foil Volume (cm^3)	Foil Mass (gm)	Isotope	Isotope Abundance (%)	Isotope Mass (gm)	Isotope Density (gm/cm^3)	Isotope Number Density (atoms/cc x 10^{24})	Efficiency*	Reaction	Mother	Decay Mode	Daughter	Halflife	Decay Constant λ (min^{-1})	Activity at Shutdown (counts/sec)	Saturated Activity (counts/sec)	Saturated Activity Efficiency (counts/sec)	Standard Deviation (%)
Na_2CO_3	0.978	0.521	0.391	0.586	$_{11}Na^{23}$	100	0.254	0.65	0.0170	0.0339	n,γ	$_{11}Na^{24}$	β^-	$_{12}Mg^{24}$	15 hr	7.7×10^{-4}	1.13×10^{1}	2.51×10^{2}		0.35
																	1.23×10^{1}	2.74×10^{2}	8.08×10^{3}	0.38
Al(b)	1.905	0.0787	0.224	0.561	$_{13}Al^{27}$	100	0.561	2.50	0.0559	0.102*	n,p	$_{12}Mg^{27}$	β^-	$_{13}Al^{27}$	9.5 min	7.29×10^{-2}	5.87×10^{3}	5.94×10^{3}	5.82×10^{4}	0.16
(t)																	6.75×10^{3}	6.83×10^{3}		0.17
(b)					$_{13}Al^{27}$	100	0.561	2.50	0.0559	0.102	n,α	$_{11}Na^{24}$	β^-	$_{12}Mg^{24}$	15 hr	7.7×10^{-4}	4.07×10^{1}	9.04×10^{2}	8.86×10^{3}	0.25
(t)																	4.63×10^{1}	1.03×10^{3}		0.30
S(b)	1.905	0.632	1.80	3.05	$_{16}S^{32}$	95.0	2.90	1.61	0.0303	0.0402	n,p	$_{15}P^{32}$	β^-	$_{16}S^{32}$	14.3 days	3.37×10^{-5}	1.92×10^{2}	9.50×10^{4}	2.36×10^{6}	0.07
(t)																	2.18×10^{2}	1.08×10^{5}		0.07
(b)					$_{16}S^{34}$	4.25	0.13	0.07	0.00124	0.0402*	n,α	$_{14}Si^{31}$	β^-	$_{15}P^{31}$	2.6 hr	4.44×10^{-3}	3.14×10^{1}	1.34×10^{2}	3.33×10^{3}	2.3
(t)																	3.71×10^{1}	1.58×10^{2}		2.1
Cu(b)	1.905	0.0170	0.0485	0.383	$_{28}Cu^{63}$	69.1	0.265	5.46	0.0522	0.06*	n,γ	$_{29}Cu^{64}$	β^-	$_{30}Zn^{64}$	12.8 hr	9.02×10^{-4}	1.44×10^{2}	2.72×10^{3}	4.87×10^{4}	0.19
(t)										0.06*							1.65×10^{2}	3.11×10^{3}		0.20
(b)					$_{29}Cu^{65}$	30.9	0.118	2.43	0.0225	0.10*	n,p	$_{28}Ni^{65}$	β^-	$_{29}Cu^{65}$	2.564 hr	4.5×10^{-3}	1.74×10^{1}	7.34×10^{1}	8.00×10^{2}	3.7
(t)										0.10*							2.06×10^{1}	8.67×10^{1}		3.8
InSn(b)**	1.905	0.0132	0.0376	0.266	$_{49}In^{113}$	4.3	0.0046	0.12	0.00062		n,γ	$_{49}In^{114m}$	γ	$_{49}In^{114}$	50 days	9.62×10^{-6}	4.14	7.18×10^{3}		4.3
(t)																	4.36	7.55×10^{3}		8.3
(b)					$_{49}In^{115}$	95.7	0.1014	2.70	0.0142	0.0860	n,γ	$_{49}In^{116m}$	β^-	$_{50}Sn^{116}$	54 min	1.28×10^{-2}	1.24×10^{4}	2.31×10^{4}	2.69×10^{5}	0.04
(t)										0.0968							1.41×10^{4}	2.62×10^{4}	2.71×10^{5}	0.06
(b)					$_{49}In^{115}$	95.7	0.1014	2.70	0.0142	0.0043*	n,n′	$_{49}In^{115m}$	β^-	$_{50}Sn^{115}$	4.5 hr	2.57×10^{-3}	8.38×10^{2}	5.86×10^{3}	1.36×10^{6}	0.13
(t)										0.0048*							9.71×10^{2}	6.80×10^{3}	1.42×10^{6}	0.23

*Estimates
**40% by weight In and 60% by weight Sn
t Top group of foils
b Bottom group of foils

The question often arises as to how reproducible the total reactivity is after a shutdown is accomplished and the reactor is started up again and restored to some previous configuration. In order to evaluate this phenomenon, the excess reactivity was measured in Composition 2 by the reactivity-vs-time code with Drum No. 6 at 116 degrees, all other drums full-in, and the scrammable reflectors full-up. The reactor was then scrammed and a new startup was carried out in which the reflectors were again raised to their up-position, Control Drums 1 through 5 were driven full-in and Drum 6 was placed again at 116 degrees. The reactivity was again measured. This procedure was repeated a total of 6 times over a period of 4 days and resulted in excess reactivity determinations of 20.32, 19.38, 19.05, 20.30, 19.95, and 20.97¢. The average is 20.00¢ and the total spread is about ±1¢. This value is typical of the reproducibility that can be expected in measurements involving a reactor shutdown and restart, and is attributed to very small variations in the positioning of the scrammable reflectors.

III. COMPOSITION 3

A. DESCRIPTION

Upon completion of the above described experiments in Composition 2, the fuel cluster was removed from each fuel element and the Hf foil was installed around the fuel cluster. Since the Hf foil was not expected to have a very large reactivity effect, no adjustment in the fuel loading was made for Composition 3. The total loading remained, therefore, at 174.96 kg with the average weight of uranium in each element being 708.35 ± 0.55 gm. The total mass of Hf added was 4.12 kg, the mass in each element averaging 16.66 gm. The values for the masses of all the other materials in the core and reflector are presented in Table 5.

B. EXPERIMENTAL RESULTS

1. Critical Mass

Inasmuch as the change in reactivity resulting from the addition of the Hf foil was expected to be very small, a 1/M approach to critical was not performed for Composition 3. Instead, a measure of the excess reactivity was made as the Hf was added to the core in a step-wise manner. These results are presented in Table 20 and the zones are identified in Figure 46. Zone 1 refers to all elements from 0-1 to 4-13, inclusive. Zone 2 refers to Elements 4-14 through 6-9, inclusive, and Zone 3 to Elements 6-10 through 8-5, inclusive. The balance of the core, Zone 4, consists of the remaining 31 elements. The first step involved the addition of Hf foil to each of the eleven fuel elements in each of the six drums. The total Hf so distributed amounted to 1.10988 kg and increased the system reactivity by 2.7¢. This process was continued in the manner indicated and resulted in a final reactivity increase of only 3.2¢, thus bringing the total excess to 189.2¢.

If it can be assumed that the conversion factor as determined in Composition 2 is applicable to Composition 3, the critical mass of Composition 3 would be

$$171.37 \text{ kg} - \frac{3.2¢}{51 ¢/\text{kg}} = 171.37 \text{ kg} - 0.06 \text{ kg} = 171.31 \text{ kg} \quad .$$

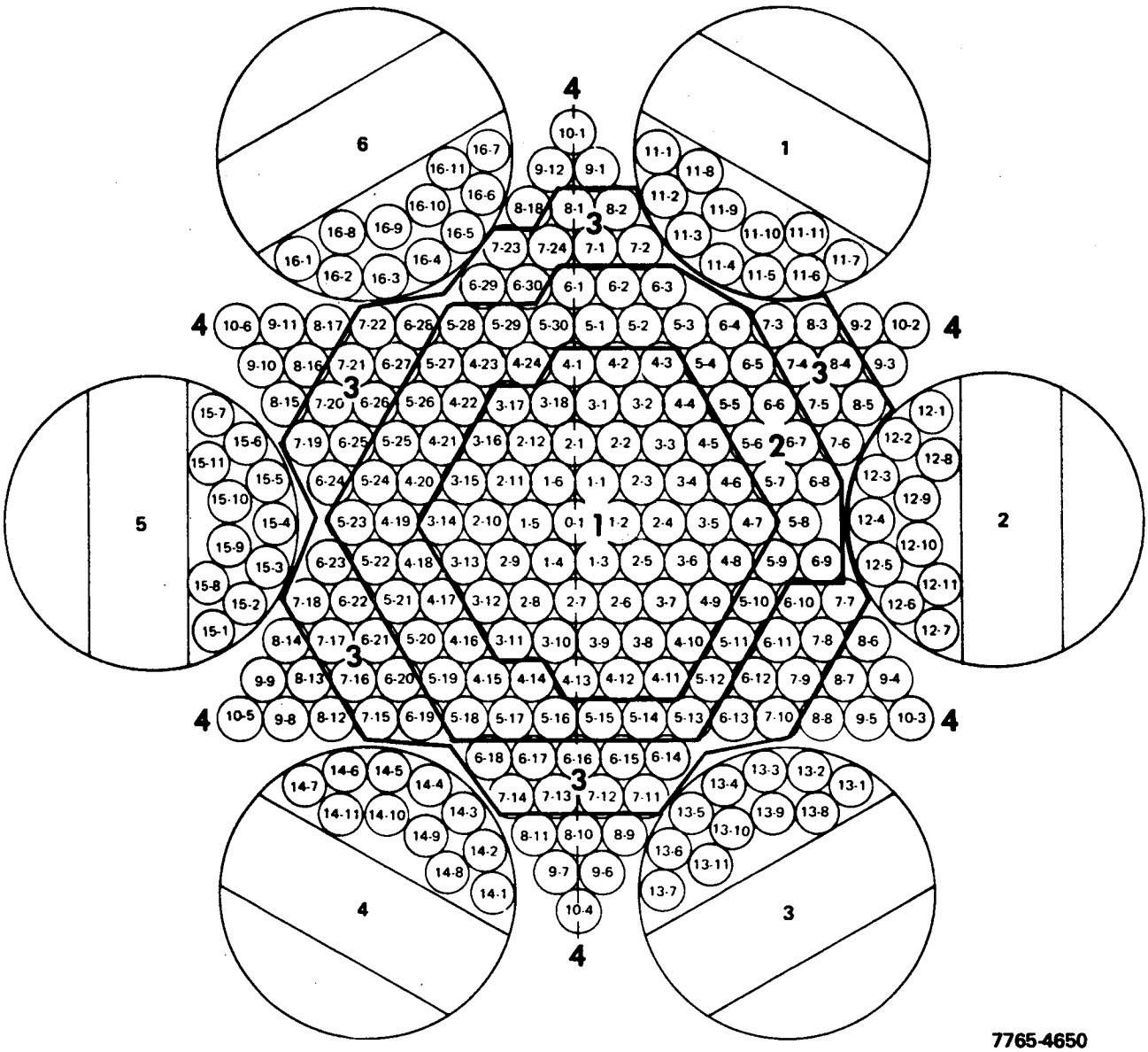

Figure 46. Zones Corresponding to Hf Addition — Composition 3

TABLE 20

REACTIVITY CHANGES ACCOMPANYING Hf ADDITION – COMPOSITION 3

Mass of Hf Added (kg)	Number of Elements to which Hf is Added	Zone* Number	Cumulative Number of Elements Loaded	Cumulative Mass of Hf (kg)	Reactivity† Change (¢)	Cumulative Reactivity Change (¢)
1.10988	66	Drums	66	1.10988	+2.7	+2.7
0.83216	50	1	116	1.94204	-2.0	+0.7
0.83307	50	2	166	2.77511	0.0	+0.7
0.82215	50	3	216	3.59726	+1.5	+2.2
0.51881	31	4	247	4.11616	+1.0	+3.2

*See Figure 46.
†Relative to the preceding Hf addition, or, in the case of the drums, relative to Composition 2.

2. Fuel Element Interchange

After loading Hf foil into each of the 247 fuel elements and establishing the reactivity of the system, a fuel element interchange was conducted in accordance with standard procedures. The reactivity change that was observed in this interchange was 0.5¢.

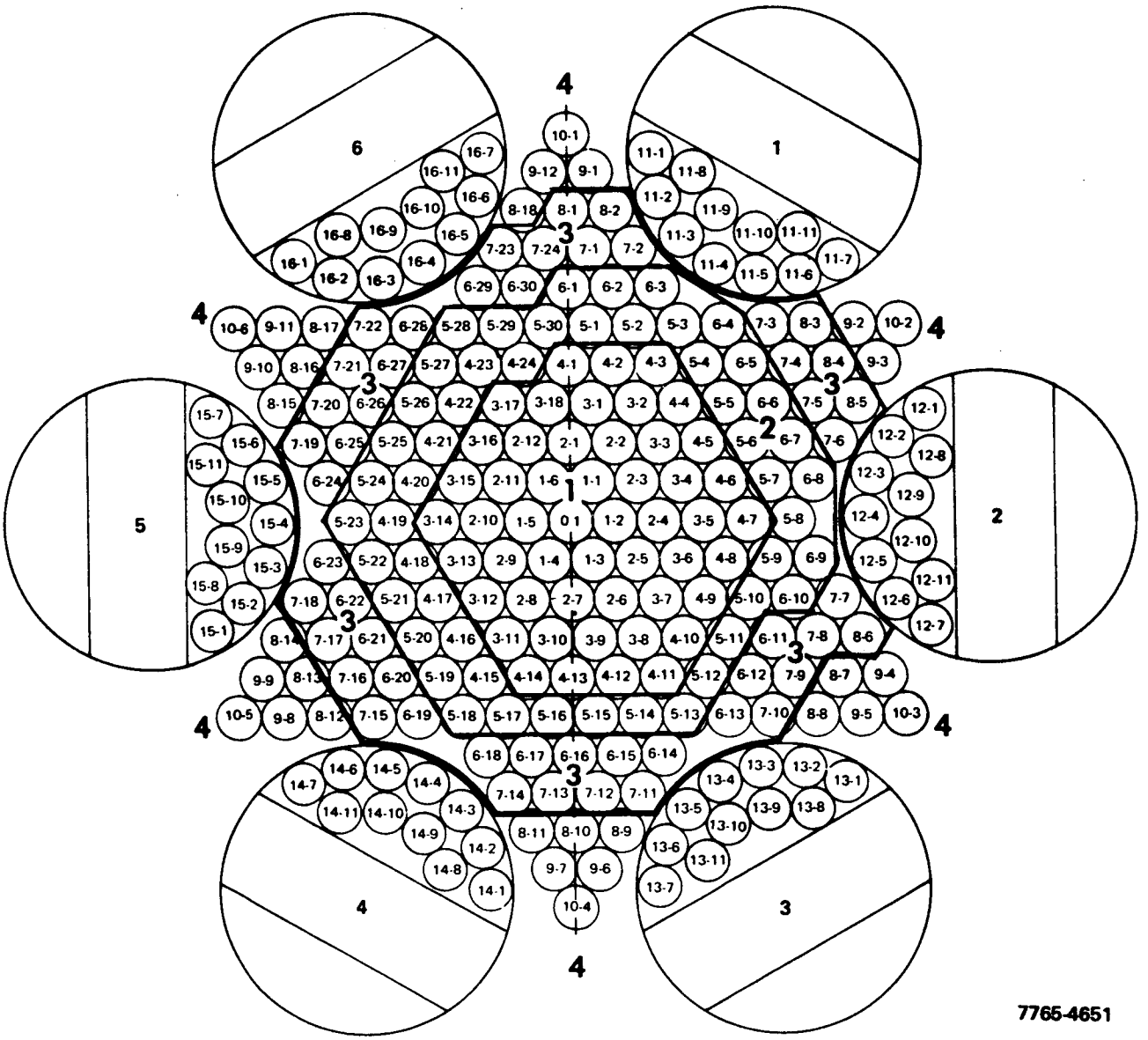

Figure 47. Zones Corresponding to Ta Wire and Foil Addition — Composition 4A

IV. COMPOSITION 4A

A. DESCRIPTION

Composition 4A involved the addition of tantalum to the reactor as it was constituted for Composition 3. This tantalum addition was in two forms: a 37.47-cm(14.75 in.)-wide by ~11.00-cm(4.33 in.) long by 0.0127-cm(0.005 in.)-thick foil coiled to fit around the fuel cluster to form a tube 37.47-cm(14.75 in.)-high between the top and bottom reflectors and a 0.279-cm(0.110 in.)-diameter by 36.83-cm(14.5 in.)-long wire which was placed in the center of the six-rod fuel cluster. The total amount of tantalum foil added in the form of a foil was about 22 kg and in the form of wire was about 9 kg, bringing the total to about 31 kg. As in Composition 3, the total reactivity change was not expected to be very large; consequently, the fuel loading was not changed and remained at the Composition 2 value of 174.96 kg. The quantities of other core and reflector materials are listed in Table 5.

B. EXPERIMENTAL RESULTS

1. Critical Mass

In accordance with previously outlined procedures, the tantalum foil and wire were added to the core in a zone-wise manner and the change in reactivity at each step was measured relative to Composition 3 using an inverse-kinetics technique in which the drum was run to the same position each time. The results of these measurements are given in Table 21. The various zones identified by arabic numerals correspond to those zones shown in Figure 47. Initially, only foil was added to Zones 1, 2, and 3, and resulted in a cumulative decrease in reactivity of 31.0¢ relative to Composition 3. Next, only wires were added to Zones 1, 2, and 3, and resulted in a further reactivity decrease of 29.8¢, bringing the cumulative change to -60.8¢. Two final steps were made and involved the addition of both wires and foil to Zone 4 and the drums. These two steps had a positive reactivity effect and resulted in a net reactivity decrease of -45.5¢.

On the basis of a drum calibration, a total excess reactivity value of 139.3¢ was established for this core, after all wire and foil was added, thus indicating that the net change relative to Composition 2 was more accurately a value of the

TABLE 21

REACTIVITY CHANGES ACCOMPANYING Ta ADDITION – COMPOSITIONS 4 AND 4A

Composition Number	Mass of Tantalum Added (kg)	Number of Elements to which Tantalum is Added	Zone Number	Cumulative Number of Elements Loaded	Form of Tantalum Added	Cumulative Mass of Tantalum (kg)	Reactivity Change (¢)	Cumulative Reactivity Change (¢)
4A	4.50357	51	1	51	Foil*	4.50357	-22.0	-22.0
	4.42117	50	2	101	Foil	8.92474	-9.0	-31.0
	4.40745	50	3	151	Foil	13.33219	-0.0	-31.0
	1.93210	50	1	51	Rods†	15.26429	-15.0	-46.0
	1.93175	50	2	101	Rods	17.19604	-9.2	-55.2
	1.92640	50	3	151	Rods	19.12244	-5.6	-60.8
	3.78821	30	4	181	Rods and Foil	22.91065	+4.6	-56.2
	8.32739	66	Drums	247	Rods and Foil	31.23804	+10.7	-45.5
4	1.203	12	III	12	Rods§	32.441	-0.9	-46.4
	1.203	12	I	24	Rods	33.644	-3.6	-50.0
	10.822	108	I	132	Rods	44.466	-31.6	-81.6
	10.835	108	II	240	Rods	55.301	-7.2	-88.8
	6.016	60	III	300	Rods	61.317	+1.7	-87.1

*Coiled foil with average weight (based on 50 samples) of 90.07 gm/foil.
†0.279 cm diameter by 36.83 cm long; average weight = 38.61 gm/rod, based on group of 21 samples.
§0.356 cm diameter by 59.69 cm long; average weight = 99.92 gm/rod, based on a group of 17 samples.

order of -46.7¢. Using the 139.3¢ value for the total excess, the critical mass for Composition 4A was therefore:

$$171.37 \text{ kg} - \left(\frac{-46.7¢}{51¢/\text{kg}}\right) = 171.37 \text{ kg} + 0.92 \text{ kg} = 172.29 \text{ kg} \quad .$$

2. Drum Calibration

A drum calibration over a portion of the drum travel was carried out in Composition 4A and has already been depicted graphically in Figure 27.

3. Fuel Element Interchange

An interchange of the 30 central fuel elements with 30 elements in the outer periphery of the core was conducted in accordance with the schedule shown in Table 17. A reactivity change of 0.4¢ was observed.

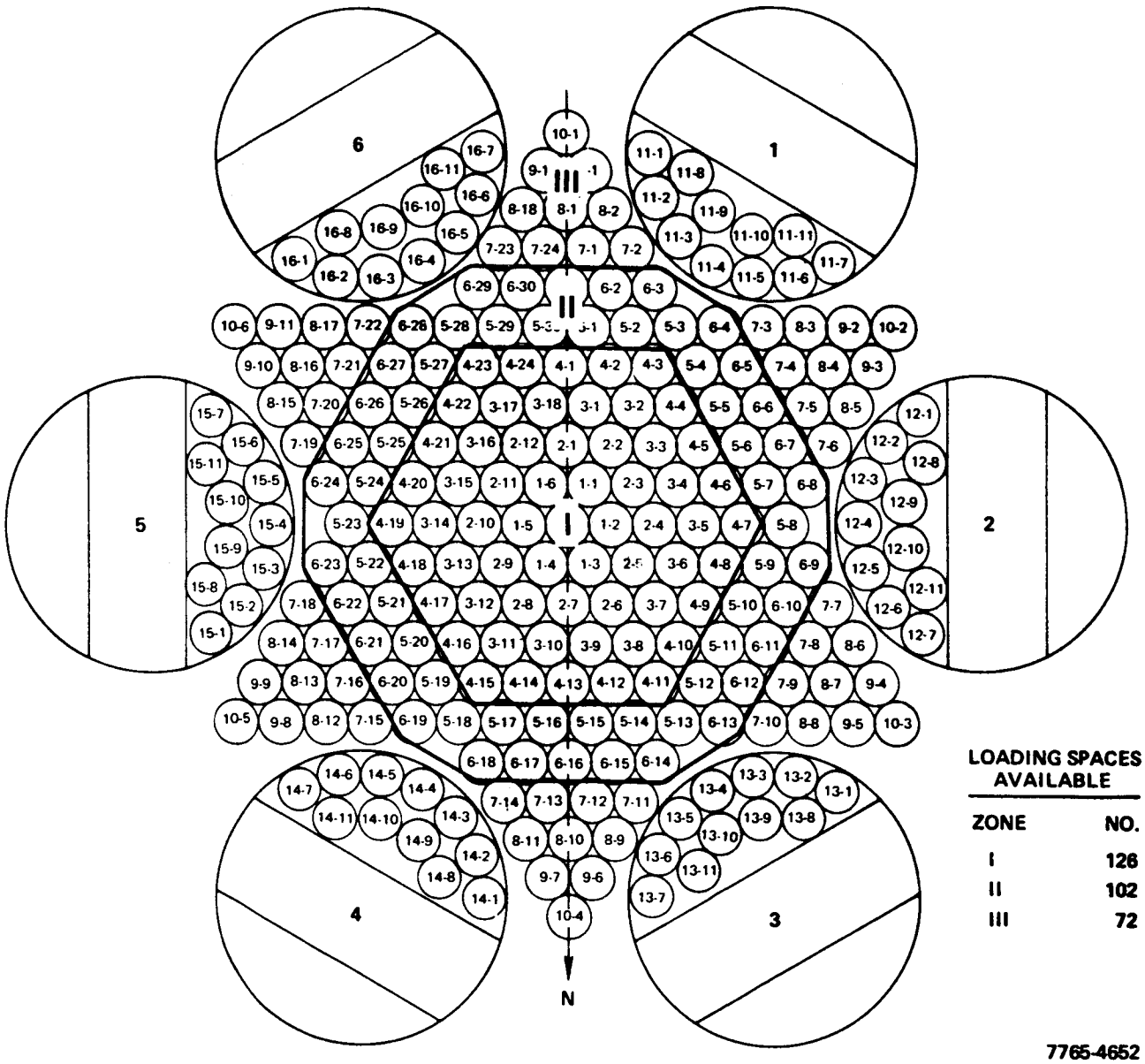

Figure 48. Zones Corresponding to Large Diameter Ta Wire Addition — Composition 4

V. COMPOSITION 4

A. DESCRIPTION

The total mass of tantalum in Composition 4A was somewhat less than that visualized for use in the reference design; consequently some additional tantalum was added to Composition 4A in the form of wire 0.356 cm(0.140 in.) in diameter by 59.69 cm(23.5 in.) high. One wire was added to each of the fully enclosed interstitial positions between the honeycomb tubes in the stationary part of the core and extended into the upper and lower axial reflector regions. On the basis of 17 samples, the average weight of each wire was 99.92 gm. Since the wire extends the full height of the reactor, only 62.8% of the wire (62.75 gm) is in the core proper.

A total of 300 Ta wires of the above type were loaded into the available spaces in the core. The total mass contained in these 300 wires was about 30 kg. As in the previous two cores, the total uranium loading remained the same (174.96 kg) as it was in Composition 2. Total masses of all materials were shown in Table 5.

B. EXPERIMENTAL RESULTS

1. Critical Mass

Since the change in critical mass was still expected to be relatively small (<$1) as a result of the addition of these larger diameter wires, the same process for establishing the critical mass was followed: the change in the excess reactivity relative to Composition 2 was ascertained as a function of the stepwise addition of wires to the core. These results are shown in Table 21 along with the Composition 4A data. The zones designated by roman numerals are depicted in Figure 48. In this type of Ta addition, Zone I refers to all interstices fully contained in the hexagon formed by drawing six lines tangent to the outer periphery of the fourth ring of fuel elements. There are 120 spaces in Zone I. Zone II is formed by the hexagonal ring around and including Fuel Element Ring 6 and therefore contains all fuel elements in Rings 5 and 6. Zone II contains 108 interstitial positions. Zone III refers to the remaining 72 interstices in the core proper. No Ta rods were added to spaces outside of the core or between the core and drums. In the initial step, 12 of the wires were added

to Zone III, one between Elements 8-3, 8-4, and 9-2 and one between Elements 8-4, 8-5, and 9-3 in each of the 6 points of the star, and the reactivity change was found to be -0.9¢. In the second step, 12 wires were added to Zone I, one between each of the elements at the center of the core and between each of the elements just inside Ring 1 (i.e., 1-1, 1-2, 1-3, etc.), and a reactivity change of -3.6¢ was observed. The remaining wires were then added in the remaining spaces in each zone. The reactivity change relative to Composition 4A was found to be -41.6¢ and therefore the total reactivity change relative to Composition 2 was -87.1¢. This value was obtained by inverse-kinetics measurements of the reactivity at fixed drum positions. As in Composition 4A, however, an accurate drum calibration was performed and showed that the total excess reactivity in Composition 4 was 94.2¢, consequently the reactivity change relative to Composition 2 was more accurately established as -91.8¢. The critical mass for Composition 4 is therefore:

$$171.37 \text{ kg} - \frac{(-91.8¢)}{51¢/\text{kg}} = 171.37 \text{ kg} + 1.80 \text{ kg} = 173.17 \text{ kg} \quad .$$

2. Drum Calibration

A step-wise drum calibration covering a portion of the drum travel in Composition 4 was conducted and the results are presented, along with a similar experiment for Composition 4A in Figure 27.

3. Drum Interaction

A series of experiments was undertaken in Composition 4 in order to ascertain whether or not any significant drum interaction existed. In order to eliminate discrepancies that could arise from the location of the chamber relative to the drums of interest, Chamber No. 6 was removed from its usual location and placed within a polyethylene cave on the sample changer table located below the core. Its axis was roughly perpendicular to and in the plane joining the axes of Control Drums 3 and 6. At a power level of about 15 watts, Drums 3, 4, and 6 were driven out individually in separate experiments and their worth was determined as a function of time and position. The worth of Drums 3 and 4, driven out simultaneously, was then measured and followed by an identical run involving Drums 3 and 6 driven simultaneously. The results of these investigations

are given for representative drum positions in Table 22 and indicate that the interaction effect is relatively small.

4. Polyethylene Worth

In order to verify that the reactivity effect of the polyethylene that surrounds the neutron detectors located on the side of the reactor has essentially the value as that determined in Composition 1, the system reactivity was measured before and after removal of the polyethylene around Detectors 5 and 6. A reactivity decrease of 6.6¢ was observed upon removal of polyethylene from one side of the reactor. This value is very close to the result (7¢) previously observed. The value of -14¢ for both polyethylene boxes is therefore assumed to still be a valid number.

TABLE 22

DRUM INTERACTION EFFECTS – COMPOSITION 4

Time (sec)	Position* (°)	Reactivity Worths (¢)						
		Drum 3	Drum 4	Drum 6	Drums 3 and 4	Sum of 3 and 4	Drums 3 and 6	Sum of 3 and 6
0	0	0	0	0	0	0	0	0
10	7.07	-0.66	-2.10	-0.70	-2.03	-2.76	-1.86	-1.36
20	14.14	-3.26	-4.98	-3.28	-7.87	-8.24	-7.23	-6.54
40	28.28	-14.19	-15.74	-14.42	-30.64	-29.93	-29.47	-28.61
60	42.42	-31.84	-32.97	-32.29	-66.47	-64.81	-64.89	-64.13
80	56.56	-55.49	-55.54	-56.06	-113.75	-111.03	-112.15	-111.55
100	70.70	-83.16	-81.86	-84.11	-168.50	-165.02	-169.31	-167.27
120	84.84	-113.69	-110.42	-114.45	-228.55	-224.11	-231.96	-228.14
140	98.98	-143.17	-138.36	-143.42	-284.27	-281.53	-290.14	-286.59

*Zero degrees corresponds to fuel full-in. The drum positions shown here are averages for Drums 3 and 6 and Drum 4. Drums 3 and 6 have a drive speed slightly different from that of Drums 1, 2, 4, and 5. The exact positions of all drums were recorded but the average is used here for brevity.

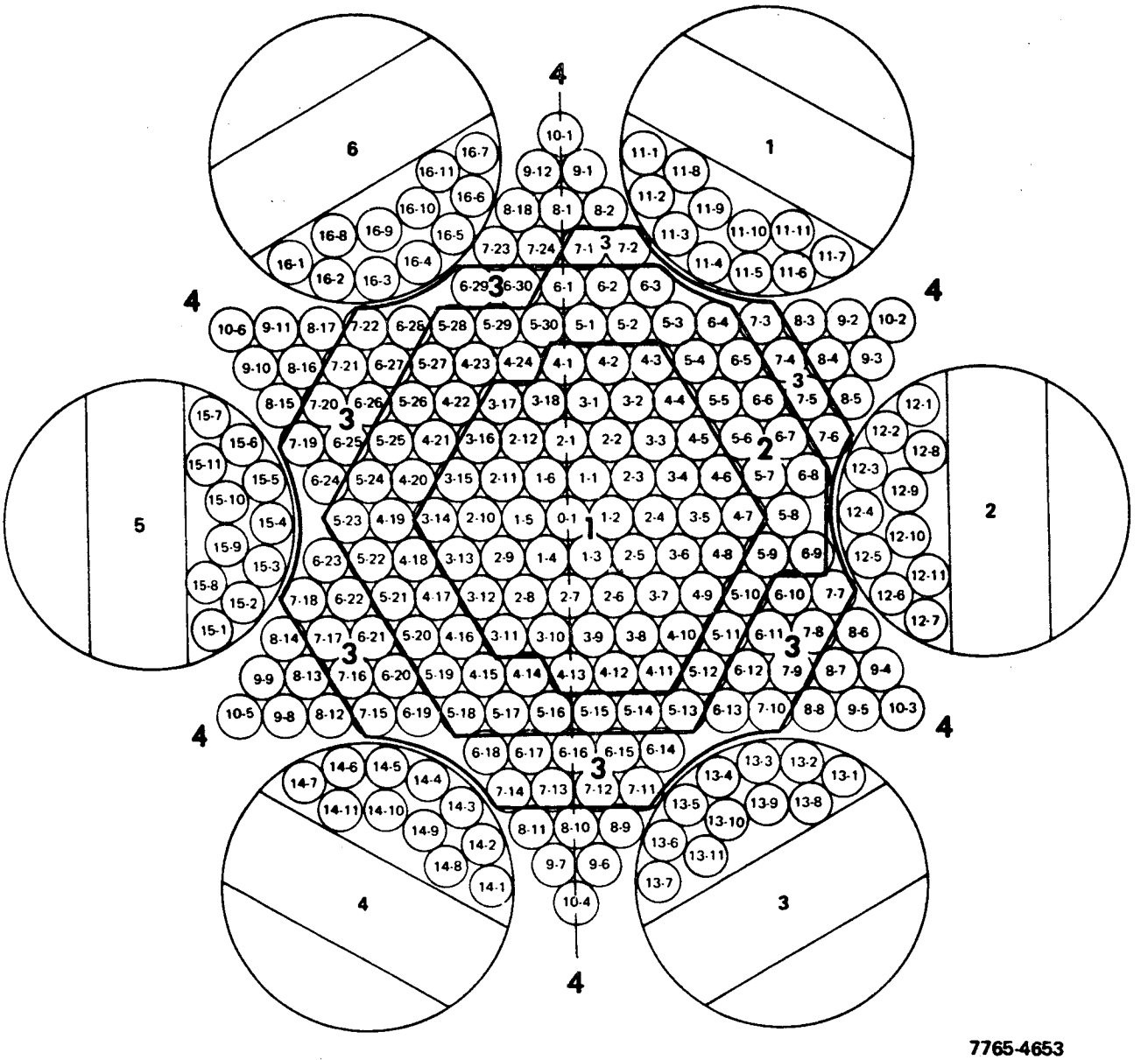

Figure 49. Zones Corresponding to W Addition — Composition 5

VI. COMPOSITION 5

A. DESCRIPTION

Composition 5 was constructed from Composition 4 by adding W foil around the fuel cluster in each of the 247 fuel elements. The foil was made into a coil with a height of 36.83 cm(14.5 in.) and an outside diameter of about 2.11 cm(0.83 in.). The nominal thickness of the foil was 0.0051 cm(0.002 in.). A total of 15.15091 kg of W was added, thus yielding an average mass of 61.39 gm per foil per element. As in the case of the previous three cores, no adjustment was made in the fuel loading; consequently the total mass of uranium remained at 174.96 kg. Reference can be made to Table 5 in order to obtain the masses of the other materials used in Composition 5.

B. EXPERIMENTAL RESULTS

1. Critical Mass

In accordance with the standard procedure, the W foil was added to the core on a zone basis and the reactivity change was measured at each step. Each reactivity change was determined by using the Composition 4 drum calibration. Since this calibration is only approximately correct by the time significant quantities of W are added, the reactivity changes recorded in Table 23 are probably not accurate to better than ±5%. The total change in reactivity, after all the W was inserted into the core, was however, determined separately and was used to establish an actual excess reactivity. In Table 23, the first four reactivity changes are listed relative to Composition 4 by using the latter's drum calibration. The last W addition yielded an increase in reactivity of +23.2¢ as determined by a new drum calibration. The cumulative change relative to Composition 4 was therefore +44.8¢. The W additions were made in zones in accordance with those shown in Figure 49. All elements were loaded in numerical order beginning with Position 0-1. The first 50 are, for example, 0-1 through 4-13. By using the actual excess reactivity of 139.5¢, the decrease in the system reactivity relative to Composition 2 is 139.5 - 186.0 = -46.5¢. The critical mass for Composition 5 is therefore:

$$171.37 \text{ kg} - \frac{-46.5¢}{51.¢/\text{kg}} = 171.37 \text{ kg} + 0.91 \text{ kg} = 172.28 \text{ kg} \quad ,$$

TABLE 23

REACTIVITY CHANGES ACCOMPANYING TUNGSTEN ADDITION – COMPOSITION 5

Mass of Tungsten Added (kg)	Number of Elements to which Tungsten is Added	Cumulative Number of Elements Loaded	Cumulative Mass of Tungsten (kg)	Reactivity* Change (¢)	Cumulative Reactivity Change (¢)
3.35314	50	50	3.35314	+1.8†	+1.8
2.94993	50	100	6.30307	+8.8†	+10.6
2.56827	43	143	8.87134	+11.0†	+21.6
2.29883	38	181	11.17017	0.0†	+21.6
3.98074	66 (drums)	247	15.15091	+23.2§	+44.8

*Change relative to Composition 4.
†Change obtained by using drum calibration curve for Composition 4 with all Ta loaded.
§Change obtained by using drum calibration curve for Composition 5.

assuming that the fuel coefficient (conversion factor) of 51¢/kg for Composition 2 is still valid.

2. Drum Calibrations

As mentioned above, an accurate drum calibration was conducted for Composition 5 after all W was installed in the reactor. This calibration was performed by the step-wise technique and is shown graphically for Drum No. 6 in Figure 28. In order to ascertain the uniformity in the worths of the drums, a similar calibration was conducted for Drums 1 through 5, inclusive. The total worths, from full-in to full-out, of each drum including Drum No. 6, are listed in Table 24 and are reasonably uniform.

A continuous drive-out of all drums ganged was also conducted without range changing; consequently, the power level rapidly became too low to provide accurate results. However, out to about 68 degrees of arc, the discrepancy between the worth multiplied by 61 of a single drum at that position (as determined in Figure 28) and the worth of all drums ganged is not greater than 16%. For example, at 29 degrees, the worth of a single drum (multiplied by 6) would predict

TABLE 24

COMPARISON OF TOTAL WORTHS OF EACH DRUM IN COMPOSITION 5

Drum Number	Total Worth (¢)
1	182.5
2	189.7
3	190.6
4	182.5
5	188.7
6	190.4

that the reactor would be 61.2¢ subcritical. At this same position, the reactor was measured to be 68.7¢ subcritical by a continuous drive of all drums simultaneously.

3. Power Distribution

A power distribution measurement was carried out in Composition 5 by irradiating a 0.066-cm(0.026 in.)-diameter uranium wire within the fuel cluster in every fuel element, except 10-5, within the 1/12 core sector defined by planes passing through the axes of Fuel Elements 0-1 and 10-5, and 0-1 and 5-23 (see Figure 50). The irradiation time was 1 hr and the power level was approximately 38 watts. Drums 4, 5, and 6 were full-in, and Drums 1, 2, and 3 were banked equally at 28 degrees 30 min. in order to maintain level power. In order to reduce the excess reactivity in the system prior to the measurement, Fuel Elements 10-1, 10-2, and 10-3 were replaced by dummy elements containing all the standard materials and components of a Composition 5 element except uranium and $Li_3{}^7N$. Similarly, Fuel Elements 10-4, 10-5, and 10-6 were replaced by dummy elements that contained all standard components except uranium. In the place normally occupied by the uranium cluster, all six elements contained a 37.488-cm(14.759 in.)-long by 1.308-cm(0.515-in.)-diameter Mo reactivity sample, ~517.83 gm each); consequently no uranium wire was irradiated in Fuel Element 10-5. For all wires except those in 0-1, 5-23, 15-8, and 9-9, 1.27-cm(0.50 in.)-long segments were cut from the core center, the top of the core, and a point halfway between these two positions, and were then counted.

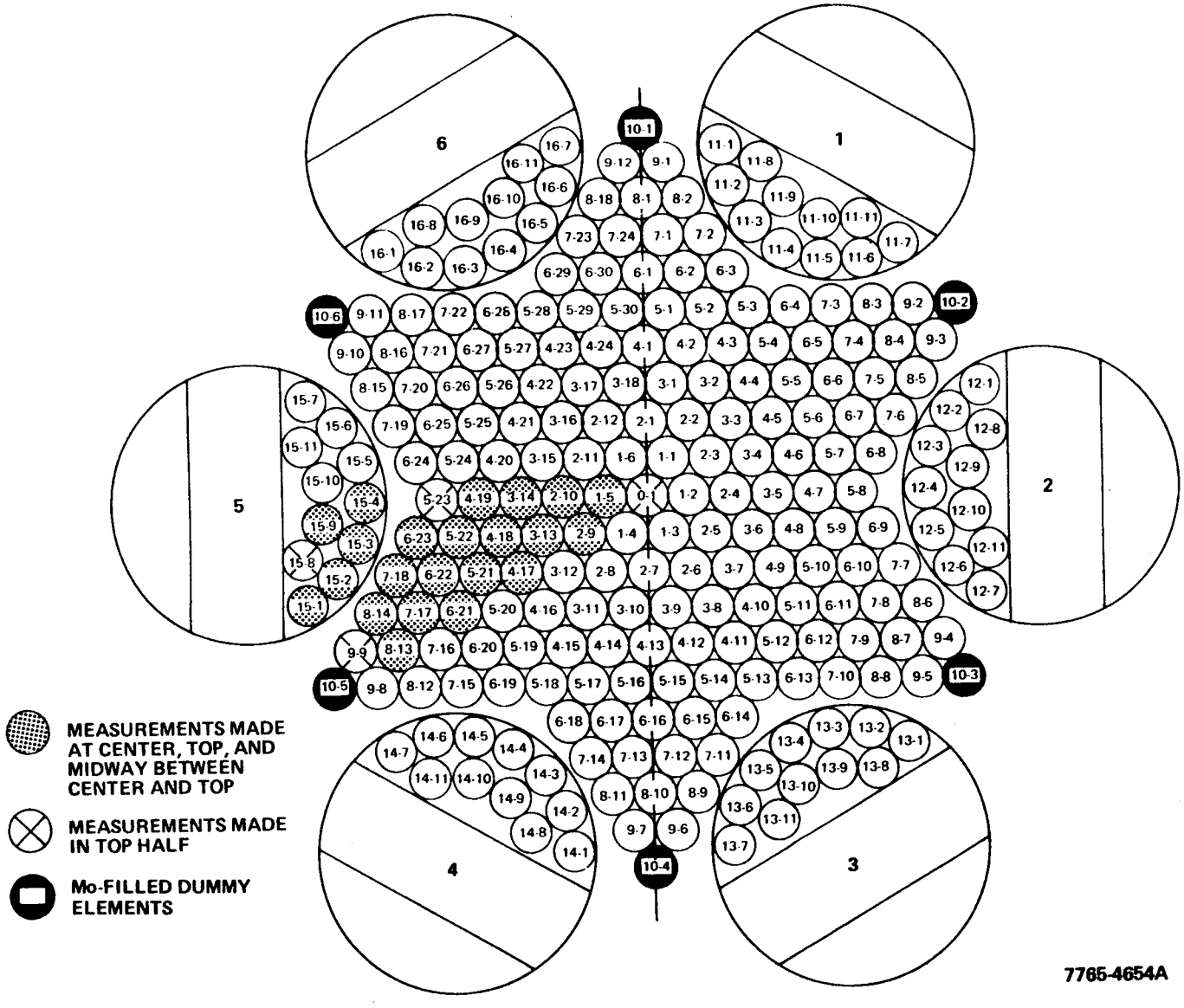

Figure 50. Power Distribution Wire Loading Scheme

The wires in 0-1, 5-23, 15-8, and 9-9 were completely segmented in 1.27 cm (0.50 in.) segments from the core center to the top of the core, and all segments were counted. A few segments were also taken from the lower half of the core and also counted. The counting technique consisted of measuring the gamma activity in the wire segment above 0.5 Mev by means of a NaI crystal.

The results obtained for the power distribution in the radial direction at each of the three heights (center of the core, top of the core, and half way in between) were shown graphically in Section IV of this report (Figure 37) and are tabulated in Table 25. The results obtained for the power distribution in the axial direction in each of the four elements (0-1, 5-23, 15-8, and 9-9) are shown in Figure 37 and are tabulated in Table 26. The table contains values from only one counting channel.

In order to facilitate the counting, three different NaI-crystal counting channels were employed. These counters were internormalized by taking the first six segments (starting at the core mid-plane) in Fuel Element 0-1 and counting them in each of the three counting channels. A normalization factor of 1.00 was derived for Channels 7 and 9 and a factor of 0.90 was found for Channel 8. After corrections for background and decay, the activities of the wires counted in Channel 8 were therefore multiplied by the ratio of 1 to 0.9. The other two channels were corrected only for background and decay. The first six positions on the curve of the power distribution in Fuel Element 0-1 are therefore made up of the three normalized values for the activity of the same wire counted in each of three counters.

In many cases, the same wire was counted twice in the same channel. In order to convey some idea of the systematic and statistical uncertainties in the points, the two values are plotted separately after corrections are made.

In an attempt to substantiate the assumption that the parting planes were the cause of the dip in the power near the core midplane, a new irradiation was performed in which a new 0.066-cm(0.026 in.)-diameter uranium wire was placed in each fuel bundle in Fuel Elements 0-1 and 8-1 and in an interstitial position around 0-1. The fuel rods in 8-1 were re-oriented in such a way that all of the 22.27-cm(8.767 in.)-long rods were placed at one end of the cluster and all of the 15.24-cm(6.00 in.)-long rods at the other. Although the effects

TABLE 25

RADIAL POWER DISTRIBUTION – COMPOSITION 5*

Radius (cm)	Relative Activity at Core Midplane (total counts)	Relative Activity 9.37 cm Above Midplane (total counts)	Relative Activity 18.10 cm Above Midplane (total counts)	Fuel Element Location
0.00	53,659	47,600*	32,799	0-1
2.18	50,713	46,407	32,995	1-5
3.85	49,900	45,602	31,729	2-9
4.40	49,855	45,513	31,904	2-10
5.87	49,086	44,072	31,296	3-13
6.67	48,718	43,212	30,913	3-14
7.70	47,107	42,944	30,490	4-17
7.98	46,411	41,670	30,090	4-18
8.85	45,593	-	29,249	4-19
9.64	-	-	-	5-21
10.16	42,967	39,711	28,015	5-22
11.07	42,435	38,450†	27,849	5-23
11.47	41,378	37,923	26,785	6-21
11.75	42,154	38,327	27,344	6-22
12.30	39,258	36,168	25,775	6-23
13.45	38,889	35,477	25,503	7-17
13.77	37,553	33,999	24,520	7-18
14.68	36,642	33,004	23,647	15-4
15.20	36,574	32,832	23,589	15-3
15.28	35,108	32,127	22,744	8-13
15.48	34,923	32,575	22,661	8-14
16.59	33,509	30,301	21,584	15-2
16.98	33,272	30,193	21,620	15-9
17.26	32,944	29,100†	20,836	9-9
18.34	31,040	27,500†	19,651	15-8
18.53	29,214	26,823	18,898	15-1

*See Figure 36.

†These wire segments were located 9.21 cm above midplane.

TABLE 26

AXIAL POWER DISTRIBUTION – COMPOSITION 5*

Distance From Midplane (cm)	Relative Activity Position 0-1 (total counts)	Relative Activity Position 5-23 (total counts)	Relative Activity Position 9-9 (total counts)	Relative Activity Position 15-8 (total counts)
0.00	53,659	42,435	32,944	31,040
1.27	52,076	42,325	32,559	29,921
2.54	52,082	42,642	33,067	30,346
3.81	52,106	42,603	32,663	31,125
5.08	50,940	41,455	31,668	29,444
6.35	50,204	41,525	31,513	28,924
7.62	49,322	40,379	30,488	28,540
9.21	47,342	38,768	28,767	27,681
10.48	46,261	37,360	28,347	26,813
11.75	44,167	35,876	27,350	25,529
13.02	42,459	34,464	25,786	24,037
14.29	40,891	33,141	24,722	23,714
15.56	38,597	31,158	23,660	22,070
16.83	35,601	29,559	22,264	20,980
18.10	32,799	27,849	20,836	19,651
-9.36	47,542	-	-	-
-16.83	36,408	-	-	-
-18.10	-	-	21,263	-

*See Figure 37.

on the flux distribution of the plane of separation of the fuel rods must perforce be widespread, it was hoped that disrupting this pattern in a single fuel cluster would enhance or degrade the effect to a sufficient extent that some indications of its existence could be ascertained.

After an irradiation of the same type as that previously discussed, the three uranium wires were removed, segmented, and counted. In order to provide more detail at the core midplane the wires were segmented 5.1 cm(2.0 in.)-long sections. Unfortunately, the smaller wires produced lower counting rates

TABLE 27

AXIAL POWER DISTRIBUTION – COMPOSITION 5 (Remeasurement)*

Axial Position (cm)	Relative Activity Position 8-10 (total counts)	Relative Activity Position 0-1 (total counts)	Axial Position (cm)	Relative Activity Position 8-10 (total counts)	Relative Activity Position 0-1 (total counts)
18.14	9,442	13,187	-0.64	14,697†	20,282†
16.97	10,132	13,985	-1.27	15,240	20,457†
15.77	10,662	14,936	-1.91	14,857	20,344†
14.58	11,367	15,597	-2.54	15,603	20,255†
13.41	12,115	16,662	-3.18	14,382	20,236†
12.22	12,422	16,803	-3.81	14,544	19,707†
11.05	12,877	17,509	-4.45	14,451	20,482†
9.86	13,013	18,164	-5.08	14,661	19,651†
8.66	13,308	18,846	-5.72	14,807	19,539†
7.49	14,165	19,233	-6.63	14,298	19,592
6.48	14,062	19,835	-7.80	14,263	19,365
5.72	14,083†	19,706	-8.99	13,731	18,927
5.08	14,593†	19,845	-10.19	13,486	18,515
4.45	14,362†	20,023	-11.35	12,935	17,617
3.81	14,244†	20,110	-12.55	12,336	17,356
3.18	14,819†	21,336	-13.72	12,011	16,677
2.54	14,619†	20,003	-14.91	11,202	15,662
1.91	14,690†	20,499	-16.10	10,984	15,273
1.27	15,176†	20,542	-17.27	10,176	14,299
0.64	15,448†	20,414†	-18.36	9,909	14,166
0.00	14,937†	20,692†			

*See Figure 38.
†Averages of Several Measurements.

in this region, and the statistical uncertainties and therefore the scatter in the data were greater; consequently a positive indication of the absence of the flux dip cannot be made (see Figure 38). The results obtained from the wire located in the interstitial position (between honeycomb tubes), although not included in the figure, were in reasonably good agreement in shape with those of Figure 38. The data are compiled in Table 27.

4. Neutron Spectrum Measurements

In accordance with the usual procedure, as outlined in Section III, the central seven standard fuel elements in Composition 5 were removed and replaced by the proton-recoil detector and thirteen special elements, eleven of which contained Hf, Ta, and W foil, in addition to fuel. The results of the spectrum measurements, which in this core involved some two-parameter analysis, were previously shown in Section IV, Figure 35. The tabulated results are given in Table 28.

As occurred in the case of Compositions 1 and 2, an internormalization between detectors was required. These factors were 0.75, 1.0, 1.0, and 1.32 for the detectors designated 0.9 H_2, 2.63 H_2, 2.63 $CH_4(He^3)$, and 8.1 CH_4, respectively. The detector designated 2.63 H_2 was used for obtaining data for two-parameter analysis, thus extending the lowest energy of measurement to about 20 kev. The relative error in the latter values were, however, somewhat larger.

Two sets of foils were again irradiated at the center of Composition 5 and the results are delineated in Table 29.

5. Fuel Element Interchange

The central 30 fuel elements were interchanged with 30 elements in the outer periphery of the core in accordance with the schedule shown in Table 17. A reactivity change of 2.1¢ was observed.

6. Fuel Element Rotation

In the normal fuel element orientation, the plane passing through the axes of the fuel and honeycomb tubes was placed at right angles to the plane passing through the axes of the honeycomb tube and the core. With the narrow part of the gap between the fuel and honeycomb tubes of all fuel elements aligned in the

TABLE 28
NEUTRON FLUX IN COMPOSITION 5
(Sheet 1 of 2)

2.63 H_2 (2-parameter)									8.1 CH_4		
Run No. 1			Run No. 2			Run No. 3					
Energy (Mev)	Flux, φ (u)	Statistical Error (%)	Energy (Mev)	Flux, φ (u)	Statistical Error (%)	Energy (Mev)	Flux, φ (u)	Statistical Error (%)	Energy (Mev)	Flux, φ (u)	Statistical Error (%)
0.019	0.09	4.5	0.021	0.02	7.4	0.033	0.11	10.4	0.744	2.24	1.4
0.021	0.08	6.1	0.024	0.07	3.8	0.038	0.15	7.6	0.788	2.16	1.7
0.024	0.10	6.4	0.027	0.08	2.9	0.043	0.13	11.2	0.844	1.95	1.7
0.026	0.11	6.5	0.030	0.11	2.9	0.049	0.11	13.9	0.899	2.00	2.3
0.029	0.13	5.6	0.033	0.09	4.0	0.056	0.21	10.0	0.955	2.18	1.9
0.032	0.15	5.2	0.037	0.09	5.2	0.063	0.38	5.9	1.021	1.83	2.6
0.036	0.08	17.8	0.040	0.10	5.3	0.072	0.43	6.8	1.087	1.86	2.9
			0.044	0.11	5.0	0.081	0.56	5.7	1.154	1.85	3.3
			0.049	0.09	7.3	0.096	0.78	1.3	1.232	1.83	3.1
			0.056	0.19	3.7	0.108	0.79	2.1	1.310	1.89	4.1
			0.062	0.27	3.4	0.119	0.90	1.7	1.387	1.80	4.0
			0.069	0.37	3.0	0.135	1.03	1.9	1.476	1.68	4.9
			0.076	0.41	3.4	0.150	1.22	2.0	1.576	1.59	5.0
						0.166	1.45	2.0	1.676	1.44	7.6
						0.181	1.66	2.0	1.776	1.41	7.3
						0.200	1.64	2.0	1.898	1.35	7.7
						0.223	1.48	2.7	2.020	1.35	10.5
						0.250	1.40	2.9			
						0.281	1.23	4.3			
						0.312	1.38	4.7			
						0.343	1.61	4.9			
						0.381	1.76	4.0			
						0.427	1.72	7.3			

TABLE 28
NEUTRON FLUX IN COMPOSITION 5
(Sheet 2 of 2)

0.91 H_2						2.63 H_2 (1-parameter)			2.63 CH_4		
Run No. 1			Run No. 2								
Energy (Mev)	Flux, φ (u)	Statistical Error (%)	Energy (Mev)	Flux, φ (u)	Statistical Error (%)	Energy (Mev)	Flux, φ (u)	Statistical Error (%)	Energy (Mev)	Flux, φ (u)	Statistical Error (%)
0.074	0.57	7.0		0.50	3.3	0.106	0.81	1.8	0.180	1.79	0.8
0.078	0.62	6.0		0.65	2.9	0.116	0.91	1.9	0.189	1.67	1.2
0.084	0.60	7.0		0.77	2.8	0.120	0.95	2.0	0.199	1.61	1.0
0.089	0.75	6.4		0.65	3.8	0.128	0.98	2.2	0.212	1.51	1.2
0.095	0.74	6.1		0.74	3.8	0.135	1.16	2.1	0.228	1.25	1.4
0.101	0.71	7.4		0.76	3.3	0.144	1.23	1.8	0.245	1.17	2.1
0.108	1.04	5.7		0.86	4.3	0.153	1.23	2.5	0.258	1.14	2.4
0.114	1.00	6.7		0.92	3.5	0.162	1.52	1.8	0.274	1.21	2.1
0.121	1.01	6.4		1.02	3.7	0.173	1.59	1.9	0.294	1.26	2.3
0.130	1.25	5.1		1.25	3.4	0.183	1.69	2.0	0.313	1.31	2.5
0.138	1.38	6.0		1.36	3.5	0.196	1.75	1.8	0.333	1.56	2.4
0.146	1.46	5.6		1.39	3.8	0.209	1.73	2.6	0.352	1.68	2.5
0.156	1.64	4.9		1.58	3.1	0.221	1.71	2.4	0.375	1.70	2.3
0.167	1.80	5.1		1.77	3.1	0.236	1.61	2.8	0.401	1.73	2.5
0.177	1 72	6.0		1.76	3.6	0.252	1.31	3.3	0.428	1.76	2.8
0.188	1.76	5.8		1.63	3.6	0.268	1.08	5.5	0.454	1.80	3.2
0.201	1.70	6.2		1.57	5.2	0.284	1.06	5.3	0.483	1.98	2.7
0.214	1.40	8.5		1.29	5.9	0.304	1.29	4.3	0.515	1.99	3.1
0.227	1.33	10.8		1.04	7.2	0.324	1.44	5.1	0.548	2.10	3.3
0.242	1.05	12.1		1.19	8.4	0.343	1.71	4.2	0.580	2.21	3.5
0.258	0.56	26.5		0.98	9.9	0.365	1.73	4.7	0.617	2.10	3.5
0.274	1.32	11.7		1.08	9.0	0.388	1.68	4.8	0.659	2.23	3.3
						0.413	1.92	4.8	0.702	2.22	4.3
						0.440	1.89	4.9	0.744	2.22	4.2
						0.469	2.05	5.1	0.793	2.10	4.5
						0.500	1.85	5.8	0.845	2.13	5.1
						0.532	2.06	5.9	0.901	2.03	5.4
						0.566	2.18	5.7	0.959	1.80	7.0
						0.602	2.39	6.0			
						0.642	1.98	6.8			
						0.683	1.89	9.0			
						0.726	2.16	7.5			

TABLE 29

RESULTS OF FOIL IRRADIATION IN COMPOSITION 5

Foil	Foil Diameter (cm)	Foil Thickness (cm)	Foil Volume (cm)	Foil Mass (gm)	Isotope	Isotope Abundance (%)	Isotope Mass (gm)	Isotope Density (gm/cm^3)	Isotope Number Density (atoms/cc x 10^{24})	Efficiency*	Reaction	Mother	Decay Mode	Daughter	Halflife	Decay Constant, λ (min^{-1})	Activity at Shutdown (counts/sec)	Saturated Activity (counts/sec)	Saturated Activity/Efficiency (counts/sec)	Standard Deviation (%)
Na_2CO_3	0.978	0.521	0.391	0.586	$_{11}Na^{23}$	100	0.254	0.65	0.0170	0.0339	n,γ	$_{11}Na^{24}$	β^-	$_{12}Mg^{24}$	15 hr	7.7×10^{-4}	1.37×10^{1}	3.04×10^{2}		0.33
																	1.53×10^{1}	3.40×10^{2}	1.00×10^{4}	0.29
Al(b)	1.905	0.0787	0.224	0.561	$_{13}Al^{27}$	100	0.561	2.50	0.0559	0.102*	n,p	$_{12}Mg^{27}$	β^-	$_{13}Al^{27}$	9.5 min	7.29×10^{-2}	5.76×10^{3}	5.83×10^{3}	5.72×10^{4}	0.11
(t)																	6.44×10^{3}	6.52×10^{3}		0.14
(b)					$_{13}Al^{27}$	100	0.561	2.50	0.0559	0.102	n,α	$_{11}Na^{24}$	β^-	$_{12}Mg^{24}$	15 hr	7.7×10^{-4}	4.12×10^{1}	9.16×10^{2}	8.98×10^{3}	0.19
(t)																	4.63×10^{1}	1.029×10^{3}		0.19
S(b)	1.905	0.632	1.80	3.05	$_{16}S^{32}$	95.0	2.90	1.61	0.0303	0.0402	n,p	$_{15}P^{32}$	β^-	$_{16}S^{32}$	14.3 days	3.37×10^{-5}	1.92×10^{2}	9.50×10^{4}	2.36×10^{6}	0.066
(t)																	2.17×10^{2}	1.07×10^{5}		0.078
(b)					$_{16}S^{34}$	4.25	0.13	0.07	0.00124	0.0402*	n,α	$_{14}Si^{31}$	β^-	$_{15}P^{31}$	2.6 hr	4.44×10^{-3}	2.85×10^{1}	1.22×10^{2}	3.03×10^{3}	2.3
(t)																	3.60×10^{1}	1.54×10^{2}		2.5
Cu(b)	1.905	0.0170	0.0485	0.383	$_{29}Cu^{63}$	69.1	0.265	5.46	0.0522	0.06*	n,γ	$_{29}Cu^{64}$	β^-	$_{30}Zn^{64}$	12.8 hr	9.02×10^{-4}	1.73×10^{2}	3.26×10^{3}	5.87×10^{4}	0.14
(t)										0.06*							2.00×10^{2}	3.77×10^{3}		0.10
(b)					$_{29}Cu^{65}$	30.9	0.118	2.43	0.0225	0.10*	n,p	$_{28}Ni^{65}$	β^-	$_{29}Cu^{65}$	2.564 hr	4.5×10^{-3}	1.80×10^{1}	7.59×10^{1}	8.38×10^{2}	3.4
(t)										0.10*							2.17×10^{1}	9.16×10^{1}		2.2
InSn(b)**	1.905	0.0132	0.0376	0.266	$_{49}In^{113}$	4.3	0.0046	0.12	0.00062		n,γ	$_{49}In^{114m}$	γ	$_{49}In^{114}$	50 days	9.62×10^{-6}	4.47	7.75×10^{3}		4.1
(t)																	5.05	8.75×10^{3}		3.0
(b)					$_{49}In^{115}$	95.7	0.1014	2.70	0.0142	0.0860	n,γ	$_{49}In^{116m}$	β^-	$_{50}Sn^{116}$	54 min	1.28×10^{-2}	1.42×10^{4}	2.65×10^{4}	3.08×10^{5}	0.036
(t)										0.0968							1.63×10^{4}	3.04×10^{4}	3.14×10^{5}	0.026
(b)					$_{49}In^{115}$	95.7	0.1014	2.70	0.0142	0.0043*	n,n'	$_{49}In^{115m}$	β^-	$_{50}Sn^{115}$	4.5 hr	2.57×10^{-3}	8.42×10^{2}	5.89×10^{3}	1.37×10^{6}	0.15
(t)										0.0048*							9.82×10^{2}	6.87×10^{3}	1.43×10^{6}	0.11

*Estimates
**40% by weight In and 60% by weight Sn
t = Top group of foils
b = Bottom group of foils

same angular direction, a critical position was established for the base case (the null position). All of the 247 fuel elements were then rotated such that the planes described above are parallel and the narrowest part of the gap was toward the core center. This manipulation displaced each fuel cluster by 0.0508 cm (0.020 in.) along the radius toward the core center. Finally, a third rotation was made in such a way that the above-mentioned planes were still parallel but the narrowest part of the gap was facing away from the core center. This step displaced each fuel cluster by 0.1016 cm(0.040 in.) along the radius away from the core center. The reactivity change that was observed by moving the gap from the null position to the position facing the core center line was +22.5¢ and the change corresponding to turning the gap outward from the null position was -25.3¢. These values were based upon the Composition 5 drum calibration. Reactivity-vs-time data were also taken as backup information.

VII. COMPOSITION 5A

A. DESCRIPTION

Because the 300 tantalum wires that were placed in the interstitial positions between honeycomb tubes presented some operational difficulties insofar as reactivity worth measurements were concerned, the wires were removed from the core and the ensuing configuration was designated Composition 5A. Again, no fuel adjustments were made; consequently, the uranium loading remained at a value of 174.96 kg. Composition 5A was, therefore, identical to the previous Composition (see Table 5) except for the removal of this Ta wire material.

B. EXPERIMENTAL RESULTS

1. Critical Mass

The excess reactivity in Composition 5A was determined by a drum calibration which indicated that a value of 193.6¢ would exist if all drums were turned to the fuel-full-in position. Relative to Composition 2, this total excess represented an increase in the overall system reactivity of 7.6¢. By using the conversion factor established in Composition 2, a critical mass of 171.22 kg was determined in the following way:

$$171.37 \text{ kg} - \left(\frac{7.6¢}{51¢/\text{kg}}\right) = 171.37 \text{ kg} - 0.15 \text{ kg} = 171.22 \text{ kg} \quad .$$

After a number of experiments were performed (experiments that involved the manipulation of a considerable amount of fuel in the outer periphery of the core), Composition 5A was reconstituted and given the designation Composition 5A(1). The latter composition was identical to Composition 5A except that, in the course of shuffling fuel around, a slight decrease in the total uranium loading took place: the loading went from 174.96 kg down to 174.84 kg as is shown in Table 5. The total excess reactivity measured for Composition 5A(1) was 182.5¢ as compared to 193.5¢ for Composition 5A.

In order to verify the accuracy of the critical mass value of 171.22 kg that was derived from previous measurements for Composition 5A, a uniform removal of uranium was carried out in Composition 5A(1). This procedure

consisted of the removal of one 0.152-cm(0.060 in.)-diameter uranium wire from each of the 247 fuel elements. This new loading was given the designation of Composition 5A(2). The mass of uranium removed was measured to be 3.225 kg. The excess reactivity of the system as measured by inverse kinetics with all drums full-in was +6.86¢. The excess reactivity for Composition 5A(1) (prior to the removal of one uranium wire) was 182.5¢. The change in reactivity was, therefore, 175.6¢. The core averaged worth of fuel is, therefore, 175.6¢/3.225 kg = 54.4¢/kg, a value somewhat greater than the Composition 2 value of 51¢/kg. The total mass of uranium in the core after wire removal was measured to be 171.6225 kg. This loading would be subcritical by 6.9 - 14 = 7¢ if the polyethylene boxes, which are worth 14¢ and which surround the neutron detectors, were removed. The value of 7¢ corresponds, on the basis of the above measured core averaged fuel worth, to 129 gm of fuel. Thus, the critical mass of Composition 5A(1) is derived to be 171.623 + 0.129 = 171.75 kg.

Since Compositions 5A, 5A(1), and 5A(2) are virtually identical except for uniform uranium loading variations, the critical masses should be identical. This condition is, for all practical purposes, met since the average of the two critical mass values is 171.49 and the deviations are ±0.16%.

2. Drum Calibrations

Drum calibrations were performed in Composition 5A, 5A(1), and 5A(2) by the step-wise technique and were found to yield identical results. A curve that is representative of all three has been presented in Section IV, Figure 29.

3. Pulsed Neutron Measurements — Composition 5A(1)

A series of pulsed neutron experiments was conducted in Composition 5A(1) in order to determine the degree of subcriticality obtained by driving all drums out to various positions. Counting times were made quite long in order to improve statistics relative to some previous measurements in which results were marginal. Pulsing was performed with the reactor at 25¢ subcritical (as determined by inverse kinetics) and also with all drums banked to 45, 90, 135, and 180 degrees. At the -25¢ position, the decay constant, α, was found to be 0.331×10^{6} sec^{-1}. Using this value in the equation

$$\alpha = \alpha_c(1 - \$) \quad ,$$

where α is the decay constant at some reactivity value, \$, in units of dollars, and α_c is the decay constant at critical, one obtains a value for α_c of 0.265×10^6 sec^{-1}.

As previously indicated, this value for α_c does not agree with the expected value of β_c/ℓ ($0.0067/41 \times 10^{-9}$ sec) of about 0.163×10^6 sec^{-1}. It also produced poor agreement when used to measure the worth of the group of seven large B^{10} samples placed in the seven central fuel element positions, where the worth of the B^{10} was assumed to be well known from inverse kinetics measurements. Assuming, nevertheless, that this measured value for α_c (i.e., 0.265×10^6 sec^{-1}) is correct, one can use it, along with the measured decay constants at 45, 90, 135, and 180 degrees, to derive a worth for all drums banked to these positions. This analysis was performed* and the results are shown in Table 30. The reactivity calculated from the measured constants are adjusted to arbitrarily make the worth of all drums equal to zero at the fuel full in position (0 degrees). The total worth of \$8.34 is in very poor agreement with the value that would be obtained on the basis of the worth of one drum (\$2.15 – see Figure 29) multiplied by six (i.e., \$12.90); consequently, the results are not considered reliable, in part because the value for α_c appears to be in error.

As was indicated in the section on Experimental Results, the value for α_c as determined by the Rossi-α method appeared to be in much better agreement with expectation than the above value and also produced excellent agreement between pulsed neutron measurements and inverse kinetics when the B^{10} samples were used as a standard. The worths of all drums banked to 16, 45, 90, 135, and 180 are also shown in Table 30, where a value of 0.211×10^6 sec^{-1}, as determined by the Rossi-experiment, is used for α_c. The 16° position corresponds to the -25¢ subcritical position that was assumed to be known. At this position, a very large discrepancy is encountered and no explanation for it has been found. Using the Rossi-α value for α_c, one obtains a worth (for all drums ganged in the full-out position) that is 17% lower than that which would be

*The more exact expression $\$ = \dfrac{1 - \frac{\alpha}{\alpha_c}}{1 - \frac{\alpha}{\alpha_c}\beta_c}$ has been used.

TABLE 30

DRUM WORTHS AS DETERMINED BY THE PULSED NEUTRON METHOD

Drum Position*	αc ($\times 10^6$ sec^{-1})	Measured Decay Constant ($\times 10^6$ sec^{-1})	Reactivity ($)	Worth of Ganged Drums ($)†
0	0.265	-	+0.70	0
16**	0.265	0.331**	-0.25**	-0.95**
45	0.265	0.446	-0.69	-1.39
90	0.265	1.062	-3.09	-3.79
135	0.265	1.661	-5.49	-6.19
180	0.265	2.179	-7.64	-8.34
0	0.211§	-	+0.70	0
16	0.211	0.331	-0.57	-1.27
45	0.211	0.446	-1.13	-1.83
90	0.211	1.062	-4.17	-4.87
135	0.211	1.661	-7.26	-7.96
180	0.211	2.179	-10.02	-10.72

*All drums banked simultaneously.

†The reactor was critical with Drum No. 6 at 65°, a position which would give an excess of $0.70 with all drums in.

§This value is based on the inverse decay constant, αc, of 4.73×10^{-6} sec as measured by Rossi-α method.

**Normalization point for all data using 0.265×10^6 sec^{-1} for αc.

expected on the basis of a single drum worth, where the latter is measured by the inverse-kinetics technique.

4. Reactivity Worth of Some Large Samples in Composition 5A

The reactivity worths of 16 different, full, core-length samples were measured in the six outermost peripheral fuel element positions (10-1, 10-2, 10-3, 10-4, 10-5, and 10-6) and in the seven central positions (0-1, 1-1, 1-2, 1-3, 1-4, 1-5, and 1-6). Each sample occupied the space normally filled with fuel rods in these fuel elements. Reactivity measurements were made by exchanging the samples and reference samples (voids) while the reactor was critical or slightly supercritical. The results of these measurements were listed in

Tables 10 and 11. Tables 10 and 11 list: (1) the mass of the prime constituent of each sample, (2) the worth relative to a void before and after corrections for isotopic and chemical impurities, and (3) the specific reactivity (worth per unit mass). Table 12 gives similar data for measurements in which a void was produced in the U^{235} samples and in the Li^{7} samples at different axial locations.

Two modes of operation were used in making these measurements. In one, the reactor was adjusted close to critical with all control drums equally turned out. After a period of time during which stabilization of the power took place, the sample changer was driven to its other position; data collection was terminated about 1 min after completion of the sample change. The difference between the prechange reactivity (which was always close to zero) and the postchange reactivity is taken as the reactivity worth of the sample. The other method involved establishing the reactor at critical with five of the six control drums turned full in. After a waiting time, the sixth drum was turned full-in, making the reactor supercritical by approximately 10¢. After another waiting time, during which the power increased to nearly full scale on the power monitor, the sample change was performed. Approximately 1 min was allowed for data collection after the completion of the change. In this case, the difference between the stable supercritical reactivity and the postchange reactivity was used as the measure of the worth of the sample.

5. Reactivity Worths of Small Samples in Composition 5(A)

In order to provide a more sensitive test of reactivity calculations than is afforded by large sample worth measurements, the reactivity worths of 9 different, nearly infinitely dilute, materials were measured in the center of the core. These small-sample measurements were made using a reactivity oscillator, with the power oscillations analyzed by means of the iterative inverse-kinetics program.

The samples were thin-walled tubes, generally 0.010 in. thick by about 2 in. long, mounted in an oscillator tube that passes through the special fuel element in the central position in the core.

The results of these measurements were listed in Table 13. This table lists: (1) the net worth, corrected for the void worth and the sample cladding, and (2) the specific reactivity, which is the corrected worth divided by the material mass.

6. Reactivity Worths of Fuel in Various Core Positions – Composition 5A

In order to establish the reactivity worth of fuel as a function of radial position, a series of substitution measurements were conducted in which a standard fuel element was removed and replaced by a dummy element containing all the usual components in a standard element except fuel and foil. On the basis of a control drum calibration, the change in drum position between the standard fuel element and dummy element was converted to reactivity. These substitution measurements were made in Fuel Element Positions 4-1, 6-1, 8-1, and 10-1 and the results were shown in Table 9.

7. Reactivity Worth of a Void in the Outer Six Peripheral Locations

A measurement of the reactivity change that accompanied the creation of a void in the space normally occupied by fuel in the outer six peripheral fuel element positions (10-1 through 10-6, inclusive) was conducted in Composition 5A. The drum position for achieving criticality with standard elements in all positions was compared with the drum position for criticality with the six dummy elements in fuel element positions 10-1 through 10-6. Three of the six dummy elements contained all of the standard fuel element components except fuel and refractory metal foils and three contained all of the standard components except fuel, the refractory metal foils, and $Li_3{}^7Ni$. The change in the excess reactivity as derived from a drum worth curve and after corrections for the absence of $Li_3{}^7N$ in three of the dummy elements, was found to be -121.1¢.

This value was confirmed in a more accurate manner by the analysis of another unrelated experiment conducted for the determination of the worth of the six B-10 samples in Positions 10-1 through 10-6. During the latter experiment, a measurement was made of the excess reactivity of the reactor system with voids in the outer six positions and Fuel Element 0-1 removed. The excess under these conditions was found to be 14.03¢. Since the worth of fuel in the central seven fuel element positions was measured to be $+77.43^*$ x 10^{-3} ¢/gm, the reactivity change attributable to the empty element in position 0-1 would be

$$(77.43 \times 10^{-3}\ ¢/gm)\ (707.44\ gm) = 54.78¢\ .$$

*The measured worth of the fuel before correction for the U^{238} content.

At the time the 14.03¢ excess value was determined, the changer table was in its full-up position and it thus added about 3.28¢ to the total excess reactivity of the reactor. The total excess reactivity with voids in the outer six positions, a standard fuel element in Position 0-1, and the changer withdrawn is therefore

$$14.03¢ + 54.78¢ - 3.28¢ = 65.53¢ \quad .$$

The total excess reactivity of Composition 5A, as previously noted was 193.6¢. The reactivity change caused by the voids would therefore be

$$193.6¢ - 65.53¢ = 128.07¢ \quad .$$

This value is in reasonably good agreement with that shown above.

After achieving the reactor configuration designated Composition 5A(1), a third measurement was made of the change in reactivity caused by creating a void in the outer six peripheral locations. In order to carry out this experiment, the fuel elements in Positions 10-1 through 10-6, inclusive, were removed and replaced by the special fuel elements that accept the sample holder tubes. Each of the 6 sample holder tubes was loaded with a large Li^6 sample in the upper chamber and then installed in the changer mechanism in the manner normally used in conducting reactivity worth measurements.

In order that the all-drums-in excess could be measured, the fuel loading in the central seven fuel elements (0-1 and 1-1 through 1-6, inclusive) was reduced in a uniform manner. The average weight of uranium in the central seven fuel elements was reduced to 617.91 gm.

The experiment was then conducted as follows:

1) The sample changer was driven to its full-up position, thus placing void zones in the locations normally occupied by fuel.

2) The reactor was brought to critical and maintained at a level power for several minutes by banking Drum No. 6 at 24°20'.

3) After equilibrium conditions were achieved, Drum No. 6 was driven full-in and the reactor power was allowed to increase for a short time.

4) The sample changer was then driven down in order to bring the Li^6 samples into the core.

The excess reactivity with all drums full-in was found, by analysis of the power trace, to be 9.214 ± 0.004¢. From the previous measurements of the worth of the large samples in peripheral locations it was found that the changer table in the up position added 3.277¢; consequently, the net excess reactivity that would exist with voids in the outer positions and the table removed would be 5.937¢.

On the basis of previous worth measurements in the center of the core as well as on the periphery, it is possible to obtain an estimate of the excess reactivity relative to Composition 5A(1) that would exist upon removal of fuel in the outer six positions and the adjustment of fuel in the central seven positions. The weight of U in the central seven elements prior to the experiment was 4953.24 gm. After adjustment it was 4325.37 gm. The difference is 627.87 gm, whose worth would be (627.87 gm) (77.43×10^{-3} ¢/gm = 48.62¢. The weight of uranium in the outer six peripheral locations prior to the experiment was 4229.71. If all of this uranium were removed, it would decrease the system reactivity by (4229.71 gm) (29.27×10^{-3} ¢/gm)* = 123.80¢. Thus the total loss in reactivity that would be expected would be 123.80 + 48.62 = 172.42¢. If the excess reactivity were 182.3¢ prior to the experiment, one would expect an excess of 182.3 - 172.4 or 9.9¢ after the fuel adjustments. The latter value, which does not take into account the removal of the foil materials that are also normally located in the standard fuel elements, is to be compared to the measured value of 5.9¢ noted above. The agreement is reasonably good.

From this experiment and the arithmetic operations outlined above, the reactivity change, relative to the unperturbed Composition 5A(1), that would be expected to occur upon removal of fuel alone (and therefore the creation of a void) in the outer six peripheral fuel elements would be 182.3 - 5.9 - 48.6 = 127.8¢. This value is in very good agreement with that quoted above.

In conjunction with the analysis of the power trace involved in the above experiment, a value for the worth of Li^6 can also be derived and compared with

*The measured worth of the fuel before correction for the U^{238} content.

that previously measured during the sample worth studies. As noted, the excess reactivity with all drums in and table down was 5.937¢. With Li^6 in the core, the system reactivity was -32.344¢. Thus the worth of six large Li^6 samples was -32.344¢ - (+5.937¢) = -38.281¢. The specific worth is the above value divided by the total mass of 126.114 gm; i.e., -0.30354¢/gm. The previously determined value was -0.30787* ¢/gm.

8. Control Characteristics — Composition 5A(2)

A series of experiments that produced results in very good agreement with expectations for the worths of all drums banked out was conducted using the inverse-counting technique. The experiment consisted of the following steps starting with Composition 5A(2):

1) Fuel Element 0-1 was removed and replaced by two of the long proton recoil fuel elements, thus creating a 3.81-cm(1.5 in.)-high cavity in the center of the core.

2) Since the creation of a cavity in the center of the core rendered it subcritical, one fuel rod was added to Fuel Element 1-1, one to Fuel Element 1-3, and one to Fuel Element 1-5.

3) A steady-state critical position was measured on all drums and on one drum alone. The excess as determined by the drum worth curve was 18¢.

4) A Cf^{252} source was inserted into the center of the cavity in the center of the reactor.

5) Channel 1, a pulse chamber, was placed on top of the core.

6) All drums were banked uniformly at 15, 20, 25, 30, 40, 60, 90, 120, 150, 160, 170, 175, and 180 degrees.

7) The total number of counts detected at each step for a uniform time interval were recorded not only for Channel 1, but also for Channels 6 and 2.

8) Using the drum calibration curve, the degree of subcriticality with all drums banked to 40° was found to be -$1.44 and this value was used to normalize the inverse counting data.

*Without correction for Li^7

The results of this experiment were previously shown in Figure 32. The total worth of all drums was found to be, for Channels 2 and 6, about -$13.20. The expected worth, assuming no drum interaction, would be (-$2.15) (6) = -$12.90, based on the stepwise drum calibration shown in Figure 29.

At the conclusion of the above experiment, an adjustment in the fuel loading was conducted at the center of the core in order to determine the change in 1/M with a change in uranium mass. This process consisted of reloading all fuel elements in Positions 0-1 through 4-24, inclusive, as well as in 5-1, 5-5, 5-6, 5-10, 5-11, 5-15, 5-16, 5-20, 5-21, 5-25, 5-26, and 5-30. At the conclusion of this manipulation, approximately 4.75 kg of uranium had been uniformly removed. Assuming an average worth of about 60 ¢/kg, one would expect a change in reactivity of $2.85. Since the core had an excess reactivity initially of about 18¢, the reactor would be a net $2.68 subcritical.

A series of inverse counting measurements was conducted in the altered core. In this case, however, all drums could also be driven full-in. The total counts measured with all drums in were used, along with the above quoted normalization value, to determine the degree of subcriticality. The resulting value was -$2.95, a number in reasonably good agreement (i. e., within 10%) with the expected result.

A calculation for the drums full-out was also performed and indicated that the reactor was -$17.38 subcritical. This result yields a worth of -$14.43 for all drums. This value is to be compared with -$13.20 shown above.

VIII. COMPOSITION 5B

A. DESCRIPTION

By the time that the experiments that were designed to measure the worths of the large samples in the central seven fuel element positions were completed, one extra fuel rod had been added to a total of 77 fuel elements in the outer periphery of the core. This fuel addition was required to offset the loss in reactivity created by removing the fuel from the central seven elements. This configuration was designated Core 5B and was used to carry out some exploratory experiments on determining large negative reactivity worths by the inverse kinetics technique.

Composition 5B was thus a nonuniformly loaded core identical in all other respects to Composition 5A. Its total uranium mass loading at the time the inverse kinetics experiments were conducted was 180.54 kg and the excess reactivity with all drums turned fuel-full-in was 45¢. The masses of all other materials were listed in Table 5.

B. EXPERIMENTAL RESULTS

1. Drum Calibration

A step-wise drum calibration was conducted on Drum No. 6 and the results were previously shown in Figure 30. As additional fuel was located in the drum, the worth increased, as would be expected, from full-in to full-out to $2.42.

2. Control Characteristics

As has already been indicated, one of the major difficulties in measuring large negative reactivities by means of inverse-kinetics concerns the low power levels that result if the reactivity change cannot be made in rather short lengths of time. If the large negative reactivity change occurs rapidly, as in a safety rod or reflector scram, the inverse-kinetics technique has been shown to be quite precise. However, in the case of the drive-out of the drums in the critical assembly, the reactivity change is made very slowly and, by the time the drums are full-out, the power level has dropped by a factor of about 5×10^4, thus reducing the power level into the zero-setting range of the instrument being used to record this parameter.

In order to evaluate the error introduced by this change in power and to obtain a measure of the improvement available through the use of range-changing, a group of drum worth measurements was conducted and are outlined in Table 31.

TABLE 31

DRUM WORTHS IN COMPOSITION 5B

Case Number	Drum Number	Date	Initial Drum Location	Detector Location	Instrument Readout	Type of Drive	Approximate Reactivity Change (¢) at		
							70°	120°	180°
1	1 - 6	10-9	13°	Side	R. C.*	Continuous	-550	-1485	-2310
2	5	10-19	19°30'	Side	Standard†	Continuous	-80	-175	-
3	5	10-19	19°30'	Side	R. C.	Continuous	-80	-185	-255
4	1 - 6	10-19	19°30'	Side	Standard	Continuous	-440	-	-
5	1 - 6	10-19	21°20'	Top	R. C.	Continuous	-550	-1510	-2380
6	6	10-26	-	Side	Standard	Step-Wise	-85	-192	-242

*Range change used.
†No range changing; standard procedure.

As can be seen, the worths of the equivalent single drums numbered 5 and 6 were approximately the same whether they were measured in a step-wise fashion (see Figure 30) or in a continuous drive with range changing. Also, out to the limits where the power level is not a problem (~120°), a continuous drive of equivalent single drums without range changing is in reasonably good agreement with the other techniques.

With regard to measurements involving the motion of all drums simultaneously, an anomalous behavior is observed insofar as comparisons with the worth of a single drum multiplied by 6 are concerned. Assuming the worth of a single drum is about -$2.42, one would expect the worth of all six drums to be -$14.52, all other parameters remaining constant. The observed value of -$23 was therefore indicative of problems in the inverse-kinetics technique at large negative reactivities.

3. A Measurement of the Ratio of ℓ/β_e

A series of Rossi-α measurements was conducted in accordance with the methods outlined in the section on Experimental Techniques. A smooth decay

curve was observed from which an exponential with a time constant of 4.73×10^{-6} sec was extracted. This time constant is defined as ℓ/β_e and is in better agreement, as has already been pointed out, with the expected value of 6.12×10^{-6} sec than is the value (4.13×10^{6} sec) as determined by pulsed neutron techniques. As indicated, a more sophisticated analysis, which takes into account a two-exponential decay, produced a value for ℓ/β_e of 6.27×10^{-6} sec, a value which is essentially the same as that calculated.

4. Pulsed-Neutron Measurements

A series of pulsed-neutron measurements, primarily intended as a check on the validity of the method, was carried out in Composition 5B at 25¢ subcritical and at $2.74 subcritical (seven B^{10} samples in place at the core center). The time constant decreased from 3.30 microsec at -25¢ to 1.31 microsec at -$2.74. If the time constant at -25¢ is used to derive a value (2.42×10^{5} sec^{-1}) for α_c and if this value of α_c is used in the equation $\alpha = \alpha_c (1 - \$)$, the expected value for the degree of subcriticality with the B^{10} samples in place is -$2.15. This value is 22% lower than the expected value.

If a value for α_c of 2.11×10^{5} sec^{-1} as determined in the Rossi-α experiment is used in the above equation, then a considerable improvement between the measured and expected value for the degree of subcriticality is achieved for the case in which the B^{10} sample is in place. The B^{10} sample would be derived to be -$2.62 by use of the Rossi-α technique for determining α_c.

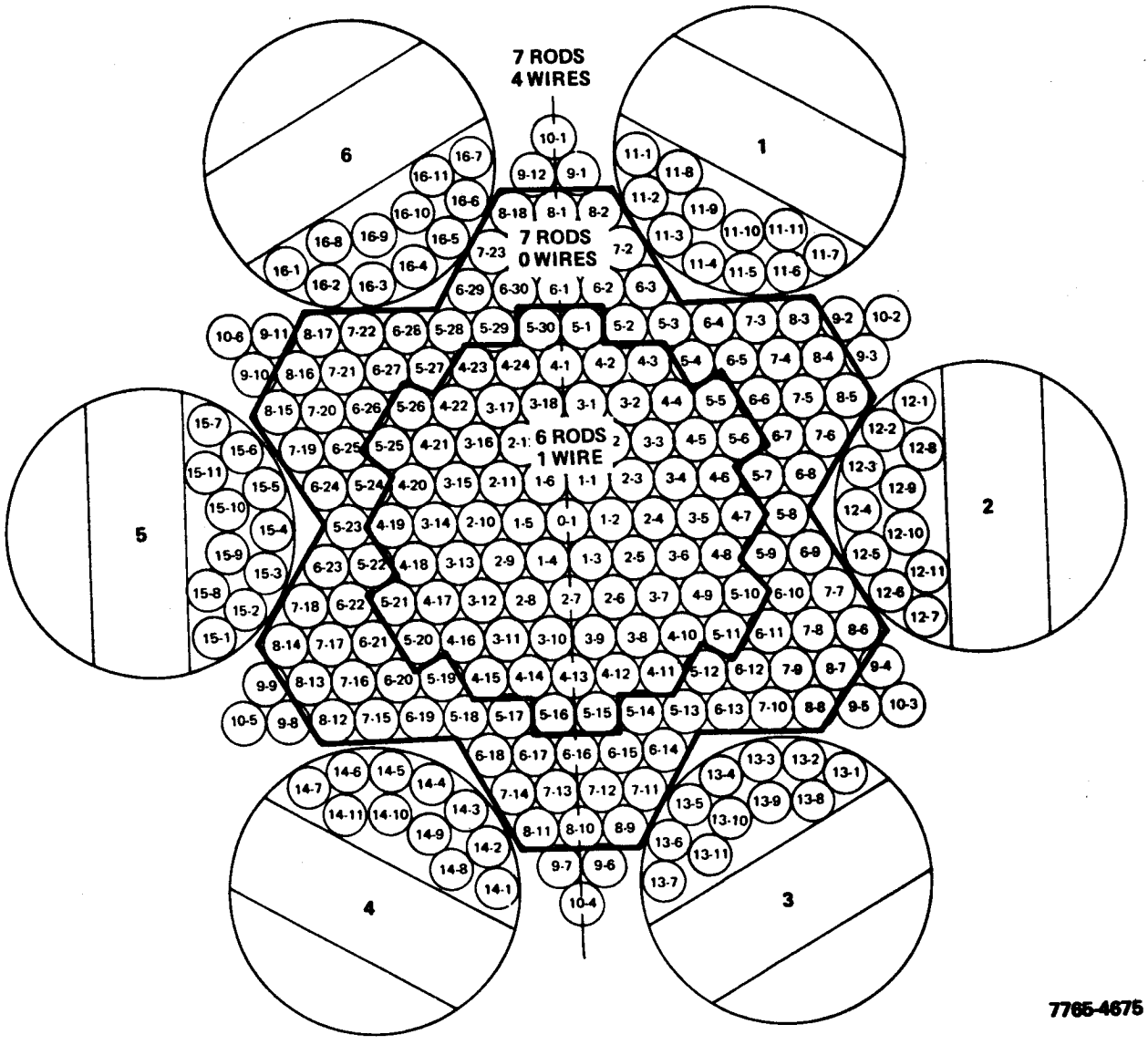

Figure 51. Three-Zoned, Power-Flattened Core Loading Arrangement

IX. POWER-FLATTENED CORE

A. DESCRIPTION

Upon completion of the experimental program for Composition 5 and its variations, the fuel loading in the reactor was modified to achieve a flatter power distribution. This task was accomplished by creating a three-zoned core as depicted in Figure 51, where the wires in each zone refer to the 0.152-cm (0.050 in.)-diameter uranium fuel. The uniformity of the uranium loading was controlled so that the standard deviation of the mass distribution from one element to the next in any given zone was ±1 gm or less. The masses of the lithium nitride, hafnium, tantalum, and tungsten were shown in Table 5, along with a value for the total amount of uranium in the core.

B. EXPERIMENTAL RESULTS

1. Critical Mass

The detailed loading arrangement by zones is given in Table 32. This loading had, before correction for the polyethylene boxes, an excess reactivity of 52.0¢ with all drums in the fuel-full-in position. If the polyethylene boxes are assumed to be worth 14¢, the total excess would therefore be 38.0¢.

TABLE 32

POWER-FLATTENED CORE LOADING SCHEME

Zone Number	Number of Rods	Number of 0.152-cm Wires	Number of Elements*	Average Fuel Mass Element (gm)	Standard Deviation on Fuel Mass (gm)	Total Fuel Mass (kg)
1	6	1	73	628.130	0.740	45.853
2	7	0	90	717.239	0.874	64.551
3	7	4	84	768.856	1.008	64.584
					Total Fuel Mass	174.988

*See Figure 51.

For purposes of facilitating measurements of drum worths, the excess reactivity in this core was reduced to 16¢ by the removal of 484 gm of uranium from Fuel Element 1-1. This manipulation reduced the total uranium loading to 174.504 kg and indicated that the specific worth of fuel in Position 1-1 is 74.4 ¢/kg, a value that is very similar to that obtained in Composition 5A.

In order to carry out an experiment associated with the measurement of the power distribution in this flattened core, one 0.152-cm(0.060 in.)-diameter uranium wire was added to each fuel element in the core. The resulting mass distribution is tabulated in Table 33. The measured excess reactivity for this arrangement was $2.25, which, when corrected for the polyethylene boxes, reduces to $2.11. The total mass of uranium added to the core relative to the initial configuration was 178.225 - 174.988 = 3.237 kg. The reactivity change was $2.11 - $0.38 = $1.73; consequently, the core-average worth-per-unit-mass of fuel is 0.534 ¢/kg. By using this value, one can convert the excess reactivity values to excess mass and derive a value of 174.28 kg (see Table 6) for the critical mass of the power-flattened core if uniform fuel adjustments were made.

TABLE 33

POWER-FLATTENED CORE LOADING SCHEME
(One wire added)

Zone Number	Number of Rods	Number of 0.152-cm Wires	Number of Elements	Average Fuel Mass Element (gm)	Standard Deviation (gm)	Total Fuel Mass (kg)
1	6	2	73	641.521	±1.741	46.831
2	7	1	90	730.332	±1.775	65.730
3	7	5	84	781.710	±1.354	65.664
					Total Fuel Mass	178.225

2. Drum Calibration

The worth of a single drum (Number 6) in the power-flattened core was determined by the stepwise inverse-kinetics techniques. This calibration, which was previously shown in Figure 31, was used to determine the excess reactivity values listed above. The total worth from fuel-full-in to fuel-full-out was $2.57.

3. Control Characteristics

The reactivity effects of turning control drums in various combinations from full-in to full-out was investigated by both the inverse-counting and continuous-drive, inverse-kinetics methods. In the inverse-kinetics method, range-changing was employed to improve statistical accuracy, although these values are not considered systematically valid at large values of negative reactivity. In the inverse counting method, the Cf^{252} source was placed at the center of the core in the standard way and counts were monitored by Channels 1, 2, and 6, with Channel 1 being placed on top of the reactor. The results of these measurements, including a value applying to the case in which the Ta absorber segment was removed from each of the six drums, were shown previously in Section IV, Table 7. Also listed in that table was the reactivity worth of Drum 6 alone, with the Ta absorber removed. Comparison of the latter value with that for Drum 6 in the initial power-flattened core indicates that, in this particular reactor configuration, the control swing of the drum with and without the Ta absorber is not very different. Therefore the segment could probably be eliminated insofar as reactor control is concerned. In a shielded reactor system, this advantage may, however, be reduced. Removing the Ta absorbers does, however, increase core leakage and therefore increase the critical mass.

In order to measure the worths of the drums with the Ta absorber segment removed, additional fuel had to be added, since the removal of the Ta rendered the reactor substantially subcritical. One fuel rod was therefore added to 45 fuel elements in the outer region of Zone 1 of the reactor in the manner depicted in Figure 52. The total mass of uranium added was 4.608 kg, thus bringing the uranium loading in Zone 1 (see Table 32) to 50.461 kg, the total core uranium loading to 179.596 kg, and the excess reactivity (without Ta absorbers) to 24.7¢. This excess value corresponds to the 52.0¢ for the initial power-flattened core, both being uncorrected for the polyethylene boxes.

4. Spatial Power Distribution

The spatial power distribution was measured in two configurations of the power-flattened, three-zoned core. The distribution was measured over a one-twelfth sector of the core as initially constituted (see Table 32) and over a one-sixth sector of the core when one additional wire was added to each fuel element

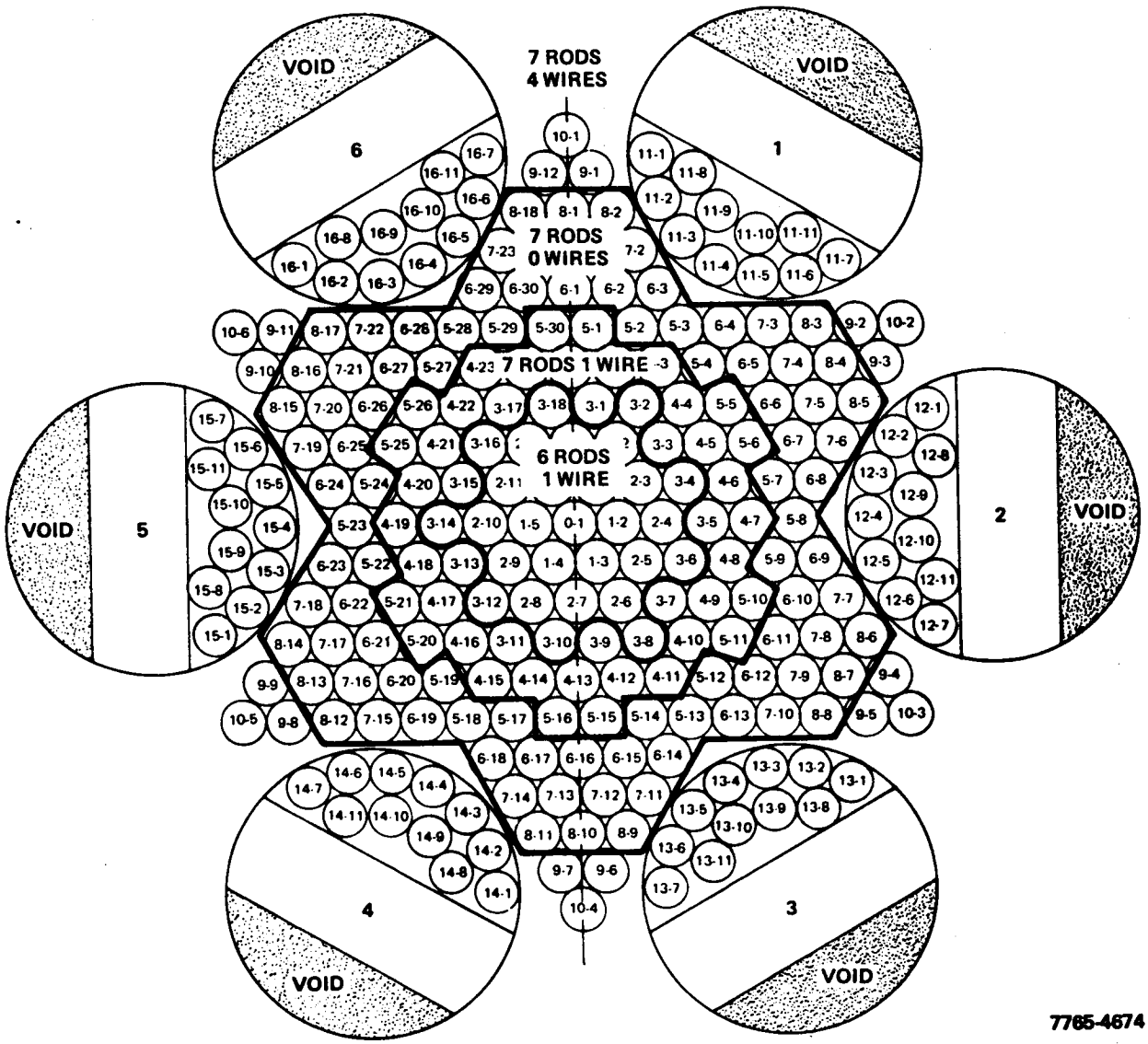

Figure 52. Three-Zoned, Power-Flattened Core With Ta Absorbers Removed

in each of the three zones (see Table 33). The latter experiment was carried out in order to establish the power distribution in a three-zoned core when the drums were turned to correspond to a 1.5% $\Delta k/k$ control change. Since the rotation of all drums as required to achieve the -1.5% $\Delta k/k$ change made the reactor subcritical, one additional 0.152-cm(0.060 in.)-diameter U wire was added in the manner shown in Figure 53.

One wire was irradiated in each of the 27 fuel elements as shown in Figure 54 and one wire in each of the 40 fuel elements as shown in Figure 53. In the usual way, the radial power distribution was ascertained on the basis of counting one wire segment from the center, from the top, and from a point halfway in between for each wore placed in the sector. Data pertaining to the axial distribution were obtained as indicated in the figures.

The wires were irradiated for 1 hour at a reactor power level of 38 watts. The drum positions for each irradiation are shown in Table 34.

TABLE 34

CONTROL DRUM POSITIONS FOR POWER DISTRIBUTION MEASUREMENTS

Drum Number	Power Flattened Core	Drums at -1.5% Core
1	Full in	42°
2	Full in	42°
3	12° 50'	42°
4	12° 53'	42°
5	12° 51'	42°
6	Full in	42°30'

Wires were removed from the core approximately 2 hours after reactor shutdown and were then segmented and started through the counting system. In the initial power-flattened configuration the segments were 1.232 ± 0.013 cm (0.485 ± 0.005 in.) long and in the -1.5% $\Delta k/k$ case were 1.245 ± 0.013 cm(0.490 ± 0.005 in.) long. The results of the measurements were previously shown in Figures 38, 39, 40, and 41 and are tabulated in Tables 35 through 38, inclusive.

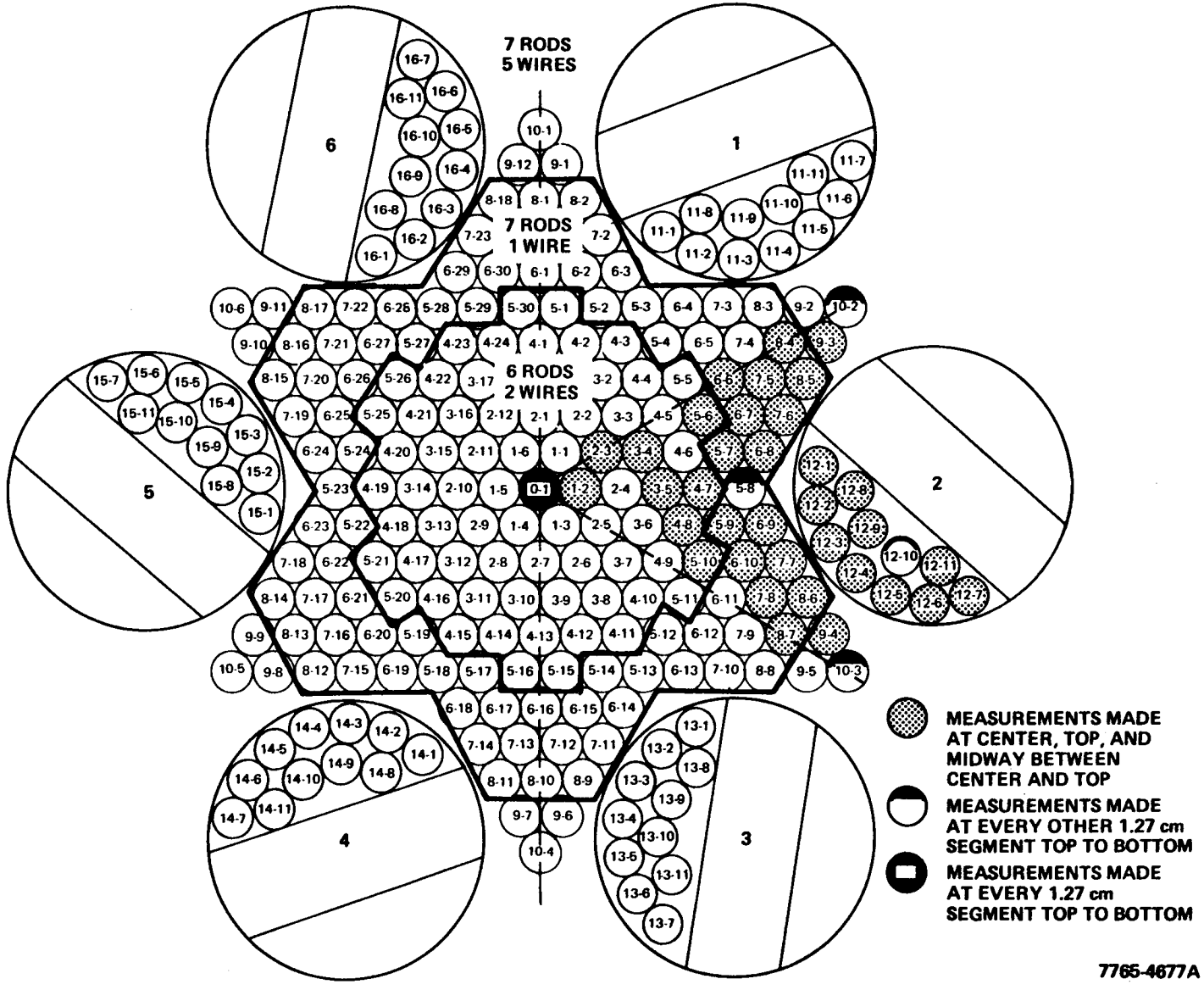

Figure 53. Power Distribution Wire Loading Scheme – Power-Flattened Core (-1.5% Δk/k)

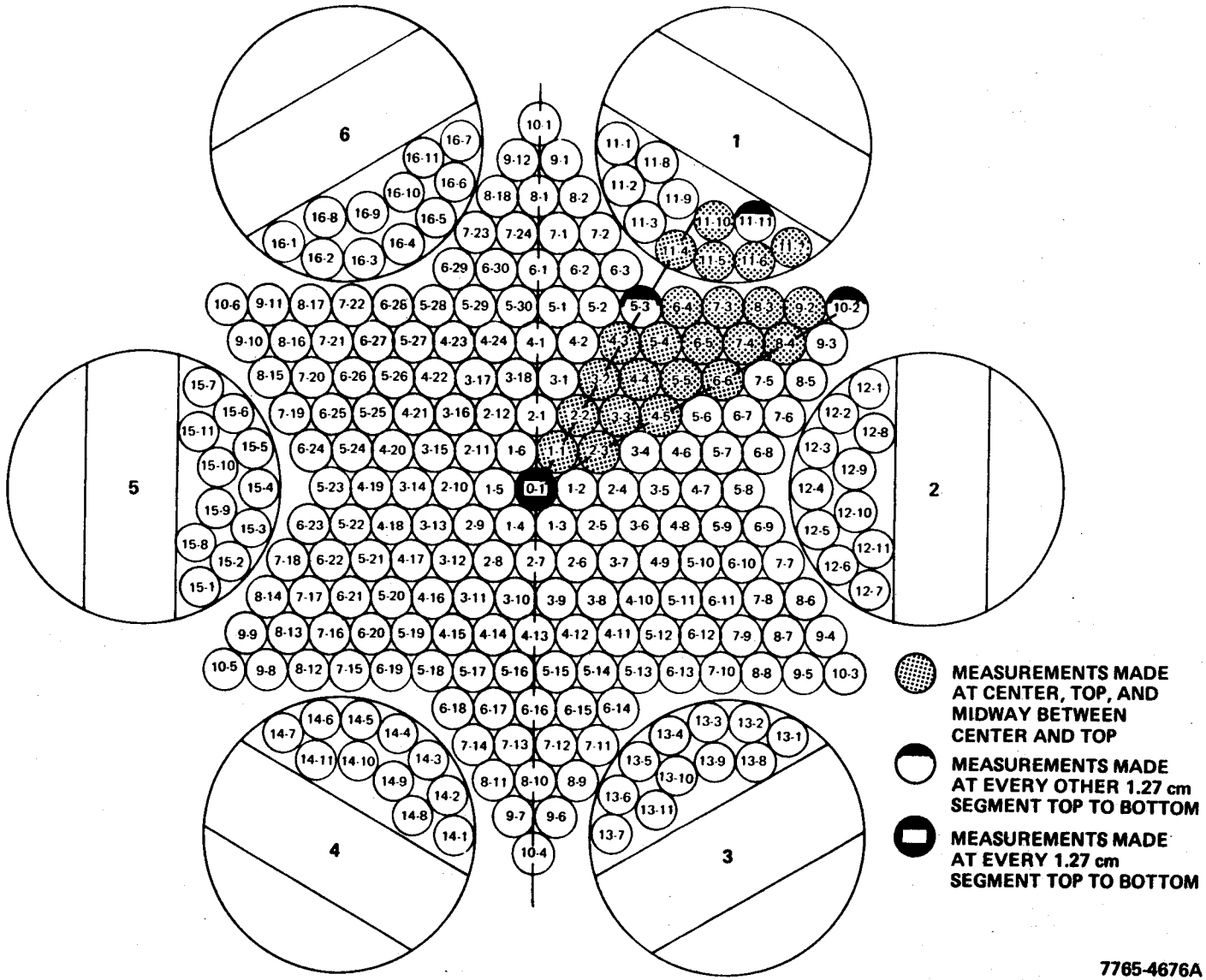

Figure 54. Power Distribution Wire Loading Scheme – Power-Flattened Core

TABLE 35

AXIAL POWER DISTRIBUTION IN POWER FLATTENED CORE*

Segment Number	Distance from Core Center (cm)	Relative Power			
		0-1 (R = 0.0)	5-3 (R = 11.07)	11-11 (R = 18.34 cm)	10-2 (R = 19.13 cm)
	Core Top				
1	17.78	0.701	0.560	0.428	0.411
2	16.55	0.727			
3	15.32	0.764	0.619	0.489	0.461
4	14.08	0.779			
5	12.85	0.829	0.684	0.537	0.518
6	11.62	0.834			
7	10.39	0.867	0.734	0.574	0.554
8	9.16	0.903	0.749	0.596	0.577
9	7.92	0.938	0.762	0.609	0.587
10	6.69	0.958			
11	5.46	0.974	0.788	0.620	0.608
12	4.23	0.976			
13	3.00	0.988	0.818	0.640	0.622
14	1.77	1.017			
15	0.53	1.016	0.814	0.653	0.629
16	-0.70	1.013			
17	-1.93	1.008	0.830	0.636	0.608
18	-3.16	1.008			
19	-4.39	0.986	0.817	0.625	0.603
20	-5.63	0.975			
21	-6.86	0.961	0.794	0.599	0.584
22	-8.09	0.951			
23	-9.32	0.947	0.756	0.569	0.549
24	-10.55	0.922			
25	-11.79	0.893	0.704	0.535	0.510
26	-13.02	0.852			
27	-14.25	0.823	0.665	0.498	0.466
28	-15.48	0.782			
29	-16.71	0.745	0.602	0.459	0.436
30	-17.95	0.708	0.559	0.422	0.398
	Core Bottom				

*See Figure 39.

TABLE 36

RADIAL POWER DISTRIBUTION IN POWER-FLATTENED CORE*

Segment Number	Radius (cm)	Fuel Element Number	Relative Power		
			Center (Z = 0.0)	Midway (Z = 8.89 cm)	Top (Z = 17.78 cm)
1	0	0-1	0.946	0.857	0.656
2	2.18	1-1	0.962	0.867	0.645
3	3.85	2-3	0.957	0.856	0.640
4	4.40	2-2	0.954	0.868	0.643
5	5.87	3-3	0.929	0.844	0.627
6	6.67	3-2	0.927	0.828	0.622
7	7.70	4-5	0.885	0.816	0.600
8	7.98	4-4	0.886	0.807	0.593
9	8.85	4-3	0.888	0.790	0.587
10	9.64	5-5	0.877	0.781	0.584
11	10.16	5-4	0.856	0.766	0.558
12	11.07	5-3	0.803	0.743	0.548
13	11.47	6-6	0.809	0.752	0.541
14	11.75	6-5	0.827	0.799	0.554
15	12.30	6-4	0.774	0.710	0.519
16	13.45	7-4	0.807	0.717	0.531
17	13.77	7-3	0.784	0.696	0.505
18	14.68	11-4	0.721	0.655	0.471
19	15.20	11-5	0.727	0.668	0.482
20	15.28	8-4	0.692	0.642	0.454
21	15.48	8-3	0.693	0.633	0.464
22	16.59	11-6	0.685	0.603	0.425
23	16.89	11-10	0.659	0.603	0.426
24	17.26	9-2	0.666	0.615	0.435
25	18.34	11-11	0.646	0.594	0.421
26	18.53	11-7	0.642	0.568	0.412
27	19.13	10-2	0.617	0.566	0.407

*See Figure 40.

TABLE 37

AXIAL POWER DISTRIBUTION WITH DRUMS AT -1.5% k*

Segment Number	Distance from Core Center (cm)	Relative Power				
		0-1 (R = 0.0)	5-8 (R = 11.07 cm)	12-10 (R = 19.0 cm)	10-2 (R = 19.13 cm)	10-3 (R = 19.13 cm)
	Core Top					
1	17.78	0.703	0.576	0.399	0.400	0.379
2	16.54	0.754	0.614	0.433	0.415	0.406
3	15.29	0.780				
4	14.05	0.810	0.690	0.483	0.476	0.458
5	12.80	0.855				
6	11.56	0.884	0.751	0.525	0.517	0.501
7	10.31	0.924				
8	9.07	0.920	0.788	0.562	0.563	0.532
9	7.82	0.976				
10	6.58	0.976	0.822	0.594	0.582	0.564
11	5.33	0.972				
12	4.09	1.003	0.844	0.608	0.606	0.577
13	2.84	1.013				
14	1.60	1.011	0.865	0.624	0.611	0.584
15	0.36	1.000	0.862	0.620	0.607	0.588
16	-0.89	1.018	0.876	0.622	0.615	0.585
17	-2.13	1.012				
18	-3.38	1.004	0.866	0.614	0.615	0.583
19	-4.62	0.987				
20	-5.87	0.978	0.839	0.607	0.603	0.571
21	-7.11	0.965				
22	-8.36	0.932	0.805	0.583	0.578	0.533
23	-9.60	0.922				
24	-10.85	0.891	0.749	0.541	0.534	0.510
25	-12.09	0.874				
26	-13.34	0.846	0.696	0.507	0.498	0.463
27	-14.58	0.813				
28	-15.82	0.776	0.655	0.461	0.455	0.432
29	-17.07	0.730	0.617	0.433	0.430	0.404
	Core Bottom					

*See Figure 41.

TABLE 38

RADIAL POWER DISTRIBUTION WITH DRUMS AT -1.5% k*

Segment Number	Radius (cm)	Fuel Element Number	Relative Power		
			Center (Z = 0.0)	Midway (Z = 8.89 cm)	Top (Z = 17.78 cm)
1	0.0	0-1	1.000	0.920	0.703
2	2.18	1-2	1.012	0.925	0.691
3	3.85	2-3	0.946	0.868	-
4	5.87	3-4	0.936	0.870	0.643
5	6.67	3-5	0.912	0.842	0.624
6	7.98	4-8	0.914	0.820	0.595
7	8.85	4-7	0.844	0.766	0.575
8	9.64	5-6	0.860	0.791	0.583
9	9.64	5-10	0.870	0.782	0.582
10	10.16	5-7	0.845	0.776	0.554
11	10.16	5-9	0.854	0.786	0.585
12	11.07	5-8	0.862	0.788	0.576
13	11.47	6-6	0.839	0.754	0.545
14	11.75	6-7	0.805	0.753	0.546
15	11.75	6-10	0.816	0.751	0.546
16	12.30	6-8	0.760	0.709	0.513
17	12.30	6-9	0.752	0.697	0.498
18	13.45	7-5	0.738	0.688	0.495
19	13.45	7-8	0.778	0.715	0.504
20	13.77	7-6	0.756	0.694	0.493
21	13.77	7-7	0.766	0.702	0.498
22	14.68	12-2	0.749	0.688	0.515
23	15.19	12-3	0.723	0.666	0.477
24	15.24	12-1	0.734	0.668	0.481
25	15.28	8-4	0.672	0.626	0.451
26	15.28	8-7	0.667	0.617	0.431
27	15.48	8-5	0.662	0.613	0.433
28	15.48	8-6	0.673	0.616	0.447
29	16.63	12-4	0.693	0.630	0.451
30	16.89	12-8	0.656	0.586	0.413
31	17.26	9-3	0.657	0.602	0.413
32	17.26	9-4	0.624	0.568	0.414
33	17.35	12-9	0.621	0.561	0.406
34	18.80	12-5	0.634	0.562	0.409
35	19.00	12-10	0.620	0.562	0.399
36	19.13	10-2	0.607	0.563	0.400
37	19.13	10-3	0.588	0.532	0.379
38	20.96	12-6	0.527	0.470	0.332
39	21.21	12-11	0.454	0.418	0.289
40	23.06	12-7	0.440	0.406	0.290

*See Figure 42.

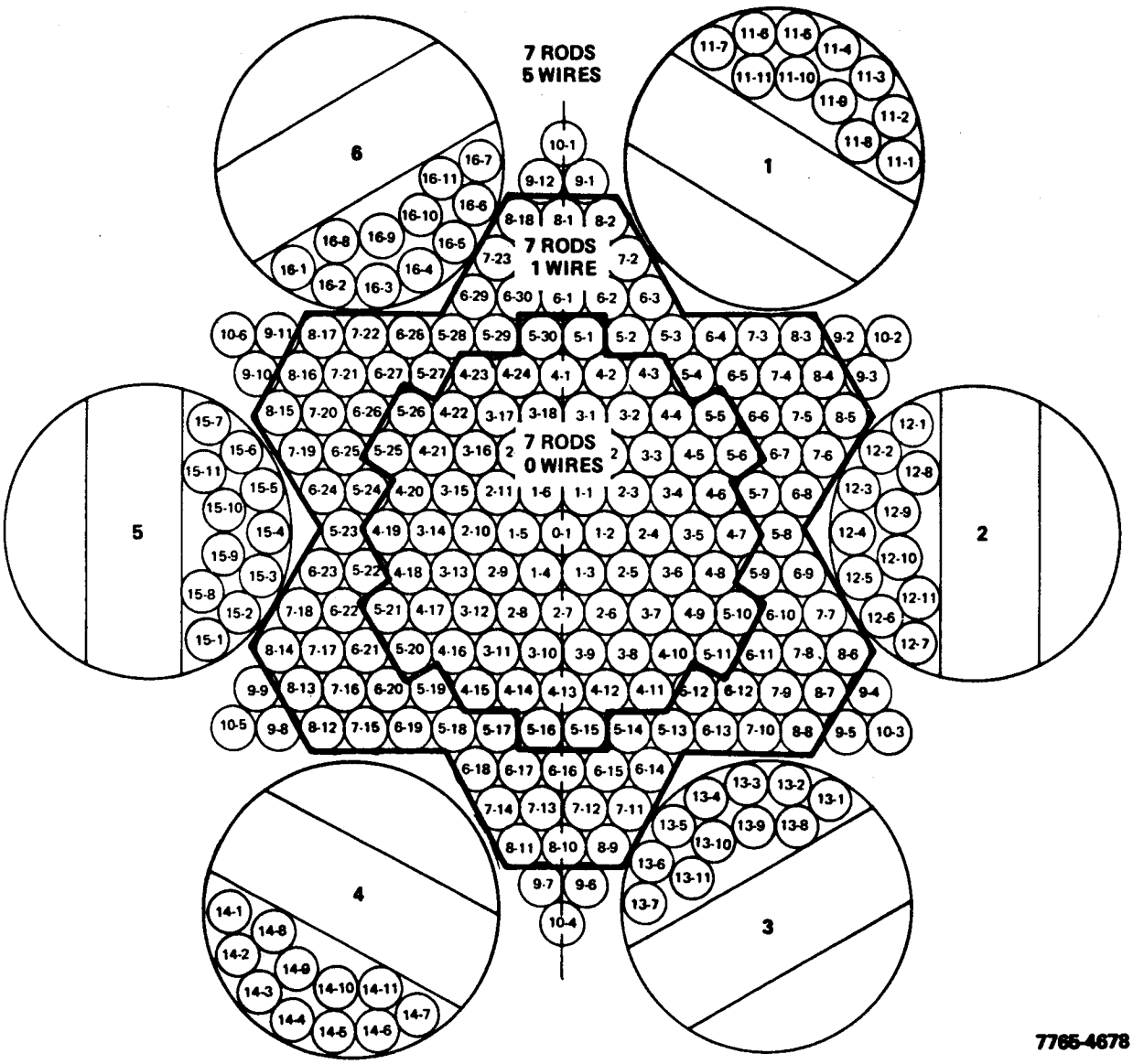

Figure 55. Fuel Loading for Criticality With Two Drums Out

Errors resulting from counting statistics only were less than 0.9%. The mass normalization introduces an error of approximately 0.2%.

Some wire segments in the power-flattened core were counted at several different time intervals. The corrected counts for a given segment decreased with increasing interval number (instead of remaining constant, as it would if it decayed at the same rate as the monitor segment). For instance, the segment from the center of the core was counted at Interval Number 4 and again at Interval Number 100 (both times in the same counter). Its corrected count at Interval 100 was 94% of that at Interval 4. Combinations of statistical errors and errors in amount of background subtracted could account for 2 to 3% of this discrepancy. However, the trend was consistent for all segments counted at different intervals. Segments for axial and radial traverses were counted over a much smaller number of intervals (usually less than 35 intervals) so their variations caused by this effect were considerably smaller (probably 2 to 3%). These results indicate that a systematic error of perhaps 6% may occur for data obtained over large counting times.

5. Critical Mass with Four Drums In and Two Drums Out

Upon completion of the experiments with the 3-zone power-flattened core, fuel loading was initiated to increase the reactivity to achieve criticality with 2 drums locked out. This was accomplished by reloading each zone as shown in Table 39 and Figure 55. The total loading was increased to 183.788 kg and resulted in a measured excess reactivity of $1.24 with two drums out. If one assumes that the core averaged worth of fuel is 0.534 $/kg, the $1.24 excess corresponds to an excess mass of 2.06 kg which, if removed uniformly from the actual uranium loading achieved, would yield a critical mass of 181.73 kg.

6. Small-Sample Reactivity Worths

Since the reactivity worth of hydrogen would be very important in terms of a safety analysis of the reference reactor, the reactivity worths of two small polyethylene samples (14.37% by weight hydrogen) were determined in a three-zoned power-flattened core essentially identical to that described in Table 32. The reactivity worth of the small U^{235} sample previously measured in Composition 5A was also measured for purposes of comparison with the uniformly loaded core. The results of these three measurements were tabulated in Table 13 of Section IV.

TABLE 39

FUEL LOADING WITH TWO DRUMS OUT

Zone Number	Number of Rods	Number of 0.152-cm Wires	Number Fuel Elements	Average Fuel Mass/Element (gm)	Standard Deviation (gm)	Total Fuel Mass (kg)
1	7	0	73	717.728	±1.449	52.394
2	7	1	90	730.332	±1.775	65.730
3	7	5	84	781.710	±1.354	65.664
					Total Fuel Mass	183.788

APPENDIX B

CHEMICAL IMPURITIES IN THE CORE AND SAMPLE MATERIALS

I. CRITERIA

Prior to the procurement of the materials for constructing the critical assembly, work was carried out to establish a list of maximum impurity levels for all impurities in core, reflector, and reactivity sample materials, impurities levels that would leak to negligible effects on the interpretation of the physics measurement relative to other uncertainties. The general philosophy of this task required development of definitive criteria in order to produce quantitiative results.

The presence of impurities or trace elements in the materials used in critical experiments may be treated in several ways. If the effects of undesired elements are sufficiently small, their presence may be neglected. Otherwise, corrections based on measurements or explicit inclusion of impurities effects in calculations must be used. To establish the level at which an impurity effect is negligible, it is necessary to compare it with other uncertainties that are inherent or allowed in the system under investigation. This process is most logically based upon reactivity worth determinations. The following uncertainties were arbitrarily established or were inherent in the reactor materials available:

1) Critical mass ±0.15% (equivalent to ±13¢);
2) Enrichment ±0.2% (equivalent to ±17¢);
3) Geometry variation ±0.10% $\Delta k/k$ (equivalent to ±15¢);
4) Uncertainty in large sample reactivity measurements whichever is the larger; ±2% or ±0.3¢,
5) Uncertainty in small sample reactivity measurements whichever is the larger. ±1% or ±0.01¢,

On the basis of these uncertainties, the negligible impurity limits were conservatively recommended as ±1¢ for reactor materials, and ±0.2% of the sample reactivity for the reactivity samples.

TABLE 40

ESTIMATED SPECIFIC REACTIVITIES

Material	Estimated Relative* Specific Reactivity	Measured Relative* Specific Reactivity				Estimated Specific Reactivity (mc/g)	Material	Estimated Relative* Specific Reactivity	Measured Relative* Specific Reactivity				Estimated Specific Reactivity (mc/g)
		TOPSY†	GODIVA†	ECEL§	ECEL**				TOPSY†	GODIVA†	ECEL§	ECEL 17**	
H	80		76.1			5600	Zn						(-7)
Li^6	-2.1	-0.05	-0.4			-147	Ga						(-7)
Li^7	-40.0	-10.6	-24.5		-154	-2800	Ge						(-7)
Li	-0.7				-1.0	-49	Br						(-0.7)
Be	1.2	1.25	1.15	1.30		84	Rb						(-0.7)
BeO	0.6	0.55	0.54			42	Sr						(-0.7)
B^{10}	-2.0	-1.11	-1.26		-49	-140	Y						(-0.7)
B	-10.0	-7.51	-7.40		-117	-700	Zr	-0.01	-0.01	-0.03			-0.7
C	0.4	0.31	0.24	0.53	-0.01	28	Nb	-0.5	-0.06	-0.09		-1.9	-35
N						(21)	Mo	-0.1	-0.20	-0.04			-7
O	0.2		0.10			14	Ru						(-7)
F	0.4		0.24			28	Cd	-0.1	-0.08	-0.10	-0.11		-7
Na						(14)	In						(-7)
Mg	0.15	0.11	0.07	0.22		10.5	Sn						(-7)
Al	0.3	0.07	0.03	0.04	-0.39	21	Sb						(-14)
Si						(14)	Te						(-14)
P						(14)	I						(-14)
S						(14)	Cs						(-14)
Cl						(14)	Ba						(-14)
K						(7)	La						(-21)
Ca	-0.2	-0.16	-0.19			-14	Rare Earths						(-42)
Sc						(-7)	Hf						(-21)
Ti	-0.01	-0.02	-0.04			-0.7	Ta	-0.3	-0.10	-0.11		-3.5	-21
V	0.01	0.03	0.00			0.7	W	-0.1	-0.05	-0.07		-1.2	-7
Cr	-0.02	-0.01	-0.04			-1.4	Re						(-210)
Mn						(-1.4)	Tl						(-21)
Fe	-0.02	-0.01	-0.05	0.0003		-0.7	Pb						(-3.5)
Co	-0.01	-0.02	-0.05			-0.7	Bi						(-3.5)
Ni	-0.15	-0.10	-0.14			-10.5	U^{235}	1.0	1.0	1.0	1.0	1.0	70
Cu	-0.1	-0.03	-0.07			-7.	U^{238}	0.1	0.13	0.13	0.05	-0.71	7

*Relative to U^{235}
†Reference 19
§Reference 20
**Reference 21

In determining significant impurity limits for the core and reflector materials for the Critical Assembly (Composition 1) and for the reactivity samples, all known chemical elements were considered initially. Some materials, such as the noble gases (He, Ne, Ar, Kr, Xe, Rn), the radioactive elements (Tc, Pm, all transbismuth elements), the voltile metals (As, Se, Hg), and the precious metals (Ph, Pd, Ag, Os, Ir, Pt, Au), were eliminated on the grounds that significant amounts would not be present. The specific reactivities of the remaining elements, relative to U^{235}, are listed in Table 40 and were selected, more or less arbitrarily, by using as a guide the experimental values shown in the columns to the right of the table. The values for GODIVA and TOPSY were obtained in a series of experiments at Los Alamos Scientific Laboratory.[19] The values shown under the heading "ECEL 1 and ECEL-17" were obtained in the Epithermal Critical Experiment Laboratory split-table critical machine.[20,21] In general, the values were selected for closer agreement with GODIVA since GODIVA and Composition 1 have somewhat similar spectra. (Because of their chemical similarity, as impurities, the rare earth elements are treated as a homogeneous group.) The specific reactivities that are enclosed in parentheses are estimates based on comparison with the other experimental values. The relative specific reactivities were converted to absolute values by using an estimate of 0.07¢/gm for the specific worth of U^{235}. This value was obtained from calculations using APC (see Appendix D), and can be derived by taking the arithmetic average of the specific reactivity change arising from a uniform core-fuel loading change (~0.05¢/gm of fuel) and from the specific worth of the fuel in the central seven fuel elements (~0.10¢/gm). The latter two values can be derived from information in Appendix D.

In order to derive an expression suitable for evaluating the effects of impurities in core and reflector materials, we define the change in reactivity as

$$\Delta\rho = M_I(\rho_{mI} - \rho_{mH}) \quad ,$$

where

$\Delta\rho$ = some arbitrarily allowed reactivity change (that we set to be 1.0¢ for these particular cases), (¢)

M_I = the mass of the impurity (gm)

TABLE 41

IMPURITY CONCENTRATIONS RESULTING IN REACTIVITY ERROR OF ±1¢ IN REACTOR MATERIALS

Impurity	U^{235}	Mo	Ta	$Li_3{}^7N$	Hf	W	Impurity	U^{235}	Mo	Ta	$Li_3{}^7N$	Hf	W
H	1	1	4	13	45	4	Ge	90	(1200)	1800	1800	18,000	(7100)
Li	30	50	180	-	1,800	160	Br	100	1000	1200	2150	12,000	3500
Be	(160)*	80	230	1400	2,300	230	Rb	100	1000	1200	2150	12,000	3500
B	30	50	180	370	1,800	160	Sr	100	1000	1200	2150	12,000	3500
C	160	200	500	(5700)	5,000	700	Y	100	1000	1200	2150	12,000	3500
N	140	250	600	5700	5,900	890	Zr	100	1000	1200	2150	12,000	3500
O	120	330	710	3700	7,100	1200	Nb	60	200	1300	980	13,000	750
F	160	200	500	(5700)	5,000	700	Mo	90	-	1800	1800	18,000	(7100)
Na	120	330	710	3700	7,100	1200	Ru	90	(1200)	1800	1800	18,000	(7100)
Mg	120	330	710	3700	7,100	1200	Cd	90	(1200)	1800	1800	18,000	(7100)
Al	140	250	600	5700	5,900	890	In	90	(1200)	1800	1800	18,000	(7100)
Si	120	330	710	3700	7,100	1200	Sn	90	(1200)	1800	1800	18,000	(7100)
P	120	330	710	3700	7,100	1200	Sb	80	1000	3500	1500	35,000	3500
S	120	330	710	3700	7,100	1200	Te	80	1000	3500	1500	35,000	3500
Cl	120	330	710	3700	7,100	1200	I	80	1000	3500	1500	35,000	3500
K	120	330	710	3700	7,100	1200	Cs	80	1000	3500	1500	35,000	3500
Ca	80	1000	3500	1500	35,000	3500	Ba	80	1000	3500	1500	35,000	3500
Sc	90	(1200)	1800	1800	18,000	(7100)	La	60	200	1300	980	13,000	750
Ti	100	1000	1200	2150	12,000	3500	Rare Earths	60	200	1300	980	13,000	750
V	100	1000	1200	2150	12,000	3500	Hf	60	200	1300	980	-	750
Cr	90	1200	1250	2000	12,000	4500	Ta	60	200	-	980	13,000	750
Mn	90	1200	1250	2000	12,500	4500	W	90	(1200)	1800	1800	18,000	-
Fe	100	1000	1200	2150	12,000	3500	Re	30	40	180	370	1,800	160
Co	100	1000	1200	2150	12,000	3500	Tl	60	200	1300	980	13,000	750
Ni	80	1000	3500	1520	35,000	3500	Pb	90	2000	1400	1900	14,000	7100
Cu	90	(1200)	1800	1800	18,000	(7100)	Bi	90	2000	1400	1900	14,000	7100
Zn	90	(1200)	1800	1800	18,000	(7100)							
Ga	90	(1200)	1800	1800	18,000	(7100)							

*Concentrations in parentheses are for indistinguishable impurities, see text.

ρ_m = the specific worth of the impurity (¢/gm)

ρ_{mH} = the specific worth of the host material (¢/gm).

According to the definition, if the specific worths of some impurity and its host are equal, then the reactivity change is zero and large quantities of the impurity can be tolerated. On the other hand, as the mass of the impurity decreases, the above equation shows that the change in reactivity decreases accordingly. Since the concentration in ppm of a small amount of impurity is given approximately by

$$C_I = \frac{M_I}{M_H} \times 10^6 \quad ,$$

it follows that

$$\Delta\rho = C_I M_H(\rho_{mI} - \rho_{MH}) \times 10^{-6} \quad ;$$

consequently, by setting $\Delta\rho$ arbitrarily equal to 1.0¢,

$$C_I = \frac{1.0¢}{M_H(\rho_{mI} - \rho_{mH})} \times 10^6 \quad .$$

The values calculated by this equation are listed in Table 41 where specific reactivities are taken from Table 40.

For those cases in which the host material and the impurity have identical estimated specific reactivities, the above equation is not valid; consequently, the limit for the impurity is arbitrarily chosen to be equal to the largest limit of a distinguishable impurity.

The above equations apply to core and reflector materials. For the case of reactivity samples, the impurity concentrations resulting in a deviation of ±0.2% of the sample reactivity were determined by the equation

$$C_I = \frac{\rho_{mH}}{(\rho_{mH} - \rho_{mI})}(0.2\%) \quad .$$

These concentrations, in parts per million, are listed in Table 42. There also, limits for nondistinguishable impurities were set equal to the largest limit for distinguishable impurities.

TABLE 42

IMPURITY CONCENTRATIONS RESULTING IN ERROR OF +0.2% IN REACTIVITY SAMPLES

(Sheet 1 of 2)

Impurity	Li	Li^6	Li^7	$Li_3{}^7N$	Be	BeO	B^{10}	C	Mo	Hf	Ta	W	Re	U^{235}	U^{238}
H	50	660	14	12	30	14	200	10	2	7	7	2	70	25	2
Li	-	-	-	680	680	400	2500	300	90	300	300	90	8400	600	80
Be	1200	1900	1800	1300			1700	1000	150	400	400	150	1400	10000	180
B	22000	2100	400	340	680	400	2500	300	90	300	300	90	8400	600	80
C	10000	1900	6600	13000	3000	6600	1900	-	400	800	800	400	1700	3000	670
N	1700	1900	4200	5500	2600	4200	1900	8000	500	1000	1000	500	1800	2800	1000
O	1800	1900	3000	3400	2400	8000	1900	4000	670	1200	1200	670	1800	2500	2000
F	1600	1900	6600	13000	3000	6600	1900	(8000)*	400	800	800	400	1700	3300	670
Na	1800	1900	3000	3400	2400	3000	1900	4000	670	1200	1200	670	1800	2500	2000
Mg	1800	1900	3000	3400	2400	3000	1900	4000	670	1200	1200	670	1800	2500	2000
Al	1700	1900	4200	5500	2600	4200	1900	8000	500	1000	1000	500	1800	2800	1000
Si	1800	1900	3000	3400	2400	3000	1900	4000	670	1200	1200	670	1800	2500	2000
P	1800	1900	3000	3400	2400	3000	1900	4000	670	1200	1200	670	1800	2500	2000
S	1800	1900	3000	3400	2400	3000	1900	4000	670	1200	1200	670	1800	2500	2000
Cl	1800	1900	3000	3400	2400	3000	1900	4000	670	1200	1200	670	1800	2500	2000
K	1800	1900	3000	3400	2400	3000	1900	4000	670	1200	1200	670	1800	2500	2000
Ca	2200	2000	1400	1400	1700	1400	2000	1300	2000	6000	6000	2000	2100	1600	670
Sc	2100	2000	1700	1600	1800	1700	2000	1600	(4000)	3000	3000	(4000)	2000	1800	1000
Ti	2000	2000	2000	2000	2000	2000	2000	2000	2000	2000	2000	2000	2000	2000	2000
V	2000	2000	2000	2000	2000	2000	2000	2000	2000	2000	2000	2000	2000	2000	2000
Cr	2000	2000	1900	1900	1900	1900	2000	1900	2500	2100	2100	2500	2000	1900	1600
Mn	2000	2000	1900	1900	1900	1900	2000	1900	2500	2100	2100	2500	2000	1900	1600
Fe	2000	2000	2000	2000	2000	2000	2000	2000	2000	2000	2000	2000	2000	2000	2000
Co	2000	2000	2000	2000	2000	2000	2000	2000	2000	2000	2000	2000	2000	2000	2000
Ni	2200	2000	1400	1400	1700	1400	2000	1300	2000	6000	6000	2000	2100	1600	670
Cu	2100	2000	1700	1600	1800	1700	2000	1600	(4000)	3000	3000	(4000)	2000	1800	1000
Zn	2100	2000	1700	1600	1800	1700	2000	1600	(4000)	3000	3000	(4000)	2000	1800	1000

*Concentrations in parentheses are for indistinguishable impurities, see text.

TABLE 42

IMPURITY CONCENTRATIONS RESULTING IN ERROR OF +0.2% IN REACTIVITY SAMPLES

(Sheet 2 of 2)

Impurity	Li	Li^6	Li^7	Li_3^7N	Be	BeO	B^{10}	C	Mo	Hf	Ta	W	Re	U^{235}	U^{238}
Ga	2100	2000	1700	1600	1800	1700	2000	1600	(4000)	3000	3000	(4000)	2000	1800	1000
Ge	2100	2000	1700	1600	1800	1700	2000	1600	(4000)	3000	3000	(4000)	2000	1800	1000
Br	2000	2000	2000	2000	2000	2000	2000	2000	2000	2000	2000	2000	2000	2000	2000
Rb	2000	2000	2000	2000	2000	2000	2000	2000	2000	2000	2000	2000	2000	2000	2000
Sr	2000	2000	2000	2000	2000	2000	2000	2000	2000	2000	2000	2000	2000	2000	2000
Y	2000	2000	2000	2000	2000	2000	2000	2000	2000	2000	2000	2000	2000	2000	2000
Zr	2000	2000	2000	2000	2000	2000	2000	2000	2000	2000	2000	2000	2000	2000	2000
Nb	2700	2000	1000	900	1300	1000	2100	800	400	2200	2200	400	2400	1200	300
Mo	2100	2000	1700	1600	1800	1700	2000	1600	-	3000	3000	(4000)	2000	1800	1000
Ru	2100	2000	1700	1600	1800	1700	2000	1600	(4000)	3000	3000	(4000)	2000	1800	1000
Cd	2100	2000	1700	1600	1800	1700	2000	1600	(4000)	3000	3000	(4000)	2000	1800	1000
In	2100	2000	1700	1600	1800	1700	2000	1600	(4000)	3000	3000	(4000)	2000	1800	1000
Sn	2100	2000	1700	1600	1800	1700	2000	1600	(4000)	3000	3000	(4000)	2000	1800	1000
Sb	2200	2000	1400	1400	1700	1400	2000	1300	2000	6000	6000	2000	2100	1600	670
Te	2200	2000	1400	1400	1700	1400	2000	1300	2000	6000	6000	2000	2100	1600	670
I	2200	2000	1400	1400	1700	1400	2000	1300	2000	6000	6000	2000	2100	1600	670
Cs	2200	2000	1400	1400	1700	1400	2000	1300	2000	6000	6000	2000	2100	1600	670
Ba	2300	2000	1300	1200	1600	1300	2000	1100	1000	(6000)	(6000)	1000	2200	1500	500
La	2300	2000	1300	1200	1600	1300	2000	1100	1000	(6000)	(6000)	1000	2200	1500	500
Rare Earths	2700	2000	1000	900	1300	1000	2100	800	400	2200	2200	400	2400	1200	300
Hf	2300	2000	1300	1200	1600	1300	2000	1100	1000	-	(6000)	1000	2200	1500	500
Ta	2300	2000	1300	1200	1600	1300	2000	1100	1000	(6000)	-	1000	2200	1500	500
W	2100	2000	1700	1600	1800	1700	2000	1600	(4000)	3000	3000	-	2000	1800	1000
Re	22000	2000	400	340	680	400	2500	300	90	300	300	90	-	600	80
Tl	2300	2000	1300	1200	1600	1300	2000	1100	1000	(6000)	(6000)	1000	2200	1500	500
Pb	2000	2000	1800	1800	1400	1800	2000	1700	4000	2400	2400	4000	2000	1400	1300
Bi	2000	2000	1800	1800	1900	1800	2000	1700	4000	2400	2400	4000	2000	1900	1300

TABLE 43
IMPURITY LISTINGS FOR REACTOR MATERIALS
(ppm by weight)

Impurity	Li_3^7N	Ta Tubing	Ta Foil	Ta Wire	Ta Retainer Ring	Ta Absorber Segment	Ta Pressure Vessel	Mo Radial Reflector	Mo Control Drum Segment (and core filler)	Mo Control Drum Trapezoid Filler	Mo Control Drum Filler Rods	Mo Eccentric Axial Reflectors	Mo Central Axial Reflectors	W Foil	Hf Foil	T-111 Support Tube
H	1000	<5	<10	<5	<5	<10	<10	4	3					<10	5	1
Li					<5							<10	<10			
Be	<2				<7							<20	<20			
B	<20				<5							<10	<10			
C	234	21	25	43	30	17	24	26	29	<20	<20	<20	<20	50	<80	40
N		40	26	18	15	44	18	16	14					50	26	30
O	2.68%	33	50	27	55	70	41	58	33	<50	<50	<50	<50	50	99	40
F					<400							<10	<10			
Na	300				-			<7	<7			<10	<10			
Mg	<20	<10		<10	<5			<1	2	<10	<10	<10	<10			<1
Al	<10	<10	<10	<10	<5	10	<10	<4	5	<10	<20	<20	<20		<20	<10
Si	20	<10	<10	<10	30	12	20	18	19	<20	60	90	<20			
P					<50											
S					<50											
Cl	12				<400											
K	20							<15	<15							
Ca	<100	<10		<10	5			1	1	<10	<10	<10	<10	-		<25
Ti		<10	<5	<10	<5	<5	<5					<40	<40		<20	20
V	<10	<10		<10								10	10			
Cr	<1	<10	<1	10	<5	<1	2	4	2	10	15	<29	10			<1
Mn	<1	<10		<10	<5			<1	<1	<10	<10	<10	<10			<1
Fe	<20	<10	11	30	25	10	3	8	13	10	30	40	10	50	<140	10
Co	<20	<10		<10	<5					<10	<10	<10	<10			<5
Ni	<10	<10	<1	<50	30	4	2	<1	7	10	30	30	30	-		<1
Cu	40	<10	<1	<10	<10	<1	<1	<1	<4	<10	<10	<10	<10		<20	<1
Sr	<10															
Zr		<10		<10	<5										3.6%	350
Nb	<20	400	39	130	<25	63	65					<50	<50		<50	1200
Mo	<4	<10	<10	<10	<5	38	<10								<10	25
Ag	40															
Cd	<6											<10	<10			
Sn	<20	<10		<10	<5			<4	<4	<10	22	40	<10			<1
Ba	<10															
Rare Earths					<100											
Hf												<100	<100			1.73%
Ta												<50	<50		<100	
W		100	<40	<50	<25	275	<40	119	134	<10	<50	<50	<50		<10	7.5%
Re					<100							<30	<30			
Pb	4	50								<10	<10	<10	<10			<1
U															<1	

II. CONFORMANCE

These impurity limits were not considered as impurity specifications, or even incisive guidelines, but were used as indications of the amounts that may be present without introducing more than trivial uncertainties in the analysis. In practice, actual impurity specifications were based on those impurities that were likely to be present in a material in an appreciable amount, with concentration limits that were economically realistic.

In general, impurity listings were obtained for each part or material used in the assembly and in the experimental program. These listings were obtained as part of the normal procurement procedure and represented standard commercial practices. The actual impurity values achieved for reactor materials are listed in Table 43, while those for the reactivity samples and associated hardware are listed in Table 44.

All entries in these tables, with a few exceptions, are in parts per million and clearly show the generally high purity of the commercially available materials. Some large impurity concentrations, such as Zr in Hf, and O in Li_3^7N, are due to chemical or processing peculiarities and could not be avoided without severe cost penalties.

Comparison of Tables 41 and 43 with Tables 42 and 44 shows that, in general, the impurity levels actually achieved are far below the specified limits. There are some exceptions to this generalization and these exceptions must be taken into account in detailed comparisons between calculational and experimental results. For the reactivity sample worth measurements this has been done for all significant chemical and istopic impurities, except hydrogen, by use of experimentally derived corrections.

The effects of the significant impurities in the reactor materials must be determined analytically. The masses of these impurities in each reactor composition are listed in Table 45. Since all masses of reactor materials reported in the core specifications are gross masses, the mass listed for each impurity must be subtracted from the mass of its host material.

Several of the materials utilized in this program were isotopically enriched. The fraction of the enriched isotope is presented in Table 46.

TABLE 44
IMPURITY LISTING FOR REACTIVITY SAMPLES
(ppm by weight)

Impurity	Li	Li^6	Li^7	$Li_3{}^7N$	Be	BeO	B^{10}	C	Nb	Mo	Hf	Ta	W	Re	Ta Tubing	Mo Cladding	Mo Reflector Plugs	Stainless Steel Cladding
H				1000	16		56	Possibly 300	<20		2.2	<5		12	<2	9		
Li					1	<1	<50	<10		<10		<60	<10	<60	<50			
Be		<2	<2	<2			<10		<1	<20		<10	<20	<100	<50			
B		<20	<20	<20	0.1	<1		1.1				<50	-	<60	<50			
C		200	448	234	660		2.46%		900-1100	<20	50	<10	<20	<200	<10	34		0.06%
N	20	45	291		200				<200		26	19		<100	67	30		
O				2.68%	4480		0.99%		<200	<50	310	46	<30	1500	82	31		
F										<10	-	-	10	<400	<trace			
Na	34	200	<60	300		30	300			<10		<400	<10	<400	<400			
Mg		<20	<20	<20	281	830	500			<10		<10	<10		<10		<10	
Al	<10	<10	50	<10	350	65	3000	125		<20	30	<10	<10	<200	<10		<8	
Si	<10	<20	<20	20		110	1000	430	<300	60		<10	<10	<100		10	<15	0.51%
P							40							<400	<trace			0.021%
S							300							<200				0.029%
Cl	31	10	7	12										<400	<trace			
K	32	20	<20	20			1000											
Ca	<10	15	<100	<100	<50	60	500	111		<10			<10		<10		<5	
Ti						5	120		<500	<40	42	<10	<10	<100	<10		<10	
V		<10	<10	<10			20	40		10		<10	<10		<10			
Cr	<10	1	<1	<1	65	8	200			15		<10	<10		<10		8	18.41%
Mn		<1	<1	<1		<2	200			<10		<10	<10		<10		<10	1.63%
Fe	<10	<20	<20	<20	625	50	700	420	<500	30	165	<10	25	<100	<10		19	
Co	<10	<20	<20	<20	5	<1	20			<10			<10		<10		8	
Ni	<10	<10	<10	<10	165	8	700			30		10	20	<100	<10	<10	6	9.88%
Cu	<10			40	25	<2	5000			<10	<20	<10	<10		<10		<4	0.18%
Zn						<20	80											
Ge							<500											
As							30											
Rb							<200											
Sr		<10	<10	<10			<100											
Zr							<500		0.9-1.1%		3.2%	<10		<200	<10		<10	
Nb		<20	<100	<20			<500			<50	<50	165	<30	<500	260			
Mo		<4	<4	<4	10	<3	<200				<5	16		<100	<10			0.29%
Ag		<1	1	40		<1	25										<1	
Cd		<6	<6	<6		-		<10		<10			-					
Sn		<20	<20	<20			120			22		<10	<10		<10		18	
Sb							<500											
Cs							<500											
Ba		<10	<10	<10			5											
Rare Earths					<50							<50		<200	-			
Hf					<20					<100		<100	<100		<100			
Ta					<25		60	40	<2000	<50	<100		<50	<400				
W							20			<50	30	55		<200	55			
Re					<150					<30		<50	<30		<50			
Pt							<500											
Hg							<500											
Pb		<4		4		<2	<200			<10		<50	<10		<50		<10	
Bi							<200											
U											<0.5							

TABLE 45

MASS OF CHEMICAL IMPURITIES IN REACTOR

Material		Mass (gm)				
Impurity	Host	Composition Number				
		1	2	3	4	5
H	Fuel	1.31	2.1	2.1	2.1	2.1
	Li_3^7N	0.0	10	10	10	10
O	Li_3^7N	0.0	271	271	271	271
Kel-F	Fuel	118	187	187	187	187
Zr	Hf	0.0	0.0	148	148	148

TABLE 46

ISOTOPIC COMPOSITIONS

Reactor Components		
Fuel	U^{235}	93.145 wt % balance U^{238}, U^{234}
Li_3^7N	Li^7	99.993 wt % balance Li^6
Reactivity Samples		
Li^6 (large and small)	Li^6	95.44 wt % balance Li^7
Li^7 (large and small)	Li^7	99.993 wt % balance Li^6
Li_3^7N (large)	Li^7	99.993 wt % balance Li^6
B^{10} (large and small)	B^{10}	92.01 wt % balance B^{11}
U^{235} (large)	U^{235}	93.145 wt % balance U^{238}, U^{234}
(small)	U^{235}	93.13 wt % balance U^{238}, U^{234}
U^{238} (large)	U^{238}	99.78 wt % balance U^{235}, U^{234}, U^{236}
(small)	U^{238}	99.973 wt % balance U^{235}, U^{234}, U^{236}

TABLE 47

LIST OF DRAWINGS

Drawing Categories	Drawing Number	Drawing Description
Conceptual Design	R-N76514001 (Sheet 1)	Critical Machine
	R-N76514001 (Sheet 2)	Critical Machine
Layouts	R-N76514002 (Sheet 1)	Layout Critical Machine
	002 (Sheet 2)	Layout Control Drums
	002 (Sheet 3)	Layout Sample Changer
	002 (Sheet 4)	Layout
Assembly Drawings	EX-N76514003	Critical Machine Assembly
	004	Reactor Core Assembly
	005	Safety Element Scram Assembly
	006	Table and Sample Changer Assembly
	007	Drive Assembly and Scram Element
	008	Control-Drum Drive Assembly
	009	Oscillator Rod Assembly
	010	Control-Drum Assembly
Massive Molybdenum and Tantalum Parts	EX-76514011	Mo Reflector – Radial Stationary
	012	Mo Reflector – Radial Scram
	013	Mo Reflector – Drum and Core Filler
	014	Ta Absorber – Drum
	017	Ta Pressure Vessel
	018	Mo Bolts
	020	Ta Oscillator Tube, Mo Plugs, Mo Drum Filler
Core Support Structure	EX-N76514015	Drum Shaft Details
	016	Drum Plate Details
	019	Core Structure Weldment
	021	Bracket – Scram Reflector
	022	Details – Grid Plate
	023	Upper Bearing Plate
	024	Details – Table and Changer Plate
	025	Details – Sample Changer
	026	Screw Jack Specification
	027	Details – Sample Changer
	028	Details – Scram Element
	029	Sample Rod Assembly
Fuel Element	EX-N7614030	Fuel Element Assembly
	031	Ta Honeycomb Spacer Tube
	032	Ta Fuel Tube
	033	Mo Axial Reflector Solid Cylinder
	034	Mo Axial Reflector Eccentric
	035	Centering Ring
	036	Jack Screw
	037	Rubber Packing
	038	Cap
	039	Alignment Pin
	040	Li_3N Segment

APPENDIX C
DETAILED SPECIFICATIONS OF THE CRITICAL ASSEMBLY

A. GENERAL LAYOUT

In Section II of this report, a brief general description of the critical assembly was given along with enough dimensional information that the basic layout, size, and function of the assembly could be understood. In Figures 2 and 3, the relative positions of the major reactor components, such as control drums, fuel elements, and reflector segments relative to the core axis and lower grid plate were pointed out and were located dimensionally. When these dimensions are known, reference can be made to Figures 4 and 5 to find the location of various material segments relative to the fuel element and the control drum. It is the intention of this Appendix to provide, in sufficient detail that accurate calculations can be performed, dimensional and weight data on each individual component making up the major parts of the reactor core. Also in this Appendix, functional descriptions are provided, not only for items associated with the core proper (if they have not already been dealt with), but also for the various auxiliary mechanisms such as the sample changer apparatus, the sample holder tubes, and the reactivity samples. A configuration summary, which lists the drawings by number and provides the title of each, is given in Table 47.

The detailed dimensional and weight data are provided for most of the reactor components in Table 48. For these components, the data in the table are sufficient, and only a simple definition of the components is given in the text. In some cases, the number of items sampled to determine a dimension or mass is given in parentheses. Dimensions for other components which have complex geometrical shapes are shown in figures with the text. These dimensions are given in centimeters and, in parentheses, in inches.

B. FUEL ELEMENTS

1. Element

A cross-sectional view of a fuel element is shown in Figure 5. The fuel elements consisted of inner and outer tantalum tubes, designated fuel and honeycomb tubes, respectively, defining: (1) an eccentric annular region which was empty or filled with $Li_3{}^7N$, and (2) a central region into which was loaded the fuel and

TABLE 48

PHYSICAL CHARACTERISTICS OF REACTOR COMPONENTS
(Sheet 1 of 2)

Component	Dimensions (cm)	Unit Mass (gm)
Fuel Rods	15.24 L by 0.43 D	42.275 (20)*
	22.27 L by 0.43 D	60.147 (20)
	combined 37.51 L	102.422
Honeycomb Tubes	59.94 L(11) by 2.16 OD by 0.025 W	180.12 (25)
Fuel Tubes	58.09 L(8) by 1.58 OD by 0.025 W	128.11 (33)
Lithium Nitride	37.34 L	41.00 (250)
Ta Foil	36.83 L by 0.014 thick	90.07 (50)
Ta Foil Spacer	37.46 L by 0.007 thick	18.78 (50)
W Foil	36.68 L by 0.007 thick	61.34 (247)
Hf Foil	36.83 L by 0.008 thick	16.66 (247)
Heavy U Wire	37.47 L by 0.152 D	13.49
Fine U Wire	37.47 L by 0.067 D also by 0.061 D	2.56
Eccentric Mo Reflectors	10.01 L (18) by 2.09 OD by 1.60 ID eccentric by 0.040	145.71 (18)
Solid Cylindrical Mo Reflectors	10.02 L (5) by 1.49 D (5)	178.95 (60)
End Fittings (aluminum)	-	8.54
Rubber Packing	2.10 D by 0.32 t, 0.48 hole	1.33 (8)
Ta Wire (0.28)	37.39 L by 0.28 D	38.61 (21)
Ta Wire (0.36)	59.66 L by 0.36 D	99.92 (17)
Ta Centering Ring	-	1.74 (40)
Mo Wire Wrap	-	0.251 (40)
Steel Wire Wrap	-	0.105 (24)
Ta Absorber Segment	60.17 L	38,438 (6)
Mo Reflector Segment	60.17 L	41,109 (6)
Trapezoidal Mo Filler	60.17 L	2,758 (6)
Rod-Type Mo Filler		
3/16	60.10 L by 0.47 D	108.85
4/16	60.12 L by 0.64 D	195.00
5/16	60.12 L by 0.79 D	302.85
Scrammable Radial Reflector	59.74 L	66,063 (4)
Stationary Radial Reflector	60.20 L	67,512 (2)
Core Filler Segments	60.17 L	11,281 (10)
Pressure Vessel Mockup		
120° sectors	59.69 L by 0.69 thick	39,720 (2)
60° sectors	59.66 L by 0.69 thick	20,441 (2)
Mo Bolts 3/8 - 24	5.66 L by 0.95 D	47 (7)
	6.79 L by 0.95 D	53 (15)
Large Reactivity Samples		
Li	37.34 L by 1.28 D	26.902 (7) cladding 44.739
Li^6	37.34 L by 1.28 D	21.019 (7) cladding 44.111
Li^7	7.38 L by 1.28 D	4.827 (35) cladding 10.559
$Li_3{}^7N$	37.48 L by 1.34 D	39.830 (7) cladding 45.221
Be	37.49 L by 1.31 D	93.749 (7) cladding 44.176

*Number in parentheses denotes the number of samples used to determine the dimension or mass under discussion.

TABLE 48

PHYSICAL CHARACTERISTICS OF REACTOR COMPONENTS
(Sheet 2 of 2)

Component	Dimensions (cm)	Unit Mass (gm)
BeO	37.48 L by 1.31 D	145.783 (7) cladding 44.577
B^{10}	37.48 L by 1.34 D	54.193 (7) cladding 44.451
C	37.48 L by 1.31 D	86.441 (7)
Nb	37.50 L by 1.27 D	405.787 (7)
Mo	37.49 L by 1.32 D	517.830 (7)
Hf	37.46 L by 1.32 D	659.344 (7)
Ta	37.48 L by 1.32 D	845.857 (7)
W	37.50 L by 1.31 D	966.379 (7)
Re	37.48 L by 1.34 D	374.19 (7)
U^{235}	Various assemblages of fuel rods were used	
U^{238}	37.48 L by 1.31 D	937.029 (7)
Large capsules	37.59 L by 1.38 OD by 0.025 W	43.295 (7)
Small capsules	7.46 L by 1.38 OD by 0.025 W	10.240 (35)
Small Reactivity Samples		
Li^6	5.08 L by 1.35 OD by 0.025 W	0.258 SS 4.708
Li^7	5.08 L by 1.35 OD by 0.025 W	0.290 SS 4.708
B^{10}	5.33 L by 1.30 OD by 0.016 W	0.816 SS 4.708
Hf	4.85 L by 1.36 OD by 0.027 W	6.564 SS 2.673
Ta	5.49 L by 1.36 OD by 0.028 W	9.918 SS 2.674
W	5.43 L by 1.36 OD by 0.022 W	9.208 SS 2.671
Re	5.08 L by 1.31 OD by 0.029	7.962 SS 4.709
U^{235}	5.49 L by 1.36 OD by 0.015	6.002 SS 2.678
U^{238}	5.42 L by 1.36 OD by 0.029 W	11.217 SS 2.677
Void capsule		SS 2.677
Void capsule with mandril		SS 4.680
Proton-Recoil Fuel Elements	28.11 23.99 18.59	
T-111 Support Sleeve		163.22
Reactivity Sample Fuel Elements	24.027	Ta 308.62 (9) $Li_3{}^7N$ 40.45 (9) Mo 291.19 (9)
Upper Grid Plate		1708.8
Sample Holder Tubes	110.33 L by 1.49 OD by 0.025 W	Ta 234.03 Mo Reflectors Top 158.59 Middle 158.49 Bottom 159.81 Mo capsule 41.89
Oscillator Rod	95.30 L by 1.49 OD by 0.025 W	

other core materials. Each end contained molybdenum axial reflectors, an eccentric sleeve in the annular region, and a solid cylinder in the central region. The ends were capped with end fittings serving to locate each fuel element with respect to the grid plates. Fuel consisted of 0.432-cm(0.170 in.)-diameter fuel rods supplemented by heavy and fine uranium wires. Tantalum was added in the core region by means of wires and foils, while tungsten and hafnium were added solely by foils.

2. Fuel Rods

The fuel rods used in this assembly consisted of pairs of rods, one 15.24 cm(6.00 in.) long, the other 22.27 cm(8.767 in.), enriched to 93.145% in U^{235} and coated with a Kel-F base point.

3. Honeycomb Tubes

These tubes consisting of tantalum, comprised the main structural member of the fuel element.

4. Fuel Tubes

These tubes, which were also made of tantalum, were located within the honeycomb tube and served to contain the fuel cluster.

5. Lithium Nitride

The $Li_3{}^7N$ was a free-standing body in the form of semi-circular cylindrical shells contained in the annular space between the fuel tube and honeycomb tube. Two segments were used in each fuel element in order to provide a cylindrical sleeve (see Figure 56).

6. Tantalum Foil and Tantalum Foil Spacer

Tantalum foil was placed within fuel tubes to increase the tantalum content of the core. Tantalum foil spacers were located in the annular space in fuel elements in Composition 1 to support the eccentric molybdenum reflector.

7. Tungsten Foil

Tungsten foil was placed within fuel tubes to simulate the tungsten content of the T-111 structural material as well as the tungsten liner on the fuel tube of the reference reactor.

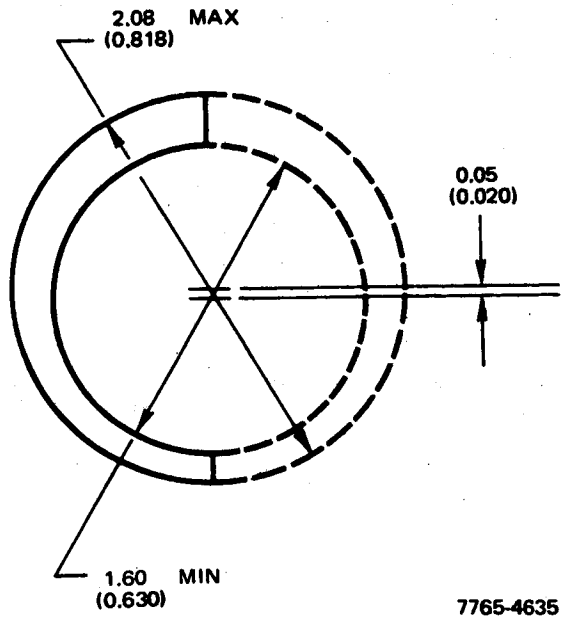

Figure 56. Li_3^7 Segment – Cross Sectional View

8. Hafnium Foil

Hafnium foil was placed within fuel tubes to simulate the hafnium content of the T-111 structural material in the reference reactor.

9. Heavy Uranium Wire [0.152 cm(0.060 in.)]

Uranium wire was produced by swaging some of the fuel rods and was then coated with Kel-F paint that was pigmented with iron oxide. This wire was used to adjust the fuel loading in the fuel tubes.

10. Fine Uranium Wire [0.066 cm(0.026 in.)]

Additional uranium wire was produced by swaging fuel rods, and was also coated with Kel-F paint that was pigmented with iron oxide. This wire was used to adjust the fuel loading in the fuel tubes.

11. Eccentric Molybdenum Reflectors

An eccentric molybdenum sleeve was placed at each end of the fuel element in the annular space between honeycomb and fuel tubes and constituted part of the axial reflector. After the experimental work had been completed on Composition 1, an air-tight seal was made at the outer end of the sleeve with an epoxy cement (see Figure 57).

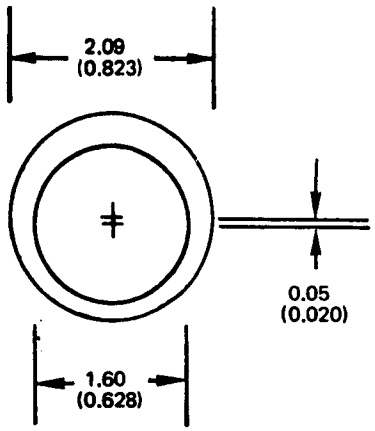

Figure 57. Eccentric Molybdenum Reflector-Cross Sectional View

12. Solid Cylindrical Molybdenum Reflectors

Molybdenum circular cylinders were placed at each end of the fuel element in the fuel tube and also constituted part of the axial reflector.

13. End Fittings

Aluminum end plugs served to seal the elements as well as to locate them in the upper and lower grid plates (see Figure 4).

14. Tantalum Wire [0.279 cm(0.110 in.) diameter]

Since the total mass of tantalum in the reference reactor is envisaged to be considerably greater than that represented by the tantalum foil and tantalum fuel and honeycomb tubes in the critical assembly, tantalum foil in the form of wire that is 0.279 cm(0.110 in.) in diameter by 36.83 cm(14.5 in.) long was added to each fuel cluster for several experiments.

15. Tantalum Wire [0.356 cm(0.140 in.) diameter]

Additional tantalum was added to the critical assembly in the form of long tantalum wire, 0.356 cm(0.140 in.) in diameter by 59.69 cm(23.5 in.) long. This wire, which extended into the upper and lower reflector regions, was placed in the 300 interstitial positions between honeycomb tubes in the stationary part of the core.

16. Tantalum Centering Ring

A ring of tantalum was used to hold the cluster of fuel rods together in the fuel tube. It was placed at both ends of the fuel element in Composition 1, at

the lower end of the fuel element of Composition 2, and was not used in other compositions.

17. Molybdenum Wire Wrap

Molybdenum wire was wrapped around the fuel rod bundles in Compositions 1 and 2 to help maintain a stable fuel arrangement.

18. Steel Wire Wrap

Steel wire was wrapped around the fuel rod bundles in Composition 3 to help maintain a stable fuel arrangement. In subsequent cores, the foils added around the fuel cluster provided adequate support.

C. CONTROL DRUMS

1. Overall Description

Each control drum had the form of a circular cylinder and was composed of a central molybdenum reflector segment, a tantalum absorber segment, and eleven fuel elements. Additional filler pieces of molybdenum were used to occupy spaces between fuel elements. A plan view of a control drum was shown in Figure 4.

The drums were driven by geared electrical motors. The theoretical drive speed of each drum, derived from the nominal motor speed and the gear reduction, and the measured drive speeds are shown in Table 49.

TABLE 49

THEORETICAL AND MEASURED CONTROL-DRUM DRIVE SPEEDS

Drum	Drive Speed (deg/sec)	
	Theoretical	Measured
1	0.694	0.692
2	0.694	0.699
3	0.720	0.726
4	0.694	0.699
5	0.694	0.696
6	0.720	0.722

Another measurement, involving a determination of the position of the drums as a function of time, showed a drive speed that was constant at 0.727 deg/sec throughout the range.

2. Tantalum Absorber Segment

A removable cylindrical segment of tantalum was mounted in the control drum to represent the T-111 absorber segment in the drum of the reference reactor (see Figure 58).

3. Molybdenum Reflector Segment

The drum reflector was a cylindrical segment of molybdenum that formed the structural member of the control drum and separated the tantalum from the fuel elements (see Figure 59).

4. Trapezoidal Molybdenum Filler

A trapezoidal strip of molybdenum was used to fill the space between the fuel elements and the molybdenum reflector segment (see Figure 60).

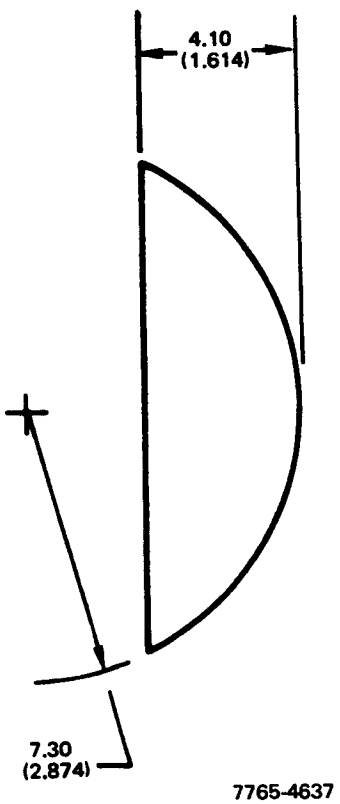

Figure 58. Ta Absorber Segment – Cross Sectional View

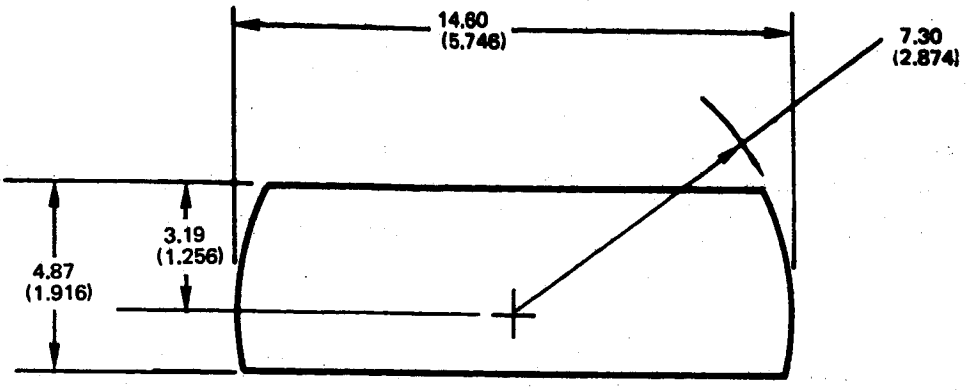

Figure 59. Mo Reflector Segment – Cross Sectional View

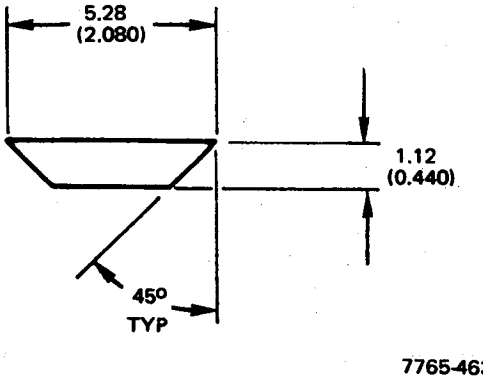

Figure 60. Trapezoidal Mo Filler Segment – Cross Sectional View

5. Rod-Type Molybdenum Filler

Rods of molybdenum of three different sizes were placed in spaces between fuel elements in the control drum to reduce the void fraction (see Figure 4).

6. Fuel Elements

The fuel elements in the control drums were identical to those used in the balance of the core and have been described and dimensioned elsewhere.

D. RADIAL REFLECTORS

1. Scrammable Reflectors

Each scrammable reflector (or safety block) is composed of two adjacent sections of the six sections making up the massive molybdenum radial reflector.

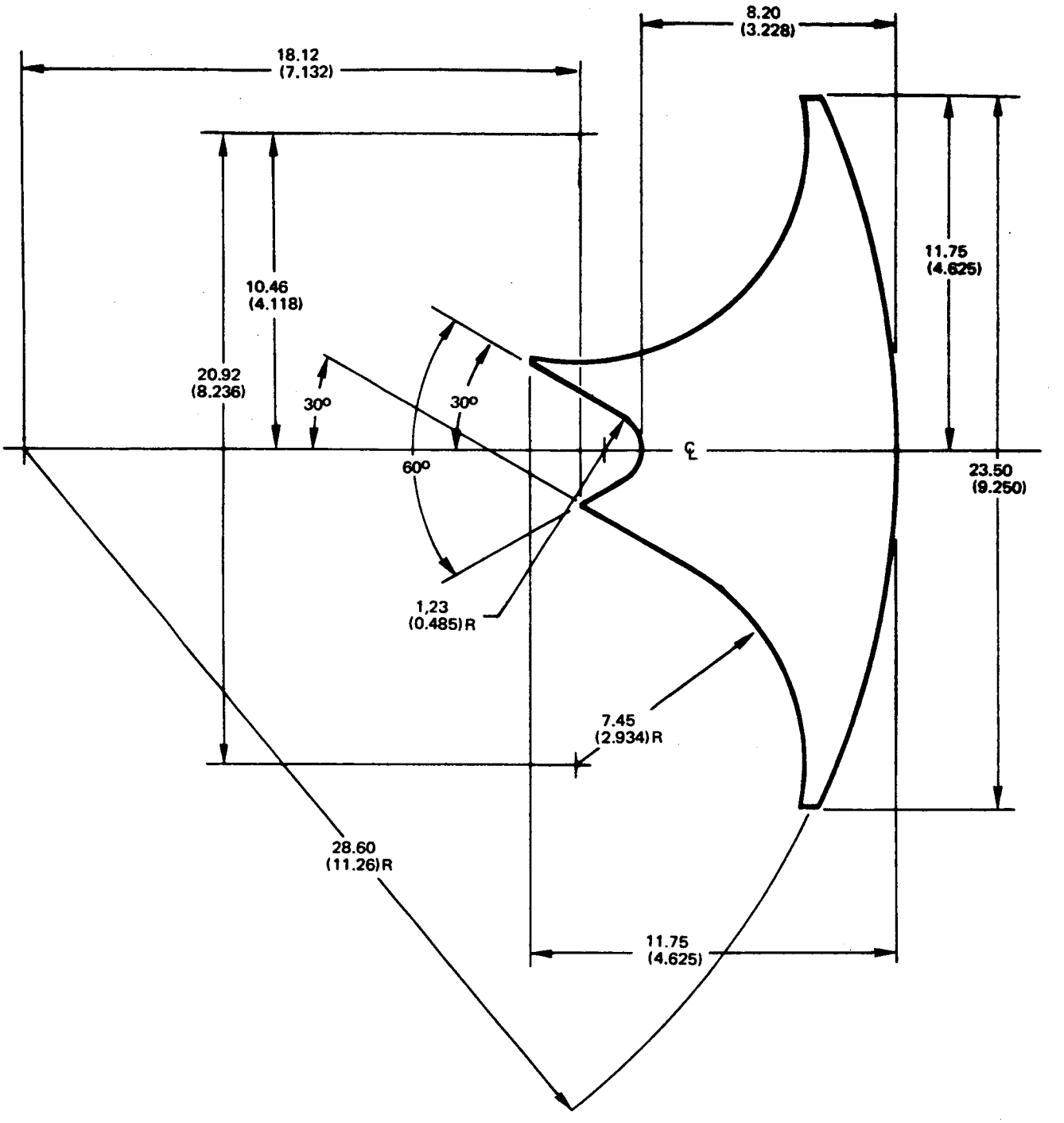

Figure 61. Scrammable Mo Reflector – Cross Sectional View

Two such scrammable reflectors were built into the critical assembly. To provide clearance for the scram motion, a portion of these reflectors was removed to allow clearance around the control drums. Triangular pieces of molybdenum were placed in the core to substitute for the portions removed (see Figure 61).

2. Stationary Reflectors

Two radial reflector sections, diametrically opposed, were stationary (see Figure 62).

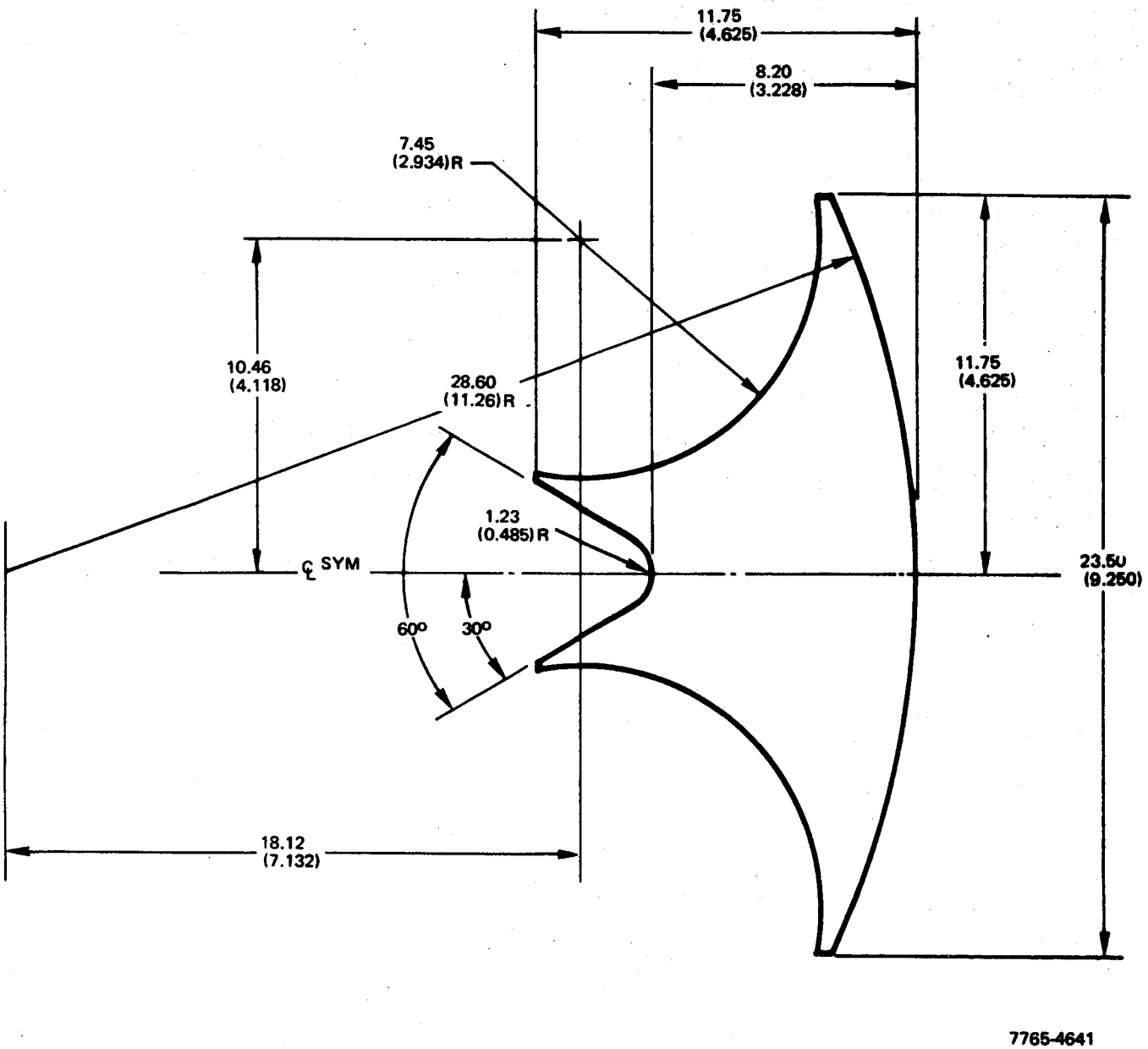

Figure 62. Stationary Mo Reflector – Cross Sectional View

E. CORE FILLER SEGMENT

A total of 10 molybdenum strips, approximately triangular in cross section, were placed in the spaces between the control drums and the core proper to reduce the void fraction in the core (see Figure 63).

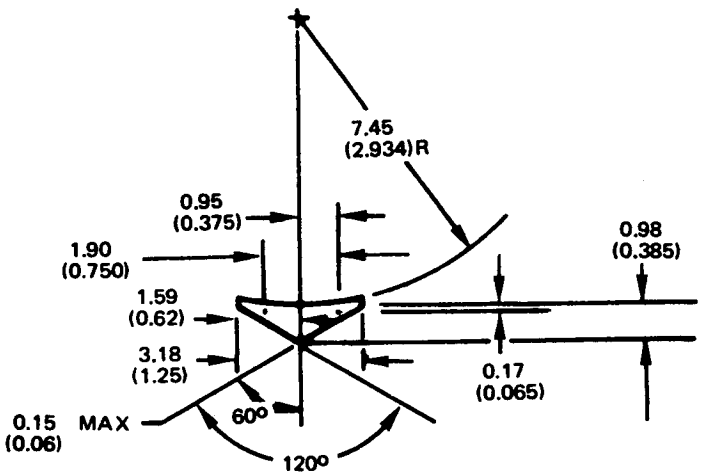

Figure 63. Core Filler Segment — Cross Sectional View

F. PRESSURE VESSEL MOCKUP

Segments of tantalum plate surrounded the reactor radially and were attached by means of molybdenum bolts to the radial reflectors sections.

G. REACTIVITY SAMPLES

1. Large Samples

Samples of various materials of full core length were used for reactivity worth measurements at the core center and at the periphery. The samples were clad in 0.0254-cm(0.010 in.)-wall molybdenum tubing with end caps. The Li^7 samples were segmented into short sections which, when stacked end to end, were equivalent in length to the standard core-length samples. This arrangement made it possible to measure the reactivity effect of coolant voiding as a function of axial position.

2. Small Samples

Short annular samples of various materials were used for reactivity worth measurements at the core center.

H. SPECIAL FUEL ELEMENTS

1. Fuel Elements for Use with Proton-Recoil Detector

Partial-length fuel elements were used above and below the proton-recoil detector at the core center. The inner ends of these elements were capped by tantalum plugs (see Figure 64). A sleeve of T-111 alloy surrounded the proton-recoil detector at the core center and supported the partial-length fuel elements.

2. Fuel Elements for Use with Reactivity Samples

"Fuel Elements" that consisted of a tantalum honeycomb and fuel tube, a $Li_3{}^7N$ segment, eccentric molybdenum reflectors, and special aluminum end fittings were used to allow a passage through the core for the sample-holder tube (see Figure 65).

I. UPPER AND LOWER GRID PLATES

An aluminum plate with location holes for 181 fuel elements was used for the top grid plate and a similar structure, made of stainless steel, was used for the lower grid plate. The deflection of the lower grid plate was measured in a fully loaded core and was found to be 0.00279 cm(0.0011 in.).

J. SAMPLE HOLDER TUBES

Tantalum tubes with integral molybdenum reflector plugs were used in conjunction with the sample changer in measurements of the reactivity worths of large reactivity samples. The lower half of each tube contained an empty molybdenum capsule. The upper half contained the sample of interest (see Figure 66).

K. OSCILLATOR ROD

A tantalum tube that held small samples at the center of the core was used in the oscillator measurements (see Figure 67).

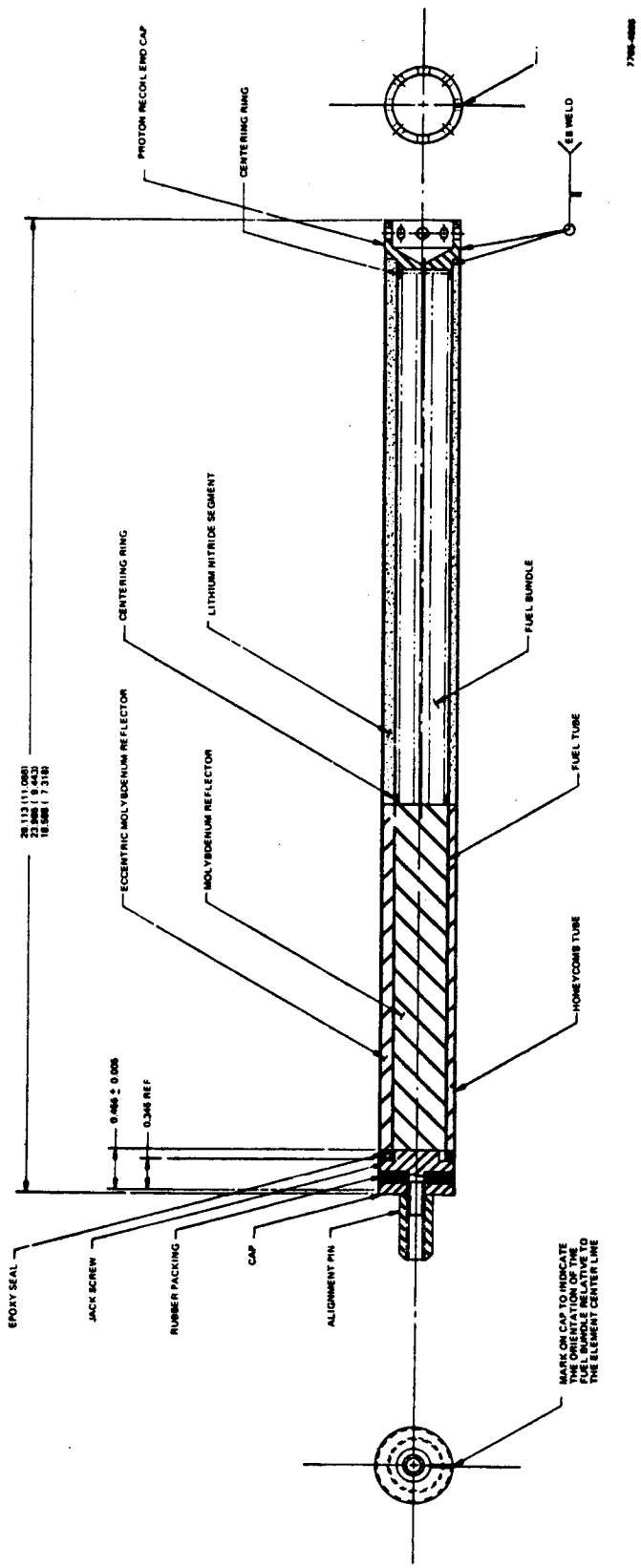

Figure 64. Fuel Element For Use With Proton-Recoil Detector

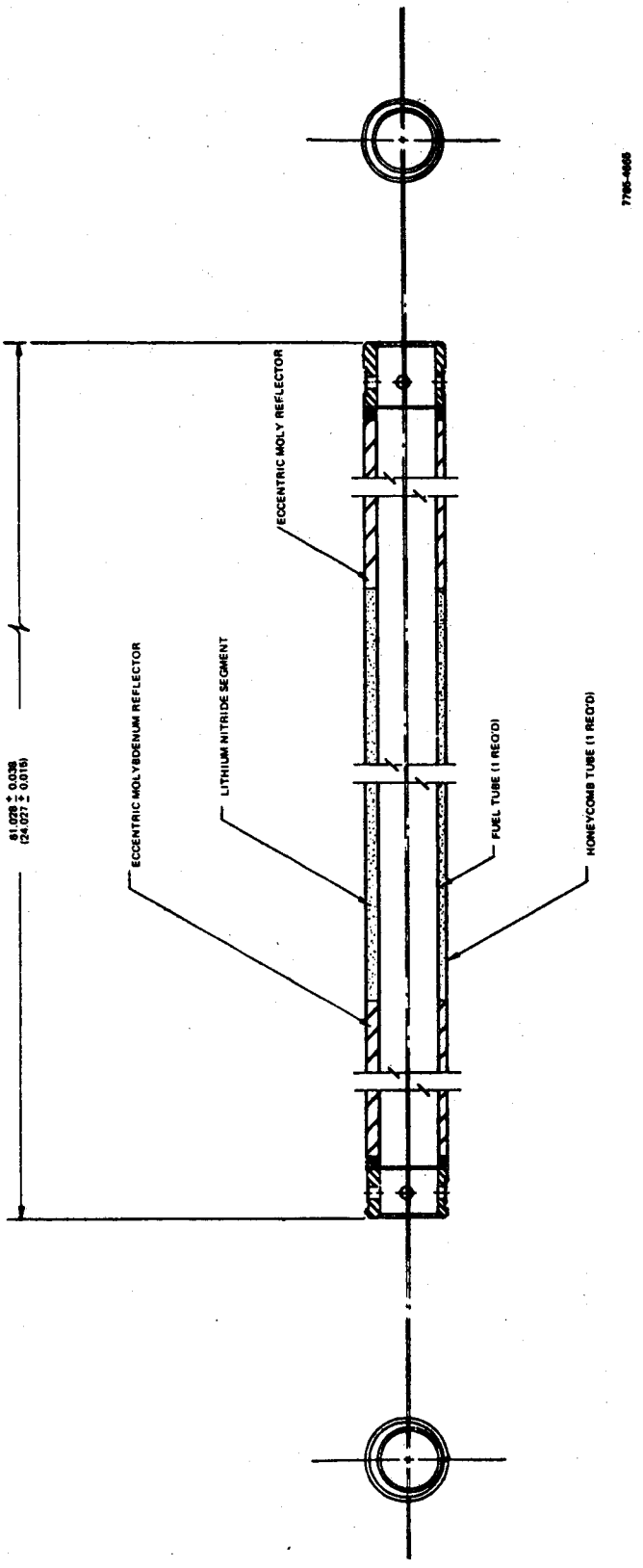

Figure 65. "Fuel Element" For Use With Sample Holder Tube

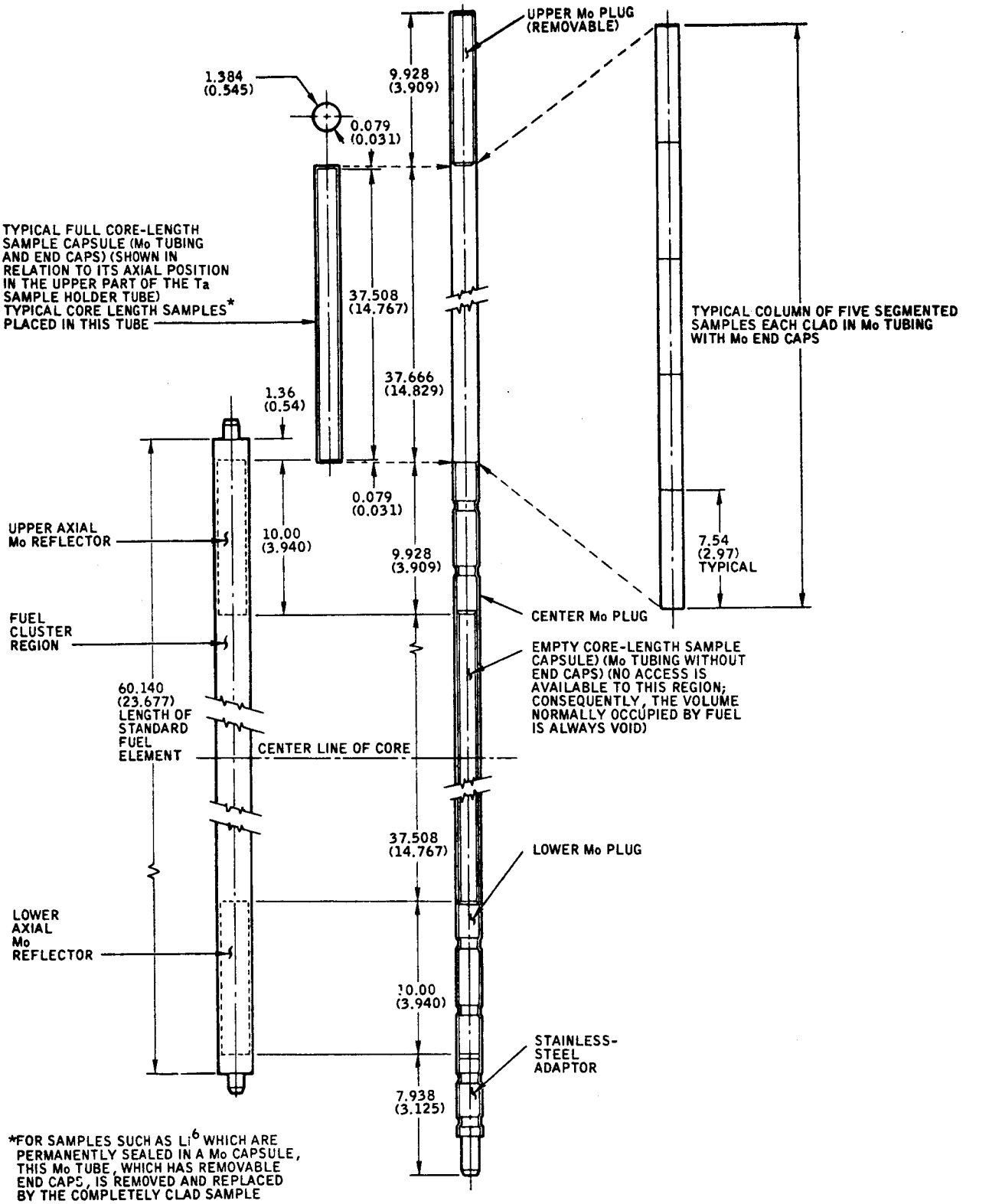

Figure 66. Sample Holder Tube

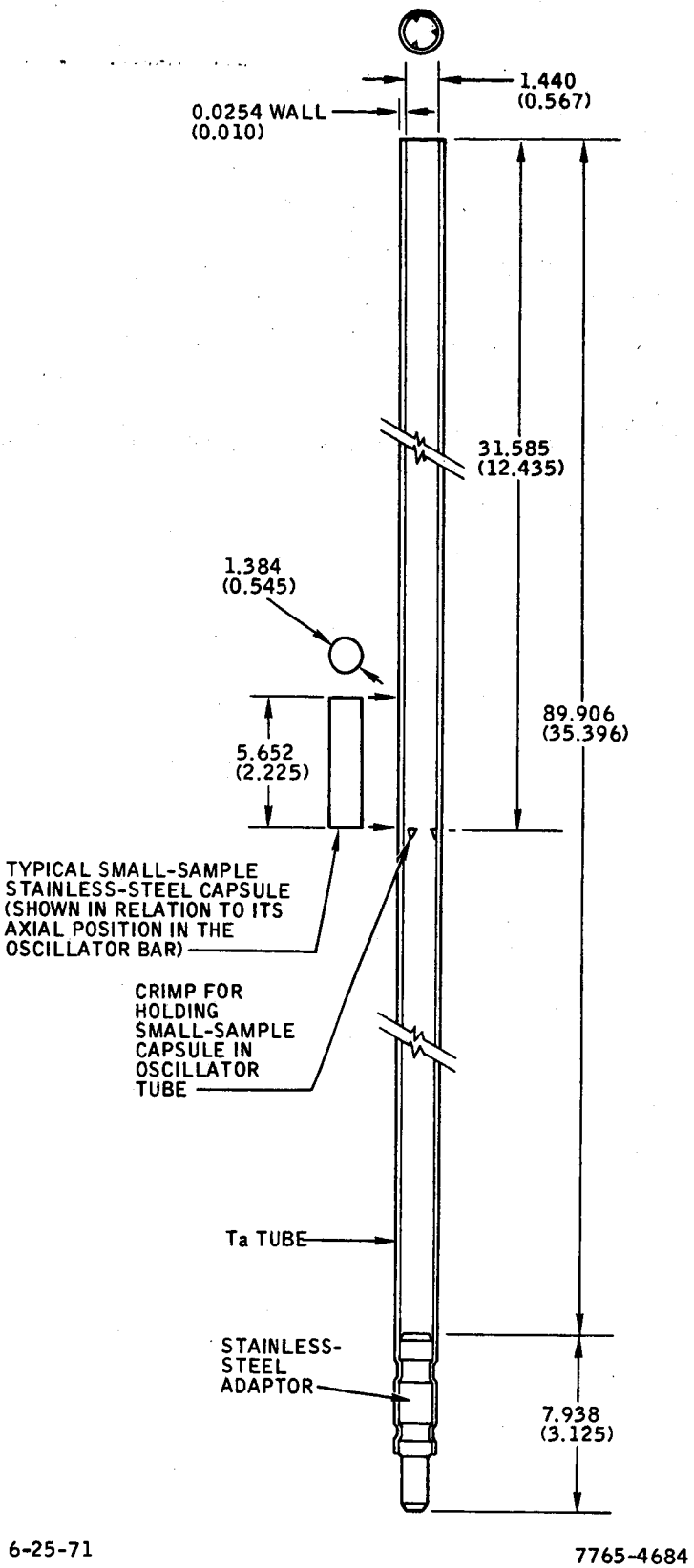

Figure 67. Oscillator Bar

L. SAMPLE CHANGER AND OSCILLATOR MECHANISM

An electrically driven table supported either 6 or 7 sample holder tubes or the oscillator rod. The stroke length with the sample holder tubes was 47.5 cm (19.9 in.) and required 103 sec from full-in to full-out. With the oscillator rod, the stroke was 34.0 cm(13.4 in.) and required 9.2 sec.

APPENDIX D

CALCULATIONS IN SUPPORT OF THE SAFEGUARDS ANALYSIS REPORT

I. INTRODUCTION

In accordance with normal procedures, an addendum to an existing safeguards analysis report[1] was prepared for and submitted to the U. S. Atomic Energy Commission in order to obtain approval to build and operate the critical assembly in an existing facility at the nuclear field laboratory at Atomics International. In this safeguards report were described, among other subjects, the physical and mechanical features of the reactor, the facility in which the reactor was built, and the laboratory site. The report also contains information concerning the administrative controls governing the operation of the reactor and the proposed experimental program. In the preparation of the report, a series of static and dynamic calculations was performed in order to scope, in broad terms, the operating and safety characteristics of the reactor. In this Appendix, the main results of these calculations and the methods used to obtain them are presented.

II. STATIC CORE CHARACTERISTICS

A. CALCULATIONAL METHODS*

Reactivity calculations were performed using the APC and APC-II[22] versions of the ANISN[23] one-dimensional multigroup transport code.

A 13-group cross section set was prepared using the GRISM[24] code for all core compositions (see Table 50). KEDAK cross sections were used for U^{235} and molybdenum. The AIENDF cross section set for U^{238} was used, and the remainder of the cross sections were taken from ENDF/B. These cross sections (zero order in scattering expansion) were punched in ANISN format. As is usual for use in ANISN, the total cross section was transport corrected.

TABLE 50

13-GROUP CROSS SECTION SET

Group Number	Energy Range	Lethargy Width
1	10 to 3.679 Mev	1
2	3.679 to 2.231 Mev	0.5
3	2.231 to 1.353 Mev	0.5
4	1.353 to 0.821 Mev	0.5
5	0.821 to 0.498 Mev	0.5
6	498 to 302 kev	0.5
7	302 to 183 kev	0.5
8	183 to 111 kev	0.5
9	111 to 40.87 kev	1
10	40.87 to 15.03 kev	1
11	15.03 to 5.53 kev	1
12	5530 to 74.85 ev	2
13	74.85 to 0.414 ev	3

*These calculations were carried out prior to the final design of the critical assembly; consequently, some of the dimensions do not correspond exactly to those existing in the as-built assembly.

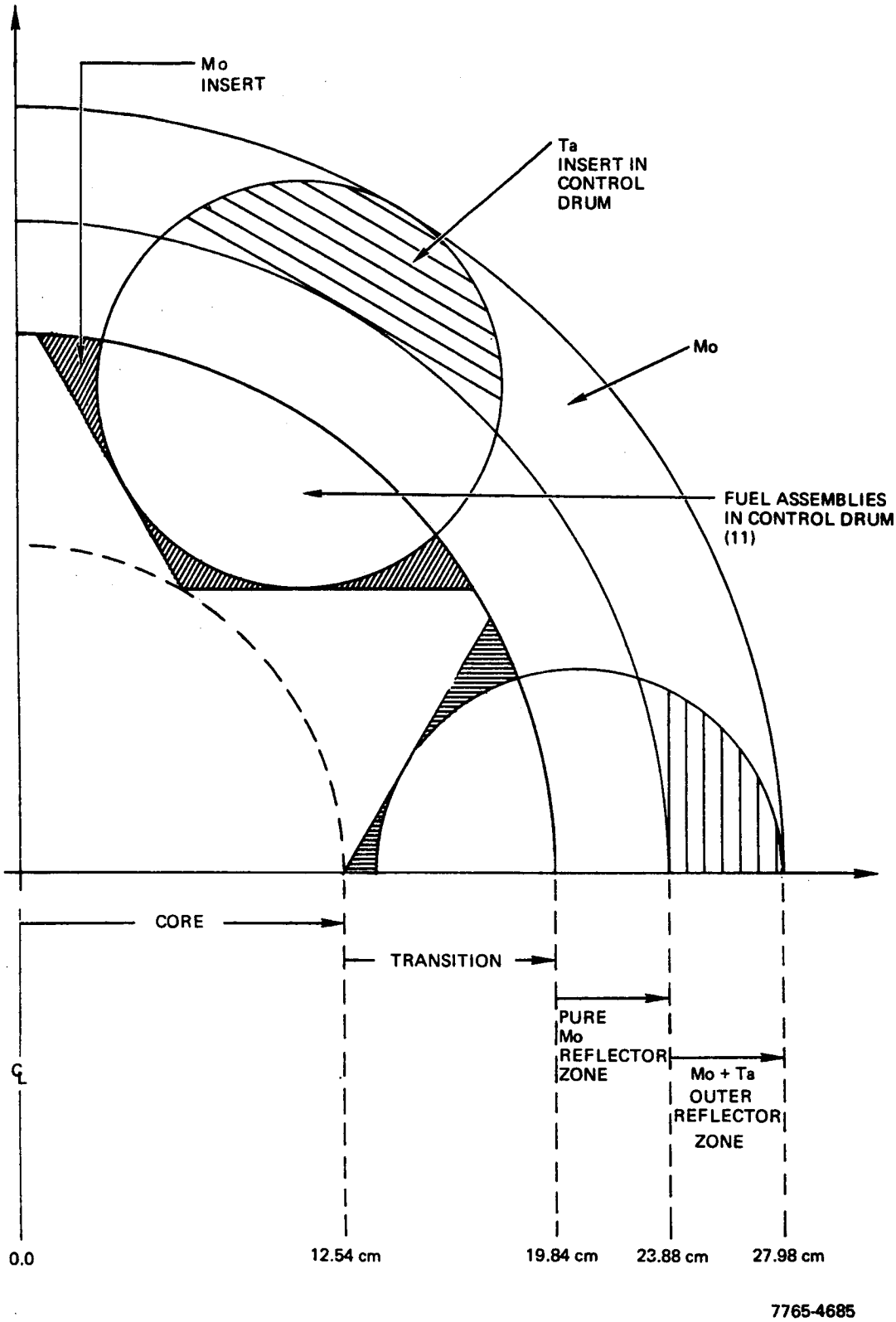

Figure 68. Core Layout

For Core Composition 1, a published GODIVA spectrum was used for cross section weighting. For Compositions 2 through 5, $MC^{2(25)}$ was used to generate the flux and current spectrum for use in GRISM. The inventory for the MC^2 calculation was appropriate for Composition 5. One dilute and two self-shielded cross section sets for molybdenum and tantalum were derived in order to have an applicable set for each core zone in which these elements occur.

Criticality calculations were done in cylindrical and slab geometry using transverse leakage corrections in an iterative fashion. This is done automatically in APC-II.

Atom densities for the calculations were obtained using standard zone smearing techniques. The reactor was divided into four radial zones and three axial zones. The core composition was smeared into a pure core zone and a transition zone as shown in Figure 68. The transition zone is followed by a zone of solid molybdenum reflector, and an outer reflector zone. For the fuel full-in configuration, the outer reflector zone is 4.1-cm thick. The tantalum inserts and molybdenum composition are smeared together. The outer reflector zone is 6.6-cm thick in the fuel full-out drum position. For this latter case, the material inventory for the 66 fuel elements in the control drums is smeared in the outer zone. The core height is 36.83 cm with an additional 10.16 cm of molybdenum reflector on top and bottom. The atom densities are given in Tables 51 through 53.

Drum worth calculations were made using buckling iterated results. For most relative worth determinations, regular APC runs were made using the converged transverse bucklings from a base APC-II calculation.

The worth of the drop-away reflector safeties was found by reducing the molybdenum atom number densities in Zones 3 and 4 to correspond to 2/3 of the fixed molybdenum reflector being removed.

The "fat-man" effect was determined by adding another radial zone around the reflector consisting of water 15-cm thick.

The worth of a 1-cm axial fuel expansion was obtained by reducing the fuel atom density by a factor 36.83/37.83. A 1-cm-thick axial zone was added between

TABLE 51
ATOM DENSITIES FOR RADIAL CASES WITH DRUMS TURNED FUEL-IN

Material	Radial Zone Number	Core Number				
		1	2	3	4	5
Lithium-7	1	-	0.015529	0.015529	0.015529	0.015529
	2	-	0.010520	0.010520	0.010520	0.010520
	3	-	-	-	-	-
	4	-	-	-	-	-
Nitrogen	1	-	0.0051765	0.0051765	0.0051765	0.0051765
	2	-	0.0035068	0.0035068	0.0035068	0.0035068
	3	-	-	-	-	-
	4	-	-	-	-	-
Uranium-235*	1	0.010849	0.010327	0.010327	0.010327	0.010327
	2	0.0073495	0.0069960	0.0069960	0.0069960	0.0069960
	3	-	-	-	-	-
	4	-	-	-	-	-
Uranium-238*	1	0.00079655	0.00075822	0.00075822	0.00075822	0.00075822
	2	0.00053962	0.00051357	0.00051357	0.00051357	0.00051357
	3	-	-	-	-	-
	4	-	-	-	-	-
Hafnium	1	-	-	0.00036752	0.00036752	0.00036752
	2	-	-	0.000248976	0.000248976	0.000248976
	3	-	-	-	-	-
	4	-	-	-	-	-
Tungsten-182	1	-	-	-	-	0.000942
	2	-	-	-	-	0.000638
	3	-	-	-	-	-
	4	-	-	-	-	-
Tungsten-183	1	-	-	-	-	0.000514
	2	-	-	-	-	0.000348
	3	-	-	-	-	-
	4	-	-	-	-	-
Tungsten-184	1	-	-	-	-	0.001092
	2	-	-	-	-	0.0007398
	3	-	-	-	-	-
	4	-	-	-	-	-
Tungsten-186	1	-	-	-	-	0.001013
	2	-	-	-	-	0.0006862
	3	-	-	-	-	-
	4	-	-	-	-	-
Tantalum, Dilute	1	0.004196	0.004196	0.004196	0.0059554	0.0059554
	2	0.002843	0.002843	0.002843	0.004121	0.004121
	3	-	-	-	-	-
	4	-	-	-	-	-
Tantalum, Reflected	1	-	-	-	-	-
	2	-	-	-	-	-
	3	-	-	-	-	-
	4	0.01921264	0.01921264	0.01921264	0.01921264	0.01921264
Molybdenum, Dilute†	1	-	-	-	-	-
	2	0.0084485	0.0084485	0.0084485	0.0084485	0.0084485
	3	-	-	-	-	-
	4	-	-	-	-	-
Molybdenum, Zone 3	1	-	-	-	-	-
	2	-	-	-	-	-
	3	0.06405267	0.06405267	0.06405267	0.06405267	0.06405267
	4	-	-	-	-	-
Molybdenum, Zone 4	1	-	-	-	-	-
	2	-	-	-	-	-
	3	-	-	-	-	-
	4	0.04178706	0.04178706	0.04178706	0.04178706	0.04178706

*Fuel number densities are for 167 kg uranium in Core 1 and 159 kg uranium in Cores 2 through 5.
†Molybdenum densities in Zone 2 will be increased to 0.012073 with the proposed addition of molybdenum to the fueled portion of the drums.

TABLE 52

ATOM DENSITIES FOR AXIAL CASES
(Same for all cores)

Zone Number	Tantalum	Molybdenum	Pure Core Materials
1 and 3	0.004196	0.053225	-
2	-	-	Same as Radial Zone 1

TABLE 53

ATOM DENSITIES FOR RADIAL CASES WITH
DRUMS TURNED FUEL-OUT

Material	Radial Zone Number	Core Number	
		1	5
Lithium-7	1	-	0.015529
	2	-	0.0049486
	3	-	-
	4	-	0.004032
Nitrogen	1	-	0.0051765
	2	-	0.00164958
	3	-	-
	4	-	0.001344
Uranium-235*	1	0.010849	0.010327
	2	0.003460	0.0032909
	3	-	-
	4	0.002815	0.0026803
Uranium-238*	1	0.00079655	0.00075822
	2	0.00025400	0.00024162
	3	-	-
	4	0.00020630	0.00019687
Hafnium	1	-	0.00036752
	2	-	0.00011712
	3	-	-
	4	-	0.0000954
Tungsten-182	1	-	0.000942
	2	-	0.0003001
	3	-	-
	4	-	0.0002445
Tungsten-183	1	-	0.000514
	2	-	0.0001638
	3	-	-
	4	-	0.0001334

(Continued)

TABLE 53 (Continued)

Material	Radial Zone Number	Core Number	
		1	5
Tungsten-184	1	-	0.0001092
	2	-	0.0003479
	3	-	-
	4	-	0.0002835
Tungsten-186	1	-	0.001013
	2	-	0.0003227
	3	-	-
	4	-	0.0002630
Tantalum, Dilute	1	0.004196	0.0059554
	2	0.001335	0.0018913
	3	-	-
	4	0.001257	0.00155648
Tantalum, Reflected	1	-	-
	2	0.017282	0.017282
	3	-	-
	4	-	-
Molybdenum, Dilute	1	-	-
	2	0.023613	0.023613
	3	-	-
	4	-	-
Molybdenum, Zone 3	1	-	-
	2	-	-
	3	0.06405267	0.06405267
	4	-	-
Molybdenum, Zone 4 †	1	-	-
	2	-	-
	3	-	-
	4	0.038585	0.038585

*Fuel number densities are for 167 kg uranium in Core 1 and 159 kg uranium in Core 5.

†Molybdenum number densities in Zone 4 will be increased to 0.041247 with the proposed addition of molybdenum to the fueled portion of the drums.

the top of the normal core and the top reflector. This zone contains only fuel and tantalum honeycomb tubes on the assumption that the fuel expansion pushes up the top reflector.

Calculations were made to determine the effect of replacing the fuel, and the hafnium, tungsten, and tantalum foil wrapped around the fuel in the central 7 fuel tubes, with a void. The worth of seven U^{235} samples (containing 1.8 times the normal amount of fuel in a standard fuel tube) relative to the seven central voids was then calculated to simulate the maximum possible sample changer reactivity insertion.

A hypothetical meltdown calculation was performed. It was assumed that an axial zone (2-cm-thick) of melted fuel formed at the center of the core, and that the top of the core slumped an amount equivalent to the additional space occupied by the fuel in the melt zone. It was assumed that the density of melted fuel was 17.5 gm/cm^3. This calculation was performed for Composition 1 only since it has the largest void volume for molten fuel.

Radial worth curves were generated for kinetics calculations. The core region was divided into i = 4 radial zones. The fuel atom density was reduced by 4% in Zone i and the transverse buckling in that zone was adjusted to correspond to a 4% increase in height of that zone. This procedure was repeated for all i zones. An axial worth curve was generated in a similar fashion except that instead of changing the buckling in each reduced density zone, the thickness of the zone was increased 4%.

An effective value for beta was determined by calculating the effective multiplication of a core with and without delayed neutrons added to the prompt neutron spectrum. The delayed neutron spectrum was obtained from work by Batchelor and Bonner as reported by G. R. Keepin.[12] The delayed fraction was taken to be 0.00692. β_{eff} was found by a prescription described in NAA-SR-11850, pages 1-38.[26]

$$\beta_{eff} = \frac{k^1 - k_o}{k^1} \quad .$$

Here, k^1 was determined by using the combined spectrum (C of Table 54) and k_o was determined by using a pure prompt spectrum (A of Table 54). It should be noted that APC does not renormalize the source to 1 neutron before proceeding with the calculation. An almost identical result was obtained using a relationship which eliminates the round-off error of subtracting two nearly identical numbers.

$$\beta_{eff} = \frac{k_d}{k_o} \cdot \beta \quad .$$

Here, k_d was determined using the delayed spectrum only (B in Table 54)

TABLE 54

13-GROUP SOURCE SPECTRA

Group	A Prompt Spectrum Xp	B Delayed Spectrum Xd	C Combined Spectrum Xp + 0.00692 Xd
1	0.13079	0.0	0.13079
2	0.21039	0.00635	0.21043
3	0.23131	0.04766	0.23166
4	0.18024	0.12713	0.18112
5	0.11483	0.24252	0.11650
6	0.06484	0.23417	0.06646
7	0.03412	0.15508	0.03519
8	0.01715	0.09956	0.01784
9	0.01252	0.08114	0.01308
10	0.00292	0.00639	0.00296
11	0.00067	0.0	0.00067
12	0.00022	0.0	0.00022
13	0.0	0.0	0.0
Sum	1.00000	1.00000	1.00692

The generation time Λ was calculated using relationships developed in NAA-SR-11850.[26] Effective multiplications were determined for various concentrations of a flux weighted 1/v absorber added uniformly to all regions of the reactor including reflectors. The amounts added, which are equivalent in this case to inverse period, ω, were chosen to give a $\Delta\rho$ of about \$1 and \$3. The relationship,

$$\Lambda = \frac{k_o - k_p}{k_o \omega} ,$$

was used to find Λ as a function of ω. k_o is for the unpoisoned reactor and k_p is for the poisoned reactor. A two-point plot was linearly extrapolated to $\omega = 0$ to obtain the value of Λ with no poison.

B. RESULTS

The critical mass results are shown in Table 55. The mass is in terms of total uranium ($U^{235} + U^{238}$). All calculations were buckling iterated in an S-4 approximation. Table 56 lists the results of various reactivity calculations for Compositions 1 and 5. Drum worths with and without additional molybdenum in the control drums are shown. The latter calculations were made in anticipation of the insertion of molybdenum rods in the fueled part of the control drums. This increases the molybdenum cross sectional area by 42 cm^2 in place of void space. The change in atom density is given in Table 51.

TABLE 55

CRITICAL LOADINGS

Composition	Loading (kg)	k_{eff} (radial)	$\frac{\Delta K}{(kg)}$	Extrapolated* Loading (kg)
1	162	0.98320	-	-
1	167	1.00417	0.0042	166.0
2	150	0.96783	-	-
2	159	1.00102	0.0037	158.7
3	159	1.00144	-	158.6
4	159	0.99697	-	159.7
5	159	0.99876	-	159.3

*These values were obtained with no molybdenum rods added to the fuel region of the drums. With the additional molybdenum the values for Compositions 1 and 5 are 161.6 and 155.5 kg, respectively.

TABLE 56

REACTIVITY CALCULATIONAL RESULTS

Calculation	Core 1		Core 5	
	$\Delta\rho$ $(\Delta k/k_1 k_2)$	\$ $(\Delta\rho/\beta_{eff})$	$\Delta\rho$ $(\Delta k/k_1 k_2)$	\$ $(\Delta\rho/\beta_{eff})$
1. Drum worth (Fuel full-in to full-out configuration)	-0.06164	-8.68	-0.0719209	-10.29
2. Drum worth (Additional molybdenum in drum)	-0.077307	-10.90	-0.082499	-11.80
3. Drop-away reflector worth (drum in, reflector safety down)	-0.131825	-18.60	-0.065396	-9.35
4. Axial expansion coefficient 1 cm	-0.019936	-2.81	-0.011168	-1.60
5. "Fat-man" worth (15-cm H_2O radially)	0.026566	3.74	0.01255	1.79
6. Core meltdown (2 cm molten fuel zone located at core center)	0.033632	4.73	-	-
7. Oralloy sample worth (relative to fuel absent in 7 central fuel tubes)	-	-	0.05848	8.35
8. Oralloy sample worth (relative to standard fuel loaded in 7 central fuel tubes)	-	-	0.02521	3.60

The additional molybdenum, according to calculations, will result in a fuel loading decrease of 4.4 kg in the case of Composition 1 and 3.8 kg for Composition 5.

The results of calculations to determine the effective delayed neutron fraction are tabulated in Table 57.

TABLE 57

DELAYED NEUTRON FRACTION CALCULATIONS

Core Composition	k			
	Combined Spectrum C*	Prompt Spectrum A*	Delayed Spectrum B*	β_{eff}
1	1.00693	0.99980	-	0.00708
1	-	0.99980	1.0309	0.00711
2	1.00803	1.00102	-	0.00695
5	1.00391	0.99687	-	0.00701

*See Table 54.

The results of the lifetime calculations are shown plotted in Figures 69 and 70. The results of a straight line extrapolation indicated that Λ = 37.0 nanosec for Composition 1 and 41.2 nanosec for Composition 5.

The relative axial and radial worth histograms are shown in Figures 71 and 72. The relative one-dimensional power density is also plotted from data in the APC-II output.

C. CONCLUSIONS

Since compositions 2 through 5 have almost the same critical mass and nuclear properties, calculations of relative worth were performed only on Compositions 1 and 5 with Composition 5 results assumed representative for Compositions 2 through 4.

To investigate the multigroup effect, a set of cross sections were generated in 24 groups for Composition 5. The 24-group library was in half lethargy interval steps. The 13- and 24-group results were very similar. The 24-group calculation made the reactor more reactive by 13×10^{-4} Δk. The values of η

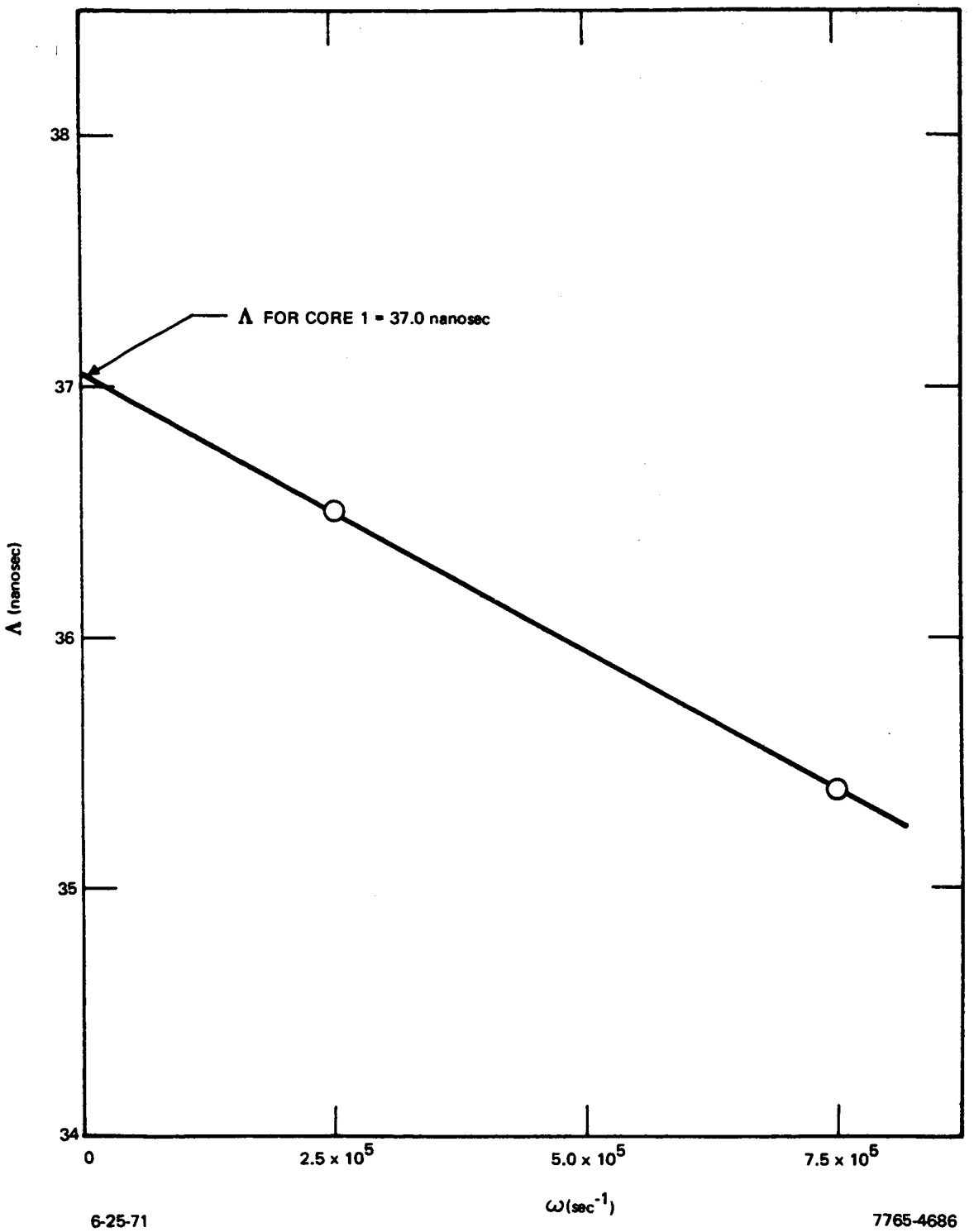

Figure 69. Prompt Neutron Lifetime for Composition 1

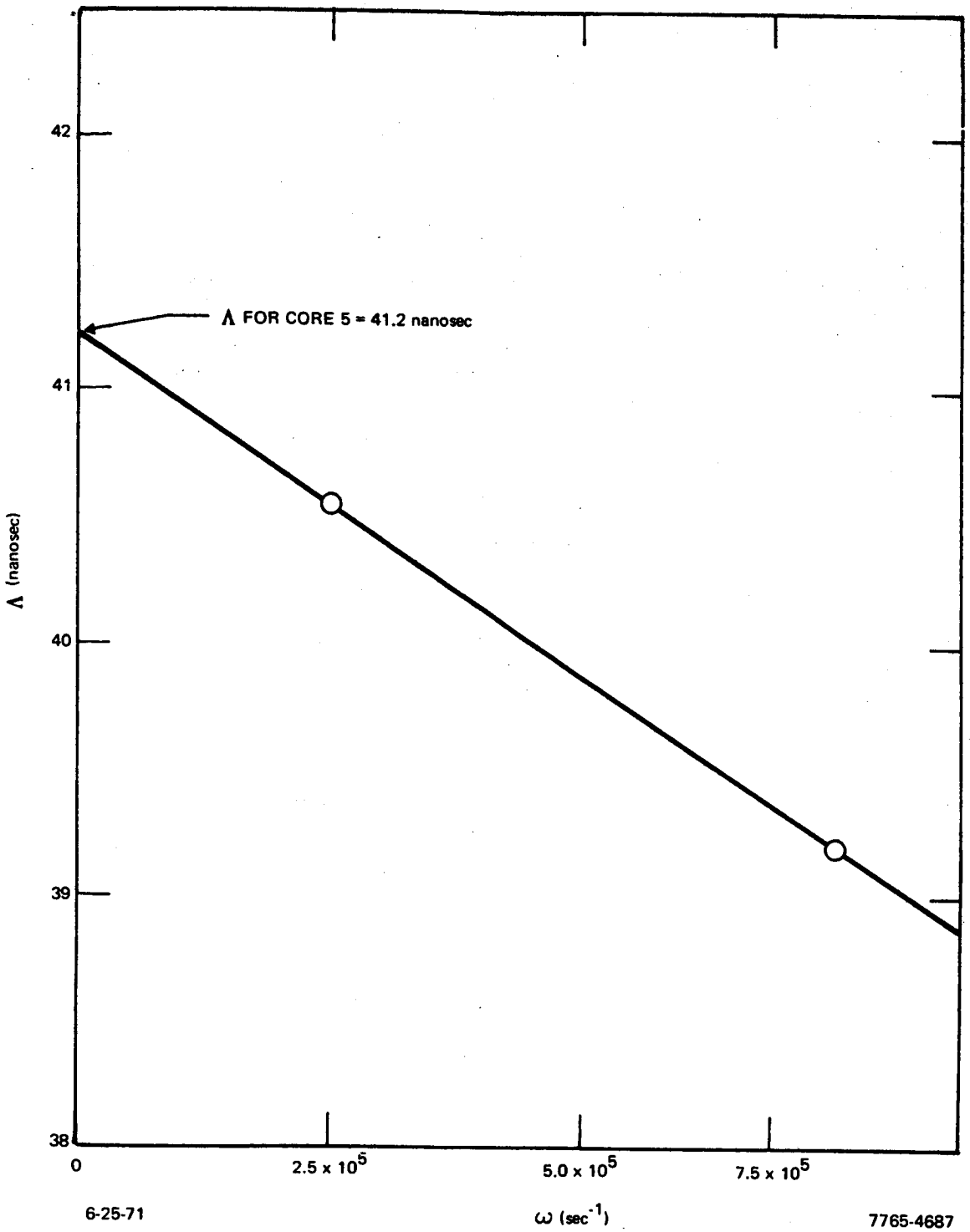

Figure 70. Prompt Neutron Lifetime for Composition 5

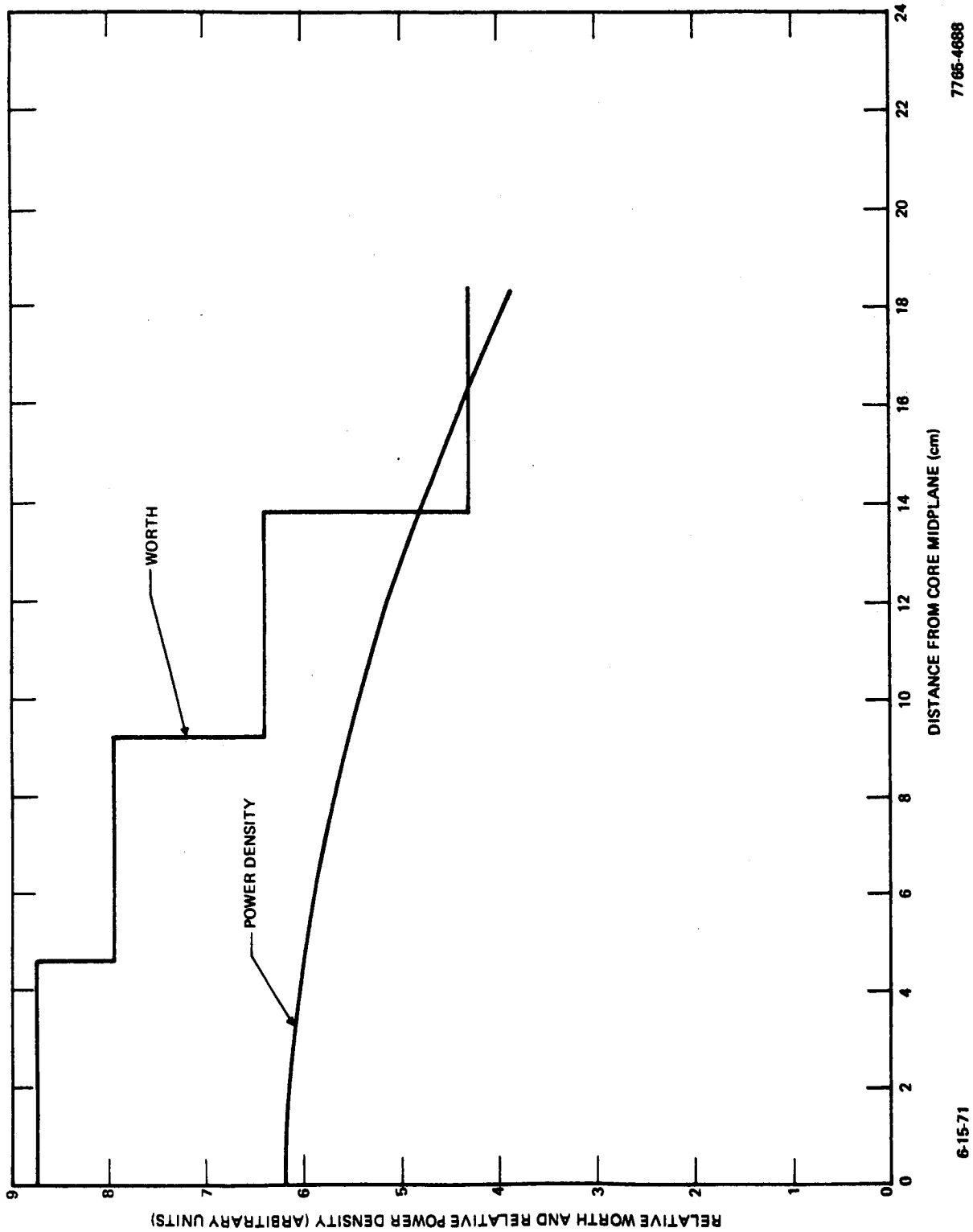

Figure 71. Relative Axial Worth and Power Density-Composition 5

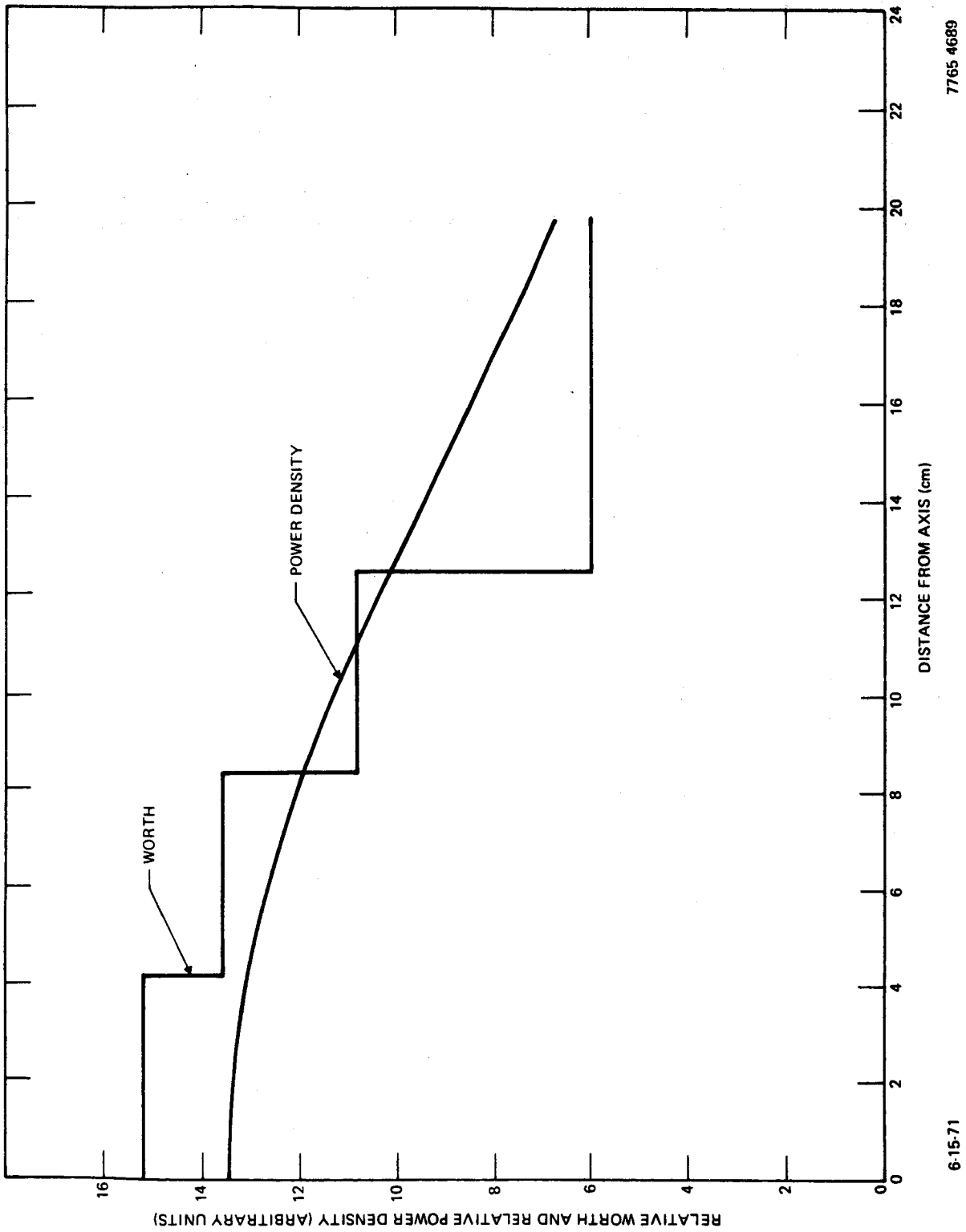

Figure 72. Relative Radial Worth and Power Density-Composition 5

and the radial leakage for both cases were essentially identical. The absorption rate of tungsten and tantalum was reduced by about 4% using the 24-group library, thus producing an increase in reactivity. The 13-group library was considered adequate for all calculations.

The drum and drop-away reflector worth calculations are only qualitative in nature because of the severe approximations made in reducing the calculation to a one-dimenional problem. A normalizing two-dimensional calculation would be required for a more quantitative data.

Calculations were not performed for sample worths in the peripheral fuel tubes. It is assumed that the importance of neutrons for this calculation would be considerably less than that determining the central worth.

III. DYNAMIC CHARACTERISTICS

As part of the Safety Analysis Report, the response of the reactor to an assumed accident condition, designated the design basis accident (DBA), was calculated. This accident is assumed to be initiated by ramp insertion of reactivity at a rate of 15¢/sec.

The kinetics code, CREKIN, was used to analyze the system up to the melting point and for some cases, up to the boiling point. CREKIN is a point kinetics code with spatially dependent feedback similar to the code, SNAPKIN VI,[27] which has been used successfully in calculating the behavior of SNAPTRAN experiments.

The only feedback mechanism for this reactor (short of disassembly) is a negative axial expansion coefficient. For Composition 5, this coefficient is lowest and is equal to -$0.59/% expansion. This coefficient is assumed to go to zero when the fuel becomes molten (per zone).

A ramp insertion rate of +15¢/sec, corresponding to the DBA was used. A β_{eff} of 0.00714 and a lifetime of 37×10^{-9} sec were used. The heat capacity of the solid fuel as a function of temperature was read in in as a table and included the phase change effects. Radial and axial worth and power density curves were obtained from the results of APC-II calculations for Composition 5. The core was divided into 4 axial zones and 5 radial zones.

The code allows for scram shutdown. The scram can be initiated on either period or power level. A delay time (before safety elements begin to move) can be read in to allow for instrument and magnet response time. The shutdown insertion as a function of time is read in as a table. The effect of period and power scrams for a range of ramp insertion rates is shown in Figure 73.

Assuming that all scrams are inoperative, the center of the core reaches the melting point at about 9.6 sec after initiation of the ramp. At this point the fuel will begin to slump with a resultant increase of reactivity. APC calculations have been performed for the following two cases: (1) Composition 1 with axial expansion corresponding to heating the core to the melting point and (2) Composition 1 with a 2-cm-high axial zone of molten fuel at the center and a reduction

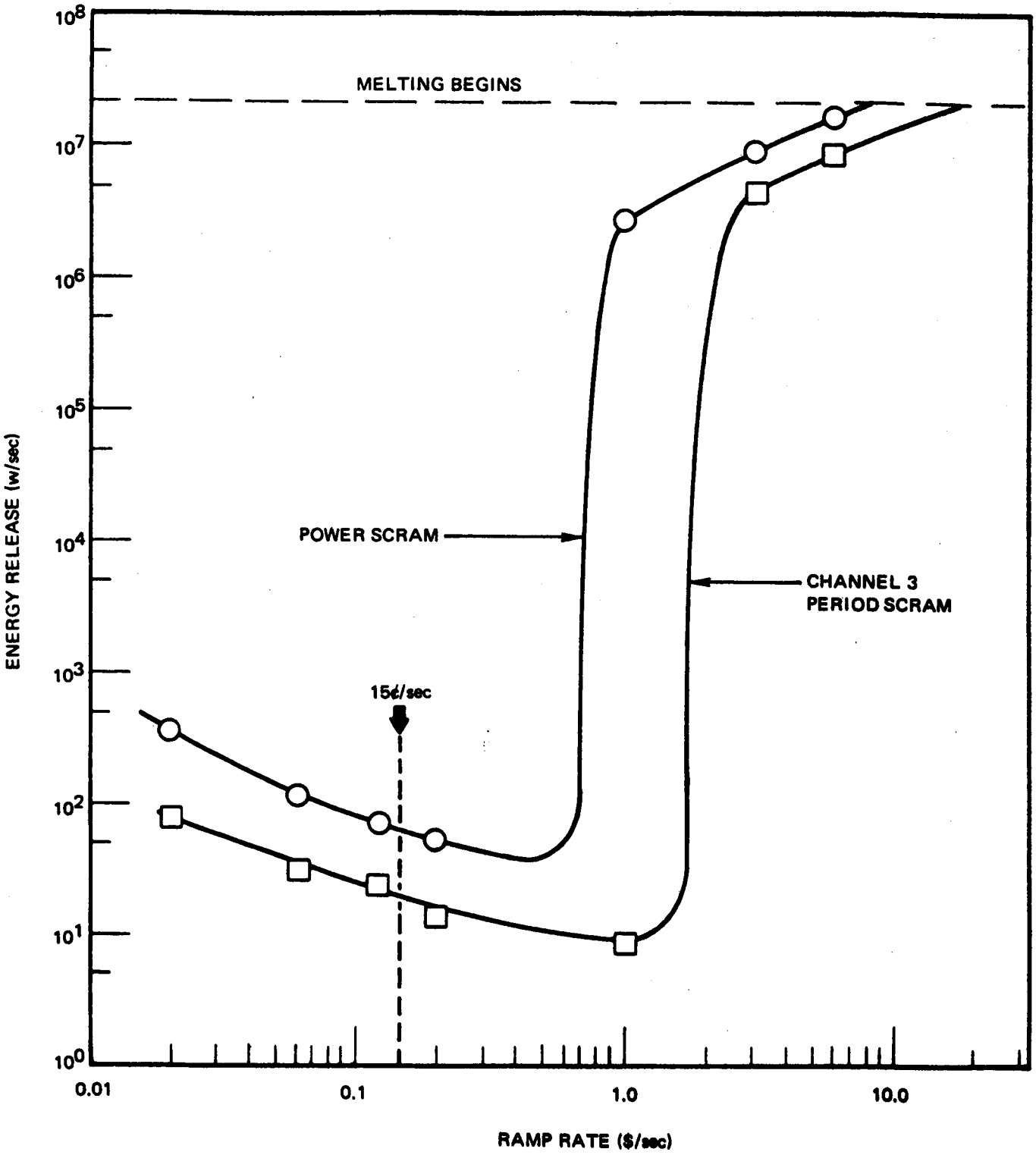

Figure 73. Energy Release vs Ramp Rate

in core height of 1.5 cm corresponding to the amount of fuel needed to fill the void space in the 2-cm zone. The difference in reactivity of these two cases gives the reactivity insertion due to a 1.5-cm drop of the entire core ($3.1/cm). The amount of void volume available in Composition 5, for fuel to slump into, is much less than in Composition 1 so that the resulting reactivity insertion rate would be lower.

CREKIN calculations were performed beyond the melting point using the following model: (1) axial expansion is zero in each molten zone; (2) as each radial zone begins to melt at the center, it is assumed that the top of the core in that raidal zone drops under the force of gravity; (3) the worth per cm of drop is linear; (4) the geometry of the core remains unchanged, i.e., the relative worth and power distributions remain unchanged up to the time of disassembly; and (5) the amount of reactivity inserted per cm drop in each radial zone is proportional to the relative radial worth-per-unit-volume of fuel multiplied by the volume of the zone.

Successive cases were run. The first case had no slumping insertion and was used to determine the time at which Radial Zone 1 begins to melt. The next case was run with Zone 1 slumping in at the time it begins to melt. The results of this case gave the time at which Radial Zone 2 begins to melt. The third case was run with both Zone 1 and Zone 2 slumping in, etc. The results of this series of calculations shows that the rate at which reactivity is being added at the time of disassembly is about $44/sec.

A series of WEP[28,29] cases with different ramp rates have been run to determine the dynamics of disassembly. Table 58 gives the input data used for WEP. A $44/sec ramp insertion gives a total energy release of 110 Mw-sec. Ramp insertions of $30 and $60 yield energy releases of 101 Mw-sec and 121 Mw-sec, respectively, so that the consequences are not very sensitive to the insertion rate. Decreasing the absolute value of the worth curve used in WEP by a factor of four increases the calculated energy release by only 25%.

The amount of fuel vaporized as a result of the DBA was determined from CREKIN calculations. The amount of energy deposited in a zone from the time that zone reaches the boiling point until disassembly occurs was obtained from the total energy release during that time interval, weighted by the power density and fuel mass in the zone. It is assumed that all of this energy goes into vaporizing the fuel. The amount of fuel vaporized is then obtained by dividing this energy

by the heat of fusion. Summing the results from all zones gives the total amount of fuel vaporized. This was found to be about 854 gm or 0.54% of the core.

TABLE 58

WEP INPUT DATA

Parameter	Value
1. Number of radial elements	100
2. Radius of sphere (cm)	22.33
3. Time increment (sec)	1×10^{-5}
4. Prompt neutron lifetime (sec)	4.2×10^{-8}
5. Initial power (Mw)	4.2
6. Initial reactivity increment	0
7. Reactivity-insertion rate ($/sec)	20, 30, 50, 1000
8. Maximum time for transient (sec)	0.1
9. Number of delayed-neutron groups	6
10. Homogenized core density (gm/cm^3)	6.97
11. k_{final}	0.95
12. Doppler coefficient (α)	-1×10^{-4}
13. Doppler coefficient form (k = 1.0)	$\alpha = T\,dk/dt$
14. Reciprocal of the core volume ($1/cm^3$)	2.15×10^{-5}
15. Power distribution $\left[P(r)\right]$	$1 - 1.71 \times 10^{-3} r^2$
16. Danger coefficient $\left[W(r)\right]$($\Delta k/cm^3$)	$3.80 \times 10^{-5} - 8.5 \times 10^{-8} r^2$
17. Equation of state: $P_r = B_e - \frac{A}{E(r,t) + E_o}$ where $A = 2.44 \times 10^4$ joules/cm^3, $B = 7.6 \times 10^{11}$ dynes/cm^2, $E_o = 6.23 \times 10^2$ joules/cm^3	

IV. SUMMARY

A summary of the calculated nuclear characteristics of the critical assembly is presented in Table 59.

TABLE 59

NUCLEAR PARAMETERS

Parameter	Composition 1	Composition 2 through 5
Nominal fuel loading (kg U^{235})	161.6	155.1 ± 0.6*
Median Fission Energy (kev)	~400	~400
Prompt-neutron lifetime (10^{-9} sec)	37	41
Effective delayed-neutron fraction	0.0071	0.0070
Prompt expansion coefficient, axial ($/cm)	-2.8	-1.6
Total worth of two safety elements ($)	18.6	9.4
Worth of six control drums, safeties up ($)	10.9	11.8
Maximum control-drum reactivity insertion rate (¢/sec)	1.6	1.6
Maximum oscillator reactivity insertion (¢)	≤20	≤20
Maximum oscillator reactivity insertion rate (¢/sec)	2	2
Maximum allowable excess reactivity ($)	2.50	2.50

*Indicates range of fuel loading for Compositions 2 through 5.

REFERENCES

1. W. H. Heneveld, V. Swanson, A. W. Thiele, "SNAP Critical Facility Safety Analysis Report: Addendum for NASA Critical Assembly Experiments," AI-69-Memo-79, November 24, 1969

2. Wendell Mayo and Edward Lantz, "Analysis of Fuel Loading Requirements and Neutron Energy Spectrum of a Fast Spectrum, Molybdenum – Reflected Critical Assembly," NASA TM X-52762, Lewis Research Center, Cleveland, Ohio, March 4, 1970

3. J. L. Anderson and Wendell Mayo, "Effect of Adding Lithium Nitride, Hafnium, Tantalum, and Tungsten to a Fast-Spectrum, Molybdenum-Reflected Critical Assembly," NASA TM X-52787, Lewis Research Center, Cleveland, Ohio, May 1970

4. Wendell Mayo, "Precritical Analysis of a Power-Tailored Fast Spectrum Molybdenum Reflected Critical Assembly," NASA TM X-52895, Lewis Research Center, Cleveland, Ohio, September 1970

5. S. G. Carpenter, "Reactivity Measurements in the Advanced Epithermal Thorium Reactor (AETR) Critical Experiments," Nucl. Sci. and Eng.: 21, pp 429-440 (1965)

6. R. J. Tuttle, "Elimination of the Effect of a Constant Neutron Source in Reactivity Measurements," NAA-SR-Memo-12290 (Revised), May 1967

7. W. G. Davey and W. C. Redman, Techniques in Fast Reactor Critical Experiments, Gordon and Breach Science Publishers, New York, ©1970, pp 172 and 173

8. N. C. Kaufman, "GRIPE-II, A Computer Program for the Analysis of Data From a Pulsed-Neutron Experiment," IN-1085, September 1967

9. N. G. Sjostrand, Proceedings of the International Conference on the Peaceful Uses of Atomic Energy, August 8-20, 1955, Vol 5, Physics of Reactor Design, United Nations Publication, New York, 1956, p 52

10. T. Gozani, "A Modified Procedure for the Evaluation of Pulsed Experiments in Subcritical Reactors," Nucleonik, 4, December 1962, pp 348-349

11. E. Garelis and J. L. Russell, Jr., "Theory of Pulsed Neutron Source Measurements," Nucl. Sci. Eng., 16, July 1963, pp 263-270

12. G. R. Keepin, Physics of Nuclear Kinetics, Addison-Wesley, © 1965, p 274

13. P. W. Benjamin, C. D. Remshall, and J. Redfearn, "The Use of a Gas-Filled Spherical Proportional Counter for Neutron Spectrum Measurements In a Zero-Energy Fast Reactor," AWRE Report No. NR 2/64, 1964

14. E. F. Bennett, "Fast Neutron Spectroscopy by Proton-Recoil Proportional Counting," Nucl. Sci. Eng., 27, 1967, pp 16-27

15. R. K. Paschall and R. J. Tuttle, "Differential Neutron Spectra in ECEL Reactor Cores 17 and 17P," AI-AEC-12855, July 15, 1969

16. P. W. Benjamin, C. D. Kemshall, and A. Brickstock: The Analysis of Recoil Proton Spectra, AWRE 09/68, 1968

17. J. L. Snidow: Wall Effect Correction in Proton Recoil Spectrometers – Spherical Counter, BAW-TM-442, 1965

18. G. Kistner, "Rossi-α Theory for Assemblies With Two Prompt Neutron Groups," Nukleonik: 7, 1965, pp 106-109

19. L. B. Engle, G. E. Hansen, and H. C. Paxton: Reactivity Contributions of Various Materials in TOPSY, GODIVA, and JEZEBEL, Nucl. Sci. Eng., 8, 1960 p 543

20. S. G. Carpenter: Reactivity Measurements in the Advanced Epithermal Thorium Reactor (AETR) Critical Experiments, Nucl. Sci. Eng. 21, 1965, pp 429-440

21. T. H. Springer et al: Annual Technical Progress Report LMFBR Physics Program, GFY 1969, AI-AEC-12857, August 1969,pp 5-23

22. W. A. Rhoades and B. J. Dray, "The APC & APC II Buckling – Iteration Discrete Ordinates Transport Codes," TI-696-13-027, Atomics International, March 1969

23. M. A. Boling and W. A. Rhoades, "ANISN/DTFII Conversion to IBM System/360," AI-66-Memo-171, Atomics International

24. R. C. Lewis et al, "GRISM – A Code to Generate Multigroup Constants From Microscopic Neutron Cross Section Data," NAA-SR-11980, Vol III, Atomics International

25. B. J. Toppel, A. L. Rago, and D. M. O'Shea, "MC^2, A Code to Calculate Multigroup Cross Sections," ANL-7318, Argonne National Laboratory, June 1967

26. J. F. Jackson, W. R. Rhoades, and L. I. Moss, "Analysis of SNAPTRAN-1 and -2 Reactor Kinetics Experiments," NAA-SR-11850, Atomics International, June 1967

27. W. A. Rhoades, "The SNAPKIN VI Computer Program for SNAP Reactor Kinetics Calculations," NAA-SR-9190, April 1964

28. R. B. Nicholson, "Methods for Determining the Energy Release in Hypothetical Reactor Meltdown Accidents," APDA-150, December 1962

29. J. W. Stephenson, Jr. and R. B. Nicholson, "Weak Explosion Program," ASTRA 417-6.0, 1961

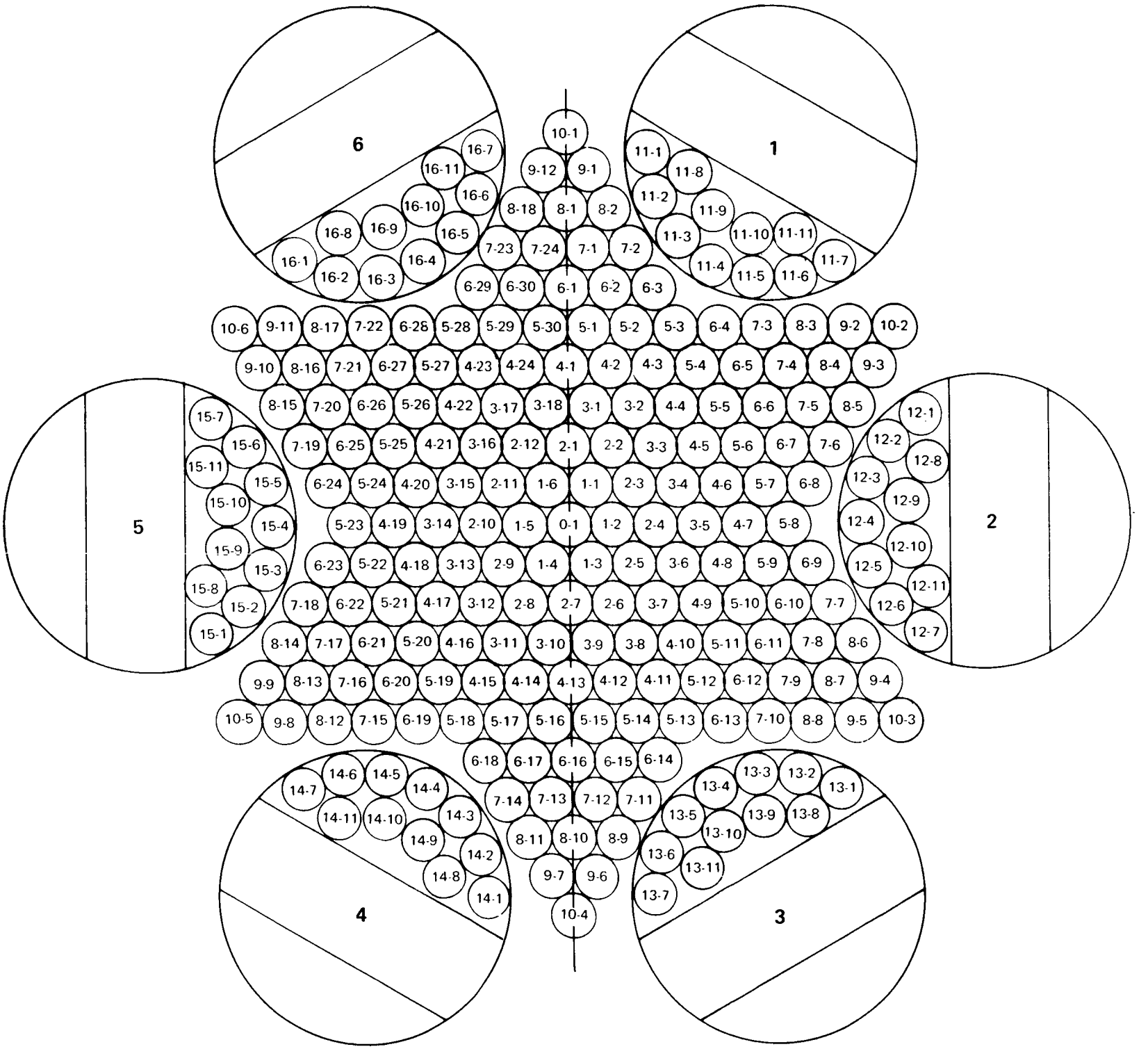

Figure 74. Core Map